Levee Stability and The Evolution of 'A'a Lava Flow-Fields

The thesis is submitted in partial fulfilment of the requirements for the award of the degree of Doctor of Philosophy of the University of Portsmouth

Marie Nolan

April 2014

School of Earth and Environmental Sciences

University of Portsmouth

FORM UPR16

Research Ethics Review Checklist

University of Portsmouth

Please complete and return the form to Research Section, Quality Management Division, Academic Registry, University House, with your thesis, prior to examination

Postgraduate Research Student (PGRS) Information			**Student ID:**	**351597**
Candidate Name:	**Marie Nolan**			
Department:	**SEES**	**First Supervisor:**	**Dr. Carmen Solana**	
Start Date: (or progression date for Prof Doc students)	**May 1st 2009**			

Study Mode and Route:	Part-time ❑	MPhil ❑	Integrated Doctorate (NewRoute) ❑
	Full-time ❑x	MD ❑	Prof Doc (PD) ❑
		PhD ❑x	

Title of Thesis:	Levee Stability and The Evolution of 'A'a Lava Flow-Fields
Thesis Word Count: (excluding ancillary data)	52,000

If you are unsure about any of the following, please contact the local representative on your Faculty Ethics Committee for advice. Please note that it is your responsibility to follow the University's Ethics Policy and any relevant University, academic or professional guidelines in the conduct of your study

Although the Ethics Committee may have given your study a favourable opinion, the final responsibility for the ethical conduct of this work lies with the researcher(s).

UKRIO Finished Research Checklist:
(If you would like to know more about the checklist, please see your Faculty or Departmental Ethics Committee rep or see the online version of the full checklist at: http://www.ukrio.org/what-we-do/code-of-practice-for-research/)

a) Have all of your research and findings been reported accurately, honestly and within a reasonable time frame?	**YES**
b) Have all contributions to knowledge been acknowledged?	**YES**
c) Have you complied with all agreements relating to intellectual property, publication and authorship?	**YES**
d) Has your research data been retained in a secure and accessible form and will it remain so for the required duration?	**YES**
e) Does your research comply with all legal, ethical, and contractual requirements?	**YES**

*Delete as appropriate

Candidate Statement:	
I have considered the ethical dimensions of the above named research project, and have successfully obtained the necessary ethical approval(s)	
Ethical review number(s) from Faculty Ethics Committee (or from NRES/SCREC):	
Signed: ***(Student)***	**Date:**
If you have *not* submitted your work for ethical review, and/or you have answered 'No' to one or more of questions a) to e), please explain why this is so:	
Not applicable to this area of research	
Signed: Marie Nolan ***(Student)*** Marie Nolan Digitally signed by Marie Nolan DN: cn=Marie Nolan, o, ou, email=mnolan2@gmail.com, c=IE Date: 2014.07.07 00:26:47 +02'00'	**Date: 06.07.2014**

Declaration

Whilst registered as a candidate for the above degree, I have not been registered for any other research award. The results and conclusions embodied in this thesis are the work of the named candidate and have not been submitted for any other academic award.

Word Count: c. 52,000

Abstract

The capability to predict the final dimensions of an 'a'a flow-field and the timeline for emplacement is key to effective lava hazard management. Levee breaching and the subsequent generation of secondary flows has been recognised as an intrinsic process in flow-field development. However, the conditions, locations and mechanisms for levee failure are not fully understood and so a multidisciplinary approach was taken utilising field studies of extant flow-fields on Mount Etna and Tenerife, analogue modelling and uniaxial compression tests to investigate levee failure.

The experimental results were used to define three stages of flow-field development – lengthening, widening and thickening, a modification of the classification of Kilburn and Lopes (1991). Levee breaching was identified to be a key process by which flow-fields widen during stage two of emplacement. Four mechanisms for breaching are identified, providing a classification system for levee failure. Secondary flows originating from breaching consistently formed at an angle of 30 – 50^{o} to the original channel, significantly contributing to overall flow-field width.

Uniaxial compression tests were performed to quantify the mechanical properties of levees. Levee strength was shown to change with direction according to the size, orientation and distribution of vesicles. Samples with vesicle alignment orientated obliquely to the angle of principal stress were consistently weaker. A set of conditions, relating to the mechanical properties of the levee, is therefore identified under which levees are more susceptible to failure.

The results of the study have been combined to produce a set of guidelines to the locations and conditions under which levee breaching is more likely to occur, aiding decision making for lava hazard management.

Table of Contents

Table of Figures

Table of Tables

Acknowledgements

I would like to take this opportunity to thank my supervisors Dr. Carmen Solana, Dr. Christopher Kilburn and Mrs. Emily Butcher for their invaluable support and advice during this PhD study, particularly during the write-up phase. Their experience and guidance were instrumental in completion of this study. I would also like to thank the Leverhulme Trust who provided the funding for this PhD (Funding contract F/00 678/J). Without their financial support, this project would not have been possible.

Apart from the main team of supervisors and researcher, many people are involved in a PhD and in particular I would like to thank the SEES department's Sue Atkins and Elaine Dyer for their skill and advice in assembling the analogue model. Special thanks should also go to Darina Brennan; the seedling ideas behind this study came from many early morning/late night discussions with her.

The fieldwork portion of this PhD represents some of the most enjoyable periods of the PhD study, down in no small part to the company I had, particularly that of Jessica Roberts. We'll always have Palermo. Thanks for assistance with the field studies also go to Samuel Murray and Patrick Boesch.

Lastly, I would like to thank my family. It's not possible for me to put into words what their support over the last four years and in particular the last year has meant. My father Sean, my sisters Sarah, Joanne and Laura and my mother Mary have devoted hours to supporting me and I can only hope that they know how much it is appreciated.

1 Introduction

Approximately 455 million people live within 100 km of a volcano that has been active in recorded history (Small & Naumann, 2001). As global population (and therefore demand for land) increases, it is inevitable that settlements on and around volcanoes will grow, increasing the amount of people and valuable infrastructure potentially at risk from volcanic activity. Volcanic hazards are diverse and not all result from eruption. Hazards such as earthquakes, ash and gas emission, tsunamis and lahars can reach significant distances from their source, with devastating effects on communities that may not perceive themselves as "at risk", such as the lahar that killed 25,000 people in Nevado del Ruiz in 1985 which reached peak discharge at 10-20 km from the summit (Naranjo et al., 1986; Pierson et al., 1990; Voight, 1990). Other volcanic products such as tephra-fall, volcanic bombs, pyroclastic flows and lava flows are more localized but no less hazardous to human life and property.

Of these hazards, lava flows are the most common and represent complex, multi-facetted flow systems which are not fully understood. Lavas can be extruded as single flows or in flow-fields made up of multiple flows termed compound flows. These multi-flow systems can reach significant distances from their source and form through a process of secondary flow generation from the growth and subsequent breaching or overtopping of levees and the formation of new flows.

Under subaerial conditions, the majority of flows are effused at temperatures below their liquidus, causing then to behave like a non-Newtonian fluid, possessing a yield strength, as demonstrated by Shaw (1969) on the Makaopuhi lava lake and proved under laboratory conditions by Murase & McBirney (1973). At their point

of origin, basaltic lavas can be effused at temperatures of up to 1200°C with a yield strength of 1.5–50 × 10^3 Pa (Fink & Zimbelman, 1986; Lyman et al., 2004). Due to its temperature dependent viscosity, lava will continue to flow downslope under gravity until heat loss is sufficient to increase the yield strength of the material, retarding its ability to flow under gravity. Cooling rates are not uniform throughout the flow, preferential cooling occurs along the top, base and sides of a flow resulting in areas with higher yield strengths that move more slowly than the hotter, more fluid material in the centre of the flow. This process results in the formation of lava levees which act as boundaries to the flow, defining its orientation and width.

Field observations have shown that lava flow-field morphology is strongly influenced by the formation and rupture of these levees (e.g. Kilburn & Luongo, 1993; Polacci & Papale, 1997; Bailey et al., 2006). When levees are breached or over topped, material moves through the breach resulting in the formation of a new flow, secondary to the main channel. Variations in flow morphologies for volcanoes such as Mount Etna, Sicily which exhibits a range of morphologies despite the uniform bulk chemical compositions of its flows (Kilburn & Lopes, 1988), can be related to differences in the complex interactions between eruptive parameters such as effusion rate, topography, volume and rheology that are not fully understood. Lava flows can occur in a single flow event but more commonly they occur in compound flow-fields, defined as one or more lava flows which can be distinguished from each other in terms of their morphology (Walker, 1971; Kilburn & Lopes, 1988, 1991; Borgia & Linneman, 1990). The behaviour of a lava flow is dependent on its rheology, temperature, underlying angle of slope, effusion rate and silica content. Lavas with lower silica content, basalts and basaltic andesites, have a

much lower viscosity and are associated with mid ocean ridges, divergent plate boundaries and hot spots. They are produced during effusive eruptions and are classified by their surface morphologies into pahoehoe and ‘a‘a lava flows.

These terms are ancient Hawaiian in origin and originally referred only to the surface features regardless of composition or emplacement mechanism. However, in cross section, it can be clearly seen that the morphological differences between these types of flows are not just restricted to the surface (Macdonald, 1953).

Pahoehoe flows are characterised by a smooth, continuous crust interspersed with areas of ropy or slabby texture. In the initial phase of eruption, pahoehoe lava may advance as a singular unit with a rolling flow-front, however in an established flow, where cooling has become the dominant parameter influencing flow behaviour, it is more common that the flow advances in multiple active fronts as a series of toey lobes which are extruded from the solidifying flow-front as the pressure of the still fluid lava overcomes tensile strength of the crust. These lobes are typically short lived and will in turn become static as the formation of solidifying crust retards their forward movement. However, if the vent is still active, lava will continue to flow causing inflation of the lobe which can overcome the tensile strength of the crust, forming a new lobe. This process is repeated and in this way the flow advances.

‘A’a lavas are the most common type of flow. Morphologically, they consist of a rough, rubbley surface at the macro and micro scale and advance as a continuous unit. ‘A’a is commonly described as having a layer of clinker or brecciated material on the surface of the flow. Observations made during the field investigation portion of this study support the hypothesis that these “clinkers” are

actually formed by autobrecciation as a function of movement of the flow and occurs on all contact surfaces including the top, base and sides of the flow. This theory along with a detailed description of 'a'a and pahoehoe flows will be discussed further in Chapter 2.

The final dimensions of the flow-field also show a systematic dependence on average ground slope and duration of eruption (Kilburn & Lopes, 1991) indicating that flow-field growth is determined by the interaction of eruptive parameters. It should thus be possible to relate the growth trends to ranges of force balances or associated process ratios (Kilburn, 1996) which are features that can be investigated both theoretically and by analogue experiments.

Field observations (Lipman & Banks, 1987; Kilburn & Luongo, 1993; Solana, 2012) have shown that there are three stages of flow-field evolution, where the flow can be divided up into proximal, medial and distal sections. The proximal section refers to the area of flow directly from the vent and may be relatively structureless. The medial section of the flow refers to the majority of the flow body between the vent and flow-front. This section is characterised by an increase in flow complexity as a function of cooling, changing topography and degassing resulting in the development of secondary flows. Secondary flows can be formed through bifurcation, overflow or breaching of levees and also by thickening. Other flow structures observed in this section include levees, tubes, hornitos, benches and overflows (Sparks et al., 1976; Dragoni et al., 1986; Guest et al., 1987; Griffiths & Fink, 1993; Griffiths, 2000; Allard et al., 2006; Favalli et al., 2010).

The final section called the distal portion of the flow-field is characterised by a cooled front and the formation of frontal lobes. The front will continue to advance until the crust has developed a yield strength greater than the force of the

fluid lava behind it. As discussed above, pahoehoe lavas advance in a series of toey lobes forming a network of interconnecting flows and lava pathways, some of which become stagnant immediately after extrusion and some of which remain active allowing still molten lava to reach the flow-front, advancing the flow-field further. ‘A’a lavas generally advance as a single unit with no part of the flow-front reaching significant distances from the other. Although pahoehoe lavas typically move more slowly that ‘a’a, they more commonly form tubes which insulate the lava as it moves downslope, allowing it to keep flowing for longer. In contrast, the open ‘a’a channels, with their constantly fracturing crust are subjected to greater heat loss.

Pahoehoe and ‘a’a lavas do not occur in isolation from each other with a rigid set of characteristics. Flows in the 1974 and 1823 pahoehoe flows from Kilauea, Hawaiian Islands were observed to be bounded by parallel zones of ‘a’a material (Soule et al., 2004). It is common to find that as a lava flow moves downslope, the surface characteristics change from pahoehoe to ‘a’a. This is indicative that chemical composition is not a controlling factor in flow morphology however chemical composition may influence the distance of the transition.. As flows are classified by their surface morphology, a result of the formation of solidified crust, cooling history must be a controlling parameter.

Both pahoehoe and ‘a’a flows develop solidified margins that act as boundaries to the flow, defining its width and orientation. In the early stages of eruption, flows may not develop lava levees. The maximum length of the flow-field is usually achieved in the first days of the eruption. Subsequent growth occurs laterally through the formation of secondary flows. This process develops when solidification of material at the flow-front and edges results in the generation of a

solid crust that retards the forward movement of the flow, resulting in the accumulation of still molten, flowing material up-flow. As the volume of lava swells, the levees constraining the flow are subject to increasing stress. If the stress being exerted on the levees is greater than their shear strength, the levee may fail, resulting in the formation of a secondary lava flow. If the levee does not fail, it may be overtopped as the volume of material exceeds its carrying capacity of the flow (Kilburn & Lopes, 1991).

The same mechanism for secondary flow formation through levee collapse or overtopping can take place when the effusion rate and therefore the volume of lava in the channel increases and exceeds either the carrying capacity of the channel, resulting in an overflow, or the yield strength of a levee, leading to levee collapse. This process can also result in reactivation of flow-front. Bailey et al., (2006) make a distinction between pluses and surges as forms of increased effusion rate. Surges occur when the channel becomes blocked by debris, resulting in lava pooling behind the blockage, increasing the stress on the levees. The force exerted by the dammed lava may eventually either clear the blockage or break through the levee, resulting in a short lived increase in effusion rate until the excess lava has either drained off through a newly formed flow or cleared the blockage and moved downstream.

In comparison, pulses are genuine increases in effusion rate generated by vent processes that can be tracked from a vent down flow. The sudden increase in volume of material can result in either levee overtopping or collapse and the formation of a secondary flow. These processes result in the development of compound flow-fields (Kilburn & Lopes, 1991). During long-lived eruptions (<14 days) the lateral growth of an entire flow-field may represent as great a hazard as

the lengths of individual flows, as illustrated during the 1669 Etna eruption, when outbreaks generated the flows affecting the city of Catania (Crisci et al., 2003) or in the 1706 eruption in Tenerife in which flows from outbreaks destroyed the city of Garachico (Solana & Aparicio, 1999).

1.1 Rationale

The principle aim of researchers studying lava flow behaviour is to gain an understanding of the parameters affecting flow-field propagation and to turn that understanding into a robust, reliable model for predicting the maximum spatial extension of a flow-field and a timeline for emplacement. This research has important implications in the field of lava hazard management as the effectiveness of hazard mitigation plans will be limited by our lack of understanding of flow behaviour. Lava flows are the most common of all volcanic hazards and their slow rate of advance (<1 km/ph. to 10 km/ph.) means that there is usually sufficient time to put in place hazard mitigation plans. Effusion rates, rheology, topography and cooling rates are all important parameters in affecting flow behaviour however, when assessing lava flow hazards, the entire system must be taken into consideration, not just the behaviour of individual flows (Kilburn & Lopes, 1988, 1991; Bailey et al., 2006).

In the past, attempts have been made to artificially manage the path of a flow, diverting lava to a more preferred orientation, away from buildings and towns by manipulation of flow orientation such as forcing flows to form new paths by blasting levees or constraining the flow using dams, barriers and walls (Stevens et al., 1997; Barberi et al., 2003; Behncke & Neri, 2003). Other methods include increasing the rate of crust formation by spraying the flow-front with water in the

hopes of halting its advance (Sheets & Grayson, 1979). However until we fully understand the processes involved in compound flow-field development, these methods of lava hazard management will meet with limited success.

Lava flows are one of the few active volcanic phenomena that can be studied at close quarters; however, direct observations of flow-field growth are limited to parts of the eruptions that are accessible and visible on the surface. If the flow-field is sufficiently large it would be impossible for one researcher or even a team of researchers observe all of its processes. Structures and breaches form only to be covered by subsequent flows. Older, channelized systems can be used as laboratories infer flow-field evolution. This is especially true of older flows that have been exposed through road cuts or some other mechanical process. These sections can give a three dimensional view through a flow-field where, for example, on Mount Etna a road has been cut laterally through the 1983 flow in a number of places. These cuts allow us to see the internal structure of a channel, not just the surface features and because the cuts are laterally through the flow-field, the relationship of each flow to the one next to it can be seen. Such observations of older inactive flows are invaluable to our understanding of how an active flow behaves. However, these "windows" into the internal morphology of a flow are not always available and where they are, their locations is dependent on civil authorities and private landowners and their needs, not on the wishes of researchers. This combined with the limitations of viewing an active eruption mean that research into lava flow processes cannot be carried out through field work alone (Mader et al., 2004).

For this reason, models, both analytical and analogue, have been developed to investigate how various parameters such as topography, effusion rate, cooling

and lava composition affect flow behaviour. More recently developments in LIDAR (light detection and ranging) technology have assisted in more accurate volumetric mapping of extant flow-fields (Favalli et al., 2010; Tarquini et al., 2012 which in turn have improved the input of data into lava flow models.

Various analytical models have been proposed to simulate lava flows; some models use a deterministic approach (Ishihara et al., 1989; Dragoni & Tallarico, 1996; Anderson et al., 1999; Dragoni et al., 2002; Zhu et al., 2003; Quareni et al., 2004; Damiani et al., 2006) and others probabilistic (Barberi et al., 1993; Felpeto et al., 2001; Del Negro et al., 2013). More recently, cellular automata have been used to predict lava flow paths (Crisci, et al., 2003; Crisci et al., 2004; Avolio et al., 2006; Avolio et al., 2008; Vicari et al., 2011; Ganci et al., 2012).

Deterministic models in general incorporate more complex numerical simulations which are capable of dealing with many parameters simultaneously (Papadopoulos, 1990; Wadge et al., 1994; Gómez-Fernández, 2000; Rongo et al., 2008). These models use data from past eruptions to simulate future flows. This approach has limited use in hazard assessment as it depends on detailed information on numerous parameters such as effusion rate, volume, temperature, viscosity, topography, tube formation, vent location etc. These parameters are difficult to predict and vary with each eruption. These data are also not always available and a miscalculation of any single variable will generate false results. This method has more uses in reconstructing past eruptions than in hazard assessment.

Probabilistic models also use data from past eruptions in order to predict the morphology of future flows. Due to the complex interactions between flow parameters, many probabilistic models simplify flow behaviour using approximations of just a few parameters based on past flow behaviour such as

volume, viscosity and effusion rate in conjunction with topographic data to determine the probability of a specific area being in the path of a lava flow, originating in a certain area under a certain set of eruption criteria. The most recent model proposed for Etnean lavas developed by (Damiani et al., 2006) incorporates data on lava flow height, length, emission point and DEM data. As a result of the simplification of the parameters, subtleties in flow behaviour are not accounted for which means there is a large margin of error in the modelling of flow paths which could render the predictions false.

The third method of flow path prediction is based on the use of cellular automata. Cellular automata are used to model systems where the global evolution of the system may be described on the basis of local interactions of their constituent parts (Avolio, et al., 2008). The method has only recently been applied to model lava flows and has been used in many different fields previously including urban planning studies and industrial applications.

This method has been applied to Etnean lavas in the form of the SCIARA model (Crisci et al., 2003 & 2004; Avolio et al., 2006). The SCIARA model – Simulation by Cellular Automata of the Rheology of Etnean lava flows – was first used by (Barca et al., 1993). Since that time, the model has been modified and refined by several research groups (Barca et al., 1994; Crisci, et al., 2003; Avolio, et al., 2006).

The model incorporates cells of a uniform size. Each cell is embedded with a finite automaton which describes the value of properties of the portion of space corresponding to the cell such as topography, temperature and flow height. The finite automaton of each cell is linked to the finite automaton of the neighbouring

cells. The condition of each cell is therefore dependent on the state of its adjacent cells.

The model was used with some success during the 2001 Etnean eruption. Measurements of flow velocity, viscosity and vent location were used to predict the flow path of the lava. Some of the hypothesized scenarios were validated by the final flow morphology (Crisci et al., 2004). Although the SCIARA model has been validated by the 2001 eruption, the model uses simplified values for the initial constraints. This means that it is impossible to use the model to understand the full complexity of a lava flow, which in turn means that the flow paths for an eruption cannot be designated with confidence. However, the model is a relatively new technique and is improving all the time.

MAGFLOW is a cellular automata model developed by the INGV and has been successfully used to recreate lava flow paths from the 2001, 2004 and 2006 eruptions on Mount Etna (Ganci et al., 2012) and also to create lava inundation hazard maps (Del Negro et al., 2013). More recently, the MAGFLOW model has been integrated with HOTSAT (a system for recording infrared data) with a web based GIS system to create LAV@HAZARD (Vicari et al., 2011a; Vicari et al., 2011b; Ganci et al., 2012), a real time lava flow hazard assessment tool. The tool was employed during the 2008-2009 Etna eruption. The final dimensions of the flow-field correlated very well with those predicted by the LAV@HAZARD model. This model represents a shift from models being used to recreate extant lava flows to real time hazard assessment which could be utilised by civil protection and local authorities during an eruption.

Analogue models are simplifications of nature (Koyi, 1997) allowing each stage of flow-field growth to be documented in detail. Parameters can be varied

systematically and the resultant flow-field morphologies compared and measured at every stage making them an ideal tool to further our understanding of flow dynamics and structures.

In the case of analogue models of lava flows, a variety of materials have been used but are commonly waxes or other materials with a temperature dependent viscosity (Fink & Griffiths, 1990; Griffiths & Fink, 1993; Gregg & Fink, 1995, 2000; Rossetti et al., 1999; Miyamoto et al., 2001; Soule & Cashman, 2004). Many studies have used analogue models to investigate the effects of variations in effusion rate (Huppert et al., 1982; Fink & Griffiths, 1990; Blake & Bruno, 2000), angle of slope (Gregg & Fink, 2000) viscosity (Bagdassarov & Pinkerton, 2004) have on flow morphology in order to determine the conditions necessary for the formation of flow structures such as domes, tubes, lobes and levees.

Although computational models have had success in modelling the effect of variations in effusion parameters on flow-field lengths and morphology none have been able to replicate the formation and collapse of lava levees and the role they play in the formation of secondary flows, enabling the lateral growth of flow-fields. In contrast, analogue models have consistently been able to replicate the formation of tubes, domes, levees, lobes and other flow structures essential to understanding flow-field growth.

While direct comparisons should never be drawn between an analogue model and the natural system, the purpose of an analogue model is to facilitate our understanding of big scale natural processes by drawing comparisons between what is observed in the field and reproduced in the lab while providing an accessible view and measurements to those internal process which are hidden in the field.

Despite the evidence provided by laboratory models and field observations on the importance of levee formation and collapse as a mechanism of flow-field propagation, there have been very few studies that have investigated the mechanical properties of lava levees to gain some understanding of the conditions under which they will fail (Sparks et al., 1976). The majority of work has been carried out on massive basaltic cores both from the point of view of their general properties (Ryan & Sammis, 1981) or applying data on both brittle and ductile failure of volcanic rocks and fracture maps to illustrate the interactions between stress, strain rate and temperature in lava flows (Rocchi et al., 2003, 2004). However, given the different emplacement, stress regimes and cooling histories of levees as opposed to flow units, the same deformation and failure behaviours cannot be assumed. Temperatures of 400-600 ºC were reported for the solidified walls of newly formed lava tubes during the 1991-1993 eruption of Mount Etna (Barberi et al., 1993) and field observations made in exposed sections through the 1983 flow on Mount Etna have shown the presence of micro-fractures, not observed in the lava flows which may affect the yield strength of the levee. Therefore investigation into the strength of levee material is a necessary part of any investigation into the growth of flow-fields through levee formation and collapse.

Although it is always preferable to carry out experiments with natural materials in analogous environments, it is not always feasible when dealing with high temperature or high pressure conditions (Mader et al., 2004). Experiments carried out at temperatures of 800^{o}C have shown that the strength and elasticity of the rock is only weakly temperature dependant between ambient room temperature and 800^{o}C (Rocchi et al., 2003). Therefore testing levee material at room temperature should yield the same results as a high temperature environment.

This study, combines datasets from field observations, rock strength tests and analogue modelling to perform in-depth analysis on lava flow behaviour that is unique in its multi-disciplinary approach. The results of the investigation can be used to support lava hazard management techniques and mitigation plans by identifying the locations and conditions under which there is a high probability of the formation or collapse of levees given the eruption parameters.

1.2 Aims and Objectives

The issues discussed previously illustrate the incomplete understanding of the complex interactions involved in compound flow emplacement and the role that the formation and collapse of levees plays in flow-field growth. As it is not always possible or feasible to study flow dynamics in situ, this project aims to improve the understanding of flow behaviour through combining the results of an analogue model with strength analysis of levees and observations from inactive flows. With that in mind the objectives of this study are:

1. To investigate the significance of levee failure and/or overtopping through field investigation of inactive flows and analogue modelling.
2. To design and build an analogue model utilizing paraffin wax capable of reproducing some of the processes and structures involved in flow-field growth and levee breaching.
3. To determine where and at what stage of eruption, breaches and overflows occur within flow-fields, with particular focus on underlying slope, levee morphology and channel orientation.
4. To measure and compare the mechanical properties of cores taken from the main types of levees at differing orientations of applied stress.

5. To produce guidelines on the conditions under which levees are more susceptible to failure or overtopping in order to support emergency services operations such as planning protection barriers or diversions.

1.2.1 Hypotheses to be Tested

In designing and defining the parameters of this study a number of hypotheses were identified:

1. *The relevance of levee failure in enlarging lava flow-fields.* Field and laboratory studies aim to prove that levee breaching is a key process controlling the second stage of growth of 'a'a lava flow-fields.
2. *External factors influencing levee failure.* Preliminary studies (Nolan, 2006) seem to indicate that morphological factors such as underlying slope or curvature of a levee influence the location in a channel where levee failure occurs. Field and desktop studies will identify the trends in slope changes and angles of curvature where levee failure occurs.
3. *Influence of internal macro-structures on levee failure.* The internal structure of levees (e.g. massive, layered, and rubbley) is representative of different emplacement, evolution and cooling histories. The susceptibility of each levee morphology to breaching will be investigated in the field in order to identify which type has shown to be more vulnerable to failure.
4. *Mechanisms of levee failure.* Levee failure is a fact that has been reported by multitude of authors e.g. (Sparks et al., 1976; Guest et al., 1987; Pinkerton & Wilson, 1994; Kilburn, 1996; Polacci & Papale, 1997; Rossi, 1997; Clague et al., 2000; Griffiths, 2000; Favalli et al., 2010). As laboratory studies on the strength of cores of basaltic rocks show, for levees

to be breached, they must be weaker than the rocks that form them. This study aims to investigate the influence the direction of loading (oblique, perpendicular or parallel to flow direction) has on levee strength.

2 Lava Flows and Structures

Lava flows are the most common product of volcanoes on Earth and cover 70% of the earth surface (Kilburn, 2000). Although they have many beneficial uses such as providing material for buildings or weathering to fertile soil, they pose a threat to human lives and infrastructure during emplacement. Lava flow dynamics and therefore emplacement behaviour such as the rate of advance, duration and overall flow-field dimensions (length, width, volume) are dependent on the complex interactions of a number of parameters, interactions which are not well constrained (Griffiths, 2000; Sakimoto & Gregg, 2001). This chapter will discuss lava flow dynamics and the primary parameters involved in flow behaviour including the development of lava flow-fields.

2.1 Introduction

Despite the complexity of lava flow dynamics, the evolution of a flow-field follows only a few distinct trends (Kilburn & Guest, 1993; Kilburn, 1996). Understanding these trends began with defining classifications for the different types of flow-field observed.

Nichols (1936) first defined flow units as “a tongue shaped structure within a flow” which indicated complexity within flow emplacement and that flows did not necessarily move as a single unit. The concept of a flow unit has since been refined (Walker, 1971; Hulme, 1974; Kilburn, 1981, 1996; Kilburn & Lopes, 1991; Kilburn & Guest, 1993) and is an accepted feature of flow emplacement. Walker, (1971) built further on Nichols study by proposing the term “compound lava” for lavas which can be separated into more than one flow unit with each consisting of a

discrete unit with a chilled top which had cooled significantly prior to being buried by a subsequent flow unit. Walker proposed that whilst simple (flows consisting of a single flow) and compound flows occur in both 'a'a and pahoehoe flows, pahoehoe flows are mostly compound in nature with the individual flow units identifiable in cross section due to the presence of vesicles concentrated in the upper most part of each flow unit, the unit itself appearing bun-like or tabular (Figure 2.1).

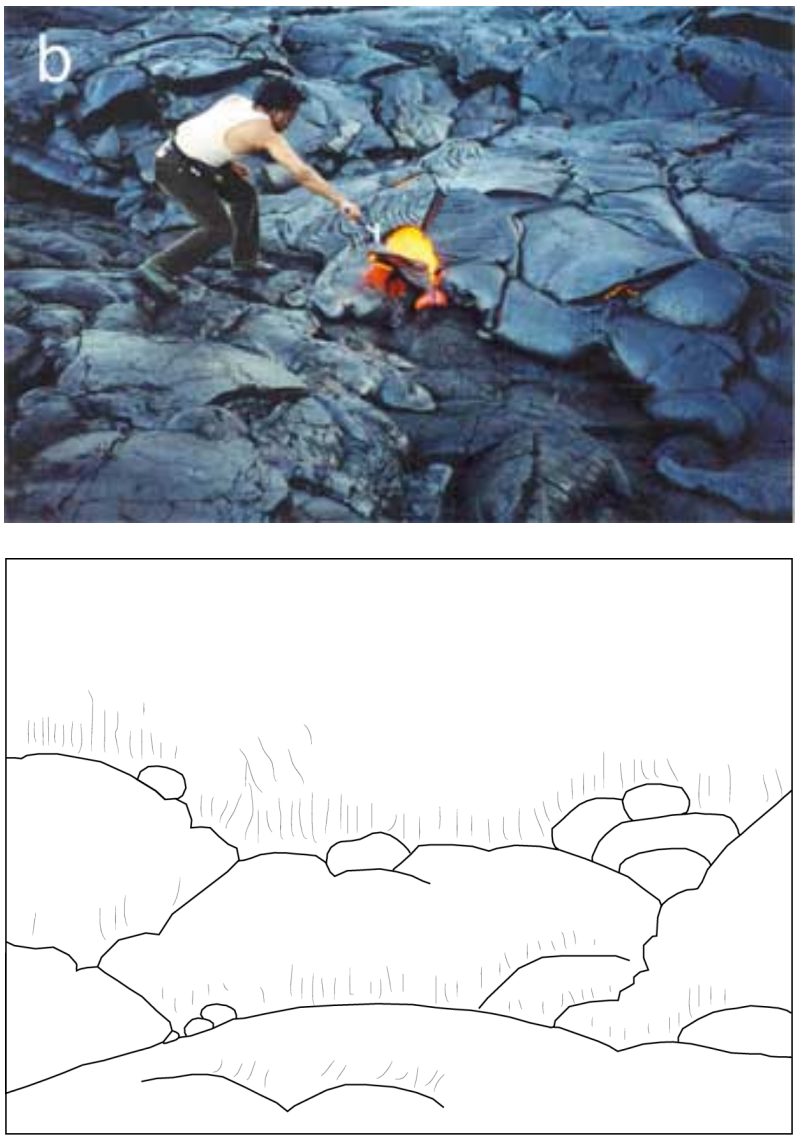

Figure 2.1 – The photograph shows a compound pahoehoe flow on Kilauea, May 2002. Image by J. Ray from www.mantleplumes.org. The bottom image is redrawn from Walker (1971) and shows a section across a compound pahoehoe basalt lava flow from the Mula Dam, part of the Deccan Traps. Pipe vesicles can be seen at the base of each unit.

'A'a flows were also described as mostly commonly compound with individual flow units more difficult to distinguish given the rubbley nature of the top and bottom of each flow unit. Each flow unit is typically tabular and between 1 and 10 m thick and consist of a massive interior with a rubbley base and top. In historical flows, compound flows from one eruptive event may be distinguished from the flows of a later event by the absence of a layer of weathering, soil or vegetation (Walker, 1971).

Walker also proposes the use of the term "multiple" to define those lavas who's individual flow units are emplaced so rapidly that there is insufficient time for cooling and the development of the rubbley layer which is normally used to distinguish between flow units. The accumulation of flows then cools to one unit where bands of vesicles can be used to identify individual flow units. These early definitions of flow unit, simple, compound and multiple flows form the basis of our understanding of the large scale morphologies of flow-fields.

2.2 Lava Flow Characterisation

2.2.1 Lava Flows

Lava flows are commonly classified by their chemical compositions. The most common lava's are silicate, characterised by ≈ 45 wt% for basalts and ≈ 60 wt% for rhyolites with typical respective eruption temperatures of 1200^{o}C and 800^{o}C (Table 2.1). Volumes from single flows can range from m^3 to km^3 and can spread out to tens of kilometres in length and reach thickness of hundreds of meters (Kilburn, 2000).

Table 2.1 – Redrawn from Kilburn (2000) showing the eruption temperatures, density and viscosities of different lava types at eruption. [1]Newtonian approximation at low shear rate.

Composition	Eruption Temperatures (°C)	Density at Eruption Temperatures (km m^{-1}) (without vesicles)	Visicosities at Eruption Temperatures (Pa s)[1]
Komatilite	> 1600?	ca. 2800	< 1?
Basalt	1050 - 1200	ca. 2600 - 2800	10^2 - 10^3
Andesite	950 - 1170	ca. 2450	10^4 - 10^7
Rhyolite	700 - 900	ca. 2200	10^9 - 10^{13}
Water at Earth Surface	20	ca. 1000	10^{-3}

When lavas are extruded onto the earth's surface, they immediately begin to cool down and solidify, losing heat to the atmosphere and the ground, forming channels which direct the flow material along a defined course. As lava moves downslope, cooling and the development of solidified crust continues until sufficient to halt the flows advance. Solidification and the development of crust is a key factor in the development of compound flow-fields and therefore overall flow-field morphology.

In addition to their chemical composition, lavas are also classified by their surface morphology. The Hawaiian terms pahoehoe and 'a'a were first used in the literature by Dutton (1884) referenced in Macdonald (1953) and are used to refer to basaltic or basaltic andesite flows. The initial classification of lavas related only to the appearance of the surface crust regardless of the internal structure of the flow. The definitions of pahoehoe and 'a'a were given as "the type of lava that in solidified form is characterised by a smooth, billowy, or ropy surface" and "the type characterised by a rough, jagged, spinose and generally clinkery surface" respectively. These definitions have not changed since their first use, however the terms have evolved to not only describe the surface of a flow but the internal structure also. MacDonald (1953) uses Hawaiian examples to illustrate how these classifications can be applied using the internal structures of a flow, demonstrating

that the surface features of the flow are an indicator of the flow emplacement mechanisms and the dynamics of the flow interior.

2.2.1.1 Pahoehoe Lava

Pahoehoe flows typically form compound flow-fields with individual flow units varying size from 50 cm to 5 m and having a characteristic smooth or ropy texture (Figure 2.2 & 2.3). The ropey textures of a pahoehoe flow surface are indicative of the crust slowing down due to cooling, whilst the hotter more fluid lava underneath continues to flow at a faster pace, pushing and compressing the crust above it. Although popularly it is thought that pahoehoe is emplaced more quickly than 'a'a flows, the reverse is actually true with pahoehoe moving up to 10 times more slowly than an 'a'a flow. This is illustrated by the presence of a continuous layer of crust, commonly seen throughout the length of a pahoehoe flow, indicative of the low imposed surface pressure caused by the slow rate of emplacement. Commonly, this continuous layer of surface crust can thicken forming tubes. MacDonald (1953) describes two principal characteristics of the internal structure of pahoehoe flows being the presence of lava tubes and the occurrence of regular spheroidal vesicles. Tubes form very close to the vent and are the principal arteries of the flow. Due to the insulating properties of the tube, pahoehoe emplacement can be much faster through these feeder tubes, facilitating flow advance, meaning that although pahoehoe flows are slower than 'a'a flows, they often reach greater distances. Flow advance can occur in one of two ways, the first mechanism – a rolling motion where the upper part of the flow moves more quickly than the lower part, causing the front to roll over and be buried by the lava coming behind it, is characteristic of fast moving flows, typical of high effusion

rate, single front flows called sheet pahoehoe. The second and more common mode of advance is found in flows with multiple active fronts, each fed by a tube causing the flow to advance in a series of protrusions from the flow-front called lobes. These lobes are only active for a short time before cooling halts their advance. The flow advances by breaking through the chilled crust of the lobes and forming a new protrusion. As cooling becomes the predominant control on flow behaviour, the entire flow-front can halt, with growth restricted to inflation of lobes as any flow material still moving is emplaced underneath the solidified crust of the lobes, resulting in thickening.

Figure 2.2 – Section of pahoehoe flow near the town of Stazzo in Sicily showing the typical smooth ropy texture.

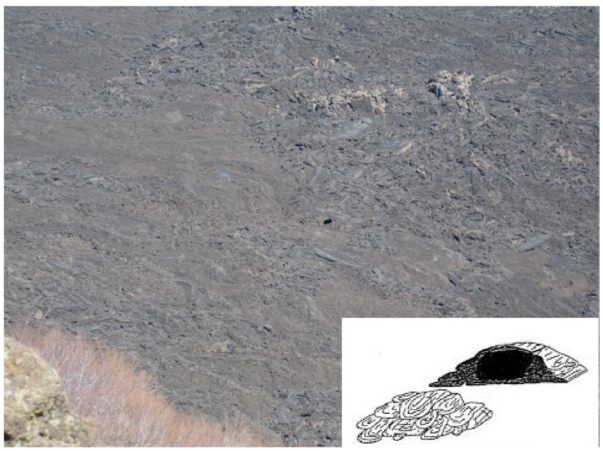

Figure 2.3 – View into the Valle del Bove on Mount Etna showing a section of a pahoehoe flow. Inset from Kilburn (2000) shows a schematic of a pahoehoe flow-front made up of intermingling tongues and toes of lava.

2.2.1.2 'A'a Lava

'A'a flows are typically more viscous than pahoehoe flows and are emplaced more rapidly, up to hundreds of meters a day. MacDonald (1953) defines 'a'a lava as characterised by an exceedingly rough, jagged or spinose surface, the majority of which is covered with loose fragmental material known as "clinker" or flow breccia. The thickness of the clinker layer can be a few cm to 1 m (Figure 2.4).

Underneath the layer of clinker material, 'a'a flows have a homogenous massive interior grading into a basal layer of clinker. The massive section of an 'a'a flow is often less vesicular than that of a pahoehoe flow with vesicularities typically below 30% compared to 50% for pahoehoe flows (Macdonald, 1953). The vesicles can often appear irregular, distorted and elongate in the direction of flow.

Jaggar (1930) noted that the clinker layer is not loose material but that it is connected with the massive flow interior. This is an early observation of what has now become known as autobrecciation. As lava cools, the mode of advance changes from ductile deformation to brittle failure, becoming dependent on the autobrecciation to move, a process which is indicative of mode of advance of an 'a'a flow (Kilburn, 1996, 2004). 'A'a flows are commonly compound and consist of a network of open channels bordered on each side by fields of clinkery 'a'a material up to 800 m wide and show simple evolutionary trends.

'A'a flows typically advance as a single flow-front that, due to cooling, develops over time from a fluid sheet to a near solidified front which moves through a combination of fracture and flow. Solidification at the flow-front causes fronts to thicken over time and the final thickness can be up to ten times that of the main flow.

Flow-fronts can be inclined at angles of up to 35^{o} – 45^{o} degrees. The backwards sloping profile of the front is a result of the top section of the flow moving more slowly than the underlying sections. The resulting instability results in material breaking off and tumbling down the flow-front, forming part of a talus bank of fragmented material that forms against the base of the flow-front MacDonald (1953).

Breaches and overflows are common in these types of channels as thickening at the flow-front moves back up channel, exerting pressure on the levees which define a flow's margins. This mechanism will be explored in more depth in Section 2.5.7 & 2.5.8. Breaches and overflows can result in the formation of a new flow which itself may undergo a cycle of cooling, thickening and breaching forming subsequent flows and in this way a single eruption can result in a compound flow-field.

Figure 2.4 – 'A'a flow-field in the 2001 flow-field on Mount Etna displaying the characteristic rubbley texture.

2.2.1.3 Pahoehoe to 'A'a Transition

Pahoehoe and 'a'a are part of a spectrum of lava types, both are often present in the same flow (Solana et al., 2004) and are chemically identical to each other and therefore differ only in their physical forms.

The surface structure of the flow depends on the rheological resistance to motion by the crust and the stresses to which is subjected (Kilburn, 1990). As previously stated, pahoehoe is characterised by a smooth or ropy continuous crust, in order to transition to 'a'a, that crust must become fractured. The energy needed to break the surface of a flow must be greater than its critical value which is a measure of how quickly a crack in surface crust can heal due to cooling. If the critical value is exceeded then cracks will form in the crust faster than cooling can repair them.

At the start of an eruption, the rate of energy supplied is too weak to exceed the critical value of the solidified crust, resulting in a pahoehoe flow. As the flow moves downslope, the energy supplied mostly by gravity increases and eventually become sufficient to overcome the critical value allowing fractures to propagate, resulting in the formation of 'a'a flow (Figure 2.5). The transition from pahoehoe to 'a'a crust has been observed in many flows with differing rates of shear acting on the crust and yet the same mechanism is observed meaning that the transition is instigated not only by effusion rate but possibly a combination of lowering effusion rate, cooling and escape of volatiles.

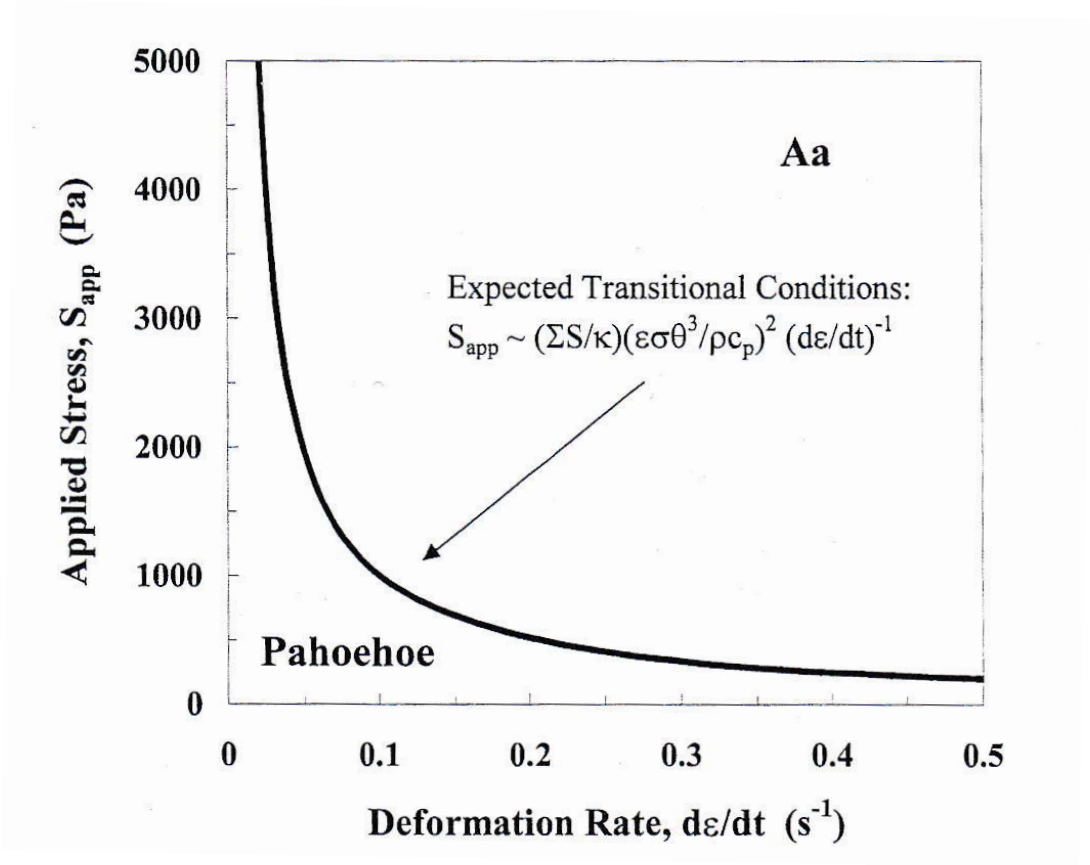

Figure 2.5 – The transitions from pahoehoe to 'a'a crust is dependent on the rate at which energy is supplied to deform the crust. Once the rate of energy supplied exceeds the critical energy flux, the crust experiences persistent fracturing which cannot be healed by cooling of the exposed surface marking the transition to 'a'a flow. From Kilburn (2000).

The reverse gradation from 'a'a to pahoehoe has never been observed and is thought to be impossible indicating that 'a'a is a more evolved state (Kilburn, 1981). Where the occurrence of pahoehoe at distances from the vent in a typically 'a'a section of the flow has been reported, it is thought to be due to the presence of boccas or tubes carrying proximal vent material to distal segments of the flow.

2.3 Flow-Field Development

Of the different types of lava flow, 'a'a lavas have posed the most frequent threat to human activity in historic times (Kilburn, 1996). Therefore it is vital to lava hazard management to understand flow-field emplacement so that the limited

resources available for hazard management can be deployed in the most efficient and effective way possible.

Flow-fields can be defined as one or more discrete flows, moving downslope under gravity, which originate from a single vent during an eruption. Although there is a great degree of variability in emplacement conditions, the flow regime within channelized basaltic lava flows is known to change over timescales of days, minutes and hours (Wadge, 1981; Lipman and Banks, 1987; Rossi, 1997; Harris et al., 2000; Lautze et al., 2004), 'a'a flow-fields form along only a few distinct trends and can be grouped into 2 main types – relatively narrow flow-fields for short lived eruptions with just a few arterial flows and wider flow-fields with several arterial flows typically associated with longer lived eruptions (Kilburn, 2000).

In general terms, flow emplacement can be broken down into three stages: Stage One – Lengthening, Stage Two – Widening and Stage Three – Thickening (Kilburn and Lopes, 1989).

Flow-fields can also be further divided into three sections based on their morphologies and distances from the vent. The proximal section of the flow is defined as the section close to and containing the vent. This section of the flow-field is the narrowest and is characterised by simple flow morphologies. The medial section of the flow-field is often the widest section of the flow and is characterised by the development of secondary flows and the occurrence of breaches and overflows. The distal section of the flow refers to the flow-front and the areas immediately behind it. These classifications also represent the sections of the flow-field that are active during the three stages of flow-field emplacement (Figure 2.6).

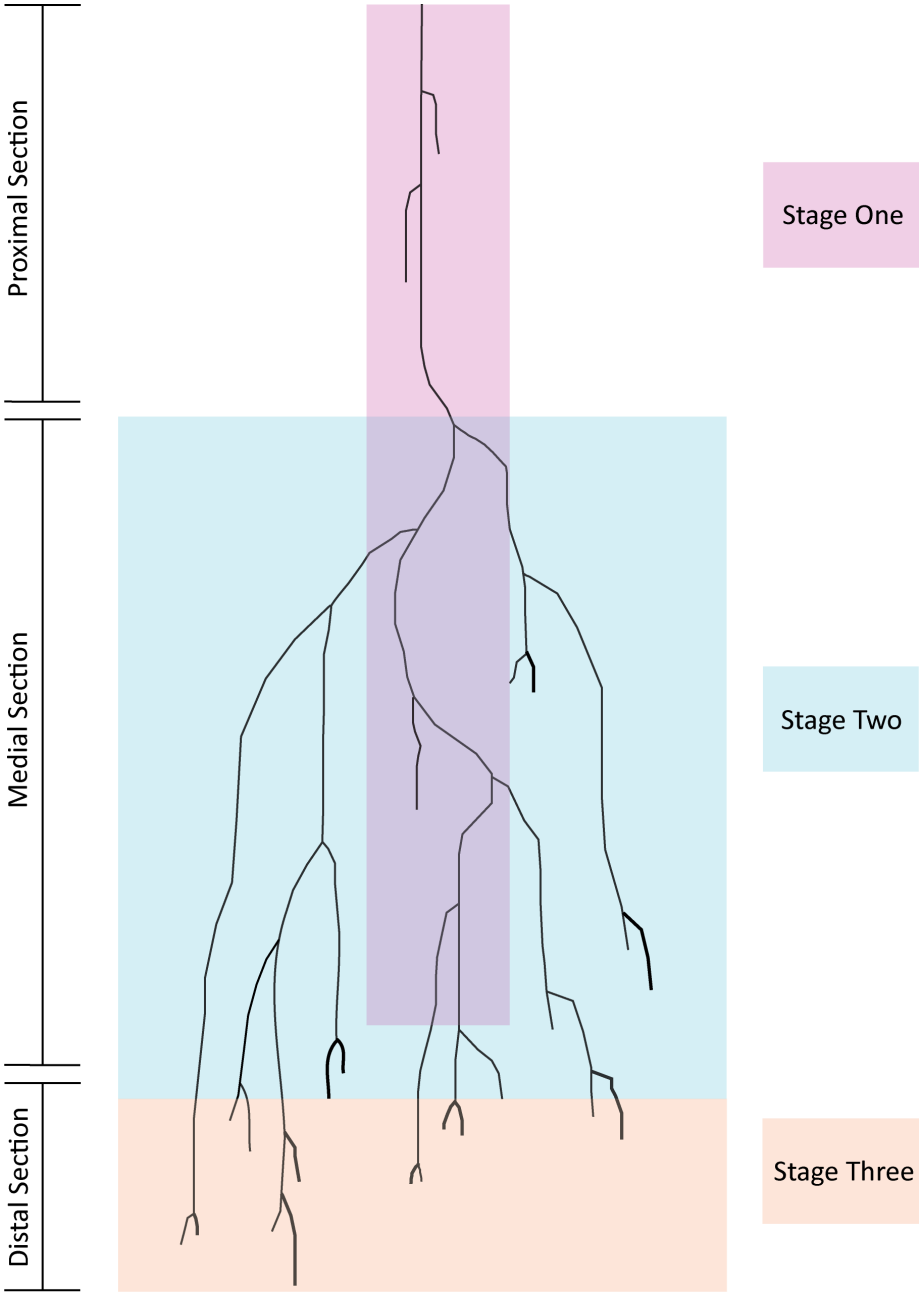

Figure 2.6 – Generalised schematic of flow-field development showing the three stages of flow emplacement.

2.3.1 Stage One – Lengthening

'A'a flow-fields typically reach 50% of their total lengths within the first 24 hours of effusion (Kilburn & Guest, 1993). Initially, lava flows are restricted to a few or even one preferred orientation, commonly following the steepest angle of slope; immediately upon effusion, lava begins to cool down, forming surface crust

and solidified flow margins called initial levees. Levees are formed in the wake of the flow-front as it moves downstream and define the flows orientation and width. As spreading is restricted to the flow-front, flow width becomes defined very close to the vent in the proximal section of the flow (Kilburn & Lopes, 1988, 1991).

The initial flows continue to lengthen until either effusion stops, the discharge rate drops sufficiently for cooling to become dominant, or the flow is inhibited by the development of solidified crust, i.e. when strength of the front is sufficient of overcome the mechanical energy of the flow behind it (Kilburn & Lopes, 1991). As cooling continues and crust develops, the flow moves from an effusion rate controlled to a cooling controlled regime.

2.3.2 Stage Two – Widening

The second stage of flow emplacement is characterised by widening through the generation of secondary flows by overflow and breaches.

Breaching is the term used to denote rupture of the channel levees, margin or the stationary flow-front and the formation of secondary flows through that rupture. Compound flow-fields result from the formation of secondary flows either through this process or bifurcation around an obstacle, for example a topographic high.

Breaching and overflow are cooling dependent events and therefore cooling is considered a key factor in the formation of a multi-flow system (Kilburn & Lopes, 1988, 1991; Borgia & Linneman, 1990). Cooling results in the growth of surface crust which retards the forward movement of the flow-front causing the flow to thicken. The rate of emplacement of the still fluid material behind the flow-front is faster than the rate of advance of the flow-front causing a build-up of

material behind the front causing it to thicken. Thickening moves back up-channel from the flow-front exerting pressure on the levees. In this manner, inflation or thickening of the flow can result in a breakout, either breaching or overflowing the levees as the volume of material overcomes the carrying capacity of the channel. Breaches of the flow-front which occur as frontal boccas provide evidence of cooling, which along with growth of surface crust are the controlling parameters of the halt of the flow-front (Kilburn & Guest, 1993). Thickening can also occur due to an obstacle, such as part of a levee breaking off and blocking the channel or from the inward growth of levees, decreasing the width of the channel.

Breakouts can result in the formation of a new arterial flow thus widening the overall flow-field. Overall flow-field morphology is defined by these main arterial flows, with short lived flows emplaced between the main flows producing little alteration to the overall flow-field dimensions. The primary result of the formation of new arterial flows is flow-field widening not lengthening as the secondary flows rarely exceed the length of the initial flow significantly (Solana, 2012). Therefore the development of surface crust through cooling is key to flow-field widening.

2.3.3 Stage Three - Thickening

Stage three of flow emplacement is characterised by thickening. Although thickening was instrumental in the development of flow-field width as described in stage two, thickening here refers to the final stages of effusion where the majority of channel margins and flow-fronts have cooled and become completely static. The rate of emplacement of new material is insufficient to break though the solidified crust or levees to form a breach. Any still fluid lava in the flow interior is emplaced

beneath the solidified crust causing it to inflate (Figure 2.7). This stage rarely contributes any growth to the width or length of the flow-field (Kilburn & Lopes, 1988).

Figure 2.7 – Close up of a flow-front in the 2001 flow-field on Mount Etna showing the steep flow-fronts.

The stages described above are commonly seen in the development of 'a'a flow-fields and show that the factors controlling flow emplacement change throughout the duration of eruption with effects of cooling becoming more predominant with time. The final morphology of a flow-field may be the result of multiple cycles of the stages described above as effusion rates at the vent fluctuate.

2.4 Factors Controlling Flow Dynamics and Morphology

The parameters affecting lava flow emplacement and resulting flow-field morphologies are numerous and the interactions between them are complex and not fully understood. In terms of hazard management the most important considerations

are the rate of emplacement and the overall flow-field dimensions – width and length. Previous studies have shown encouraging results for certain empirical analysis for relationships such as effusion rate and length (Walker et al., 1973; Booth et al., 1975; Wadge, 1978; Lopes & Guest, 1982; Kilburn & Guest, 1993), volume and length (Malin, 1980; Lopes & Guest, 1982) and angle of slope and flow width / speed of emplacement (Guest et al., 1987; Calvari & Pinkerton, 1998).

However, these studies show best results when applied to single flow systems using constants derived from a specific flow or set of flows and therefore their usefulness in application to future events is limited. However, the fact that any correlation exists and also that despite endless variations in flow parameters, 'a'a flows show a systematic evolution into a just a few distinct trends proves that there are measurable relationships between flow parameters and morphology. Improved methodologies for mapping lava activities such as LIDAR or ALTM (airborne laser altimeter) have provided detailed data on flow morphology over time, improving our understand of lava flow evolution (Mazzarini et al., 2005).

2.4.1 Effects of Slope on Flow Emplacement and Morphology

Slope has long being recognised as an important factor in flow-field emplacement. Studies have tried to not only correlate slope and flow length (Fink & Griffiths, 1992; Gregg & Fink, 2000; Griffiths, 2000; Kilburn, 2000), but also flow width (Guest et al., 1987; Polacci & Papale, 1997; Calvari & Pinkerton, 1998; Bailey et al., 2006; Nolan, 2006).

Changes in slope have number of different effects on flow morphology. On steeper slopes, flows are narrower with higher levees. As the slope becomes shallower, emplacement rates decrease and flows widen and can become braided

(Polacci & Papale, 1997; Calvari & Pinkerton, 1998; Bailey et al., 2006). Decreasing slopes also cause the flows to thicken as the flow-fronts slow down causing the more fluid, faster moving lava to build up behind the flow-front (Digby & Murrell, 1976; Guest et al., 1987; Kilburn & Guest, 1993).

The primary result of decreasing slope is increasing the width of the flow-field (Figure 2.8). Individual flows widen as flow-fronts spread out on shallow slopes, however the most significant increases in width stem from the creation secondary flows which can occur as a result of both increasing and decreasing slopes.

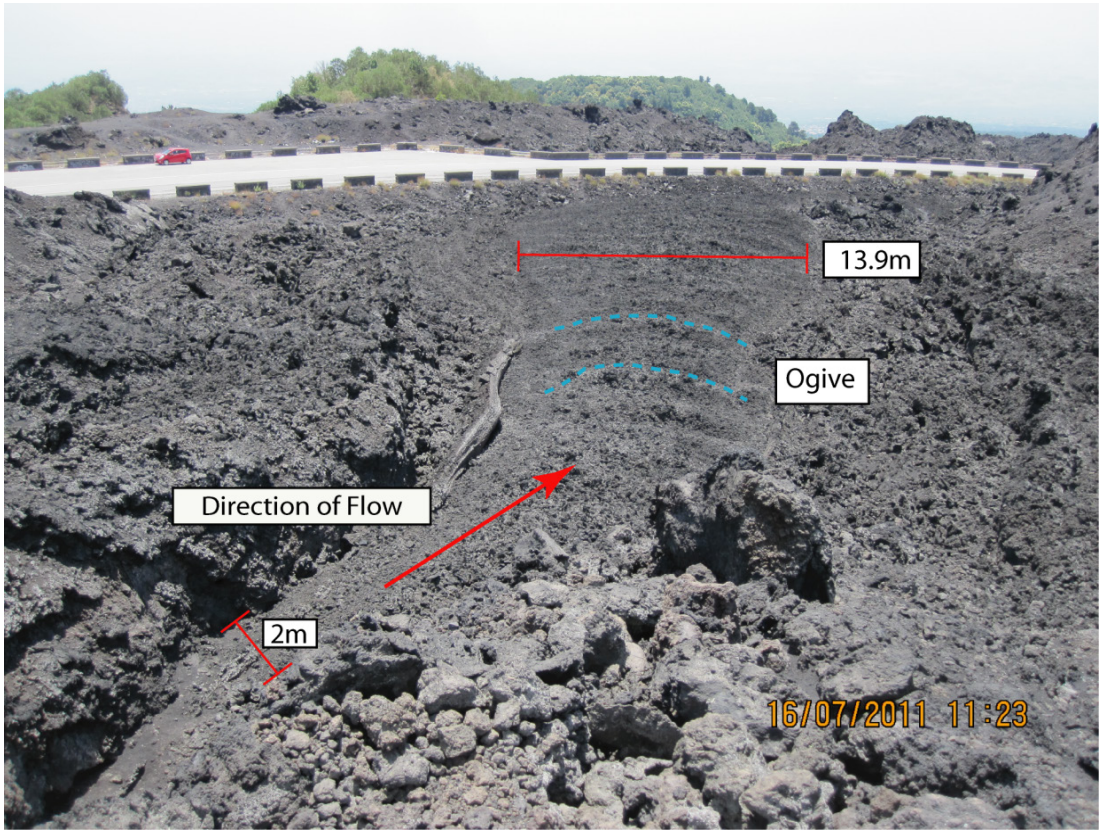

Figure 2.8 – Lava flow in the 1983 flow-field on Mount Etna. This picture was taken from the top of a lava fall where the flow falls over a small (7 m) cliff. The flow can be seen spreading out from the base of the fall. The flow measures 13.9 m in width where it reaches the road. Slope change is from 8^{o} to 5^{o}.

On decreasing slopes, flow thickening can overcome the retaining force of the levees bounding the channel in the form of breakouts or breaches. Breakouts in

the form of overflows or short lived breaches in levees do not result in the creation of new arterial flows and may only increase flow-field width locally by a matter of meters. However, if a breakout occurs of sufficient energy to become an established breach, new arterial flows can be created. This can occur in a cyclic manner with each secondary flow succumbing to breaching and the formation of new flow as long lava supply continues.

Increasing slopes can also cause flow-field widening due breakouts or breaching. As a flow moves over an area of increased slope, the channel margins narrow, resulting in less accommodation space for the volume of material in the channel causing inflation which may overtop the levees resulting in an overflow (Guest et al., 1987). Obstacles within the channel such as rafts of solidified crust or broken-off sections of levee may become wedged in the narrower channel causing a blockage which in turn causes inflation. The force of flowing lava building up behind the obstacle may become sufficient to remove the blockage, if not the pressure may be relieved by overflowing or breaching of the levees behind the blockage and the formation of secondary flows (Figure 2.9).

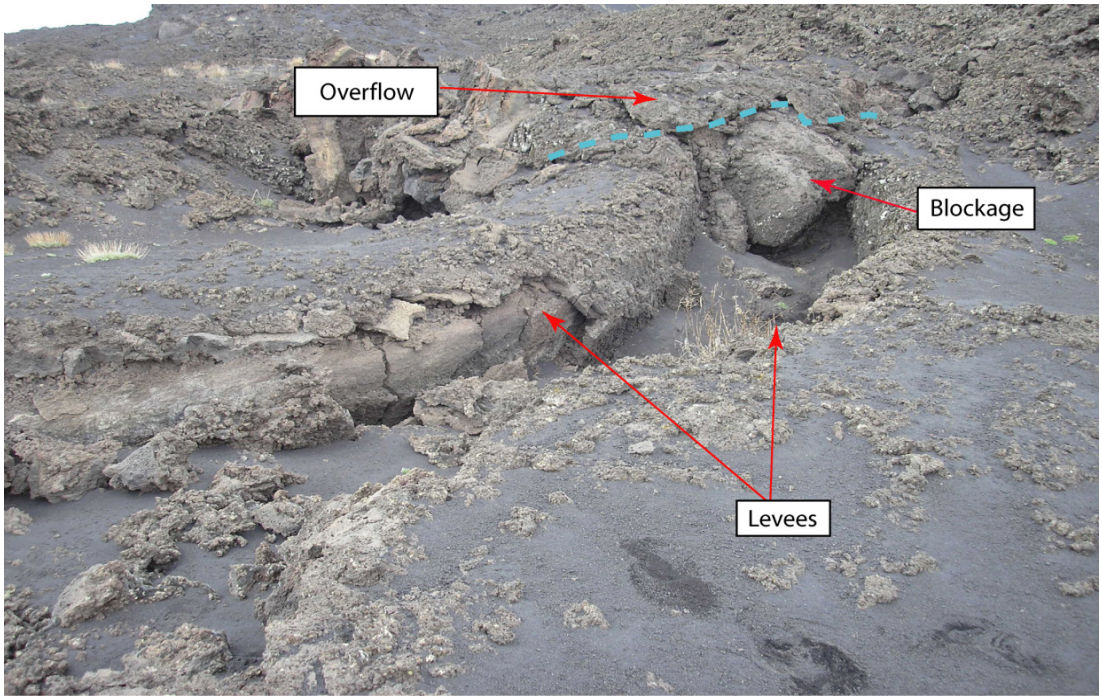

Figure 2.9 – Overflow in the 1983 flow-field of Mount Etna. The small secondary flow became blocked by debris causing an overflow.

Intuitively it could be assumed that increasing the angle of slope would increase the rate of flow under gravity, allowing a flow to reach greater distances before cooling caused the flow-front to become static. However, as discussed, decreasing the slope results in thicker flows as flows must increase their thickness on shallower slopes to provide enough energy to sustain crustal fracture. Thicker flows require longer cooling times than thinner flows and therefore the maximum length of a flow could increase with decreasing slope. Kilburn (2000) gives an equation for the maximum potential length (L_m) showing this relationship using the crustal fracture criterion where the terms in square brackets refer to the physical properties of lava crust which can be considered a constant for a given composition of lava:

$$L_m \approx \left[(1.5\ \varepsilon S/\rho g)^2(\Sigma\sigma\Theta^3)/\left(k\rho c_p\right)\right]/sin^2\beta \qquad \text{Eq. 2.1}$$

$$\approx [3\varepsilon S/\rho g k]^{1/2} Q^{1/2} \quad \text{Eq. 2.2}$$

Where: β is slope (^{o}), C_p is Specific heat capacity (J kg^{-1} K^{-1}), εS is Energy per unit volume for failure (J m^{-3} (or Pa)), g is acceleration due to gravity (m s^{-2}), k is thermal diffusivity (m^2 s^{-1}), L_m is maximum potential length of a flow (m), Θ is eruption temperature (absolute) (K), ρ is density of lava crust (kg m^{-3}), Σ is surface emissivity, σ is Stefan-Boltzmann constant (J m^{-2} s^{-1} K^{-4}) and Q is mean discharge rate along flow (m^3 s^{-1}).

In reality, slow moving flows rarely reach their predicted length as cooling and breaching halts flow advance or diverts material down a secondary flow, spreading the total active material in the flow-field over a number of different flows. The equation is however useful for hazard maps and emergency planning as it defines the maximum potential distance of a flow.

2.4.2 Effects of Volume on Flow Emplacement and Morphology

The work of Malin (1980) on historical Hawaiian flows, refuted the assumption that effusion rate was the single most important factor in the length of flow-fields, particularly the work of Walker et al., (1973). Malin (1980) proposed that volume was a more limiting factor to length and that large volume eruptions produced longer flow-fields. He compared the lengths, volumes and effusion rates for 87 flows on Kilauea and Mauna Loa and included the values Walker et al., (1973) had used for Etnean flows. The results showed that while the Etnean flows

showed a positive trend for length with increasing effusion rates, the Hawaiian flows did not.

Plotting both datasets against volume showed a stronger correlation between large volume, long distance flows for the Hawaiian data. It is worth noting that the majority of the data collected by Malin was for tube fed pahoehoe flows as opposed to the open channel 'a'a data collected by Walker et al., (1973). Therefore it is difficult draw direct comparisons between the data sets as the effects of cooling and/or insulation for the tube fed flows are not accounted for. At most, results preliminarily indicate that volume may be a more significant consideration for pahoehoe flow emplacement than 'a'a. Indeed, a reanalysis of Malin's data by Pinkerton & Wilson (1994) which excluded tube-fed flows from the dataset, showed a result for effusion rate vs length that was consistent with the theory of Walker et al., (1973) on effusion rate controlled flow lengths.

A comparison of the of 1981 and 1983 flow-fields by Guest et al., (1987) showed that despite the fact that the 1983 flow had a volume five times greater than that of the 1981 flow-field, both eruptions produced flow-fields with a maximum length of circa. 7.5 km. Therefore, whilst volume is certainly a consideration in overall flow-field length, for open channel 'a'a flows, it is unlikely to be the most significant.

2.4.3 Effects of Effusion Rate on Flow Emplacement and Morphology

Effusion rate is generally considered to be one of the most important parameters affecting flow-field development (Walker, 1971; Walker et al., 1973; Wadge, 1978; Guest et al., 1987; Kilburn & Lopes, 1988; Kilburn, 1990, 1996; Kilburn & Guest, 1993; Pinkerton & Wilson, 1994; Calvari & Pinkerton, 1998,

2002; Calvari et al., 2003). Walker et al., (1973) proposed that effusion rate was the single most important factor in both length and morphology of a flow-field. Walker et al., (1973) stated that high effusion rates generate longer flows in a simple configuration, that is to say a single or small number of flows and low effusion rate eruptions generate shorter compound flow-fields, citing the example of two flows from Etna, one from the Northeast Crater in 1966, the other from near Fornazzo in 1971. The flow from the Northeast Crater had a mean effusion rate of 1 m^3 s^{-1} and resulted in a complex compound flow-field. In contrast, the flow near Fornazzo in 1971 flowed quickly through simple channels almost 6 km downslope. Walker et al., (1973) plotted the lengths of several flows against effusion rate to illustrate this theory. Deviations from trend in the datasets were explained as the result of using mean effusion rates from the entire duration of emplacement as opposed to the average of the first few days or hours of emplacement when flows achieve the majority of their maximum lengths. Walker et al., (1973) do not discount viscosity completely from the formation of either simple or compound flows. The authors surmise that the boundary between simple and compound flow is viscosity related (Walker, 1971) and that it is a combination of viscosity and effusion rate that determines the length of a flow in addition to the form – simple or compound – that that flow will take.

While many studies have supported the role of effusion rate in flow-field length and morphology, they have attributed this relationship to the effects of cooling and the development of surface crust (Pinkerton & Sparks, 1976; Hulme & Fielder, 1977; Wadge, 1978; Kilburn & Lopes, 1988; Griffiths, 2000). Lower effusion rates allow the surface of flows to cool more quickly, forming surface crust

which will lead to flow thickening, the occurrence of breaches and breakouts and therefore flow-field widening.

The 1981 and 1983 eruptions of Mount Etna provided a unique opportunity to directly compare flow parameters like volume, effusion rate and cooling as both eruptions showed very different values and yet reached similar flow lengths of ~7.5 km. Guest et al., (1987) describe the flow-field development in detail including estimation of the dominate flow parameter for each stage of the flow.

The 1981 flow originated on the north flank of the volcano and was a short duration, high effusion rate event producing a simple flow-field (Figure 2.10). The 1983 event was from the south flank and was a long duration, low effusion rate event producing a complex flow-field (Figure 2.11). The 1981 flow appeared to be a volume controlled event in which the flow-front halted due to a cease in lava supply whilst the 1983 flow-field appeared to halt due to cooling.

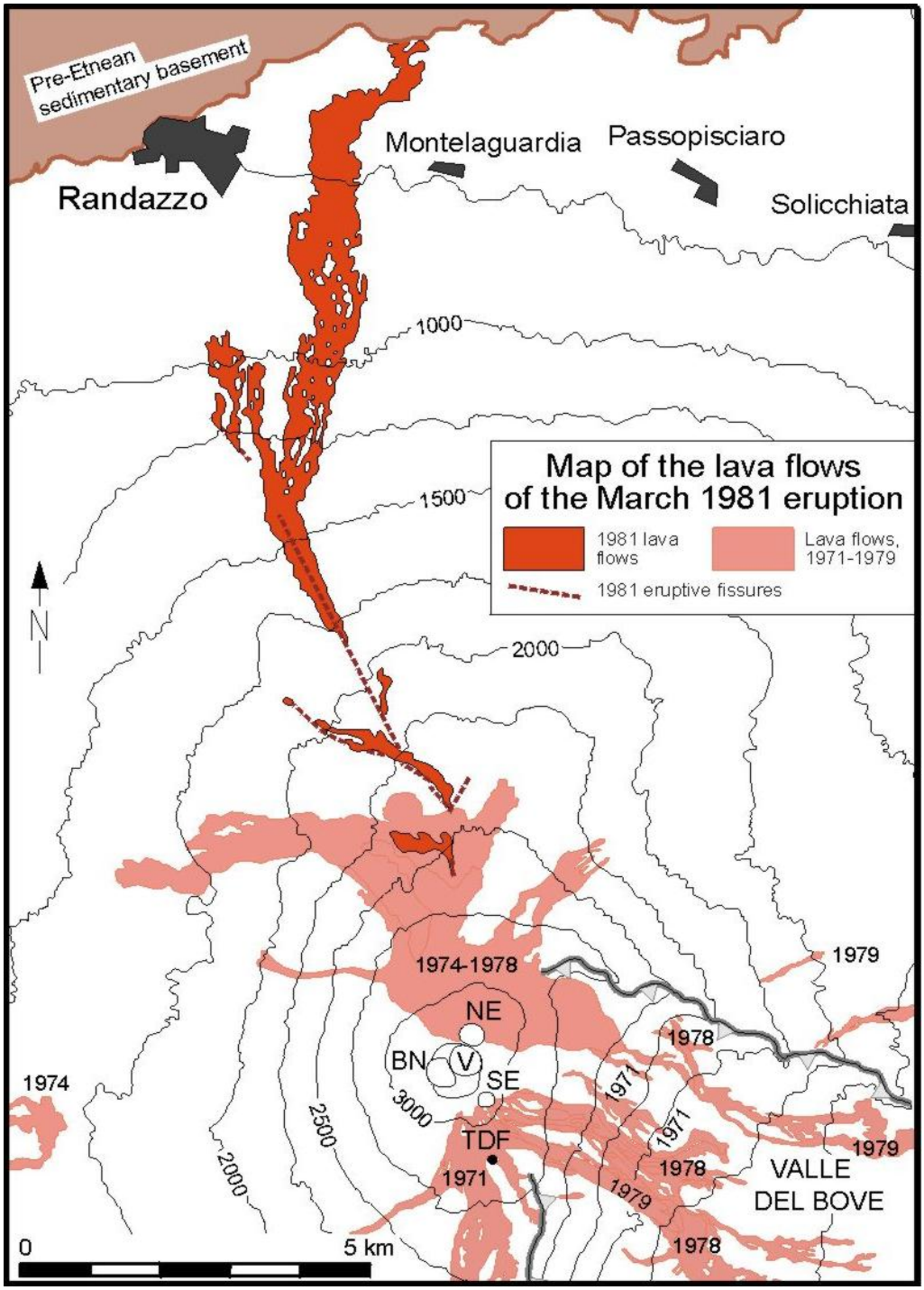

Figure 2.10 – Schematic of the 1981 flow-field on Mount Etna. The eruption resulted in the formation of a narrow. compound flow-field that reached a distance of ~7.5 km. Diagram by B. Behncke from www.italysvolcanoes.com.

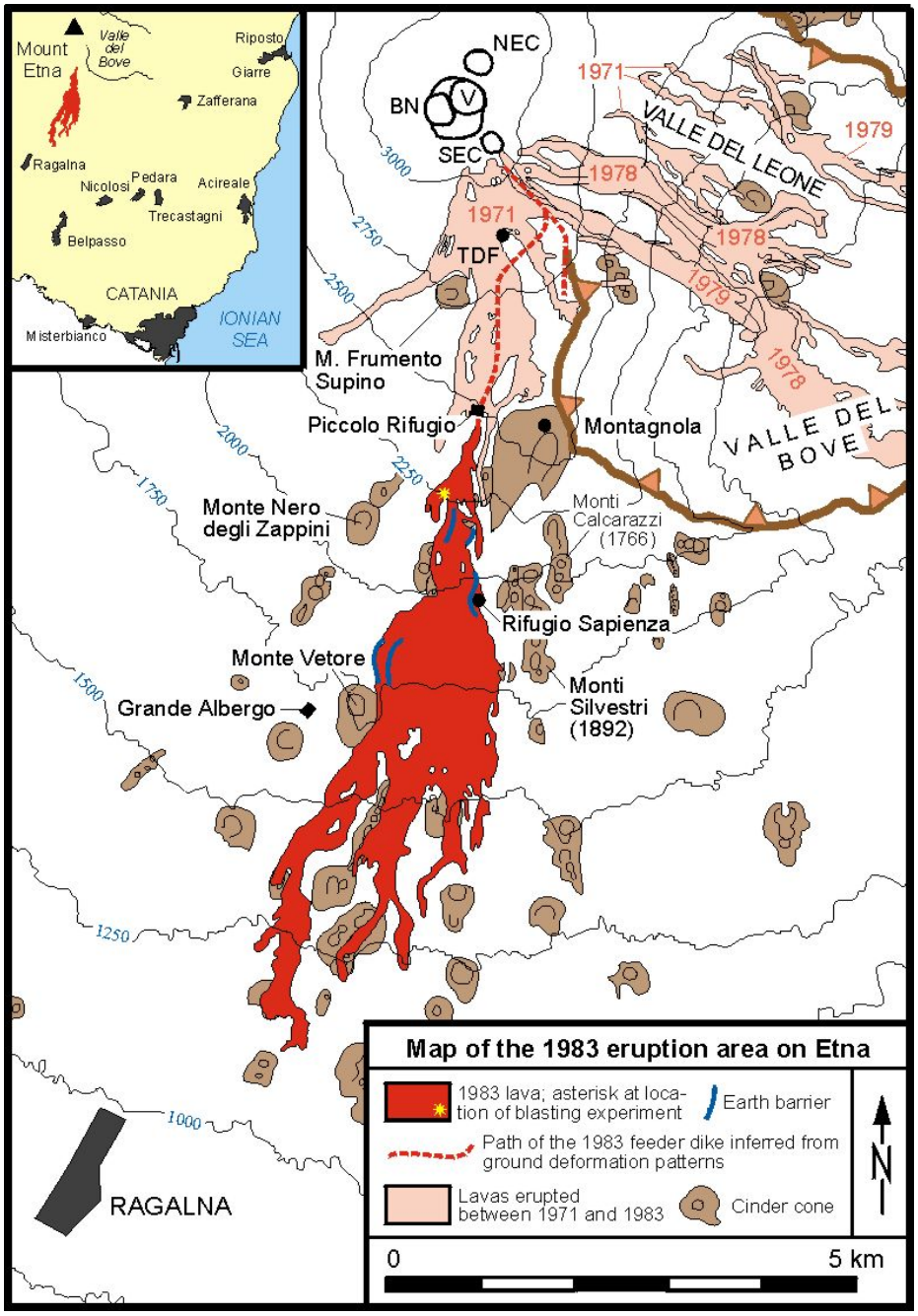

Figure 2.11 – Schematic representation of the 1983 flow-field on Mount Etna. This was a long duration eruption which resulted in the development of a complex compound flow-field which reached ~7.5 km from the vent. Diagram by B. Behncke from www.italysvolcanoes.com.

The flow-fields were divided in to three sections and chronology of both flows was documented including the formation and location of flow structures in each zone. In the 1981 eruption, the proximal zone formed in the region of the flow-field less than 3 km from the vent and was characterised by the presence of numerous small flows with accretionary levees approximately 2 m in height on

average slopes of 8-11^{o} emanating from individual vents along a fissure. This section of the flow was predominately effusion rate controlled.

The central zone was located between 3 and 6.5 km from the vent where average slopes were between 2 and 5^{o}. This section of the flow had none of the well-defined flows which existed closer to the vent with the flow advancing in an almost continuous sheet behind a wide moving front which was approximately 1 km wide 800 m wider than in the proximal zone. The flow in the central zone underwent significant thickening and lateral spreading as expected due to the decrease in slope.

The distal zone referred to those parts of the flow which were at distances greater than 6.5 km from the vent and represented the thickest parts of the flow with levees reaching 11 m in height compared to 9 m for the central zone and 2 m for the proximal zone. Secondary boccas formed at the flow-front producing pahoehoe like lavas and draining the channels upslope, showing that the main arterial channel still contained very fluid material which had not undergone significant cooling, proving that flow-field growth was volume controlled and halted due to ceasing supply from the vent.

In contrast to the simple form of the 1981 flow, the 1983 flow-field was more complex. During the first stage of emplacement, the flow reached its maximum length of 7.5 km, advancing through a cycle of breaching and emplacement with each successive flow halting as lava was diverted into a new flow. The flow reached its maximum length approximately 1/3 of the way through eruption. Emplacement style then changed to small, short lived flows from ephemeral boccas which resulted in thickening and widening of the upper and middle section of the flow.

The central zone of the flow was located between 1.5 and 3 km from the vent as was characterised by shallower slopes (from 15^{o} in the proximal zone to 11^{o} in the central) causing the flow-front to widen and thicken forming levees of up to 6 m in height and resulting in multiple breakouts from the flow margins.

The distal zone extended from 3 km away from the vent to the final flow-front over 7 km away. Ground slopes decreased once more in this zone, from 11 to 6^{o} resulting in the formation of lobes produced by the branching and breaching of existing flows. The snout of the main flows continued to move forward by draining the channels and forming a lobate flow-front.

Neither models of Walker et al., (1973) or Malin (1980) fit the emplacement of these two flows. Plotted onto Walkers empirical maximum length envelope, the two flows should have had lengths of 45 and 18 km respectively. Both flows reached roughly the same distance, 7.5 km, from the vent. The 1983 flow contained five times the volume of the 1981 flow which according to Malin's model should have resulted in a flow considerably longer than the 1981 event. Although the lengths of flow-fields show no positive trend with volume neither do they display a simple relationship to average effusion rate.

Frazzetta & Romano (1984) calculated values for effusion rate throughout the duration of emplacement based on velocity, flow width and the estimated depth of flow in the vent region. The results show that the effusion rate during the few days of eruption was about twice the effusion rate achieved during the rest of the first half of the eruption. Coltelli et al., (2012) have estimated an effusion rate of as high as 640 m^3/s/. The decreasing effusion rate in addition to the decreasing slopes contributed to the slowing down of the flow-fronts, resulting in inflation up flow which in turn led to breaches. Observations (Guest et al. 1987) made during

emplacement of the 1983 flow show clearly that each of the major flows stopped advancing due to a breakout from their margins several km's upslope. During the 1983 eruption, there were several large breakouts from the proximal section of the flow which formed new flows. After 11 days they ceased and breakouts only occurred in the medial and distal zones (Guest et al., 1987).

The chronology provided by Guest et al., (1987) for these two eruptions gives evidence for the theory that the controlling parameter for flow morphology changes throughout the life cycle of the flow, beginning with effusion rate and slope in the proximal zone in the hours immediately after eruption. In this stage the flow is either emplaced as a simple, single flow event, facilitated by high angles of slope and high effusion rates or as a complex compound flow favoured by lower effusion rates and to a lesser extent shallower slopes.

The complex interactions between emplacement rates (decreasing due to shallower slopes), cooling and the development of crust and decreasing supply from the vent define the structures seen in the next stage of emplacement including inflation, increasing levee height and/or secondary flow formation. During this stage, changes in local topography can also lead to the formation of secondary flows, widening the flow-field. Frazzetta & Romano (1984) describe how prior to the creation of two major flows in the 1983 flow-field, there were large "occlusions of the main lava channel and the breaking down of its western levee".

The final halting of the flow-front can occur due to supply from the vent ceasing, characterised by the presence of drained channels upslope and more commonly found in high effusion rate, simple flows. Low effusion rate, long duration flows are more likely to become static due to cooling and solidification of

the flow-front. Such flows are characterised by breakouts, breaches and the systematic creation of secondary flows.

Calvari et al., (2003) refute the theory of Wadge (1978) that neither high nor low effusion rates are responsible for flow morphology, rather the consistency of effusion may have a greater effect on flow-field growth. Tubes and simple channels are favoured by stable sustained effusion rates whilst fluctuating effusion rates is more like to cause overflows, breaches and the formation of new flows (Guest et al., 1987, Jurado-Chichay and Rowland, 1995).

The eruption chronology of two flows from the 1999 eruption of Etna as reported by Calvari et al., (2003) describe the occurrence of overflows following paroxysmal events at the vent and a temporary increase in flow rate. In contrast, steady supply over weeks to months led to the formation of lava tubes and a thick compound flow-field consisting of mostly cooling limited lava flows and large tumuli. Therefore fluctuations in effusion rate, cooling and slope may have the greatest control on flow emplacement to differing degrees dependent on the stage of eruption.

2.5 Levees

As described in the previous section, cooling and the formation of flow structures such as tubes, levees and lobes are an integral part of flow-field evolution (Macdonald, 1953; Walker, 1971; Kilburn, 1981, 2000; Griffiths, 2000; Burkhard, 2003; Favalli et al., 2010) and the role of tubes in rapid flow emplacement (Macdonald, 1953; Walker, 1971; Digby & Murrell, 1976; Pinkerton & Wilson, 1994; Calvari & Pinkerton, 1998, 1999; Merle, 2000).

However, of all of these structures, levees are the most important in terms of lava hazard mitigation. The location of a breach or overflow which results in a secondary flow will, to a certain extent, define the path of the new flow. Therefore, in order to properly understand lava flow hazards it is vital to understand how levees form in addition to how and where breaches and overflows occur along a channel margin (Section 2.5.7 & 2.5.8).

'A'a flows are characterised by the presence of solidified or semi-solidified material at their margins called levees. These levees, whilst still part of the flow, are stationary or move more slowly than the hotter more fluid material in the channel. Due to levees near the vent being the oldest and therefore with the longest exposure to flow material, they can account for up to 80% of the width of the flow whilst downstream it may be as little as 5-10%. Due to later stage drainage and the lowering of the flow level, levees may be left standing meters above the final flow height. Geometry on Etna for drained channel is roughly rectangular or slightly upward widening (Kilburn & Guest, 1993).

MacDonald (1953) provides an early description of levees, defining the fluid part as the main flow and the massive clinkery fields to the sides of the main flow as the flow margins. He describes how these margins are fed by a central pasty layer of material from the flow and can move slowly over the lifetime of the flow.

The first classification of the different types of levee and their mode of formation was provided by Sparks et al., (1976). They classify levees under four different categories (initial, accretionary, rubble and overflow) based on their morphology and infer their formation mechanisms from their appearance. The classifications of Sparks et al. (1976) have been confirmed and used by many authors (Kilburn & Guest, 1993; Bailey et al., 2006; Harris et al., 2009). However,

these classifications are best suited to the proximal section of a lava flow. Subsequently other authors (Kilburn & Guest, 1993) have created more detailed classifications of levee morphologies which can be found throughout the length of the flow.

2.5.1 Initial Levees

Sparks et al., (1976) describe the formation of static, cooled flow margins in the early stages of flow emplacement as initial levees (Figure 2.12). These types of levee are found predominately in the proximal section of the flow-field. Although rarely preserved in the medial section of the flow, it is likely that as the flow-front moved downslope, extending the flow longitudinally, it created initial levees that have since either been buried by subsequent flows or evolved into another levee type.

Kilburn & Guest (1993) use the term lateral levee to describe the initial morphology of the chilled margin of a flow. They are described as having massive interiors and are initial levees only when incandescent and without a layer of surface rubble. When they do become covered in autobrecciated material they can be termed rubble levees. They still have their massive interior and therefore both these types of levee can be termed massive levees

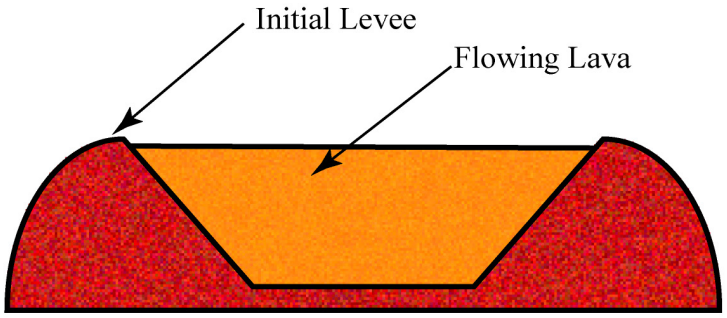

Figure 2.12 – Cartoon schematic of the structure of an initial levee. The channel margins consist of homogenous, massive material. Redrawn from Sparks et al., (1976).

2.5.2 Accretionary Levees

Several authors, (Sparks et al., 1976; Kilburn & Guest, 1993) describe the growth of accretionary levees as hot ductile clinkers being carried by the flow becoming attached to the sides and tops of an initial levee often exhibiting shear in the direction of flow. They then weld themselves together to form a solid levee. These levees are the commonest found close to boccas and are characterised by outward sloping inner walls and steep-sided outer walls from 50^{o} to 80^{o}. Interestingly, Sparks et al., (1976) remark that these levees occur before the lava has fully transitioned into an 'a'a flow (Figure 2.13).

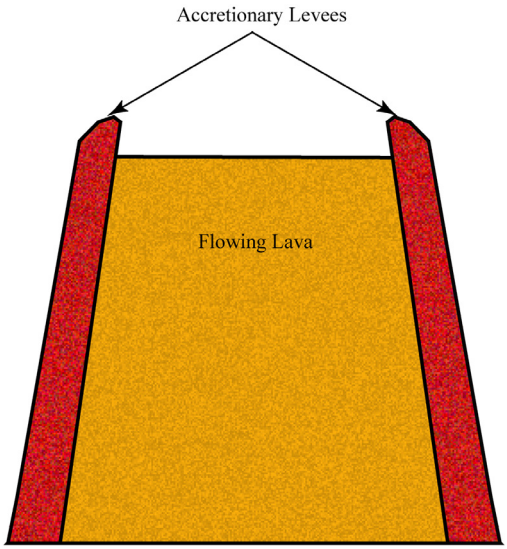

Figure 2.13 – Accretionary levees evolve from initial levees by the addition of clinker material that wields itself to the initial levee. These types of levee are characteristic of flows mid-transition from pahoehoe to 'a'a flow. Redrawn from Sparks et al., (1976).

2.5.3 Rubble Levees and Debris Levees

Sparks et al., (1976) classify rubble levees as those which are found in 'a'a flows and form as a result of the talus of rubble which collects from avalanching of the steep front and sides of a well-developed 'a'a flow. The typical angle of repose of these levees is $30 – 35^{o}$ (Figure 2.14).

Kilburn & Guest (1993) differentiate debris levees from the classification "rubble levees" by Sparks et al., (1976) by the thickness of the loose coating formed when massive levees are modified by lateral overflow or accretion caused by flow thickening (overflow) or migration of broken crust (accretion) to the sides of the flow, resulting in a massive core with a coating of breccia.

The texture that gives rubbley levees their name is the result of autobrecciation and as such will have a similar thickness to that of the flow material which is also undergoing autobrecciation. The debris levees will have a much thicker coating of loose material due to accretion.

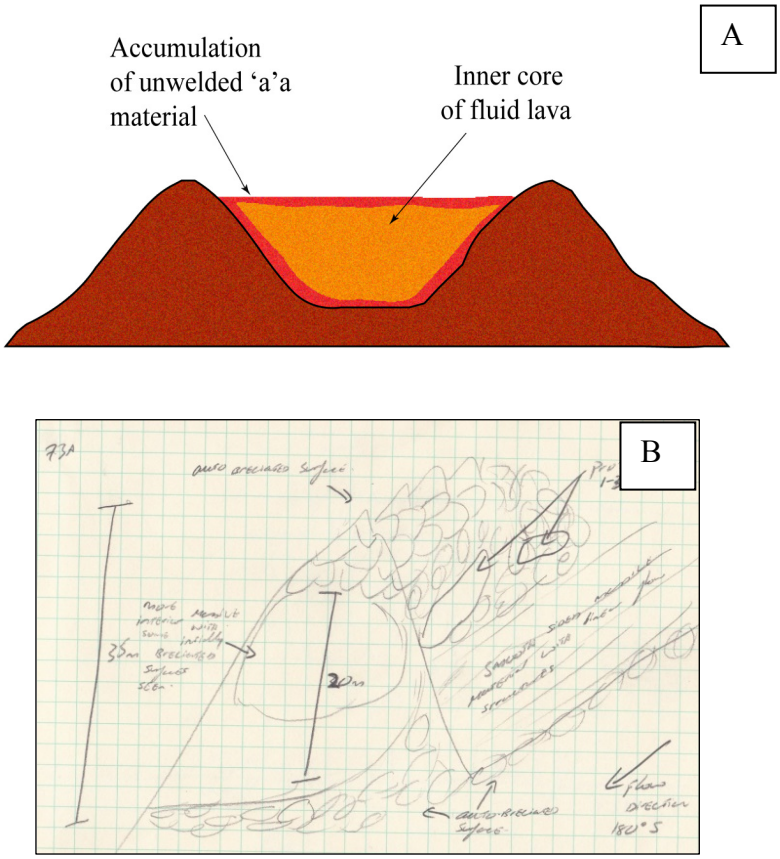

Figure 2.14 – Debris and rubble levees, whilst on the surface may appear to be morphologically similar have two different origins. The cartoon (A) is redrawn from Sparks et al., (1976) and describes the debris levee consisting of a levee with a massive interior, coated with flow debris. The field sketch (B) is of a rubble levee (following the classification of Kilburn and Guest (1993) in the 1983 flow-field on Mount Etna). A road cut exposed the interior of the levee, showing the massive interior and autobrecciating surface.

2.5.4 Overflow Levees

Overflow levees are formed when material from the channel overtops the flow boundaries and can evolve from any of the three previous classifications of levee. The material escaping the channel drapes over the existing levee, increasing its height and width. In cross section, these levees will contain alternating packages of pahoehoe or 'a'a material (Kilburn & Guest, 1993). Overflows can occur due to fluctuating effusion rates, thickening due to channel blockage, slowing flow-fronts or changes in slope (Figure 2.15).

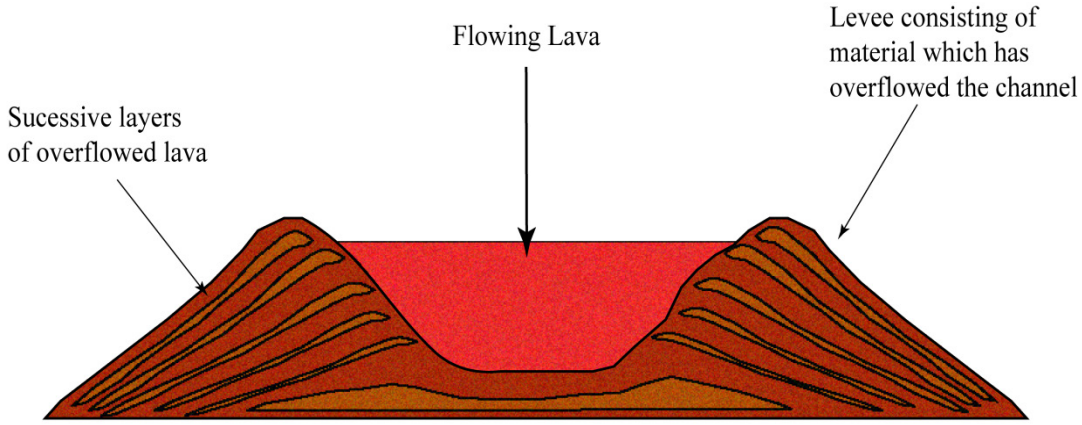

Figure 2.15 – Schematic of an overflow levee showing the alternating layers of pahoehoe and 'a'a material. Redrawn from Sparks et al., (1976).

Building on the classification of Sparks et al., (1976), Harris et al., (2009) give a detailed morphological description of the overflow levees which can be found in a 200 m long section of Muliwai a Pele lava channel on Mauna Ulu, Kilauea. The levee structure is broken down into three segments – the basal segment comprising an 80 – 150 m wide 'a'a flow in which a 2 m deep and 11 m wide channel became centred. The basal 'a'a package was capped by thin (<45 cm) pahoehoe overflows which extended up to 50 m from the channel. The third and top layer consisted of localised 'a'a overflows. During periods of decreased effusion, the level of material in the channel dropped, causing the levees to become

unsupported. This resulted in localised failures in the levee wall, weakening the structure and causing sections of the wall to break off during subsequent pulses of effusion. These chunks of levee entered the main channel, in some cases causing the channel to become temporarily blocked. The 'a'a overflows which cap the levees can be related to the position of blockages within the flow and extend no more the 23 m from the channel.

2.5.5 Active Levees

Guest et al., (1987) classify active levees as the typical levees of large flows away from the vent area having similar characteristics as the flow-front, consisting of an active talus slope at angles of up to 45^{o}. These types of levee occur during periods of high emplacement rates where initial static levees become remobilised and begin to move outwards to accommodate flow thickening with two outcomes, the first is that the material will overflow the channel. The second occurs when flow thickening results not in overflow but in the intrusion of flow material into the levee. This can occur along the length of a flow but overflow is more common closer to the vent and swollen levees are more common towards the flow-front in the rubbley 'a'a zone (Figure 2.16).

They typically form where the surface of the lava is close to or convex above the level of the levees. Once these levees become strong enough to withstand the pressure from the channelled lava they are considered static levees. Static levees may reactivate when the pressure in the channel grows past the point of their ability to withstand it morphing back into active levees.

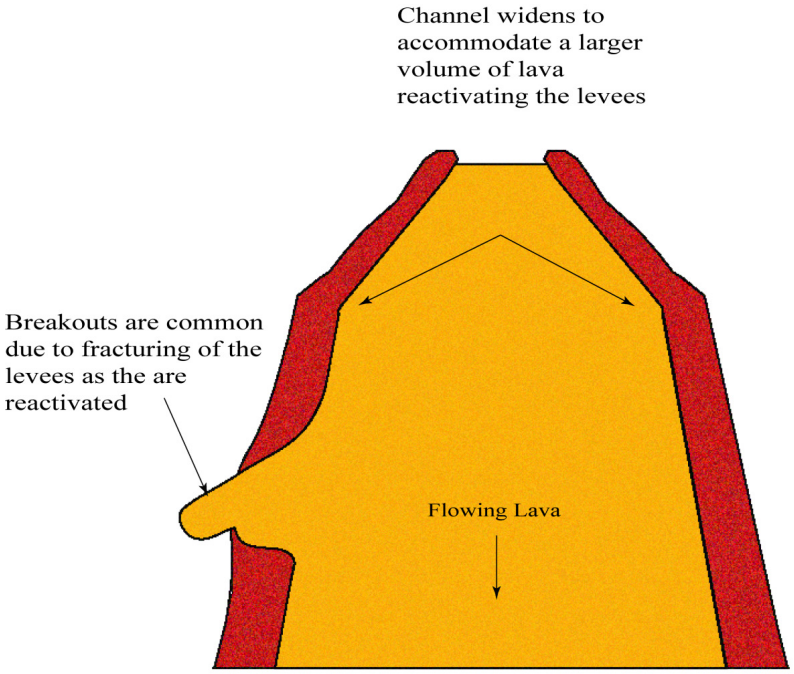

Figure 2.16 – Cartoon schematic of an active levee showing the static levee becoming reactivated to accommodate increased volume of material in the channel. In some cases, the levee deforms as channel material in intruded into the levee. In other cases, the levee fails or is overtopped.

2.5.6 Multiple, Medial and Compound Levees

Levees may be found in more than parallel sets of two. Multiple levees can be associated with a decrease in flow volume and can look like inward descending steps or sets of levees of comparable heights distinguished by angular depressions at their junctions or differences in their coating of debris (Figure 2.17). Although ideally each levee should have a corresponding opposite number this is not always the case. For example when one side of the channel is constrained by an obstacle and the other side is unconstrained. The unconstrained side will show an inward progression of levees as the channel volume drops whilst the constrained side may continue to have only one levee abutting the obstacle.

Their symmetry may also be broken by the development of medial levees associated with topographic irregularities and a waning effusion rate. Medial levees can cause channels to split into braided networks (Figure 2.18). Compound levees

form in flow-fields where small flows fill the gaps between arterial flows. The existing flows act as barriers/levees to the new flows in gaps which are so narrow that the development of their own levees is not possible.

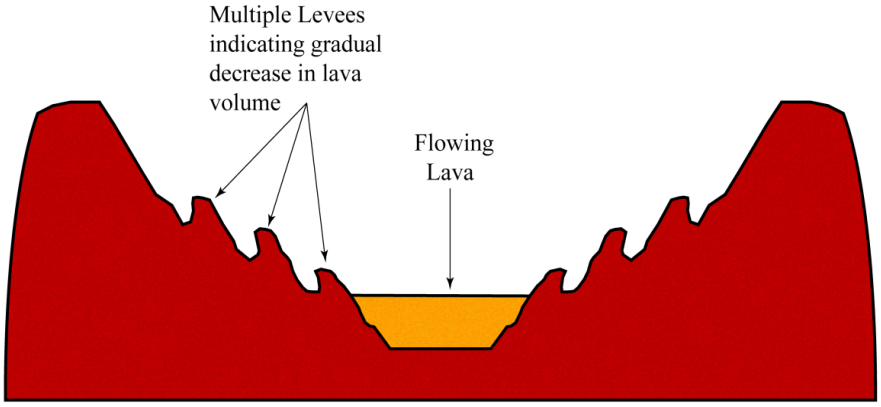

Figure 2.17 – Multiple levees reflect the dropping level of material in an active channel and are an indication that emplacement rates are waning for that channel.

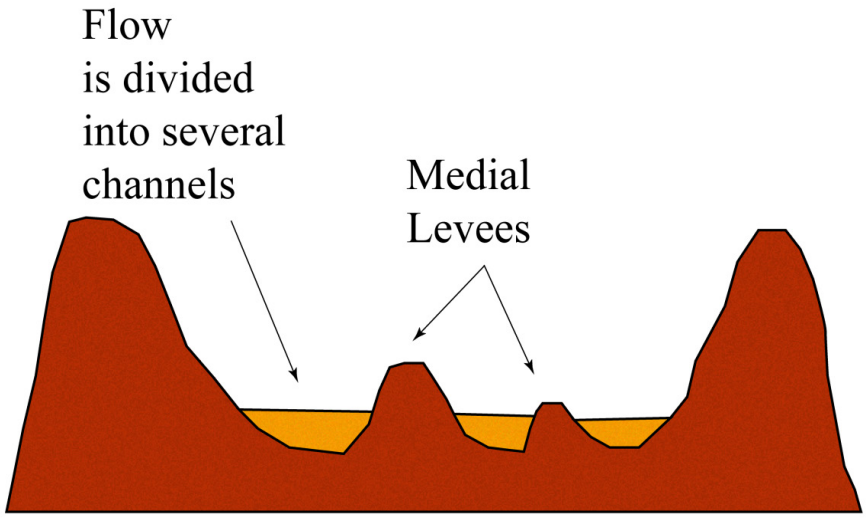

Figure 2.18 – Medial levees are characteristic of flows on shallow slopes where the channels has spread out and formed a braided network of channels and channel margins.

2.5.7 Breaches

The preferred locations and mechanisms by which levees fail are not well understood and are the subject of this study, however some observations of active flow-fields have identified some large scale trends in location and modes of failure.

Mechanism

It is generally recognised that periods of flow thickening regardless of the mechanism can lead to breaching (Pinkerton & Sparks, 1976; Kilburn & Lopes, 1988). Guest et al., (1987) observed three different mechanisms for failure in different sections of the 1983 flow-field on Mount Etna. The first was in the distal portion of the flow-field near the flow-front where, due to localised topography, the flow margin started to advance faster than the flow snout, diverting lava from the main channel causing it to flow in a new direction resulting in two different flow-fronts being active at the same time. This type of disruption of a flow margin very near the flow-front could result in the original flow halting and the new flow-front taking over as the primary flow.

The second failure mechanism observed by Guest et al., (1987) was specific to active levees in the distal section of the flow-field at flow-front. The front was moving in a series of overlapping, horizontal sheets. The sheet extrusion was large enough to undermine the levee, causing it to become unstable. This type of breaching indicates that the flow-front halted due to cooling and that the flow interior is still fluid enough to flow (Kilburn & Guest, 1993).

The third method of failure observed by Guest et al., (1987) was relating to changes in lava levels within the channel and resultant overflows and was observed to occur in both the distal and medial sections of the flow-field on overflow and debris levees. Guest et al., (1987) observed that if an overflow had sufficient energy, it could cause part of a levee to break off, creating a breach, lowering the level of the levee with the result that lava could still flow through the breach even after the level of lava in the channel had returned to normal. The causes of overflow are discussed in more detail in Section 2.5.7.

The process of breaching is restricted as the relative thickness of the crust increases (Pinkerton & Sparks, 1976). Kilburn & Lopes, (1988) expressed this process using the function S_R/S_D where S_R is the crustal retaining strength and S_D is the stress driving lava movement. S_R is derived from the tensile strength of the crust and its thickness with respect to the dimensions of flow margin. During periods of thickening, S_D increases. Breaching is more likely to occur when the rate of thickening is faster than the rate of crustal growth.

Location

Other than identifying broad locations in the flow-field such as distal, medial or proximal sections where a breach is likely to occur, very little work has been done on the more specific locations of levee failure or linking the morphology of the levee with a propensity to failure. Given that the formation of breaches is linked to cooling and that growth of flow-fields moves from lengthening to widening with time, the occurrence of breaches must follow a systematic process (Kilburn & Lopes, 1988). Indeed a number of authors (James et al., 2007, 2011) have observed that breaching migrates back up channel towards the proximal section of the flow-field with time, giving support to cooling as a controlling factor in breaching.

Topographic controls on breaching were also observed. Changes in gradient, where the underlying slope became shallower, resulted in flow sinuosity. It was observed in the 1983 flow-field on Mount Etna that breaches occurred on the outer curve of a flow suggesting that the angle of applied pressure from the interior flow may have a control on the location of breaches (Nolan, 2006). The same process

was observed by James et al., (2007) in the Valle de Bove in the 2008-2009 eruption of Mount Etna.

2.5.8 Overflows

Overflows occur when the level of lava in the channel rises above the height of the channel levees, spilling over the side of the levee, some forming localised, short lived flows other merely draping over the top of the levee but having insufficient volume to reach beyond the flow margins. Overflows can be triggered by a variety of causes discussed below.

Variations in Slope

As a flow moves down a slope, local variations in the underlying topography can have an effect on the flow dimensions. When the gradient becomes shallower, the flow-front spreads out and slows down causing the flow behind it to thicken as the hotter, more fluid material up-flow continues to be emplaced at a faster rate behind the slower flow-front, causing inflation. If the increase in height of the lava is sufficient, the flow will overtop the constraining levees, adding to the levees height and width (overflow levee) and forming a small fan shaped flow down the outer wall of the levee.

Localised increases in slope can also result in overflows. As the flow moves over areas of increased gradient, the flow becomes narrower, reducing the amount of accommodation space within the mobile part of the flow. If the level of the flow increases, for example through slowing down of the flow-front or a pulse of increased effusion rate, the lava will overtop the constricted channel forming an overflow.

Blockages

The level of lava within a channel can also increase locally due to blockages. These can take the form of local topographical highs which slow the flow-front down, causing the lava to become backed up until the flow either bifurcates around the obstacle or thickens sufficiently to provide enough energy to flow up and over. Blockages can also be caused by sections of levees breaking off and being pulled into the lava flow. The sections can block the channel either individually or where several pieces become jammed together forming a raft that effectively dams the flow. This may cause an overflow behind the obstacle until the pressure in the channel behind the blockage becomes sufficient to move it, returning the level of the flow to its previous height, effectively starving the overflow. Channels become more easily blocked the narrower they are and overflows frequently occur as a result of the combination of slope variation and blockage. An example of this is described by Bailey et al., (2006) when an overflow of slow moving 'a'a material occurred due to a blockage in the 2001 flow-field on Mount Etna. Once the pressure caused by the blockage had removed the obstacle, the level of lava in the channel fell to below the height of the levee and starved the overflow.

Variations in Effusion Rate

Pulses of increased effusion rate can propagate downstream causing localised increases in flow level leading to overflows. Bailey et al., (2006) describe overflows and the flow dynamic during and after pulses in the 2001 flow-field on Mount Etna. Pulses propagated down channel, initiating overflows of pahoehoe

material which extended for 20 m from the channel and were no more than 0.5 m thick. The overflows were short lived events as they would become starved as the pulse move down channel. The lava from the overflows draped over the levees increasing their heights and causing them to become inward sloping which, given enough time, could form a tube. Pulses also removed channel blockages and therefore the efficiency of the channel was increased immediately following a pulse.

The mechanism for disruption of the flow margin has been discussed in the previous section and is the same for breakouts except that the breach is quickly healed by solidification of the in-filling lava and therefore forms only a short lived flow that does not greatly extend the width of the flow-field.

2.6 Summary

Although many studies have provided descriptions and chronologies of the emplacement of individual flow-fields, there are as yet, no guidelines which can be applied during active eruptions to help forecast final flow-field dimensions. Key to providing these guidelines will be a clearer understanding of levee formation and collapse and the generation of secondary flows. These processes have been documented in the field but there is very little data available which describes the likely mechanisms, locations and timings of levee failure and secondary flow formation.

3 Field Investigation

The study of the morphology and structures of inactive flow-fields is invaluable to understanding the processes relating to flow-field development. Whilst some features may have been buried by subsequent lavas, it is often possible to infer emplacement conditions from the solidified flows. Sites were chosen in the flow-fields of the 1983, 1985, 2001, 2002 and 2003 eruptions on Mount Etna and in the 1705 Arenas and 1909 Chinyero eruptions on Tenerife. In the case of the flows studied on Mount Etna, particularly the 1983 flow and the Arenas flow on Tenerife, road cuts through the flow-field allowed for the study of the internal structure of the flows and levees, something that would not be possible in an active flow-field.

3.1 Selection of Field Sites

The field sites for this study were selected on the basis of satisfying a number of primary criteria. The criteria included well developed flow-fields which had well documented emplacement histories and timelines and which formed over different underlying slope angles. Mount Etna and the flows from Arenas and Chinyero were chosen as they fit the criteria, having complex flow-fields which are characterised by breaching and the formation of secondary flows and had emplacement histories which had been documented by contemporary authors.

Mount Etna is the largest sub-aerial volcano in Europe and also one of its most active. It has a roughly elliptical base which measures 38 x 47 km with a maximum elevation of 3300 m (Kilburn & McGuire, 1997) (Figure 3.1).

Figure 3.1 - Map of Sicily, Italy which shows the location of Mt. Etna on the upper east coast (www.travellingitaly.info).

Etnean lava flows have very similar bulk compositions (Kilburn & Lopes, 1988) and form 'a'a compound flow-fields with similar emplacement characteristics which make it an ideal study area as measurements from a vast number of different flows can be compared and contrasted. Etnean lavas are typically formed of basaltic andesites with a vesicle concentration ranging from 10 to 45%, an important consideration in selecting field locations as preliminary studies (Nolan, 2006) indicated that vesicle concentration and orientation may have an effect on the strength of a levee.

Field sites were chosen from Google Earth images, where it was possible to identify the location of overflows, levee breaches and the formation of secondary flows. Each site was assayed in terms of levee composition (structure and texture), mechanism of failure where applicable and topographic characteristics. The observed morphologies were used to infer flow-field development in an effort to identify the local characteristics of the channel which were a controlling factor in the location of the breach or overflow. Samples were taken from levees and also from locations above and below breaches for rock strength analysis.

A full list of the field sites where samples were taken is available in Appendix A but some of the key field sites from Mount Etna are shown in Figures 3.2 & 3.3 on both geological maps, (which make it possible to distinguish between different generations of flows) and on a Google Earth image, showing the location of secondary flow formation.

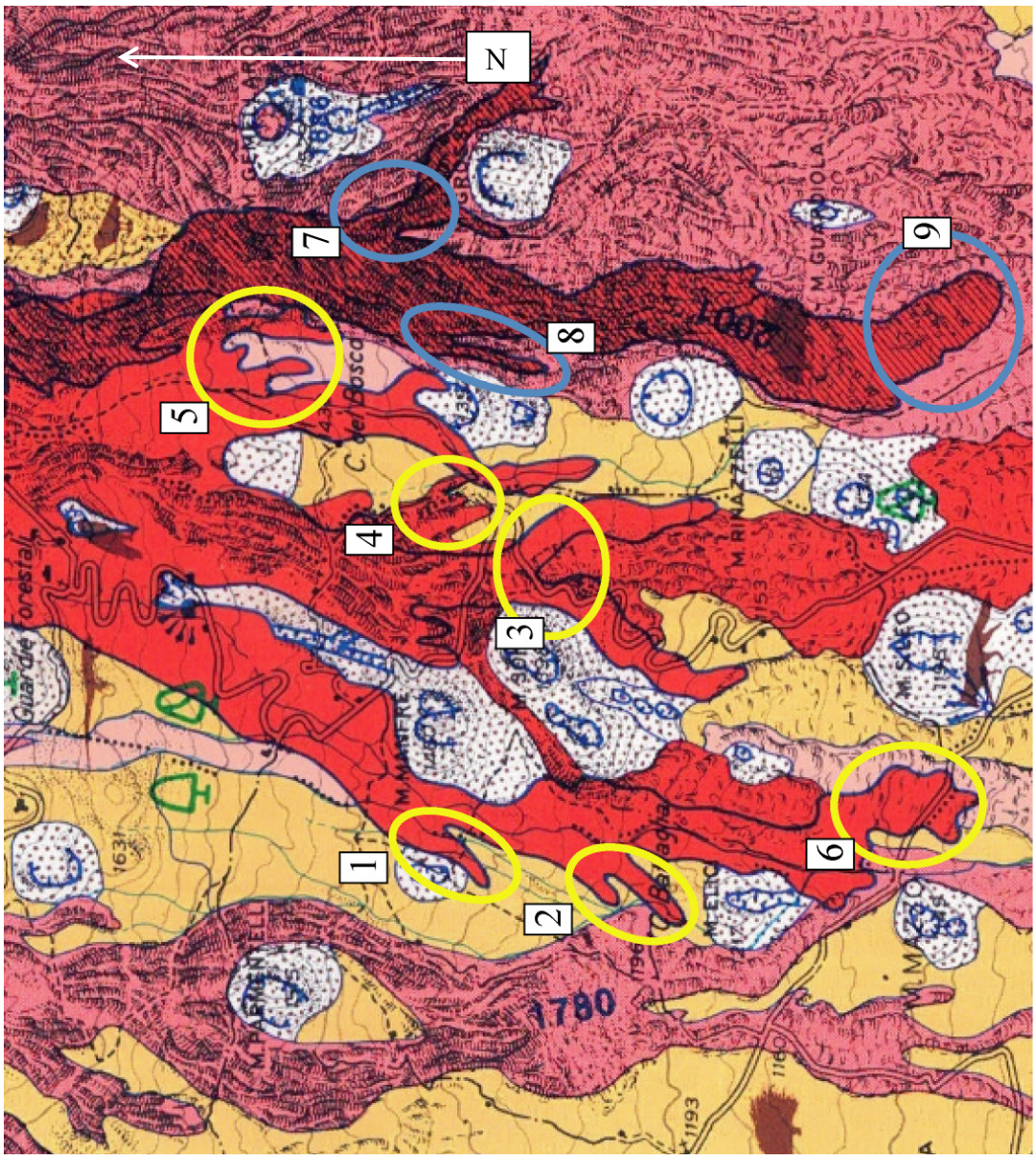

Figure 3.2 – Extract from the 2005 1:60000 S.E.L.C.A geological map of Mount Etna showing the 1983 flow-field (bright red). Some of the field locations visited are marked in circles, yellow for the 1983 flow-field and blue for the 2001. Field locations were chosen where there are breaches and overflows and where secondary flows formed.

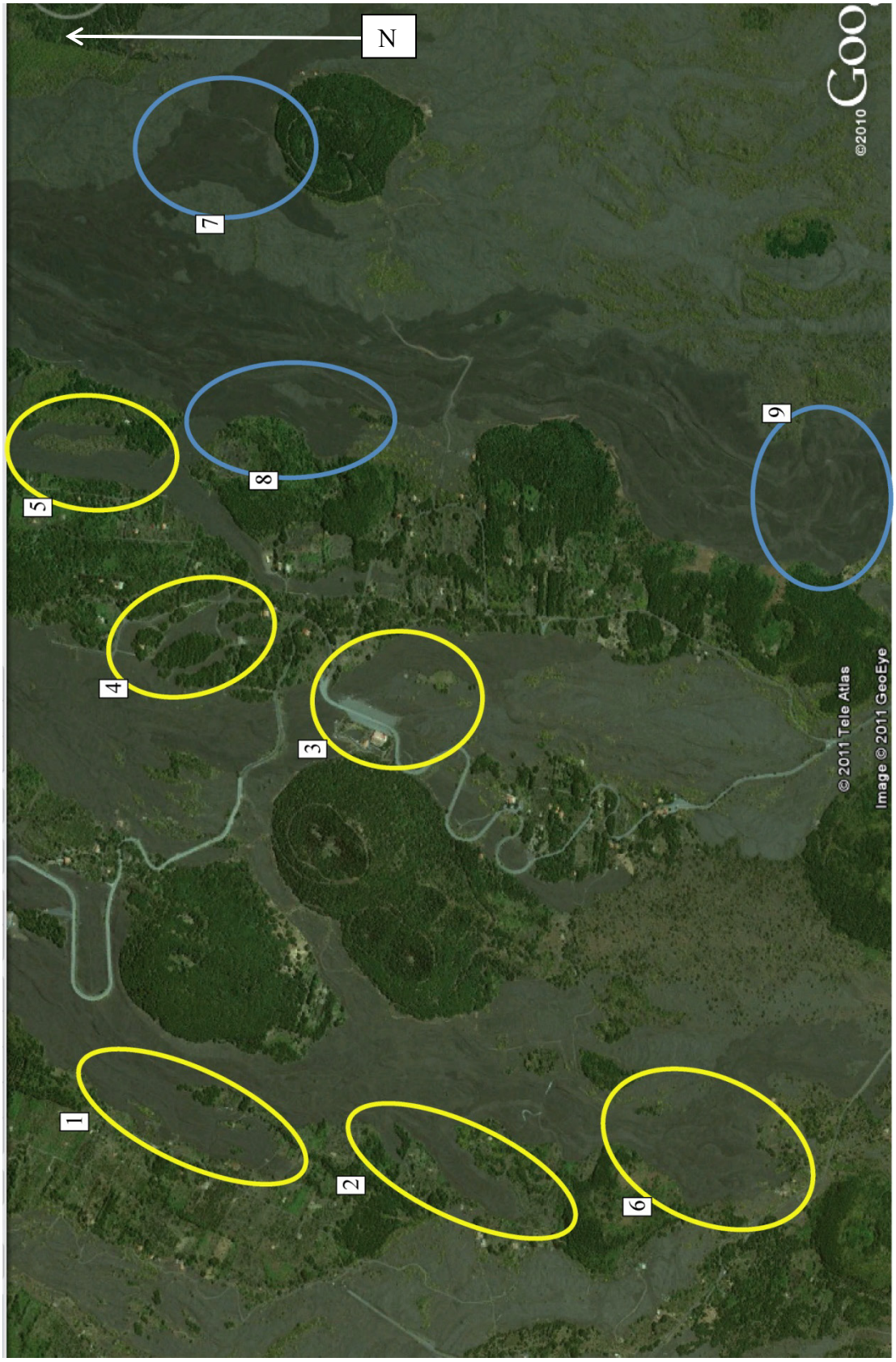

Figure 3.3 – Google Earth image of the 1983 flow-field (same section as shown in the map in Figure 2.19). Field locations are circled in yellow for the 1983 flow and blue for the 2001 flow

The second field area chosen was on Tenerife in Canary Islands. Historic and recent eruptions have been both effusive and explosive but the vast majority of the island mass is formed from lava flows (Solana, 2012). Field sites where chosen at Arenas, Garachico and Chinyero using the same criteria as previously mentioned for Mount Etna (Figure 3.4 & 3.5).

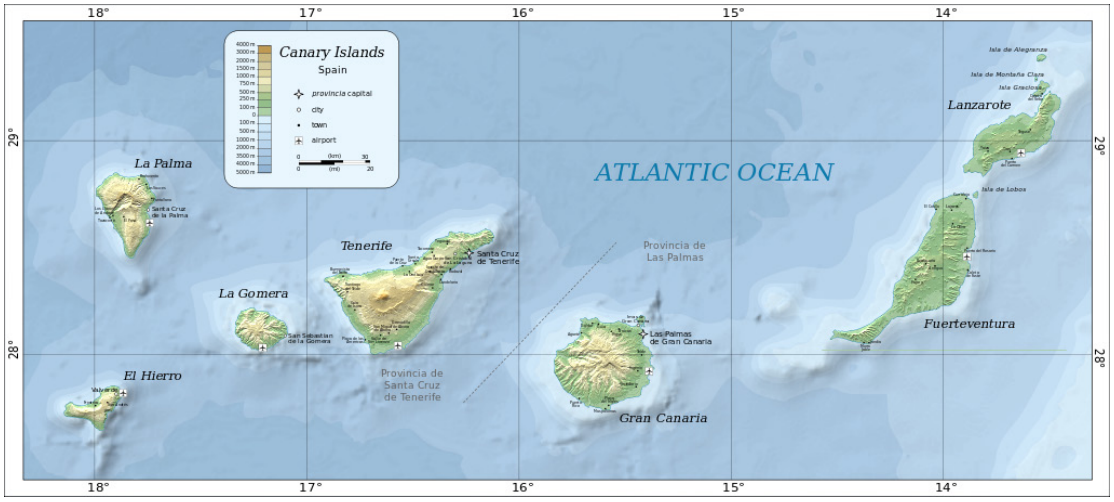

Figure 3.4 – Map of the Canary Island showing Tenerife taken from www.wikipedia.com.

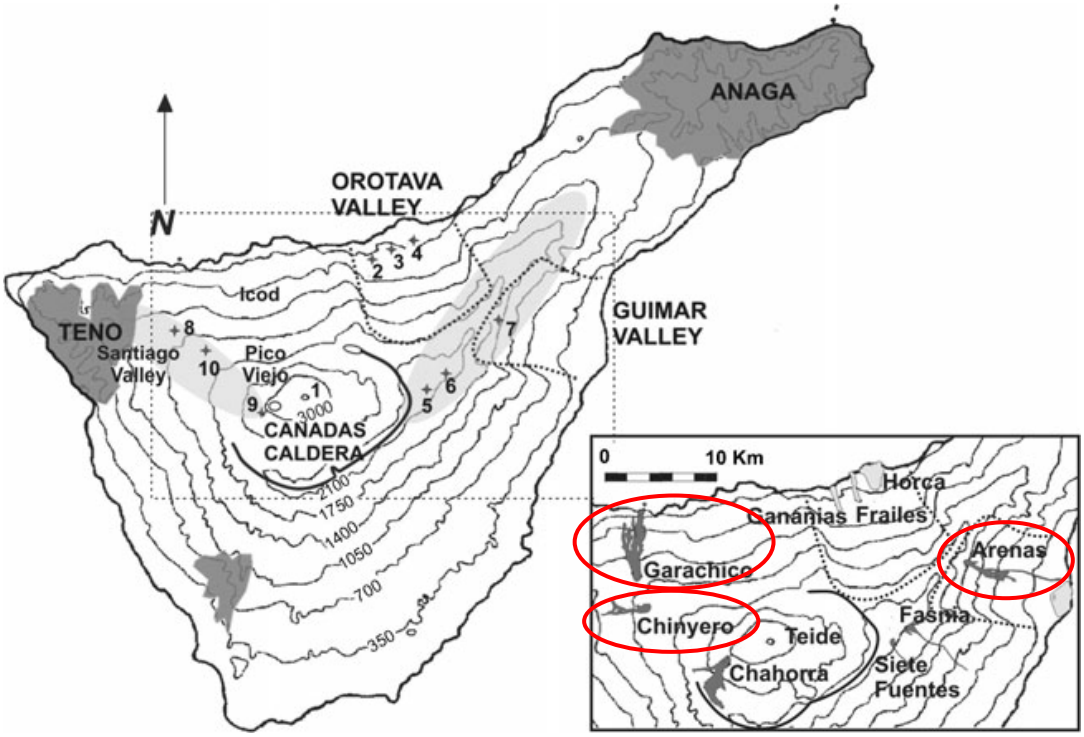

Figure 3.5 – Figure taken from Solana (2012) shows the location of the three field sites (circled in red) chosen in relation to the island as a whole and the Las Cañadas caldera.

The Arenas and Chinyero flows on Tenerife consisted of basanite and phonolitic tephrite respectively. The Arenas flow, situated between the towns of Guimar and Arafo, originated from the "Las Arenas" cinder cone, which formed in the northern end of a 12 km NE trending fissure, parallel to the predominate NE ridge on the island. The flow-field is 9 km long and 1.25 km wide with two main arterial flows (Solana, 2012) (Figure 3.6).

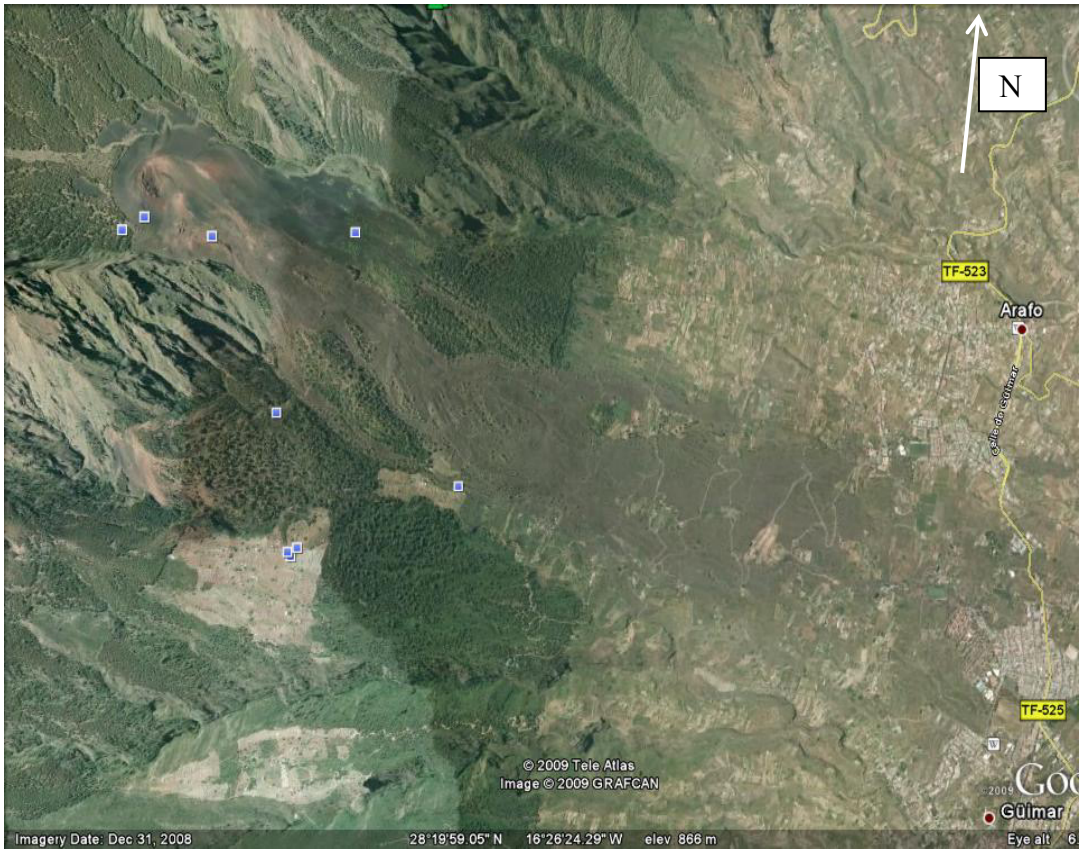

Figure 3.6 – Google Earth image of the Arenas flow on Tenerife and the strombolian cone from which it originated.

The Chinyero flow originated from the "Volcan Chinyero", an 80 m high strombolian cone and consists of two main branches to the west and north of the cone that underwent breaching and bifurcation to develop into a compound flow-field. The northern arm of the flow reached 1.2 km from the vent and the western flow reached 4.6 km (Figure 3.7).

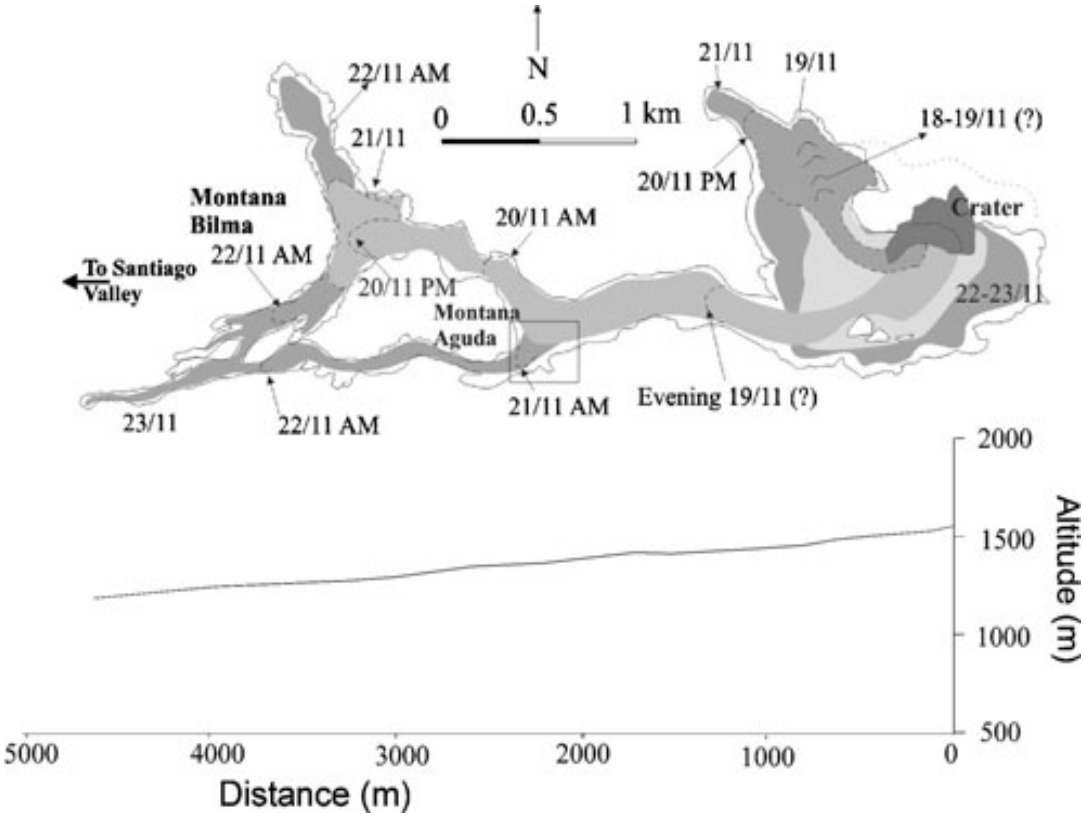

Figure 3.7 – Map of the flow-field resulting from the Chinyero eruption on Tenerife. The square on the map indicates where the main flow underwent bifurcation around a topographic high. From Solana (2012).

The field-sites in Tenerife were chosen to contrast with the basaltic andesite flows of Etna, to compare levee morphology between the two different lava types and also to compare the strengths of samples with different size profiles for vesicles and % amount vesicularity. In some samples, the basanites from Tenerife also contained a high concentration (10-20%) of phenocrysts of olivine orientated in the direction of flow. Strength analysis of these samples gave insight into the effects of crystallinity on levee strength. The petrology of the samples is described in Section 6.3 Petrology.

3.2 Observations from Field Investigation

The primary goal of the field investigation was to use extant flow-fields and structures to infer emplacement conditions and in particular to look for evidence of breaching and secondary flow formation, the mechanisms by which those breaches formed and to document levee structures and changes to their morphology throughout a flow-field. In addition to looking for evidence of individual breaches, another goal of the field study was to look for patterns or controls on the locations of breaches and parameters affecting overall flow-field morphology.

3.2.1 Changes with Slope – Widening and Sinuosity

Slope changes have a well-documented effect on flow dimensions. When a flow experiences a decrease in slope, the flow-front and correspondingly the flow behind becomes wider and more spread out. As a result, the aspect ratio (the ratio of the width to the height) of the levees constraining the channel changes as their heights decrease and widths increase.

As the flow spreads out, the angle of applied stress at which the infilling lava puts on the levees changes. It had been assumed that the levees would spread in an outwards and down-channel direction. However, a gate post in a levee of a secondary flow in the 1983 flow-field on Mount Etna, gives evidence that the direction of spreading is almost 90^{o} to the direction of flow.

This could be an important consideration in the failure of levees as the direction of applied stress to the levee becomes oblique to perpendicular rather than a parallel shearing motion (Figure 3.8)

Figure 3.8 – Gate post buried in the margin of a channel in the 1983 flow-field on Mount Etna within 200 m of the flow-front. The angle of tilt of the post indicates the direction of spreading of the levee. The post is pushed out obliquely from the flow indicating that the levees were being pushed outwards behind the flow-front.

Measurements taken on flows show that decreasing slopes also caused thickening. This was especially noticeable at the flow-fronts. Slope changes of just 2^{o} were observed to have this effect on flow dimensions.

Lava flows were observed to become sinuous as the gradient decreased, causing the levees to become curved. Material in inactive sinuous channels was observed to be thicker on the outer bends of the flow suggesting that as the lava moved through a sinuous channel, the flow material was pushed towards the outer flow margin. As well as imposing larger stresses on this area of margin, this may have also caused some additional mechanical erosion to the levees at these points (Figures 3.9, 3.10 & 3.11).

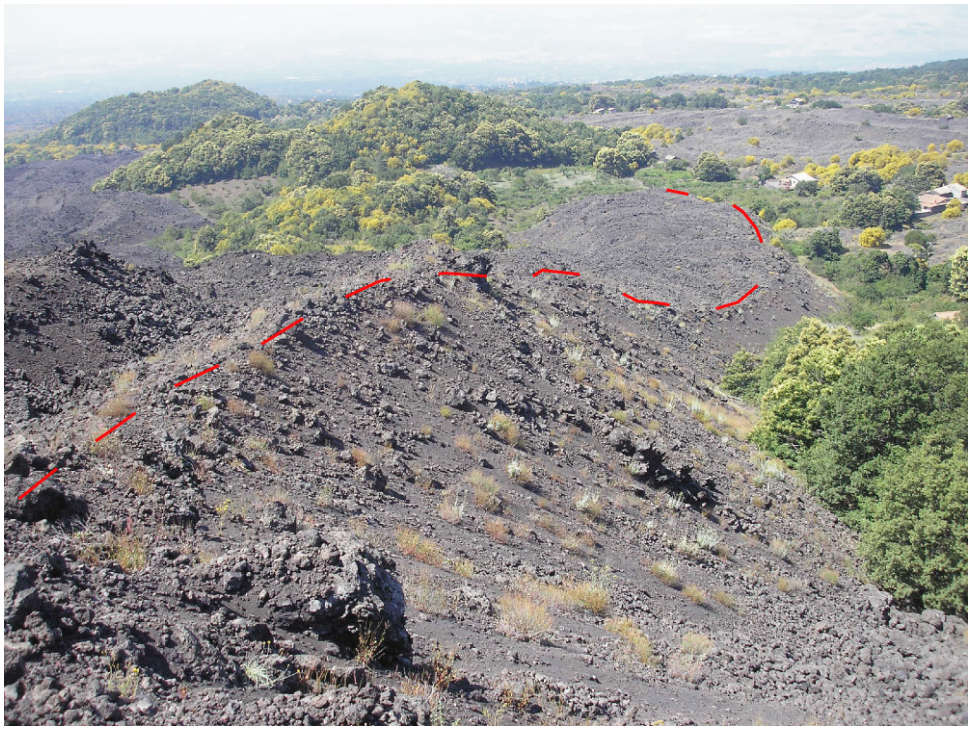

Figure 3.9 – Flow within the 1983 flow-field on Mount Etna. The channel can be observed to curve as the slope decreases from 11° in the foreground of the picture to 8° in the background where the flow font is located (curve outlined in red).

Figure 3.10 – Flow near the summit of Mount Teide, Tenerife. The channel was observed to curve due to a change in slope. The depth of material in the channel was greater on the outer bend of the flow and the corresponding levee was higher (approx. 5 m) than its inner bend counterpart (approx. 4 m).

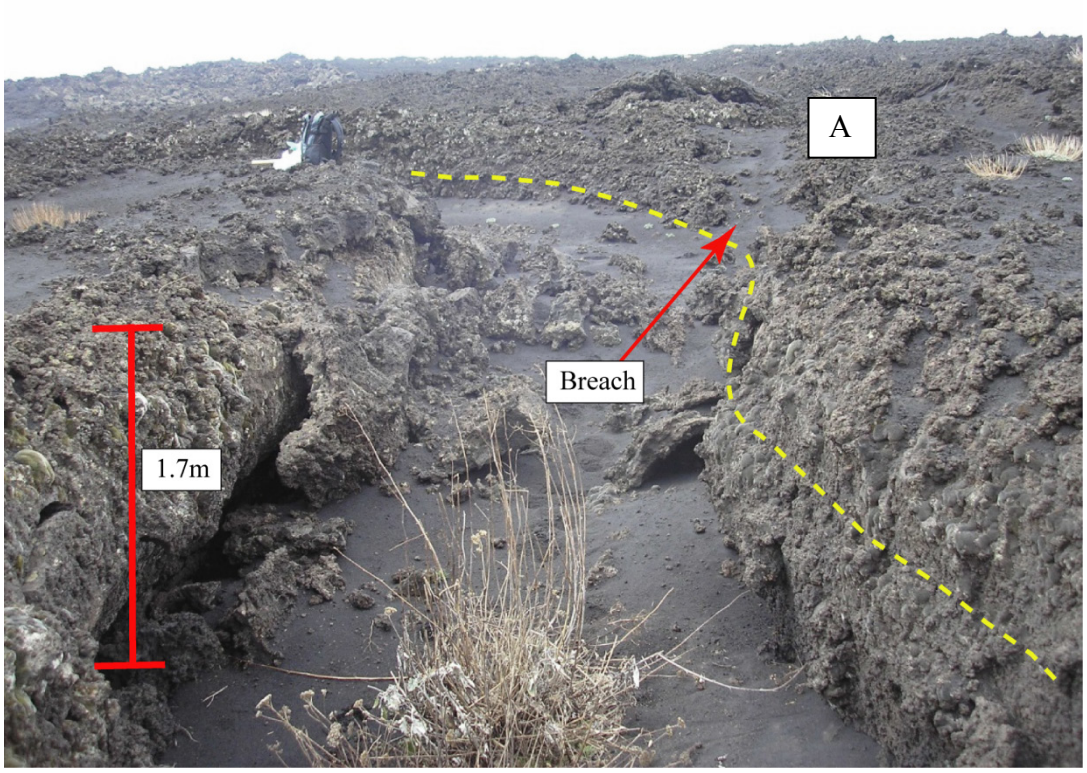

Figure 3.11 - A short section of an exposed flow in the 1983 flow-field on Mount Etna. A breakout (A) can be seen originating from the outside bend of the curving channel marked with the red arrow.

3.2.2 Overflows – Angle to the Original Channel

As expected from the observations in the literature, overflows were found to occur commonly where either channels had become blocked, became narrower or where flows experienced sinuosity. Where an overflow occurred in a sinuous channel, the overflow was found to originate on the outer curve.

Overflows were observed to reach only tens of meters from the original channel before supply ceased. This classifies them as short lived events as no new arterial secondary flow was formed. The angle which overflows made to the original channel was very consistent at almost every site studied with the angle being between 30 - 50^{o} (Figure 3.12). The same was true for secondary flows originating from breaches. The angle that the new arterial flow was emplaced to the initial channel was also found to be between 30 – 50^{o}.

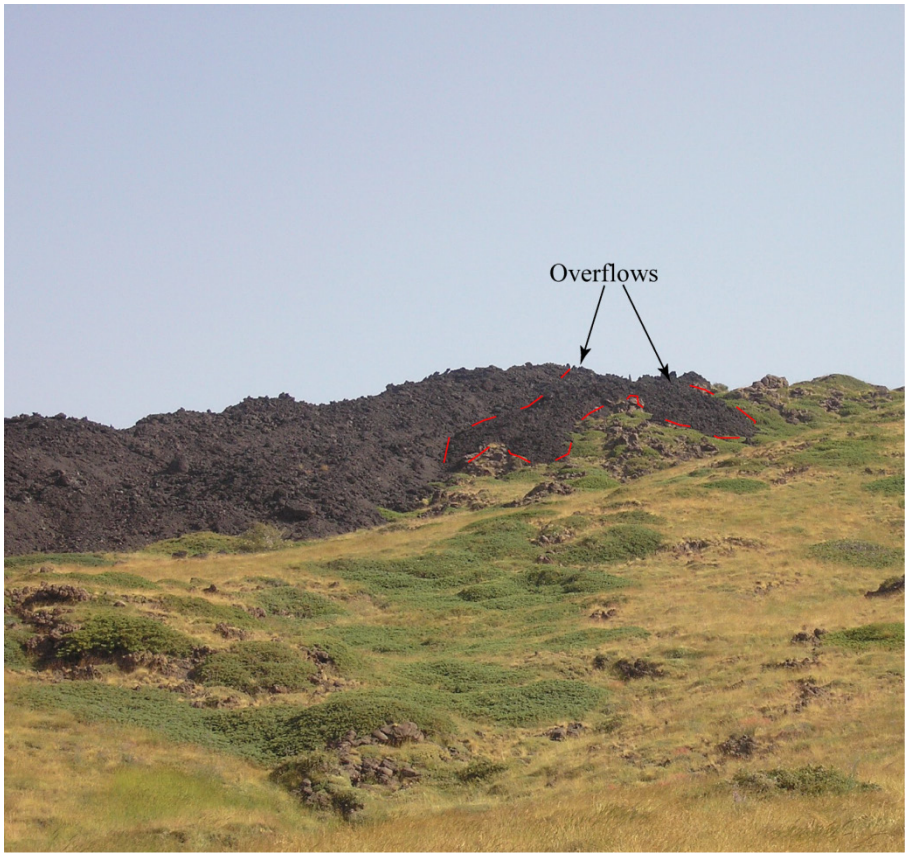

Figure 3.12 – Overflow in a channel in the 2003 flow-field on Mount Etna. This short lived overflow was one of a series propagating down channel that only reached a few meters past the flow margins. They all formed at the characteristic angle of 30 – 50^{o} to the original channel.

3.2.3 Levees – Morphology

The majority of levees observed in the field were either of the active, rubble or overflow morphology. The rubble and overflow morphologies were characterised by the occurrence of auto-brecciated layers of material in the overflow levees and by autobrecciation throughout the structure in the rubble levees. Through road cuts on Mount Etna, it was possible to see that levees do not exist separately from the interior lava flow but are a part of it, albeit slower moving (Figures 3.13, 3.14, 3.15 & 3.16).

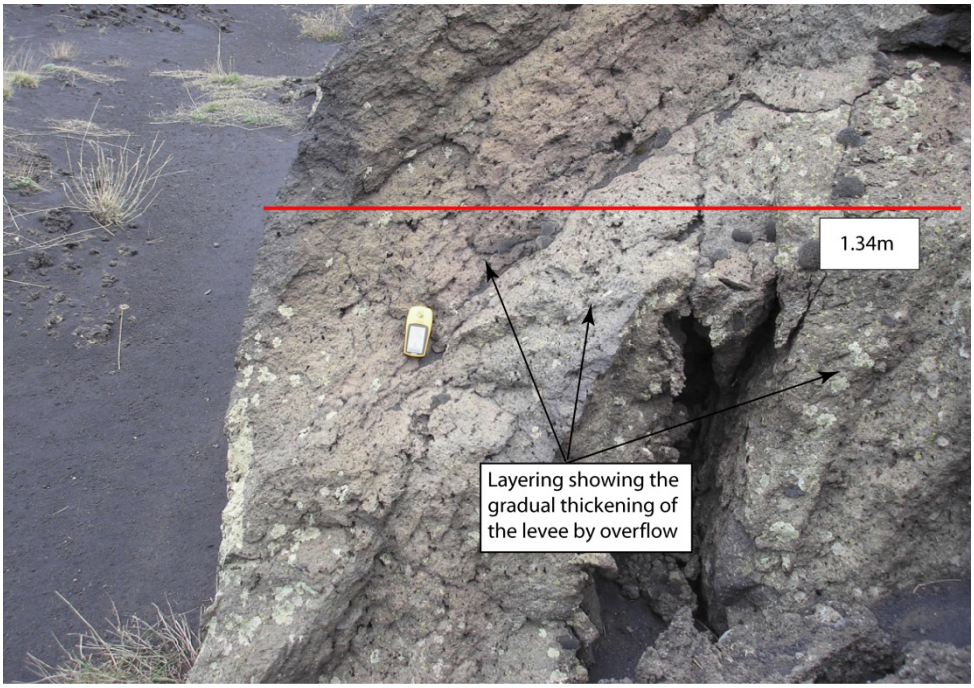

Figure 3.13 – Overflow levee in the 1983 flow-field on Mount Etna displaying the characteristic layered structure.

Figure 3.14 – Rubble levee in the 2003 flow near Lingualagosa at Etna Nord. The levee experienced the same degree of autobrecciation as the flow material.

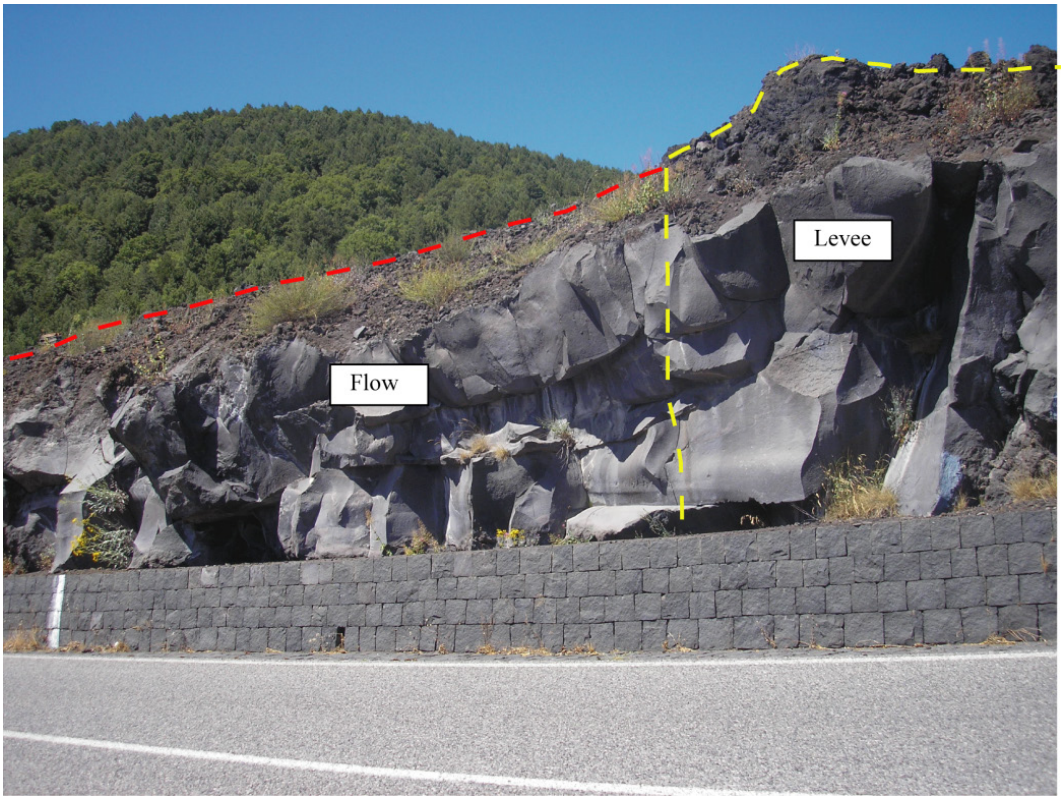

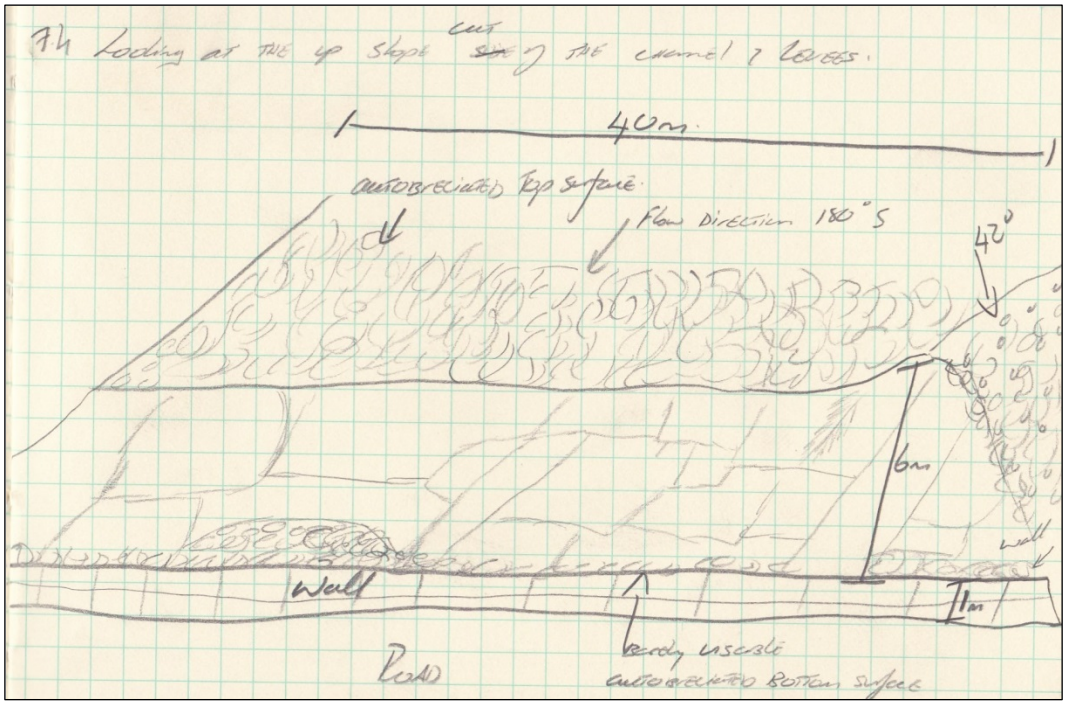

Figure 3.15 – Road cut though a channel/levee in the 1983 flow-field on Mount Etna. In the photograph, the top surface of the infilling flow is marked with the red dashed line and the top of the levee is marked with the yellow dashed line. From above the flow and the levee appear to be separate units but as can be seen from the section the levee and infilling lava are part of a single unit. The field sketch shows the dimensions of the flow and levee.

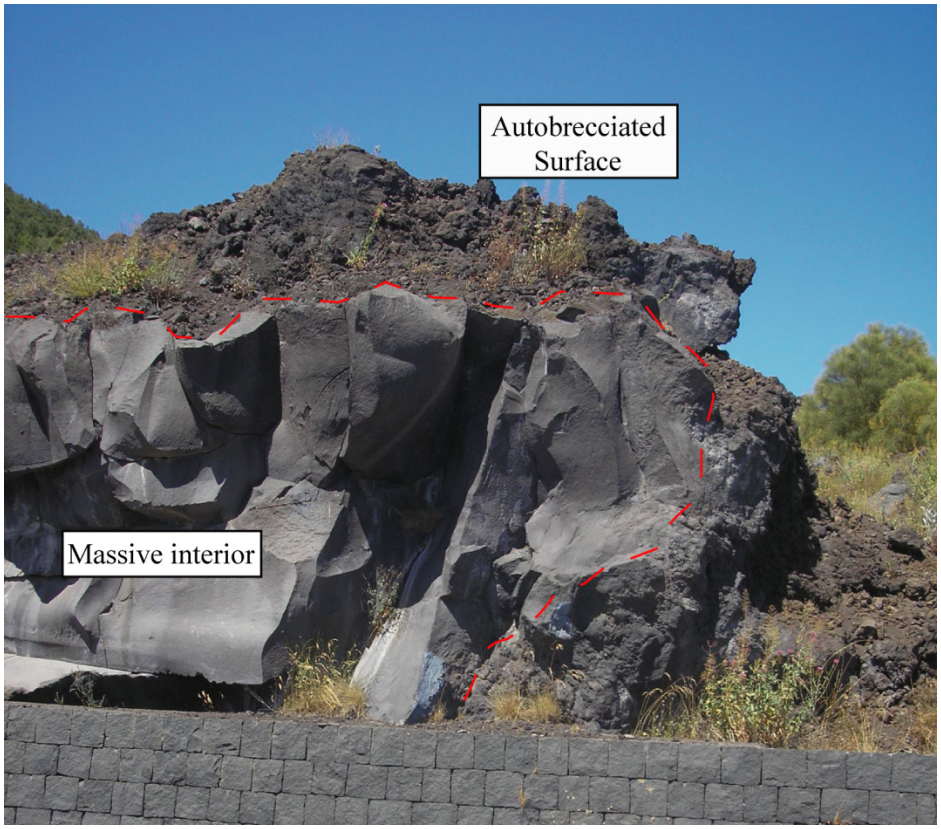

Figure 3.16 – Close up of the section through the levee in Figure 2.30. The interior of the levee is massive whilst the outer surfaces appear rubbly in texture due to autobrecciation.

Levees of the active morphology type were also observed in the flow-fields. These were identified by the existence of protrusions of sheet like lava through the levee. The levees were observed to be bulged or tilted at these locations.

3.2.4 Locations and Mechanisms of Breaching

Predicting the location and probability of a breach is very difficult and there has been almost no research into attempting to define a set of criteria for levee collapse. However, through this study, a number of interesting trends were observed that merit more detailed investigation in the future.

Breaches were found to occur just after a flow had undergone widening e.g. after a slope change or due to slowing down of the flow-front. It was also observed that channels that had become sinuous, typically in the medial and distal parts of the

flow-field, experienced a number of breakouts from the outer curve of a bend (Figure 3.11).

Both of these observations suggest that the angle of applied stress to the levee is an important factor in levee breaching; potentially the changing orientation of the levees or the stress due to widening reduces the strength of the levee and increases its susceptibility to failure.

The angle of slope and the direction of applied stress relating to flow sinuosity seemed to have a much greater control to whether a levee breached or not rather than the actual dimensions and construction of the levee.

A number of different modes of breaching were inferred from the remnant flows and are illustrated in Figure 3.17 (the arrows show the direction of movement of the levee and in C1 & C2, the grey shaded areas referred to a more detailed look at the failure mechanism in the corresponding grey box directly below).

- "Push Translational" illustrated by diagram (A) is a simple mechanism whereby a section of the levee is remobilised and pushed outwards by the lava. The section remains upright and may become incorporated into the new lava flow as a raft or debris.
- "Trapdoor" illustrated in (B) is the mechanism where a fracture forms in the levee and is gradually widened. The momentum of the lava moving toward the breach forces the section of levee directly behind the fracture outwards like a door opening.
- "Toppling" can be split into two variations (C1 & C2) depending on the direction of movement of the remobilised section of levee.– These are also variations on the "Push" mechanism in (A). The force of the lava moving against the levee causes it to topple, forming a

breach. C1 refers to a mechanism where a section of levee topples outwards, away from the channel. C2 refers to a mechanism where the force of the lava is concentrated more at the base of the levee, a section begins to be pushed outwards at the base, causing the levee to become unstable and topple backwards into the channel.

- "Swing" illustrated by diagram (D) is a variation on the push mechanism where the section of remobilised levee is broken into pieces and pushed to either side of the emerging flow.

The mechanisms for A, C1 and C2 are more suitable for active levees where part of the levee has remobilised due to a sheet of more fluid material from the channel being injected into the levee. This may cause the levee to be carried outwards (A) or become unstable (C1 & C2), toppling either forwards or backwards dependent on the levees morphology and centre of gravity. The other mechanisms, B and D are more suited to rubble or debris levees.

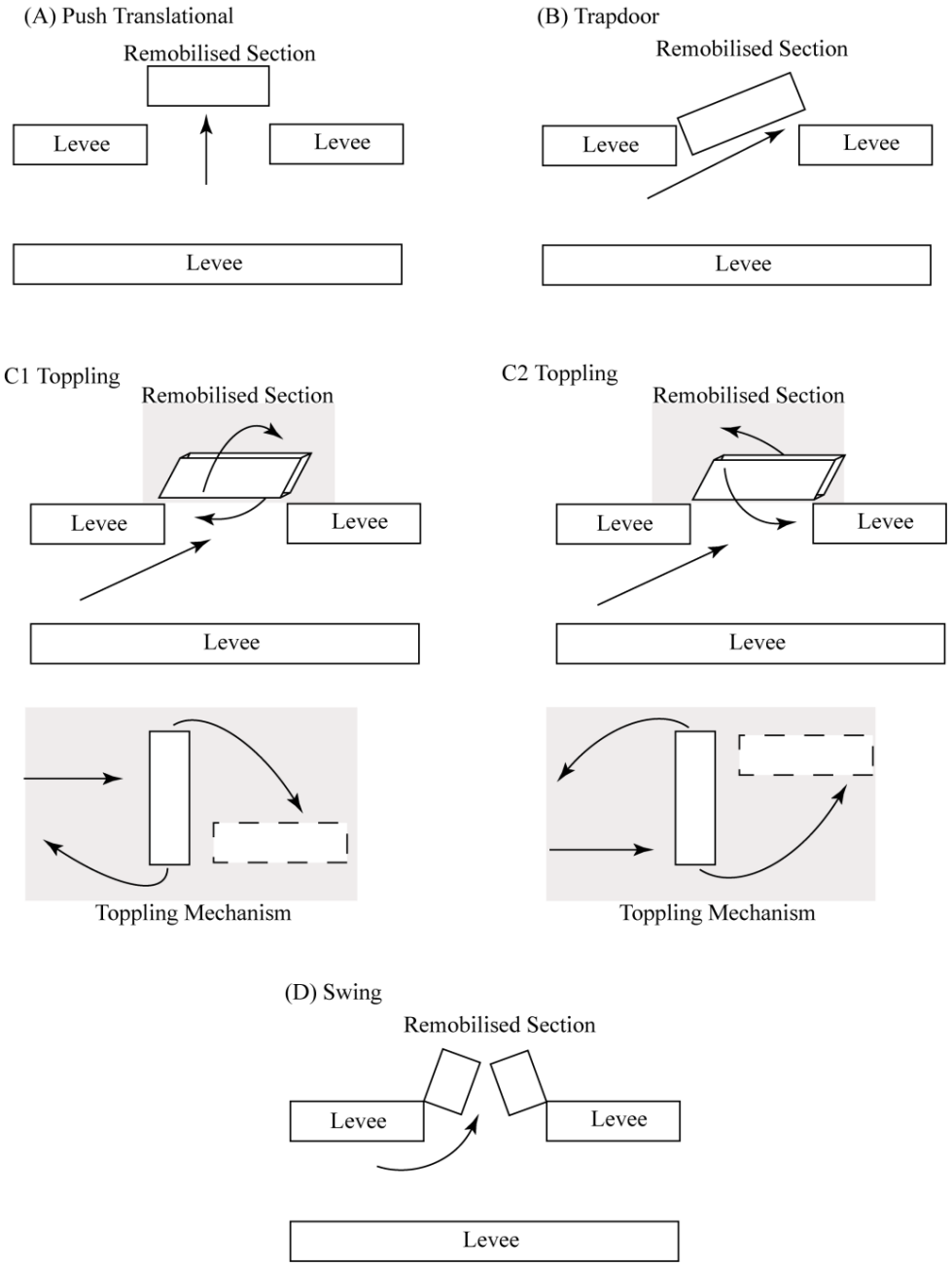

Figure 3.17 – Proposed methods of failure for levees leading to the formation of a breach. Arrows indicate the movement of levees. The grey shaded areas relate to the grey boxes directly below them which show the failure mechanism in more detail. The mechanisms of failure can be broadly categorised into four types (A) Push Translational, (B) Trapdoor, (C1 & C2) Toppling and (D) Swing.

It is difficult to decipher the mode of failure of a levee from the remnant of a flow as evidence for the breach is often buried by subsequent lavas. However, examples of all of the mechanisms described in Figure 3.17 have been observed in the field.

An example of the Push Translational mechanism (mechanism A) was seen in the 1983 flow-field where a small secondary flow developed from a breach in an arterial channel (Figure 3.18). The section of levee that was breached, was pushed directly outward from the main channel and the remnants could be seen, still in the correct orientation in the smaller secondary flow.

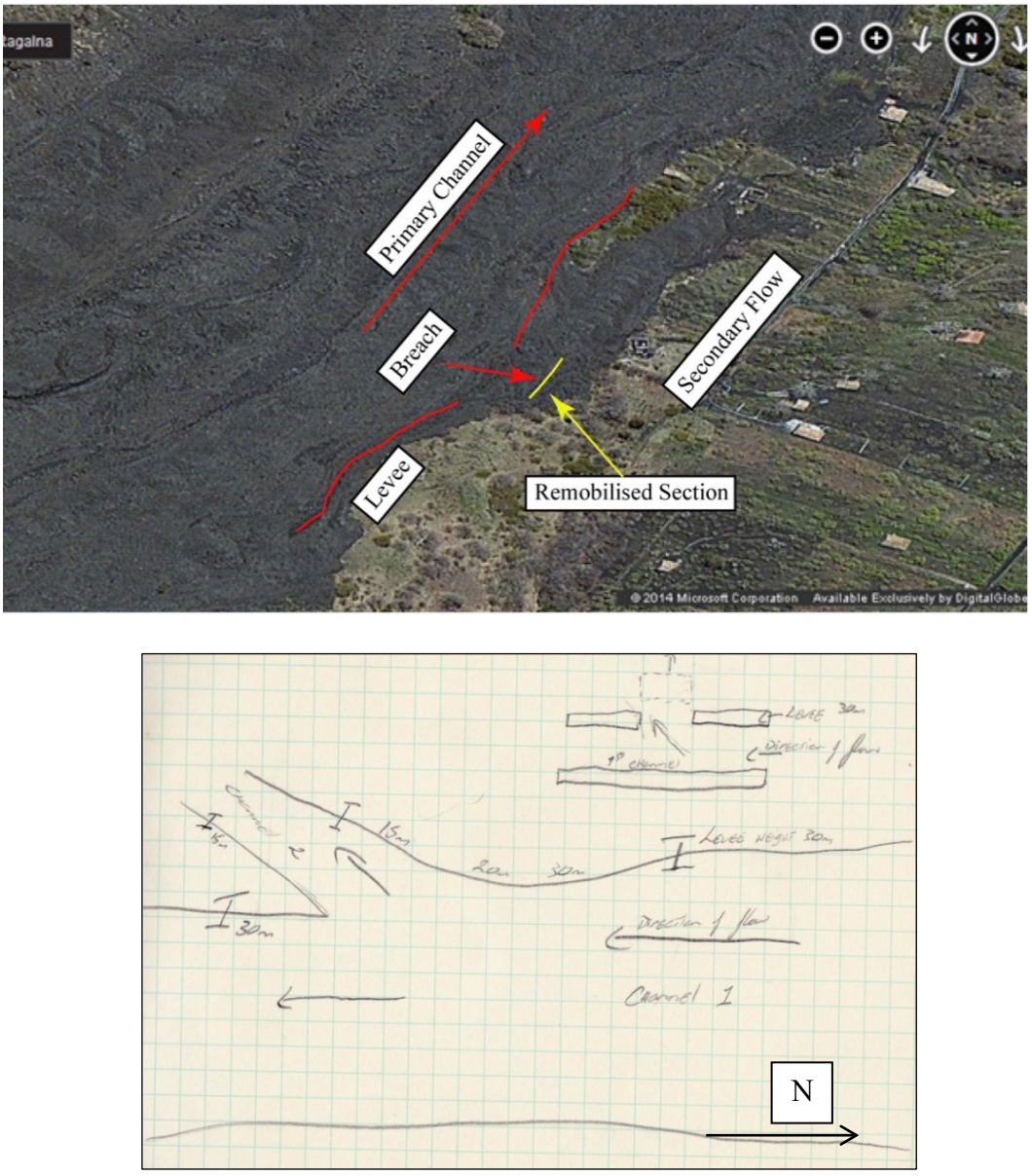

Figure 3.18 – Push Translational. This mechanism describes how the remobilised section of levee is simply pushed forward by the lava exiting the main channel. An example was seen in the 1983 flow-field at the location labelled 2 in Figures 3.2 & 3.3. The annotated Google Earth image shows the relationship between the original channel and the secondary flow. The first field sketch describes the same relationship whilst the second field sketch illustrates the mode of levee failure.

An example of the Trapdoor mechanism was observed in part of the Chinyero flow-field on Tenerife. The section of levee which had been moved to allow the breach to stabilise was visible in the secondary flow (Figure 3.19 & 3.20). The breach occurs where a channel within the Chinyero flow-field passes around a cinder cone from a prior eruption: the original flow is trending 270^{o} to the WSW. When the channel encounters the cinder cone, the orientation changes to 330^{o} NW causing the channel to become curved. The flow is also thicker in the section which abuts the cinder cone. A breach formed in the levee of the outer curve forming a secondary flow which flows around the south side of the cinder cone, whereas the original channel flows to the N side. The original section of levee can still be seen in Figure 3.20, pushed outwards at an angle to accommodate the new secondary flow, giving an example of the trapdoor mechanism for levee failure.

Figure 3.19 – Google Earth image of the breach in the Chinyero flow-field. The lava channel can be seen curving as it meets the cinder cone. The dashed blue line represents where the levee was breached on the outer curve of the bend, forming a two new short-lived secondary flows. The three black arrows show the orientation of the flows. More detail of the relationship between the original channel, the cinder cone and the secondary flow is given in the field sketch.

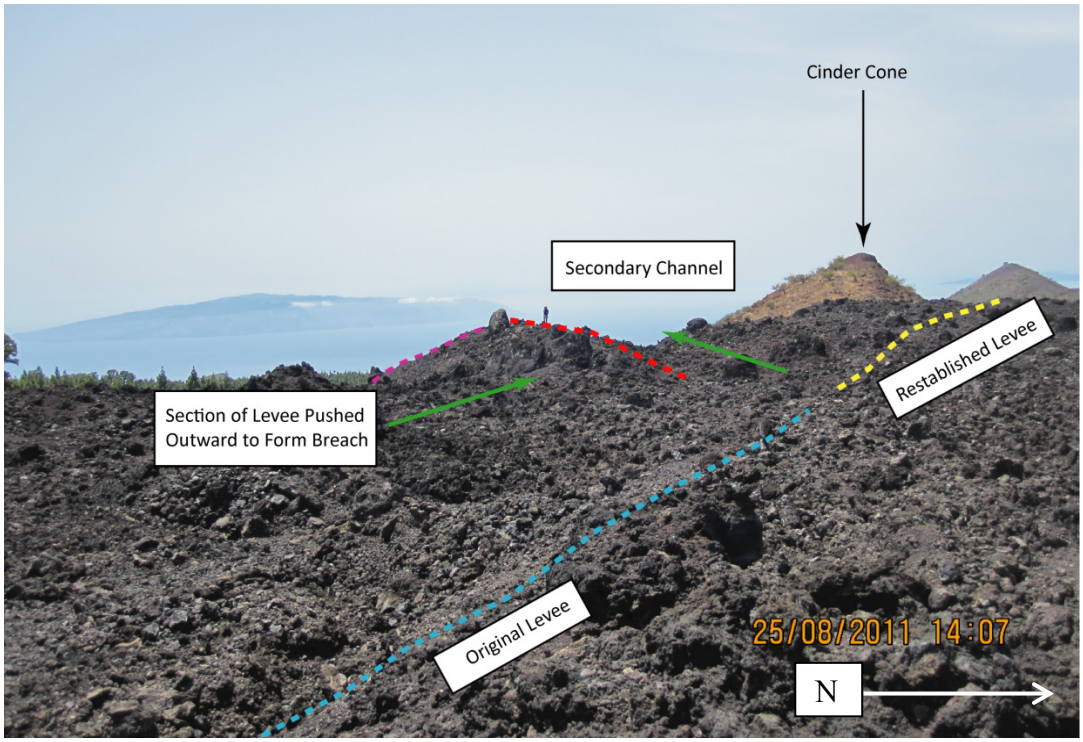

Figure 3.20 – A photograph of the breach in the Chinyero flow showing the same section as the Google Earth image in Figure 3.18. The dashed blue line shows the original levee. The dashed red line shows how the levee was breached and pushed outwards in a single section to allow a secondary flow to form. The yellow dashed line shows the levee that formed after the breach.

The toppling mechanism can take place in one of two ways as described in Figure 3.17, where the lava exiting the channel can topple the levee forward away from the arterial flow or backwards into the main channel. An example of toppling where the remobilised section of levee was toppled forwards was seen in the 1983 flow-field on Mount Etna (Figure 3.21). In this example the levee had not toppled completely but was tilted outwards from the main channel. It was observed that the material leaving the main channel was flowing underneath the levee, causing it to become unstable and topple outwards from the channel. The secondary flow that originated from this breach was small and short lived without well-defined margins.

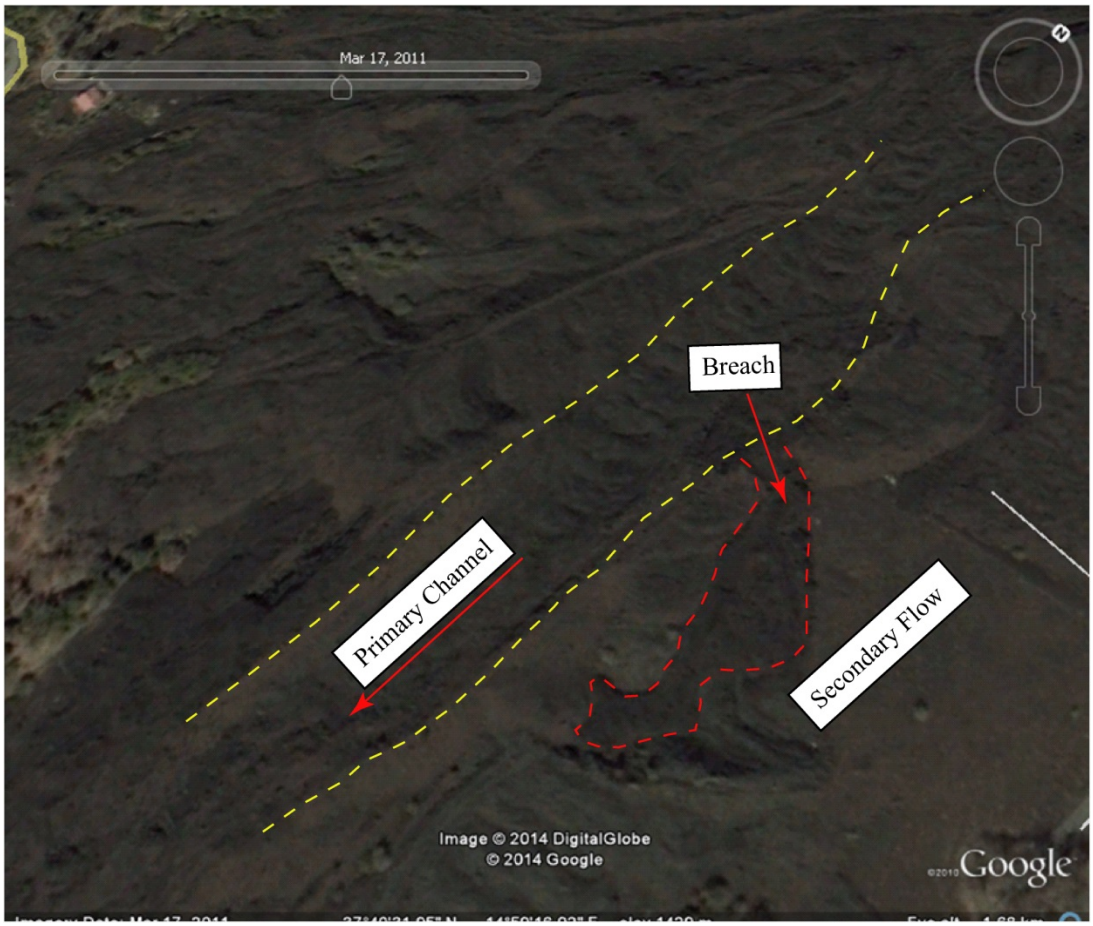

Figure 3.21 – An example of the Toppling mechanism described in Figure 3.17. The levees of the arterial flow are outlined in the dashed yellow line and the direction of flow is shown by the red arrow. The secondary flow is outline in the red dashed line. As can be seen, it did not develop levees and instead had a topographic controlled morphology.

The Swing mechanism describes how the mobilised section of levee breaks during breaching with broken sections being pushed outwards and to the sides by the movement of lava through the breach. An example of this was also observed in the 1983 flow-field on Mount Etna. The breach occurred in a relatively small flow with well-defined margins which had a number of breaches that developed small, short lived secondary flows. In the example shown in Figure 3.22 it can be seen that the secondary flow reached only approximately 50 m from the original channel and did not develop levees. Remnant sections of the original levee were visible in the secondary flow partially covered by the flow.

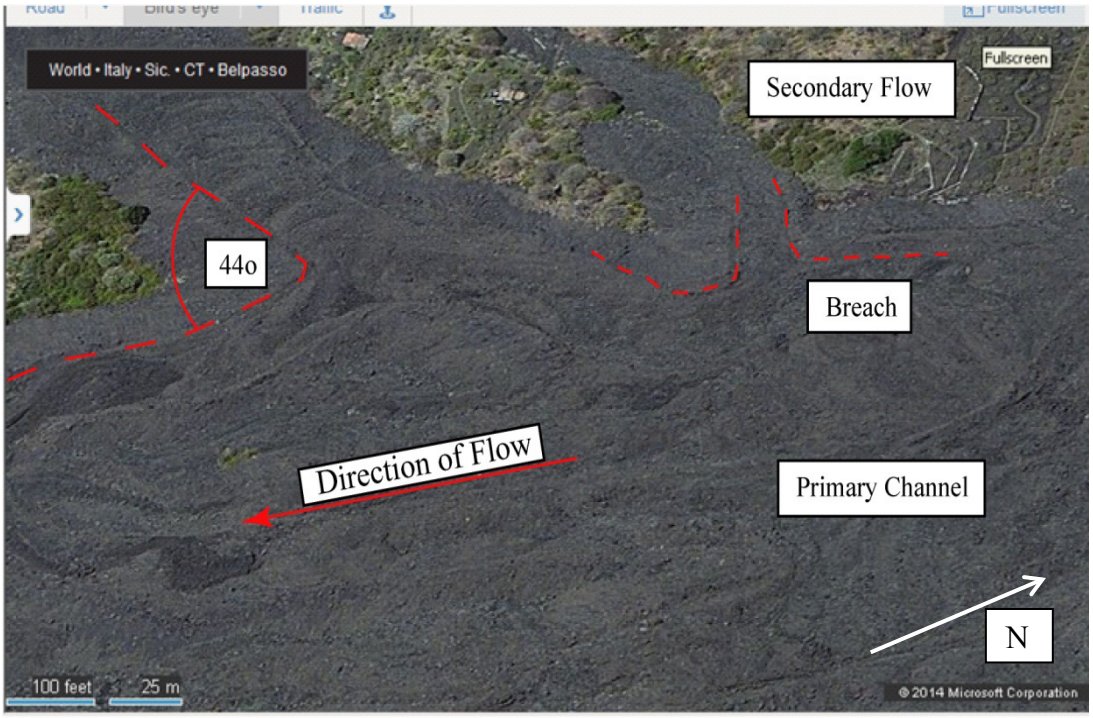

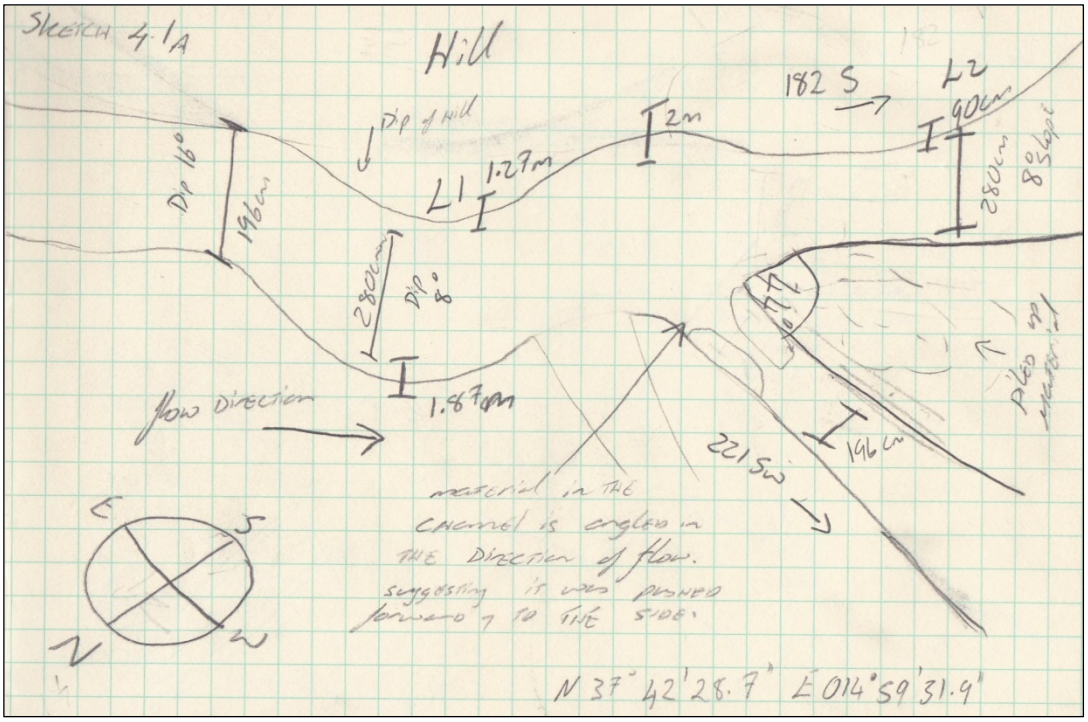

Figure 3.22 – Swing mechanism. This breach took place in a section of the 1983 flow-field below the Rifugio Sapienza which was characterised by a number of breaches along its margin. The breach which occurred via the Swing mechanism is shown in the middle background of the photo with the breach outline in the dashed red line. Also shown in this photo is the angle that another secondary flow made to the original channel. The angle was approximately 44°. The field sketch gives the dimension of the flows and the mechanism of failure for the breach.

3.3 Sample Collection

Samples for rock mechanics and petrological purposes were taken from a variety of locations within field-sites on Mount Etna and the Arenas and Chinyero flows. A list of sampling localities can be found in Appendix A. As the focus of this study was to understand the factors controlling levee breaching and to constrain a range of strengths representative of different levee types, samples were taken from a number of different levee types. Particular attention was paid to collecting samples on or close to breaches in a levee. Where samples were taken on or close to a breach, a further sample was taken from the same levee but at a distance from the breach in order to understand if the mechanical properties of the levee varied in and around the location of the breach.

Samples were also taken from the interior of a massive flow on Mount Etna in order to quantify the difference in strength between flow and levee material. In both field locations, samples were taken from levees constraining basaltic 'a'a flows.

When collecting the samples, the orientation in relation to the direction of flow was marked on each sample so that when they were brought back to the lab to be cored, cores could be taken at different angles to the direction of flow. This was done to quantify the impact changes in the direction of applied stress had on the cores and also the effect orientation of vesicles had on the strength of a sample. The three chosen orientations were parallel to the flow direction, 90^{o} to the flow direction and oblique to the flow direction. It was difficult to core obliquely at an exact angle but all cores were taken between 35^{o} and 50^{o} to the direction of flow.

Given the field observation that breaching seemed to be more common at the outer bends of curved flows, where the mechanical erosion by the material

flowing in the channel would be oblique, it was important to calculate a range of strengths for the levees based on this orientation.

3.4 Summary

The study of flow-fields on Mount Etna and Tenerife have highlighted a number of interesting trends and patterns with flow-field emplacement and the generation of secondary flows through breaching.

- Secondary flows were observed to form at an angle to the original channel (between 30 – 50^{o}) which significantly increases flow-field width and influences the orientation of subsequent flows.
- Changes in slope were observed to cause the flows to become sinuous, which in turn may have influenced the location of secondary flow formation with breaches appearing more common on the outer curve of sinuous flows.
- A number of different failure mechanisms for the levees were identified and described which could help further our understanding of where and how breaches occur.
- The probability of a breach occurring appeared to be independent of the morphology of the levee. Location along a channel combined with the angle of applied stress to that levee appear to be the control on levee breaching.

4 Analogue Modelling

Flow-field growth is dependent on the complex interactions of a number of parameters including volume, cooling rates and topography (Walker et al., 1973; Lopes & Kilburn, 1990; Kilburn & Lopes, 1991). From the moment of eruption, lava begins to lose heat through radiation, particularly on the surface and sides of the flow forming a thermal boundary layer or initial crust. This layer develops strength as it thickens over time, eventually developing into a thick crust which begins to reduce the ability of the lava to flow under gravity favouring the formation of lava levees and other flow structures. Given the limitations of research in the field during an active eruption discussed in Chapter 1, it was decided that an analogue model, should be developed that was capable of reproducing structures observed during fieldwork and investigating their origins by systematically varying the effusion parameters and documenting the evolution of the flow over time. Analogue modelling is a tool used to simplify nature and to facilitate our understanding of complex phenomena. Cloos, (1955) said of his experiments relating to fracture patterns that

"I have presented little that is really new. Experiments have been made ever since the first geologist wrinkled his wife's tablecloth to demonstrate folding".

The first recorded analogue experiment was communicated to the Royal Society of Edinburgh by Sir James Hall in 1815 where he describes a deformation experiment using different types of cloth stacked horizontally, upon which a length of wood was placed to represent rock strata. The cloth pile was then bounded either

side by two vertical sheets of wood which were then hammered together, resulting in uplift of the horizontal wooden layer and deformation in the cloth strata in the form of folds (Koyi, 1997). Analogue models have been used to investigate a variety of geological processes. Applied to lava flows, early models such as the 1792 experiments of James Hall who used a blacksmiths forge to melt basalt (Watt, 1804), focused on qualitative analogue modelling. Initial experiments explored the rheology of lava flows and whether lava exhibited Newtonian or non-Newtonian behaviour. The apparatus and materials used for analogue modelling have become more sophisticated over time as the discipline has developed and analogue modelling has moved from a qualitative to quantitative tool. Many analogue experiments have been performed in order to understand the behaviour of lava flows, a summary table of the key studies, their materials, objectives and primary conclusions is provided in Table 4.1at the end of this section.

As illustrated in Chapters 2 and 3 in addition to the effects of cooling, slope, volume and effusion rate play a significant role in flow morphology. To investigate the effects of these factors, experiments were performed at a fixed ambient temperature (20^{o}C) and angle of slope, volume and analogue material temperature as variables.

The model was intended not to draw direct comparisons between wax and lava but rather be used to facilitate our understanding of the development of structures observed in the field.

4.1 Early Models

A crucial step in any analogue model is to find a material with a similar rheological behaviour as lava. However, there is some debate on the classification

of lava as a Newtonian or non-Newtonian, (specifically Bingham) fluid. Newtonian liquids are the most common fluid type they have no strength and a constant viscosity for which the rate of strain varies in applied shear stress. Examples include water and air. If lava behaved as a true Newtonian fluid, it would flow under gravity until it became pooled in a topographic low or was restrained by a solid crust. Field observations of both static and active flow-fields have demonstrated that lava flows do not behave in this manner. Flows come to rest regardless of topography once supply has ceased and although widths are by no means uniform along the length of a flow; their dimensions are not defined by underlying slope or topography. This, coupled with flow thickness, demonstrates that on eruption, lava does not behave as an isothermal Newtonian fluid.

Viscosity measurements carried out in Makaopuhi lava lake by Shaw (1969) and Shaw et al., (1968) demonstrated that lava exhibited a range of rheological behaviour based on its temperature and composition. For a homogenous melt of constant composition, the behaviour was approximately Newtonian but with the onset of crystallisation, acquired a yield strength that increased with crystal content.

4.1.1 Isothermal Model of Hulme 1974

Hulme (1974) provided the first comprehensive paper to link an analogue and theoretical model of lava flows. He showed that restraint by a cooling crust could not account for the short times observed for lavas to stop spreading and form channels. From a force balance between the hydrostatic pressure during spreading and the resistance due to a surface crust cooling by conduction, Hulme (1974) defined the timescale for a crust of sufficient thickness to halt spreading as:

$$t = \frac{\left(\frac{g\rho}{S_T}\right)^2 . {d_m}^4}{8K} \qquad \text{Eq. 4.1}$$

Where t is time, g is gravity, ρ is density, S_T is tensile strength, d_m is mean flow depth and K is thermal diffusivity.

Equation 4.1 shows that the time needed for crust to halt spreading is proportional to the fourth power of flow depth. Here for a flow 1 m thick, the time taken to halt spreading is less than 30 seconds but a flow 8 m thick will take more than one day. Lava flows on Mount Etna are frequently meters thick and field observations have shown that channel width is fixed within hours (Kilburn & Lopes, 1988), much more quickly than predicted by Hulme's equation. He concluded that the spreading of a flow was controlled by an inherent strength of the lava and proposed a Bingham fluid as a more appropriate rheological model. Robson (1967) also proposed that in the final stage of a flow lava in fact behaves as a Bingham fluid and that the thickness of Etnean flows could be calculated by the formula:

$$h sin\alpha = \frac{S_Y}{\rho g} \qquad \text{Eq. 4.2}$$

Defining that if the stress (ρg) acting on the flow is smaller than S_Y, movement of the flow will cease.

Bingham fluids are characterised by a yield strength that must be exceeded by the applied stress before they can flow. Once the yield strength has been

overcome, the fluid deforms with a constant viscosity (Figure 4.1). The stress-strain rate relation is given by:

$$S - S_Y = \eta \frac{\partial u}{\partial z} \qquad \text{Eq. 4.3}$$

Where: S is shear stress, S_Y is yield stress, $\frac{\partial u}{\partial z}$ is the shear rate and η is the Bingham viscosity.

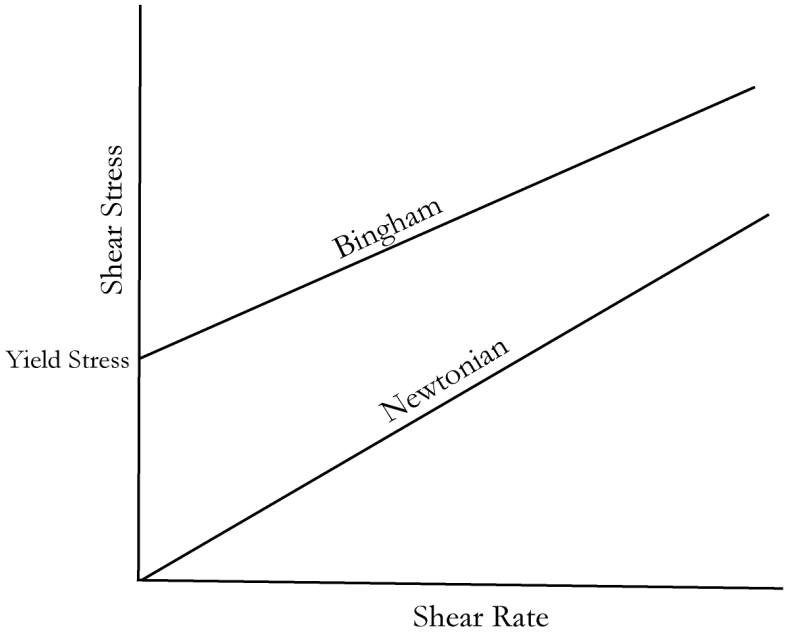

Figure 4.1 – Stress vs. strain rate for Newtonian and Bingham liquids. Redrawn after Hulme (1974).

Hulme's equation states that for a Bingham liquid such as lava, yield stress accounts for the formation of stationary bodies of fluid at the margins of the flow, formed as the lateral spread of the flow decreases until the shear stress is less that the yield strength and that the flow itself will have a characteristic thickness as per Robson (1967).

For a flow over a surface, a fluid with a yield strength will continue to flow only while the basal shear stress for spreading is governed by the decrease in flow

thickness towards its margins. Away from the flow-front, the shear stress downslope increases the local flow thickness and angle of slope. On an inclined plane, therefore, a Bingham fluid will spread until its lateral basal stress has decreased below the yield strength. It will also form stationary margins where the flow thickness is too small for downstream stresses to exceed the yield strength. A yield strength thus favours the formation of fixed channels in which motion is directed downslope between self-made stationary margins.

From a force balance during steady flow, Hulme (1974) related the channel structure of a Bingham fluid to its rheology by:

$$\left(\frac{2}{15}W^{5/2} - \frac{1}{4}W^{2} - \frac{1}{6}W - \frac{1}{20}\right)\left(\frac{1}{Ftan^{4}\alpha}\right) = \frac{(\rho g)^{3}\mu}{S_Y{}^{4}} \qquad \text{Eq. 4.4}$$

Where the terms on the left represent quantities measured in the field and those on the right the physical properties of lava. W is $\frac{Flow\ Width}{2\ x\ Levee\ Width}$, F is flow rate in $m^3\ s^{-1}$ and μ is viscosity.

Hulme tested equation 4.4 using measurements of a kaolin and water mixture on an inclined plane. The inclined plane was completely featureless, so that there was no outside influence on the depth and width of the flow. Kaolin clay particles were suspended in water to give a close approximation to an ideal Bingham fluid. This mixture flowed on to an inclined glass surface through a pipe with a 1 cm diameter (Figure 4.2). Pressure was provided by water in the header tank which was separated from the mixture by the diaphragm. The model produced

leveed flows and showed that the rate of lateral spreading became negligible within 10 cm from the point of effusion.

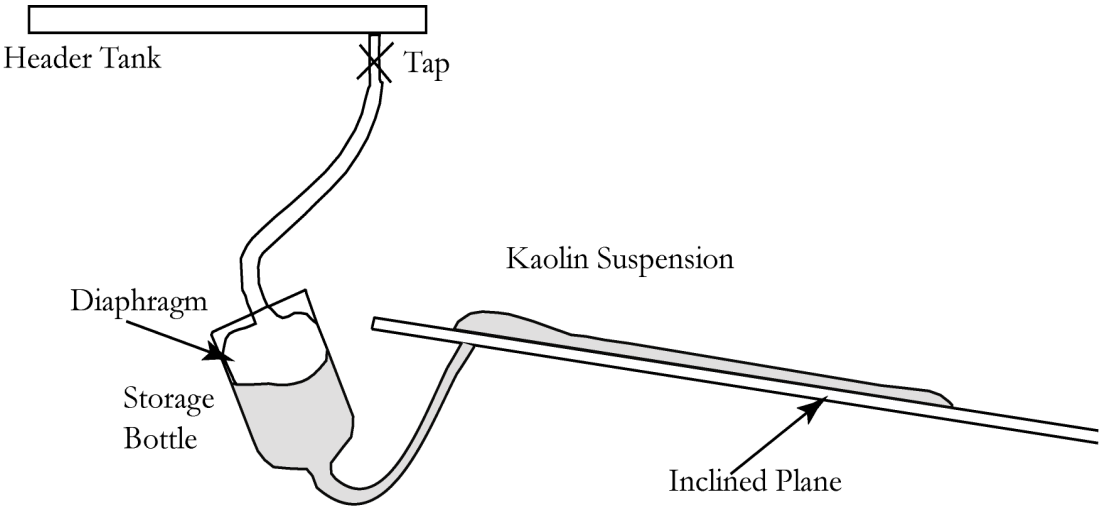

Figure 4.2 - Hulme's experimental apparatus. The wax (grey) was allowed to flow under gravity on to an inclined glass plane. Redrawn after Hulme (1974).

Hulme's experimental results showed that equation 4.4 could be used as a first approximation to relate the channel structure of a flow to its rheological properties. He acknowledged some discrepancies between the measurements of the kaolin mixture and the predictions of the equation and attributed these to uncertainties with the experimental measurement. Levee widths varied throughout the flow and in the case of multiple levees, only the outer most set were measured. However, the data from the experimental model were in the same order of magnitude as the predictions from the equation. Hence Hulme proposed that the final dimensions of 'a'a lava channels could be used to infer rheological properties. However, there were some inconsistencies with the field data, some of which could be attributed to poor data on the rheological properties of the flows studied and others which could be attributed to cooling and its importance in the structural

evolution of lava channels which Hulme's model did not account for. Hence the need for additional models which incorporate the effects of cooling.

4.1.2 Non-isothermal Analogue Models

Other studies (Hallworth et al., 1987; Fink & Griffiths, 1990, 1998; Griffiths & Fink, 1992a, 1992b, 1993; Stasiuk et al., 1993; Gregg & Fink, 1995; Blake & Bruno, 2000; Garry et al., 2006; Miyamoto & Crown, 2006; Robertson & Kerr, 2012) have focused on parameters such as cooling, effusion rate, viscosity and underlying slope angle as the primary controls on flow morphology by using materials with a temperature dependent rheology as analogues for lava.

Hallworth et al., (1987) investigated cooling effects using PEG (polyethylene glycol) wax. The wax has Newtonian rheology above the liquidus and has a temperature dependent rheology. The modelling apparatus was similar to Hulme's in that it involved the effusion under gravity of the analogue material from a suspended reservoir on to an inclined glass plane. However, in contrast to the methodology of Hulme, Hallworth et al., (1987) designed their apparatus so that the wax was effused under water in a flume tank to lessen the effects of surface tension on flow behaviour. Three suites of experiments were conducted to model the effects of effusion rate, slope angle and temperature flow morphology. In order to investigate the effects of effusion rate on morphology, ten experiments were run with a varied effusion rate (Q) $cm^3\ s^{-1}$ at a constant slope (15^o) and effusion temperature (50^oC) and the results classified into three morphologically distinct categories.

The high effusion rate experiments where $Q \geq 3\ cm^3\ s^{-1}$ produced simple flow-fields with straight open channels, approximately 10 cm in width with low

aspect ratios which were bounded by flat, smooth levees. The intermediate effusion rate (3 cm^3 s^{-1} < Q > 1.5 cm^3 s^{-1}) experiments generated flow-fields with narrower channels (4 cm) and wider levees. The lower effusion rate meant that solidification at the flow-front had the effect of retarding the forward advance of the flow-front, causing the channel in the medial section of the flow to thicken until the wax either overflowed or broke through the channel margins to form a new flow. Several flows were produced during individual experiments leading to the development of a compound flow-field. The channels developed a weak sinuosity and at the point of inflection; the levees tended to be thicker on the inner wall.

Low effusion rate experiments (Q < 1.5 cm^3 s^{-1}) produced the most morphologically complex flow-fields, with the narrowest channels (1 cm). The levees bounding the channels had a higher aspect ratio than those in the other two flow regimes. The channels quickly developed a flow-front with a chilled crust that inflated as wax continued to move down channel resulting in a raised hummock at the front which the authors likened to tumuli. This stagnant flow-front resulted in channel thickening until overflows or breakouts occurred either from the inflated flow-front or in the medial portion of the flow, a process which repeated itself many times, resulting in the development of a complex flow-field (Figure 4.3).

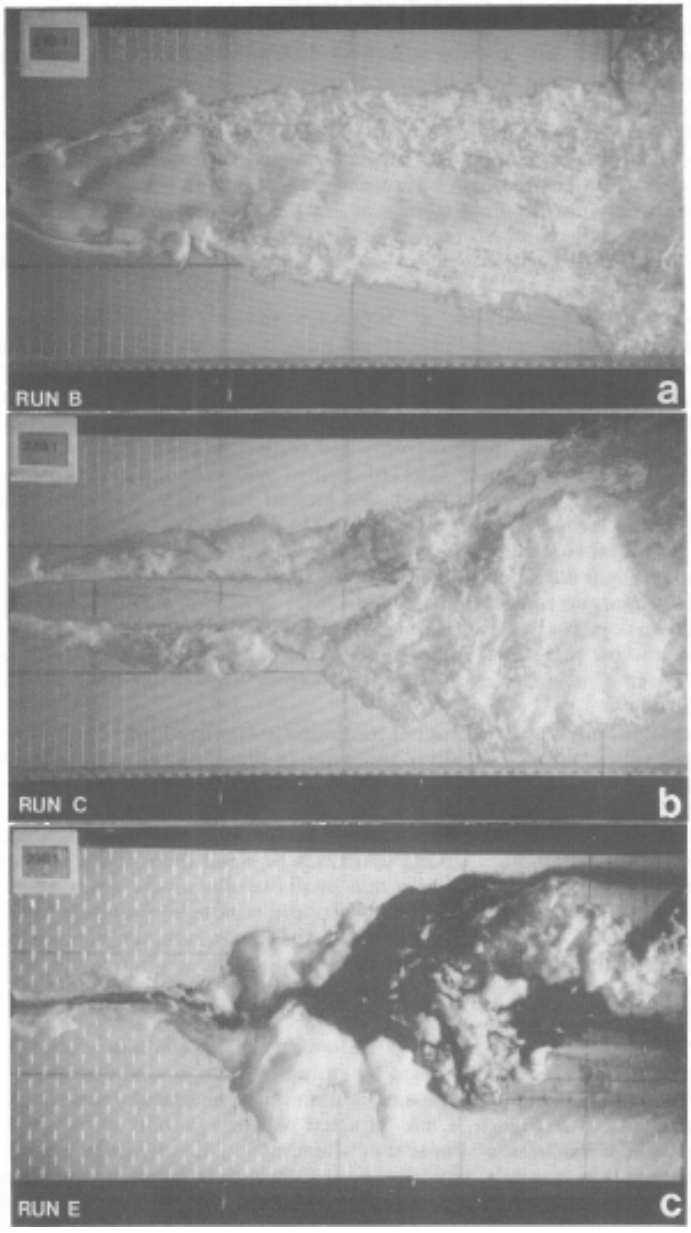

Figure 4.3 – Plan view photographs of flows which are representative of the morphologies produced by high effusion rate (A), medium effusion rate (B) and low effusion rate (C) experiments. From Hallworth (1987), plate II.

The experiments were carried out at ambient room temperatures between 40^{o}C and 60^{o}C. Lowering the temperature favoured faster rates of increase in the wax viscosity, the more rapid growth of a strong frontal crust and slower rates of flow advance. In combination, therefore, lower temperatures favoured channels with higher aspect ratios and the growth of more complex flow-fields, whereas

higher temperatures favoured channels with lower aspect ratios and the growth of simple flow-fields.

As the slope angle was increased from 15^{o} to 30^{o}, the flow propagated more quickly downslope in straight open channels. Crust on the top of a flow was fractured more easily and carried down a channel by the momentum without the breaching of levees.

Hallworth et al., (1987) concluded that flow morphology and channel distribution are controlled by solidification of the flow-front. When the wax interior had insufficient momentum to break though the crust, the medial portion of the channel would experience thickening, leading to breakouts, overflows and the development of a multi-channel system. When the flow momentum was sufficient to break up the developing crust and overcome any blockages in the channel, the flows developed wide, straight channels, bounded by levees with a low aspect ratio. Qualitatively, therefore the experiments demonstrated that the development of complex multi-channel flow-fields was promoted by lower effusion rates, ambient temperatures and angles of slope.

4.2 Incorporation of Scaling in Wax Models

Fink & Griffiths (1992) and Griffiths & Fink, (1992a) extended the qualitative analysis of Hallworth et al., (1987) by quantifying regimes of flow-field emplacement in terms of thermal and dynamic criteria. Their experiments followed the design of Hallworth et al., (1987) but PEG wax was injected into a sucrose solution instead of water. The use of sucrose reduced the density contrast with wax. The wax was pumped at a constant flow rate through a point source onto the floor

of the tank in order to investigate the effects on flow morphology of basal roughness, effusion rate, temperature and slope.

The rate of crustal growth depends on the rate of advection within the flow and the effectiveness of heat removal from the flow surface (Fink & Griffiths, 1990; Kilburn & Lopes, 1991). Stresses acting on the crust will cause it to deform, giving rise to characteristic surface morphologies. Griffiths & Fink (1992a, 1992b) expressed the influence of cooling and supply rate in terms of the timescale ratio:

$$\Psi = t_s/t_a \qquad \text{Eq. 4.5}$$

Where t_s is the time for the wax to solidify after leaving the source and t_a is the timescale for the lateral advection of viscous fluid. The advection timescale is given by:

$$t_a = \left(\frac{\mu}{\rho g\left(1-\frac{\rho a}{\rho}\right)}\right)^{\frac{3}{4}}\left(\frac{1}{Q}^{\frac{1}{4}}\right) \qquad \text{Eq. 4.6}$$

Where ρ and ρa are the density of the wax and ambient fluid, μ is the wax viscosity, g is acceleration due to gravity and Q is the effusion rate.

Experiments onto a horizontal surface showed that lowest effusion rates or solution temperatures, where Ψ is < 0.65, caused crust to form immediately upon effusion. The wax formed a dome or lobe with no other structures visible. The pressure exerted by wax accumulating underneath the solidified crust caused the

crust to fail allowing a small amount of wax to flow from the lobe. The molten wax quickly developed a solidified skin forming a new lobe. Flow advance thus occurred through successive breakouts and new lobe formation.

At higher effusion rates, corresponding to $0.65 < \Psi < 2.8$, crust began to develop at a distance from the vent, propagating backwards over time. The crust was unable to form one coherent unit due to the shear stress being applied by the molten wax flowing underneath, forming rifted areas that are morphologically similar to transform faults at areas of mid-ocean spreading centres.

Increasing the effusion rate for $2.8 < \Psi < 6.5$ resulted in crust developing radially from the source in narrow strips that experienced surface folding in the direction of flow as a result of compression. At $\Psi > 6.5$, surface crust developed only in the most distal portions of the wax flow. In some cases, crust development was sufficient to form a continuous, solid barrier or levee around the circumference of the flow, ponding the more fluid wax. These levees were frequently overtopped. At the highest values of Ψ, insufficient time was available for crust to form before the wax flow reached the side of the tank.

The experiments of Griffiths & Fink (1992a, 1992b) were later extended to investigate the influence on flow development of surface roughness (Griffiths & Fink, 1993) and changes in slope (Gregg & Fink, 2000). In a further analysis of their experimental results Griffiths & Fink (1993) describe that, once effusion had ceased, flows with the lowest cooling rate, (without a significant crust), continued to spread laterally and thus behaving like a Newtonian fluid. For experiments where $\Psi < 0.65$, and the wax advanced in a series of lobes, breakouts from the lobes were observed after effusion had ceased. The authors theorised that the breakouts resulted from the overpressure within the lobe exceeding the tensile strength of the

crust and that overpressure was a significant parameter for flows containing lobes. It was also observed that in flows with a high Ψ number > 0.65, the flows reached their maximum length and radius quickly and had smaller depths than flows with a low value of Ψ. All values of Ψ are from Gregg & Fink (2000) which have been altered from the original study by Fink & Griffiths (1990) to correct an error in their equation.

The experimental run also included some preliminary investigations into the effects of slope and basal roughness on flow morphology. On a slope of 6.5^{o}, under the same variations of effusion rate as the previous experimental suite, the morphology of the flow became, to differing degrees, asymmetric in the downslope direction, but the types of surface features formed remained unchanged. For experiments incorporating basal roughness, a wire mesh was placed on the floor of the tank.

For a given set of parameters, the model consistently reproduced morphologically similar flows. Progressively decreasing the temperature of the sucrose solution and therefore increasing the cooling rate, lead to the development first of levees, then rift zones, surface folds and finally lobes in agreement with the work of Fink & Griffiths (1990) and Gregg & Fink (1995). The same sequence of morphologies was created by decreasing the effusion rate, demonstrating that flow behaviour and morphology are therefore strongly influenced by cooling rates and the development of surface crust. Griffiths & Fink (1993) used a scaling analysis to support the hypothesis that crust development is the dominant parameter controlling flow advance when the ratio of crust thickness to flow length is greater than the ratio of the crust's yield stress to the basal shear stress acting on the bulk of the flow.

The greater effusion rates resulted in smaller flow depths supporting the theory that the effective thickness of strong crust increases with time (Griffiths & Fink, 1993). These results were supported by the work of Stasiuk et al., (1993) who found that channel depth increases with time and cooling. For experiments where crust had developed, spreading stopped immediately once effusion had ceased. This suggested that cooling resulted in the fluid change of behaviour from the Newtonian to Bingham, this last factor being a major control on flow propagation.

Gregg & Fink (2000) developed further the effect of slope on the PEG models of Griffiths & Fink (1993). Experiments were carried out on slopes of between 0^o and 60^o in 10^o degree increments. The model produced the same four morphologies as the previous experiments of Fink & Griffiths (1990, 1992), Gregg & Fink (1995) and Griffiths & Fink (1992a, 1993) which were carried out on a horizontal surface. This study confirmed the observations of Griffiths & Fink (1993) that at small slope angles < 6^o, the effect on flow morphology is negligible although they also state that the morphology of flows with a lower viscosity were more affected by increased slope while high viscosity flows showed almost no change in behaviour. Effect of increasing the slope up to 30^o was to reduce the value of Ψ need to produce certain morphology. On slopes of 40^o to 60^o the opposite trend was identified: the value of Ψ for a particular morphology was increased, a trend which was attributed to effect of gravity becoming the dominant parameter controlling morphology as opposed to crust controlled spread. Therefore Gregg & Fink (2000) propose that the morphology of a flow channel is best described using the original Ψ classification of Fink & Griffiths (1990) combined with underlying slope angle.

4.2.1 Compound Flow-Field Models

Blake & Bruno (2000) followed the experimental methodology of Fink & Griffiths (1990, 1992) and Griffiths & Fink (1993) to examine the conditions under which breakouts occur and compound flow-fields develop. They found that breakouts occur on a time scale which is proportional to the product of fluid viscosity and effusion rate divided by the strength of the crust squared.

For radial spreading over a horizontal surface, the time t_{crust} for advance to be controlled by the crust is given by;

$$t_{crust} = \frac{g\Delta\rho\mu Q}{\sigma^2 s^2 k} \qquad \text{Eq. 4.7}$$

Where g is acceleration due to gravity, Δρ is the density contrast between the wax and water bath, μ is viscosity, Q is effusion rate, σ is the yield strength of solidified crust, s is a constant of order 1 whose value depends on the details of the thermal exchange between the lava and its environment and the thermal boundary conditions and κ is the thermal diffusivity of the lava.

After t_{crust} has been exceeded, the flow propagates by the deformation of weak spots within the crust, which rupture to form breakouts. Therefore t_{crust} can be defined as the time at which even radial spreading changes to the formation of an irregular margin due to the development of breakouts and flow lobes.

For all experiments, the wax initially spread radially from the point source. After a critical time (1-16 sec) crust began to develop, either around the circumference or on the surface of the flow. Except at very high effusion rates, (Q =

3.5 cm^3 s^{-1}) the crust was either overtopped or ruptured, so that the flow continued to spread in an irregular manner. The liquid wax formed a new lobe which developed crust, which was itself ruptured forming a successive lobe. This process repeated itself for the duration of the experiment resulting in the development of a network of overlapping lobes and the growth of a compound flow-field. Breakouts formed more frequently during low effusion rate experiments which are morphometrically comparable with the $\Psi < 0.65$ experiments of Gregg & Fink, (1995) and Griffiths & Fink (1993). For experiments with a higher effusion rate ($2.8 < \Psi < 6.5$) lobes were observed to be broader and flatter. Blake & Bruno (2000) also showed that the same ratio is true for flow-fields as a whole, field length increases with increased effusion rate and/or angle of slope i.e. on a given slope flows with a higher value of Ψ reach greater lengths. This ratio is also seen in the natural system where Wadge & Lopes (1991) state that lava channels were observed to be narrow with increasing angle of slope. The results of Blake and Bruno's model also correlates with the work of Walker et al., (1973) who stated that low effusion rates favoured the development of compound flows.

4.2.2 Modelling Small-Scale Flow Morphologies

While the studies discussed have investigated the overall morphology of flow-fields, few have focused on the micro-scale processes that give rise to the gross field morphology. Miyamoto & Crown (2006) considered the development of lobes in pahoehoe flows in terms of their cooling histories. Having identified that lobe behaviour is crust controlled, they hypothesise that successive lobe formation is a result of fracturing of lobe crust due to the change in pressure caused by the liquid lava being confined by crust. In order to test their hypothesis, they developed

a model that used an analogue material – paraffin wax – which develops surface crust on cooling. The methodology was similar to that of Fink and Griffiths where paraffin wax was extruded onto an inclined plane from a point source. It was observed during the experiments that the development of crust led to halting of the flow-front causing inflation of the channel behind the static margin. Inflation was not equally distributed throughout the flow-field, with the majority occurring at the flow-front. The point of greatest inflation did not correlate with the location of breakouts indicating the presence of weak spots within the crust and that the strength of the crust in terms of its resistance to fracture can only be defined as its weakest point. Given the complexities of quantifying the rheological behaviour of the crust at temperatures above its liquidus, a constant was assumed for the tensile strength of weak spots. Therefore the inflation required for the crust to fail Δh was defined as:

$$\Delta h \sim \frac{\beta \delta}{D \rho g} \qquad \text{Eq. 4.8}$$

Where β is the tensile strength of the crust, δ is thickness of surface crust, D is the radius of the cross section which is assumed to be semi-circular, ρ is density and g is acceleration due to gravity.

The results of the paraffin wax experiments gave good agreement with the values predicted by the equation.

4.2.3 Summary

The previous studies have demonstrated that analogue models are a useful tool to model large scale, complex natural phenomena in a controlled and systematic manner. A summary table outlining the primary objectives and conclusion is given in Table 4.1. In particular they provide insights into understanding the interactions between parameters such as cooling, slope and rheology and the control they have on flow-field morphology.

The models (Fink & Griffiths, 1990; Griffiths & Fink, 1992a, 1992b) showed that increasing the effusion rate resulted in crust first developing further away from the source of the wax, and that flows had smaller depths and few breakouts. Increasing the rate of cooling by decreasing the ambient temperature, produced levees, rifts and lobes (Fink & Griffiths, 1990; Gregg & Fink, 1995). The same sequence of morphologies was created by decreasing the effusion rate, demonstrating that flow behaviour and morphology are strongly influenced by cooling and the development of surface crust. Increasing the angle of slope was found to have a similar effect as to increasing the effusion rate (Gregg & Fink, 2000).

Table 4.1 – Summary of previous analogue models.

Authors	Analogue Materials	Rheology	Environment	Objective	Primary Conclusions / Outcomes
Allen, J. 1966	Plaster of Paris	Newtonian Fluid	Sub-aerial	Flow Visualization	Obstruction in a channel results in strong curvature as the flow seeks to avoid the high pressure region upstream of the obstruction
Hodgson, G.W. 1969	Carbowax (PEG wax)	Newtonian Fluid	Sub-aerial	To investigate the effect of slope, extrusion rate, volume, viscosity and temperature on lava flow morphology	PEG waxes have merit in modelling lava flow emplacement but demonstrate highe surface tension forces lavas resulting in delayed formation of flow characteristics
Dragoni et al., 1986	Bingham Fluids	Bingham Fluid	Sub-aerial	Studying the effects of varying flow parameters such as slope and effusion rate on flow height and velocity as a function of flow rate	Assuming lava behaves as a Bingham flu flow heights are independent of flow rate and therefore changing effusion rate resul in a change of velocity only
Hallworth et al., 1987	PEG	Newtonian Fluid	Under Water	Modelling the effects of controlled variation in slope, temperature and effusion rate on morphology	Study modelled in the emplacement of compound flow fields using dyes to distinguish the chronology of flow-field growth.
Fink & Griffiths 1990	PEG	Newtonian Fluid	Under Sucrose Solution	Modelling the effect of solidifying crus on the processes and resultant morphology of viscous gravity current	The dynamics of the current is controlled by the relationship between extrusion rate and cooling. Decreasing the extrusion rat produced the same morphologies as increasing the cooling rate.
Griffiths & Fink 1992 (a)	PEG	Newtonian Fluid	Under Sucrose Solution	Identifying extrusion rate as the primar controlling factor in submarine flow morphology	Extrusion rate is the primary flow paramet in determining flow morphology.

Authors	Analogue Materials	Rheology	Environment	Objective	Primary Conclusions / Outcomes
Griffiths & Fink 1992 (b)	PEG	Newtonian Fluid	Under Sucrose Solution	Using analog experiments to infer spreading and cooling rates for planetar	Validates the Fink and Griffiths 1990 mod
Griffiths & Fink 1993	PEG	Newtonian Fluid	Under Sucrose Solution	To model the effect development of a crust has on the movement of lava flow and domes	Crustal strength was the primary control i controlling movement of the wax flows.
Stasiuk et al 1993	Glucose Syrup	Newtonian Fluid	Under Aqueous Solution	To determine the effects of cooling on flow dynamics of fluids with a temperature dependent viscosity	Cooling results in steeper and thicker flow fronts, leading to gravitational instability which can result in avalanching at the fro
Gregg & Fink 1995	PEG	Newtonian Fluid	Under Sucrose Solution	Investigating the effect of slope, extrusi rate, volume, viscosity and temperature on submarine lava flow morphologies	Under laboratory conditions, low effusion rates & slopes and high cooling rates resu in pillows. Varying these parameters resulted in the formation of other morphologies including rifts, lobate flows folded flows and lineated flows.
Fink & Griffiths 1998	Kaolin Powder Suspended in Liquid PEG	Bingham Fluid	Under Water	Investigation into the morphology and rheology of lava domes	Definition of a classification system for la domes and silicic lava flows, relating morphology to rheology and cooling histo
Merle 2000	Silicone Gel	Newtonian Fluid	Sub-aerial	Investigate internal strain within lava flows	Analysis of bubble deformation and vesic foliations with in existent flows can be us to infer emplacement mechanisms when th strain profile for the lava flow as a whol has been evaluated.

Authors	Analogue Materials	Rheology	Environment	Objective	Primary Conclusions / Outcomes
Rossetti et al 1999	Paraffin Wax	Newtonian Fluid	n/a	Assessing the suitability of Paraffin wa as an analogue material for lava crust	Paraffin wax can satisfy the scaling requirements to be used as analogue material for lava crust
Blake & Bruno 2000	PEG	Newtonian Fluid	Under Water	Modelling the emplacement of compound lava flows	Flow duration is an controlling factor in th formation of compound flow-fields
Gregg & Fink 2000	PEG	Newtonian Fluid	Under Sucrose Solution	Investigating the effect of slope on flov morphology	Increasing the slope had the effect increasing the effusion rate and lowering t cooling rates changing the boundary conditions for each distinct morphology.
Miyamoto et al 2001	Kaolin/Water Slurry and Paraffin Wax	Bingham Fluid (slurry) & Newtonian Fluid (Wax)	Sub-aerial	Study of the suitability of Non Newtonian fluids as analogues for lava flows	Paraffin wax was more suitable to model the effects of crustal growth on flow behaviour
Sakimoto & Gregg 2001	PEG	Newtonian Fluid	Under Sucrose Solution	Applying combined analytical and analogue data to lava flows	Good agreement between analogue and analytical models
Bagdassarov & Pinkerton 2004	Golden Syrup	Thixotropic	Sub-aerial	To asses the regime changes in a thixotropic liquid over time with variations of applied stress	Where stresses exceed the yield strength o the material, viscous flow is possible and the material can transition from slip free t slip boundary conditions

Authors	Analogue Materials	Rheology	Environment	Objective	Primary Conclusions / Outcomes
Lyman et al 2004	Kaolin Powder Suspended in Liquid PEG	Bingham Fluid	Under Water	Calculating yield strength and effusio rate of lava domes from their morphology and underlying topograph	As angle of slope increases, the boundary conditions for the formation of specific morphologies change
Soule & Cashman 2004	PEG	Newtonian Fluid	n/a	Investigating the suitability of PEG as analogue for lava	Suitable for modelling silic flows
Garry et al 2006	PEG	Newtonian Fluid	Under Sucrose Solution	Studying the formation of submarine la textures	Model capable of recreating morphologie observed in the natural environment. Surface textures can be used to infer emplacement conditions
Miyamoto & Crown 2006	Paraffin Wax	Newtonian Fluid	Sub-aerial	Using a two component model to investigate pahoehoe lobe behaviour	Model considered the crustal strength and overpressure of the inner core of the lobe and can be used as a qualitative tool in lob growth
Applegarth et al 2010	Silicone Gel	Newtonian Fluid	Sub-aerial	Investigating the effect surface clinker h on the dynamics of a'a' flows	Behaviour is dependent on crustal thickne
Castruccio et al 2010	Sugar crystals suspended in sugar syrup	Non-Newtonian	Sub-aerial	Investigating the effect of crystals on th rheology of a liquid	At concentrations of >30% crystals, liquic behaved in a non-Newtonian fashion
Robertson & Kerr 2012	Kaolin Powder Suspended in Liquid PEG	Bingham Fluid	Under Water	Studying solidification behaviour of a Bingham fluid in a constrained channe	Both analogue model and field investigati show that the development of surface crus reduces heat loss through radiation

5 Analogue Modelling Experiments

5.1 Materials

To aid comparison with published works, paraffin wax was chosen for the new analogue model. It is a commercially available material with a temperature dependent viscosity and a small range of solidification temperatures which are easily reproducible in the laboratory. This makes it ideal for use in large experimental suites as it requires no specialised equipment.

Paraffin wax is a solid at room temperature and has low solidification point meaning that it can be handled easily and safely. It exhibits Newtonian behaviour above the liquidus and acquires a Bingham rheology with cooling. The wax is also suitable for investigating the effects of crust on flow structures as it forms a crust on cooling. The wax has a melting point of 56^{o}C (Rossetti et al., 1999), a density of 0.81g cm^{-3} at 15^{o}C and an α-β phase transition temperature of 35^{o}C, at which point the wax undergoes a reduction in strength. The thermal diffusivity is 8 x 10^{-8} m^{2} s^{-1} (Rossetti et al., 1999). The tensile strength of the wax is strongly temperature dependant and is thought to range from 4 x 10^{6} Pa (27^{o}C) to 10^{4} Pa (57^{o}C) (Miyamoto & Crown, 2006).

In order to more easily identify the flow dynamics, a small amount (≤ 5 ml) of dye was added to the wax. It was assumed due to the small volume of coloured wax in proportion to the volume of paraffin wax (200 – 300 ml) that the introduction of dye did not significantly affect the properties of the analogue material.

5.2 Methodology

Previous studies (Table 4.1) investigated the potential role of lava crusts on the structural evolution of lavas. They focused on the radial or quasi-radial spreading of lava and so most closely resembled domes, coulees and other simple structures. The new model was intended to investigate extended flows, the formation of channels and flow-fields by breaching or overflow of levees.

Three parameters – slope, effusion rate and volume – were chosen as variables which were systematically altered and the resultant changes in flow-field morphology recorded quantitatively and qualitatively. In total 94 experiments were carried out of which 10 were considered control experiments to calibrate the model.

5.2.1 Apparatus

As described in section 5.1, it was decided to use paraffin wax, effused at ambient room temperature (20^{o}C) as the analogue material in experiments where angle of slope, temperature and effusion rate were the variables. The apparatus consisted of an inclined glass sheet measuring 206 cm by 50 cm, resting on a solid wood plane measuring 220 cm by 70 cm which could be inclined from 0^{o} through 40^{o} by means to two jacks positioned underneath the upper section the wooden plane. The angle was measured using a clinometer. A spirit level was used to confirm the horizontal. The wooden frame was attached by two hinges to another heavier wooden board directly beneath it in order to stabilise the structure and prevent the frame slipping as the slope of the board was increased. The hinges allowed the wooden frame to be tilted at the correct angle for each set of experiments. The wooden plane was sanded, varnished and then painted white to

provide contrast for the wax. The plane was divided into sections measuring 10 cm by 10 cm which were drawn onto the painted surface of the wood and then labelled alphabetically on the horizontal and numerically on the vertical proving a grid map which was visible through the glass plane once it was placed on top of the wooden frame. The grid square was used to provide a reference when mapping structures within the wax flow-field and as a scale bar for photographs of the macro structures.

Experiments were carried out on slopes representative of a shield volcano at 2^{o} to 12^{o} at 2^{o} increments. The wooden frame was adjusted to the correct angle by extending the jacks. The wax reservoir was a 1000 cm^3 cylindrical glass dropping funnel, with a glass stop cock which was suspended on a retort stand approximately 30 cm above the glass sheet. Fink & Griffiths (1990) performed experiments on both smooth and roughened surfaces. They scaled wax flowing over a smooth surface to lava moving over old flow-fields or open terrain. Therefore, as the two case study sites were Mt. Etna and Garachico, Tenerife, both areas with significant extant flow-fields, it was decided to use a smooth glass plane as the experimental surface.

The dropping funnel was insulated using packing materials and a chamois. One of the aims of this research was to model the effects of slope on flow-field morphology particularly in the medial and distal sections of the flow where the majority of eruption energy has dissipated and the lava is flowing under gravity. Therefore it was decided to design an apparatus that allowed the wax to flow under gravity instead of using a pump as in this case would artificially increase the effusion rate and potentially mask some of the effects of variations in slope. The

dropping funnel was attached to 20 cm section of clear plastic piping with a 0.8 cm aperture. The open end of the tube rested on the horizontal 0 cm mark in grid square C1, held in place by a plastic pipe bracket attached to the wooden frame. The bracket insured that the tubing did not move during the experiment, providing a consistent location for the point of effusion and insuring movement in the tubing did not skew the path of the wax. The tubing was encased foam pipe insulation to prevent heat loss and subsequently solidified wax from building up in the pipe causing a blockage. A digital thermometer with a stainless steel probe was used to record the temperature of the wax as it exited the tube onto the glass sheet. The probe was pushed through the piping approximately 2 cm from the opening. A stainless steel tray was placed at the base of the inclined plane to collect any runoff. The experiments were filmed using a Canon Digital IXUS 10015 with a 12.1 mega pixel lens. Additional photographs were taken with an Olympus Camedia 5.0 megapixel digital camera. A schematic of the apparatus is provided in Figure 5.1.

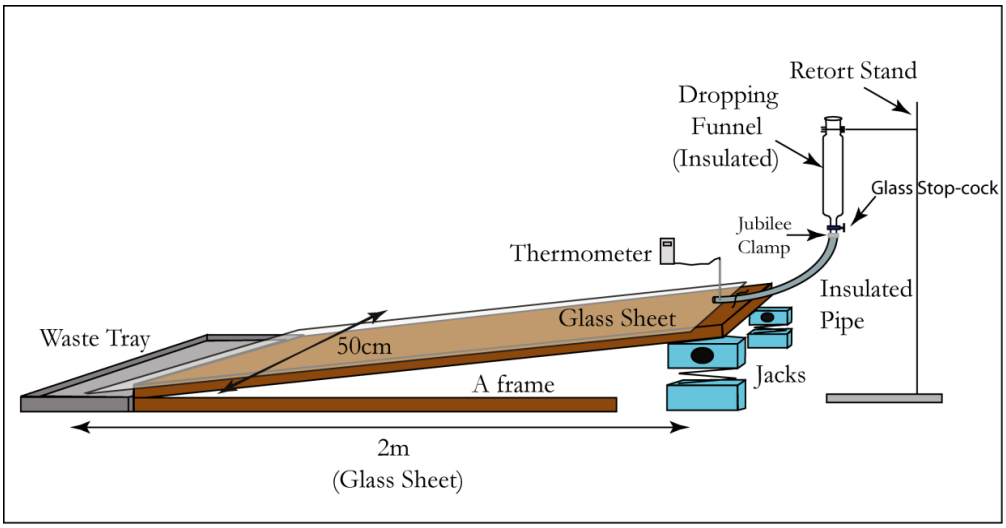

Figure 5.1 – Diagram showing the construction of the analogue model. A 2 m glass sheet was placed on a wooden frame which was hinged to a based board which helped to stabilize the frame. The angle of the glass sheet could be adjusted by the jacks underneath the wooden frame. The wax was placed in the dropping funnel

5.3 Experimental Procedure

5.3.1 Control Experiments

The initial experiments were designed to gain an insight into the structural evolution of a gravity flow with a temperature dependent rheology, which is allowed to flow downslope under gravity. Control experiments were run for variations of all three chosen parameters to determine the validity of the model, optimum position of the recording equipment and to insure that experiments could be consistently reproduced and to identify any issues with the experimental equipment. It was determined from the results of these experiments that the model was valid for slopes of 2^{o} to 12^{o} with volumes from 200 to 300 cm^3 of wax. The optimum temperature for the wax was determined to be 52-56^{o}C.

5.3.1.1 Identified Issues

At this stage some issues were identified with the experimental equipment. The wax had a melting point of 56^{o}C and the optimum temperature for effusion was found to be 52-56^{o}C. When the wax was introduced to the dropping funnel at 52^{o}C, it immediately began to cool and cause blockages in the neck of the dropping funnel and rubber tube. The issue was resolved by wrapping the dropping funnel and tubing in insulation and flushing the equipment with boiling water immediately before introducing the wax.

A secondary problem was caused by the glass stop cock in the dropping funnel. A small amount of wax was leaking around the stop cock and solidifying preventing the stop cock from rotating and releasing the wax. This issue was

overcome by coating the stopcock in an oil based lubricant which facilitated the smooth movement of the stop cock and acted as a sealant between the stopcock and the side of the dropping funnel, preventing almost all wax from infiltrating around the mechanism.

The wax used appears white/opaque once solidified, which led to issues distinguishing features within the flow against the white background of the painted wooden frame, a situation which appear even worse on the experimental video log. To rectify this situation a small amount (<5 cm^3) of paraffin wax dye was added. It was also discovered during the control experiments that once a multi-channel system had formed that it was difficult to differentiate between which flows were active and which were inactive. In order to more easily identify the flow dynamics, it was decided to use two different dyes in the wax. The pink dye was used in the first 50% of volumes effused and a contrasting blue dye was used for the remaining 50%, facilitating the documentation of the evolution of the wax flow-field.

5.3.2 Modelling the Effects of Slope on Flow-Field Morphology

As discussed in Section 5.2.1 slopes of between 2 and 12^o were chosen as representative of effusive eruptions on a shield volcano. Experiments were carried at increments of 2^o. The angle of the glass sheet was adjusted using the jacks as illustrated in Figure 5.1 and verified using a clinometer and spirit level. The glass was cleaned and polished prior to each experiment to ensure there was no residue left on the glass that would obstruct or influence the wax flow. The total volume of wax was split evenly between two beakers, one coloured with pink dye and the second containing blue dye was heated to 65^{o}C in an oven. The wax was then

removed from the oven and the temperature was monitored constantly as it was allowed to cool to 56^{o}C. While the wax was cooling to the correct temperature for effusion, the apparatus was flushed with boiling water to reduce heat loss due to conductivity and to avoid the development of solidified wax within the valves and tubing of the apparatus, causing blockages.

Once the wax had reached the correct temperature – 56^{o}C, it was poured into the dropping funnel. The pink wax was introduced first, followed by the purple/blue. The wax was allowed to flow under gravity through the stop-cock, into the tubing and onto the glass sheet. Each experiment was video recorded with additional photography taken of the flow-field once the experiment was completed.

A table of results is available at the end of Appendix B, Table B.0.1

5.3.3 Modelling the Effects of Volume on Flow- Field Morphology

The experiments investigating the effects of variable volumes on flow-field morphology were carried out using the same methodology as with the slope investigation apart from the volume of wax used. Two volumes were chosen – 200 cm^3 and 300 cm^3. As described in the materials section above, 50% of the volume for each experiment was dyed with contrasting wax dyes in order to more easily distinguish the chronology of the flow emplacement. In total of the 22 experiments carried out, 11 were carried out with 200 ml of wax and 11 were carried out with 300 ml.

A table of results is available at the end of Appendix B, Table B.0.2

5.3.4 Modelling the Effects of Effusion Rate on Morphology

In order to determine the effect of variations in flow velocity and effusion rate on flow-field morphology, experiments were carried out in which the flow rate of material was varied and the resultant flow processes recorded and categorised into three groups low effusion rate E_rL, medium E_rM and high E_rH. Effusion rate group E_rL is comparable with the effusion rates recorded in the slope variation experiments. The input of material was controlled by varying the degree to which the aperture of the stop cock in the dropping funnel was open. The mean flow velocity, V_{mean} was calculated from the Jeffrey's equation for steady, laminar flow (Jeffreys, 1925) where flow velocity - V_{mean} was calculated using the formula:

$$V_{mean} = \rho g sin(\alpha) d^2 / n\mu \qquad \text{Eq. 5.1}$$

Where ρ is wax density, g is acceleration due to gravity, α is the slope of the channel floor, d is the depth of the wax, μ is viscosity and n is a constant dependent on channel width. For the purposes of this model n = 3 following the work of Booth & Self (1973) which defined the constant for Etna wide channel flows. Effusion rate E_r was then quantified by the formula:

$$E_r = V_{mean} wd = w\rho g sin(\alpha) d^3 / n\mu \qquad \text{Eq. 5.2}$$

Where w is flow width.

A full table of results is available in Appendix B, Table B.0.3

5.4 Scaling

Although the wax models are not formally scale-dependent analogues of lava flows, they can be used to investigate the breaching of levees provided that local conditions at a wax breach are physically plausible also for lavas. Levees breach when the outward force from fluid in a channel exceeds the resistance of a levee. The factor determining the resistance lies between the extremes of the tensile strength of levee crust restraining a fluid core and of the yield strength of a completely solidified levee. In the analogue models, the wax solidifies by conduction and the thickness of the crust:

$$s \approx (8\kappa t)^{1/2} \quad \text{Eq. 5.3}$$

Where κ is thermal diffusivity and t is the cooling time (Hulme, 1974).

For conductive cooling toward the surface and base, a wax margin will have completely solidified when its thickness $d \approx 2s$, which will occur after a time:

$$t_d \approx d^2/32\kappa \quad \text{Eq. 5.4}$$

Provided the duration T of the wax experiments exceeds t_d, therefore, the conditions for breaching will encompass the range of conditions expected in lava flows. The wax has a thermal diffusivity of 8 x 10^{-8} m^{-2} s^{-1}. Hence, for typical thicknesses of 5 mm, t_d will be on the order of 9.77s. The durations of the

experiments were ~ 160 s, so that $T/t_d > 1$. The wax flows thus incorporate the full range of potential breaching conditions expected among 'a'a lavas and so provide physically plausible analogues.

5.5 Results

The purpose of the analogue model was to both qualitatively and quantitatively examine the effect of variations in slope, effusion rate and volume on the flow morphology of a material with a temperature dependent viscosity. The qualitative descriptions of the flow-fields will follow the logic of Hallworth et al., (1987) who consistently described their individual experiments using the same set of criteria in order to comprehensively illustrate the effects of parameter variation on flow-field morphology. For the purposes of this study the criteria are:

- Time taken for a flow to achieve its maximum length
- Flow-field Dimensions
- Channel and flow-field aspect ratio
- Surface features of the flows
- Timing of the development of secondary flows
- Number of secondary flows formed
- Angle of breakouts to the original channel

5.5.1 Effect of Slope Variation on Flow-field Morphology

The effect of slope variation on flow-field morphology was examined by conducting experiments on slopes from 2^o to 12^o degrees in 2^o increments with otherwise identical emplacement mechanisms. All experiments produced multi-channel flows where, in the majority of cases (70%), the first flow to form reached the greatest distance. The general pattern of flow-field emplacement was characterised by three stages – effusion rate controlled, cooling controlled (development of secondary flows and flow structures such as tubes and lobes) and thickening and lateral growth.

The first stage – initial flow construction was characterised by rapid emplacement rates and lengthening. Immediately after the aperture in the dropping funnel was opened, wax flowed through the tubing onto the glass sheet forming the initial flow. Flow widths became stable within 1-2 cm of the vent and maintained a roughly uniform width for the duration of the experiment. The rate of flow-front advance reduced with time as viscosity increased, the wax developed a yield strength and surface crust developed.

The second stage of emplacement was characterised by cooling and the formation of flow structures such as lobes, levees and secondary flows. The progenitor of all flow structures is the development of surface crust and/or thermal boundary layer which can be defined as the layer that forms between the air and the internal flow where temperature of the wax changes. Flow structures arising from the development of crust include lobes and secondary flows both of which form as surface crust develops sufficient yield strength to retard forward momentum of the flow, moving the flow regime from effusion rate controlled to crust controlled

emplacement. Thermal boundary layers form on the outer edges of a flow and can usually be identified as a band of opaque wax adjacent to the clear more fluid flow interior. The development of the thermal boundary layer is a precursor to the formation of channel levees.

The third stage of emplacement was characterised by lateral flow-field growth and flow thickening. Flow-fields grow laterally as secondary flows form through breakouts from lobes or channels, the mechanism of which will be discussed in a latter part of this section. Cross-sections through the flow-field show the age relations of the different flows aided by the use of two different coloured waxes at different stages in the experiment. Cross sections also showed how secondary flow orientation and width can be defined by adjacent flows (Figure 5.2, 5.3 & 5.4). To illustrate the general pattern of flow development eight images from Experiment 1.2 are displayed below (Figure 5.5).

All experiments followed this general pattern of emplacement. However the time-taken to transition between the stages and the dimensions of the flow-fields and structures showed distinct trends with increasing slope. It was observed that as the slope increased, flow-fields became longer and narrower (Figure 5.6). The flows were spaced more closely together and flows became narrower and thicker with increased gradient. Correspondingly, flow and flow-field aspect ratios were also higher for experiments carried out on slopes of 2^o and 8^o – 10^o with an obvious decrease for slopes of 4^o – 6^o degrees. V_{mean} increased with increasing slope angle and therefore the time taken for flows to reach their maximum length decreased. The lower value for V_{mean} favoured the growth of tubes at lower slope angles while leveed channels were more commonly observed in experiments with a higher slope

angles (Figure 5.2). The results of the experimental suite will be discussed qualitatively in Section 5.5 & 5.6.

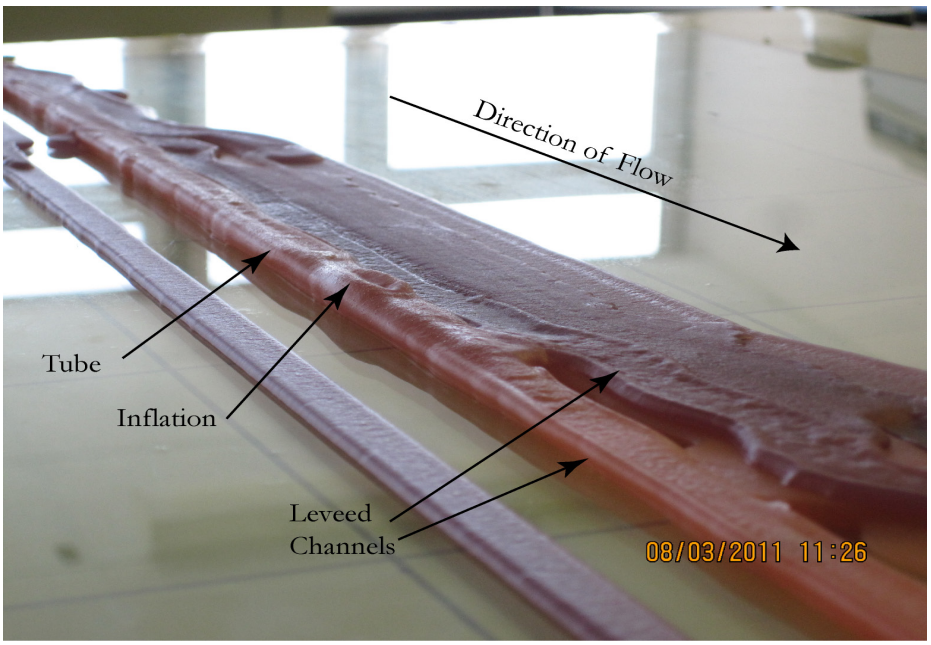

Figure 5.2 – Experiment 1.2 Volume 300 ml, Slope 2°. Overview of the compound flow-field showing the levees, tube and inflated sections of flow in relief.

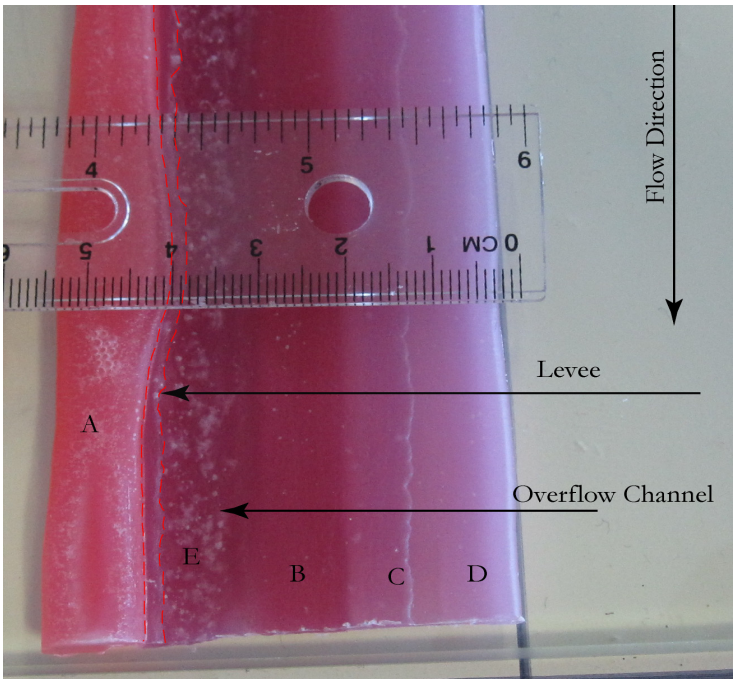

Figure 5.3 –Experiment 1.2 Volume 300 ml, Slope 2°. The image shows a multi-channel flow from the medial section of the flow-field. The flows are labelled chronologically from A to D. Flow A is a

well-developed flow which became inflated as the flow-front cooled down, retarding forward movement. Flow E was formed from an overflow of material from Flow B which flowed in-between Flows A and B, and formed a levee using the side of Flow A.

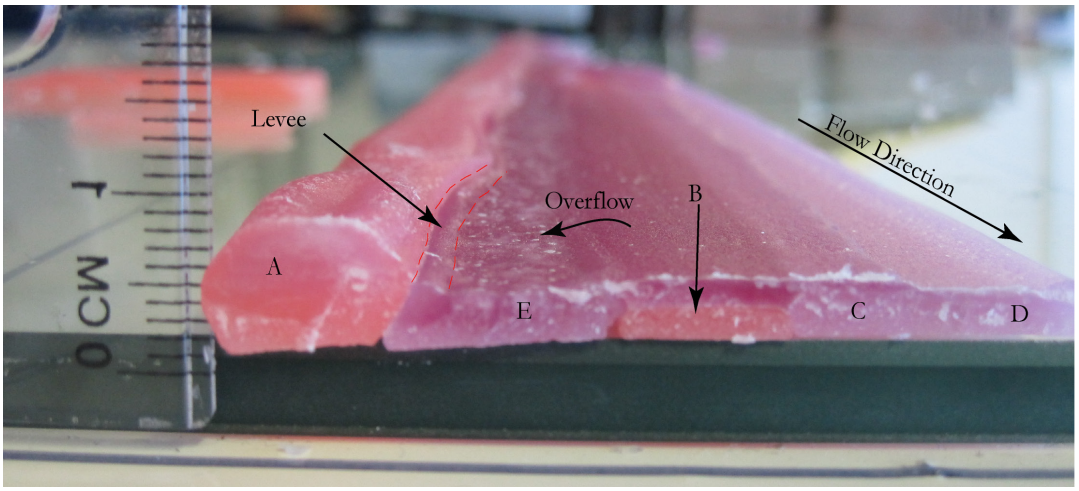

Figure 5.4 – Cross-sectional view of Experiment 1.2. The age relationships of the flows can be identified from their superposition and from the colour of the wax. The pink wax was the first to be effused followed by the purple. This view shows the height of inflated flow A in relation to the other flows. It is also possible to identify the levee formed in Flow E where it is in contact with the side of Flow A.

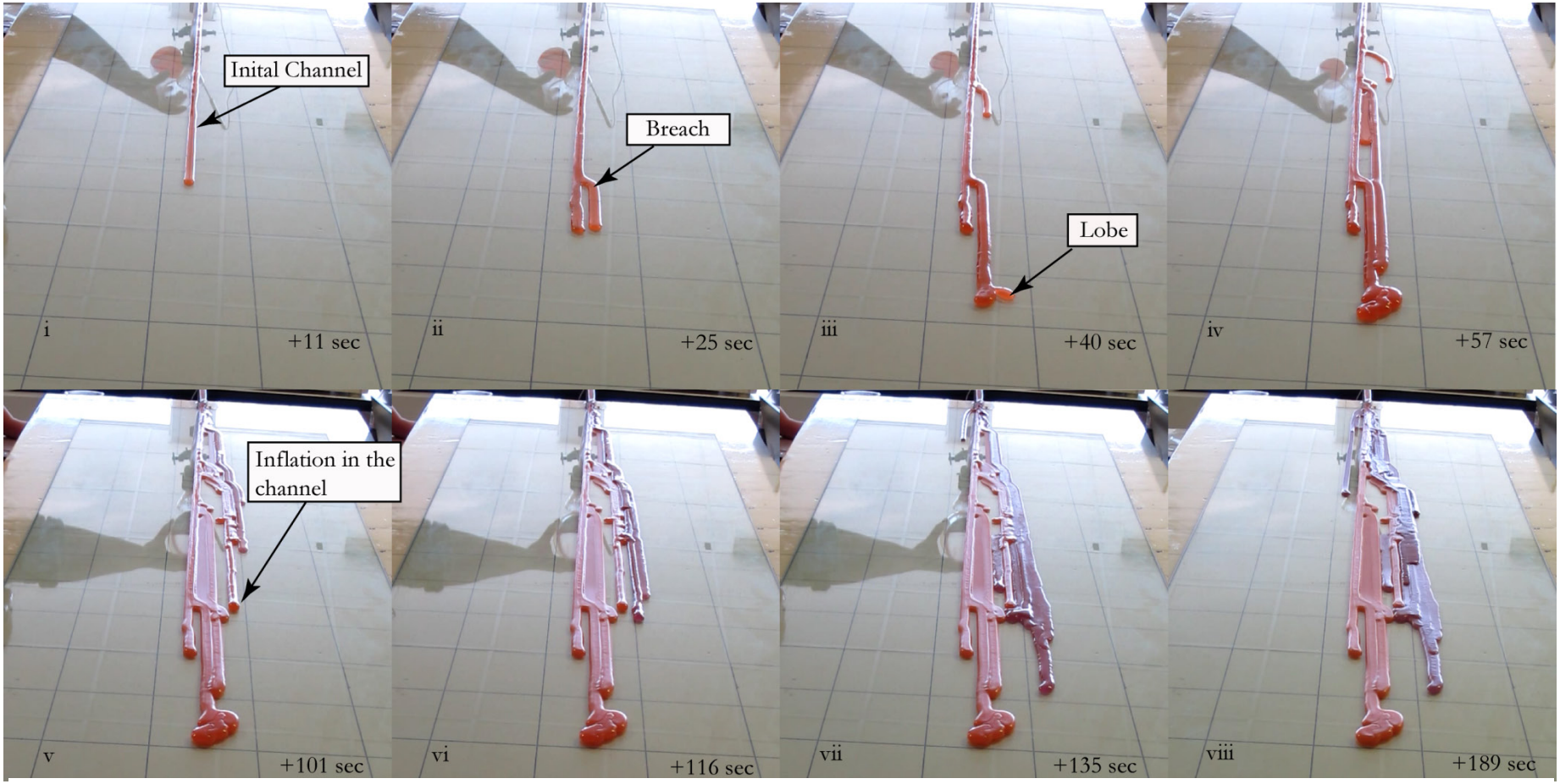

Figure 5.5 - Experiment 1.2 - Eight images showing the development of a flow-field. 300 ml of wax at 2° slope. Some of the structures that are discussed in this section are labelled. The wax is released through a tube with a 0.8 cm aperture and flows toward the bottom of the photograph. Each square is 10 cm by 10 cm.

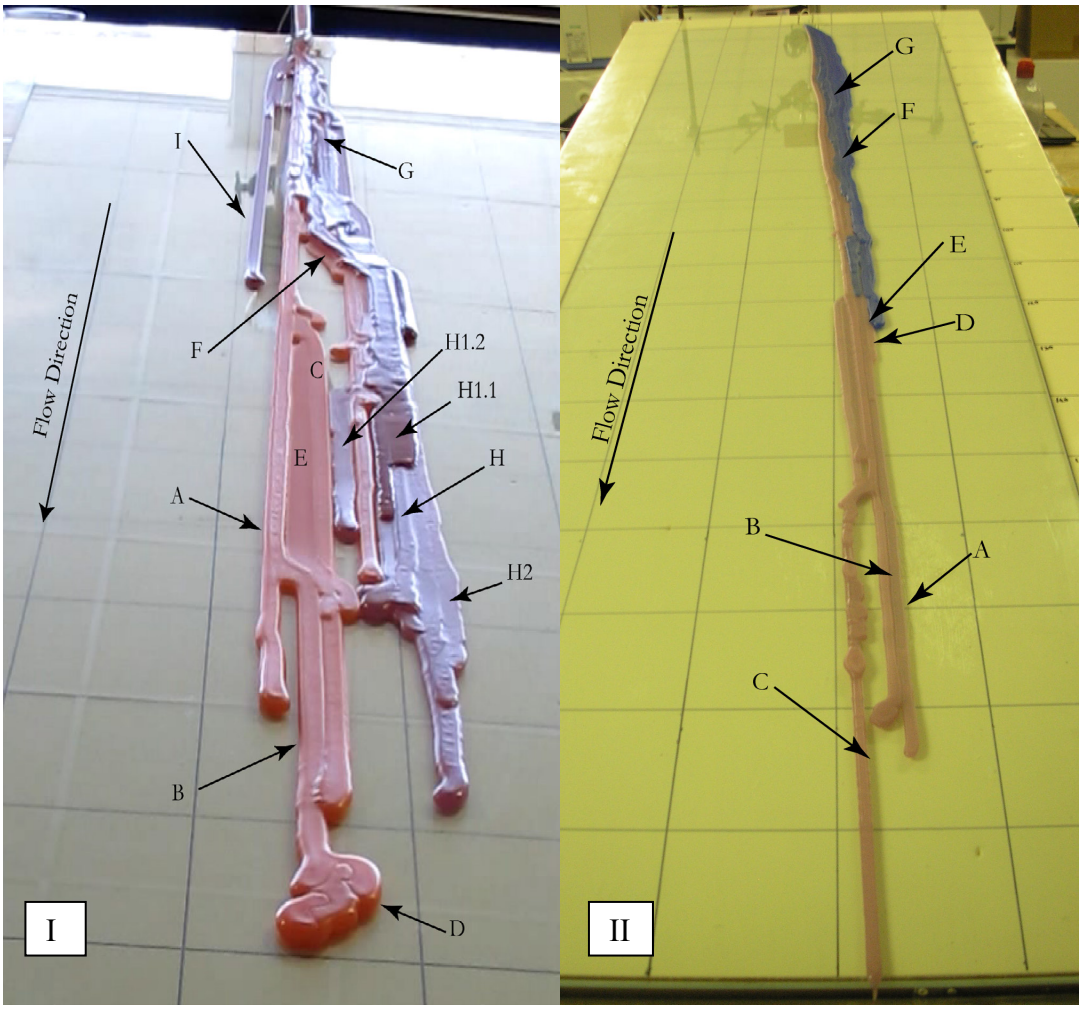

Figure 5.6 – Experiment 1.2 Volume 300 ml, Slope 2° (I). Experiment 6.6 Volume 300 ml, Slope 12° (II). Flow-field widths decreased and length increased with increasing angle of slope. Each grid square is 10 cm by 10 cm. Flow-field length in Experiment 1.2 is 139.50 cm and maximum width is 9.70 cm. The flows are labelled alphabetically in order of development. The original flow A halted due to the development of solidified crust which caused the flow to inflate leaded to a breakout and the development of secondary flow B which was short-lived before it also halted and developed lobe D which is an agglomeration of 4 different lobes. As can be seen by the position of the secondary flows A, C, F and G, the position of breakouts migrated up channel towards the source over time. Experiment 6.6 over-ran the slope making it in excess of 200 cm in length and 6.10 cm wide at its widest point. Flow A was the first to form, followed by breakouts B and C. Flow C developed a series of inflated lobes, none of which resulted in a breakout as Flow D formed and diverted material away from Flow C. Flows E, F and G formed in the latter stages of effusion and as seen in experiment I, the position of the breakouts migrates back up-channel over time.

5.5.1.1 Flow Lengths and Fronts

Emplacement and dimensions of initial flows characterises the first stage of emplacement – effusion rate controlled. The experimental suite was designed to allow the wax to flow under gravity. For the slope and volume variation experiments, the effusion rate at the point of origin was kept at a constant. However, emplacement rates were observed to increase with increasing slope leading to an increase in initial flow lengths and time taken for a flow-front to develop.

More viscous flow-fronts developed as a result of cooling and deceleration of the fronts was an indication that the flow is moving from an effusion rate to cooling dominated regime. Flow-fronts appeared as a zone of material at the head of a flow with a rheology that was different to the material up-channel. The wax in this zone was more opaque than the hotter wax in the flow interior and had an apparently increased viscosity, moving more slowly than the material in the upper part of the flow. Although the velocity of the flow-front decreased, material continued to flow in the channel resulting in a build-up of material, causing thickening. Flow-fronts were observed to move up-channel overtime due to cooling. Increasing the slope meant an increase in time taken for flow-fronts to develop meaning that the first stage of emplacement had the longest duration of all three stages for high slope angle experiments (Figure 5.7, 5.8)

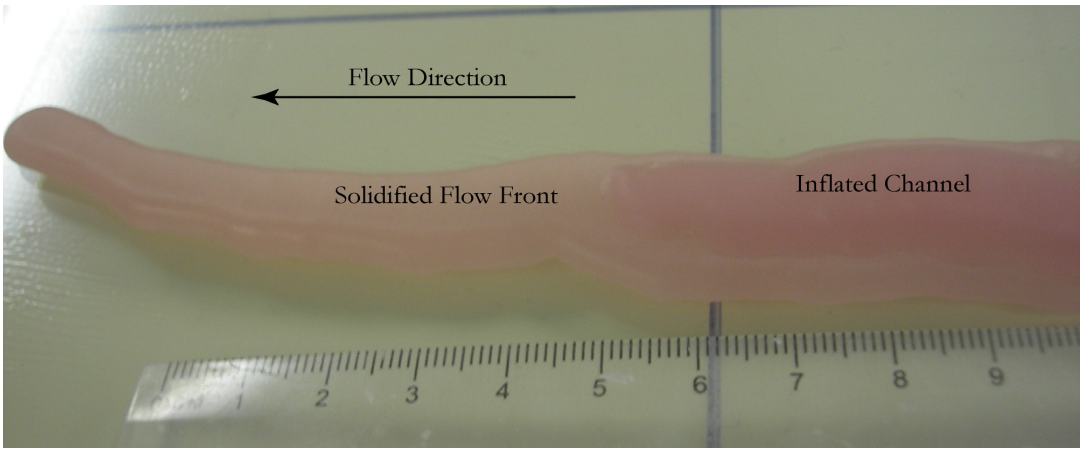

Figure 5.7 – Experiment 2.5 Volume 300 ml, Slope 4°. Flow-front migrated up-channel over time causing inflation behind the solidified front.

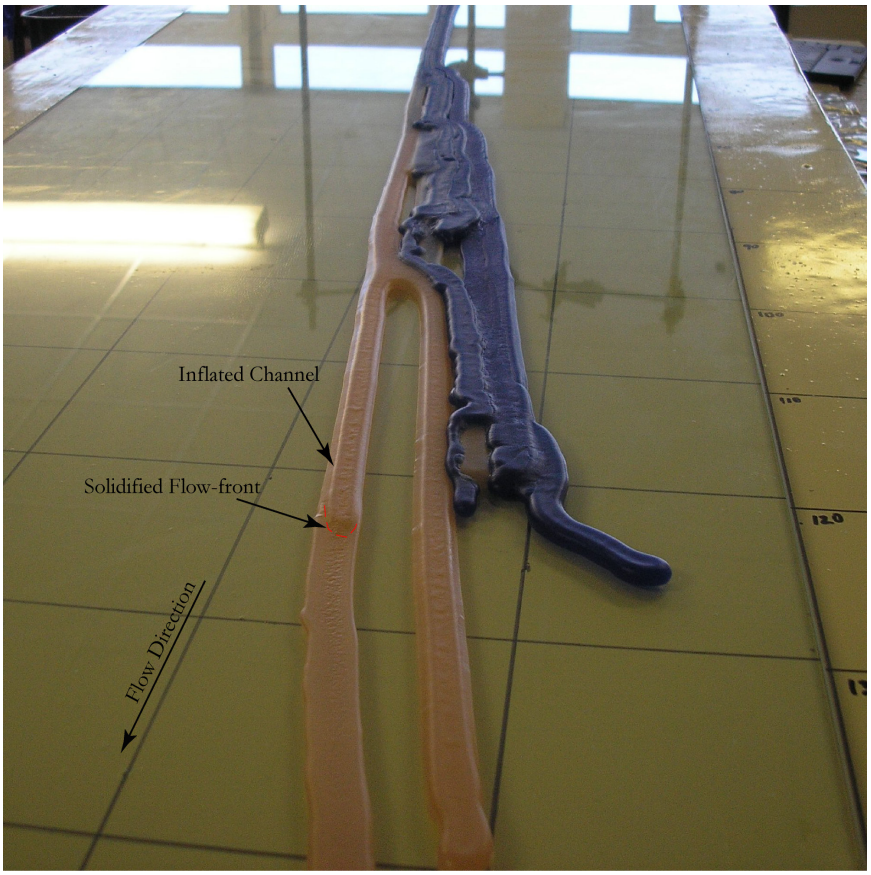

Figure 5.8 – Experiment 2.10 Volume 300 ml, Slope 4°. Cooling causes the flow-front to migrate up channel with time, causing thickening in the channel behind.

5.5.1.2 Break-outs

The development of crusted flow-fronts was the precursor to the formation of breakout. In the absence of topographic constraints, break-outs were the most common process by which flow-fields propagated and their presence marked the transition to the second stage of emplacement. Breakouts can be classified into two categories based mode of formation – overflows and breaches.

Both mechanisms result from material build up behind a cooled flow-front or obstacle. Overflows flow up and over a levee without altering its internal structure. Breaches either wholly or partially break through the levee.

Overflows occurred when wax overtopped the existing levees, flowing over the existing channel boundaries, based on their rate of supply, forming either short lived lobes or new flows. The mechanism by which overtopping occurs is not fully constrained but it was observed during the experiments that the material at the base of the channel, in contact with the glass slope, cooled preferentially to the material in the mid-section of the flow. In an established flow the thickness of the solidified wax at the base of the flow increases with time resulting in a decrease in the overall carrying capacity of the channel. The volume of wax eventually exceeds the capacity of the channel and overtops the levees to form a new flow (Figure 5.9, 5.10, 5.11). In some cases, levees were observed to migrate outwards in order to accommodate the volume of material in the channel; however this was a rare occurrence and was confined to new flows with semi-plastic levees. Overflows were also observed to be a common result of a pulse of fluid in the channel which occurred when a channel became temporarily blocked, causing material to build up behind the obstruction. Once the blockage was removed, the accumulated material

was released forming a short lived surge in flow volume before the flow rate stabilised. If the volume of the pulse exceeds the carrying capacity of the channel, material overflowed the flow boundaries and formed either a new flow or more commonly a lobe which was cut off from supply once the normal flow rate resumed. Overflows were most common on slopes in excess of 6^{o} and 10^{o}.

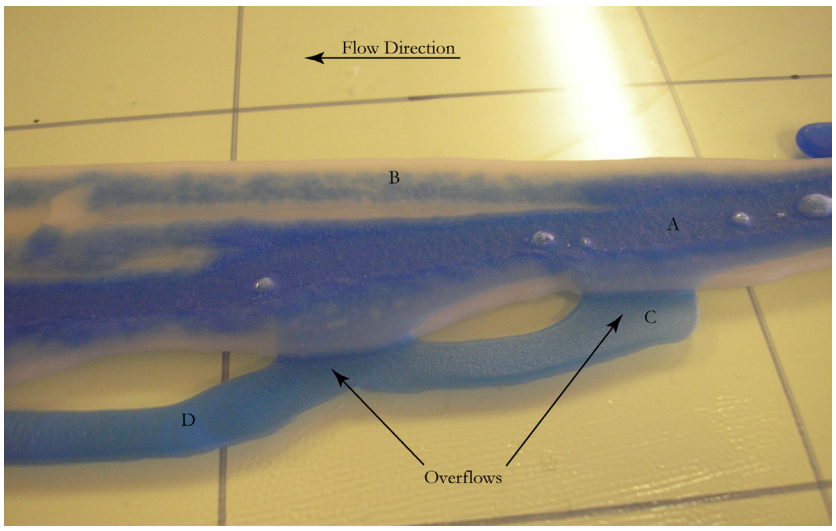

Figure 5.9 –Experiment 4.10 Volume 300 ml, Slope 8^{0}. Overflows from Flow A. Overflows can be distinguished from breaches as they drape over the sides of the channel and do not alter the morphology of the levees.

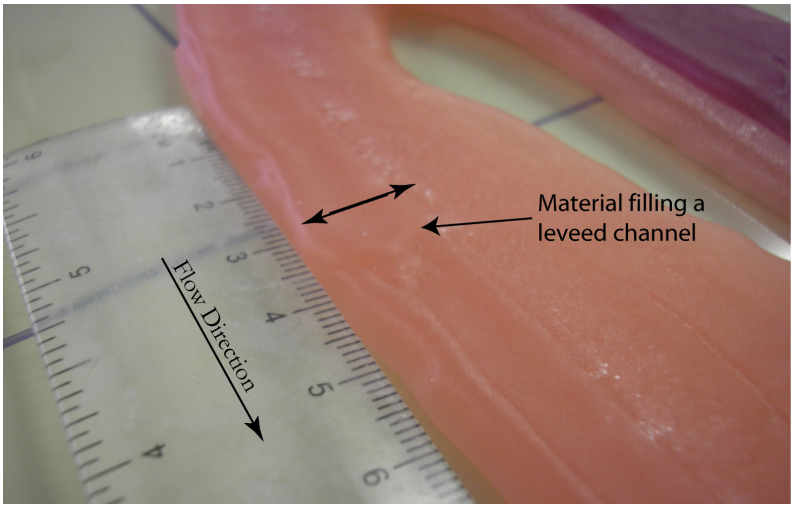

Figure 5.10 – Experiment 1.6 Volume 300 ml, Slope 2^{o}. Material can be seen filling a leveed channel to capacity. Supply of fluid material stopped before the material could overflow the channel margins forming an overflow.

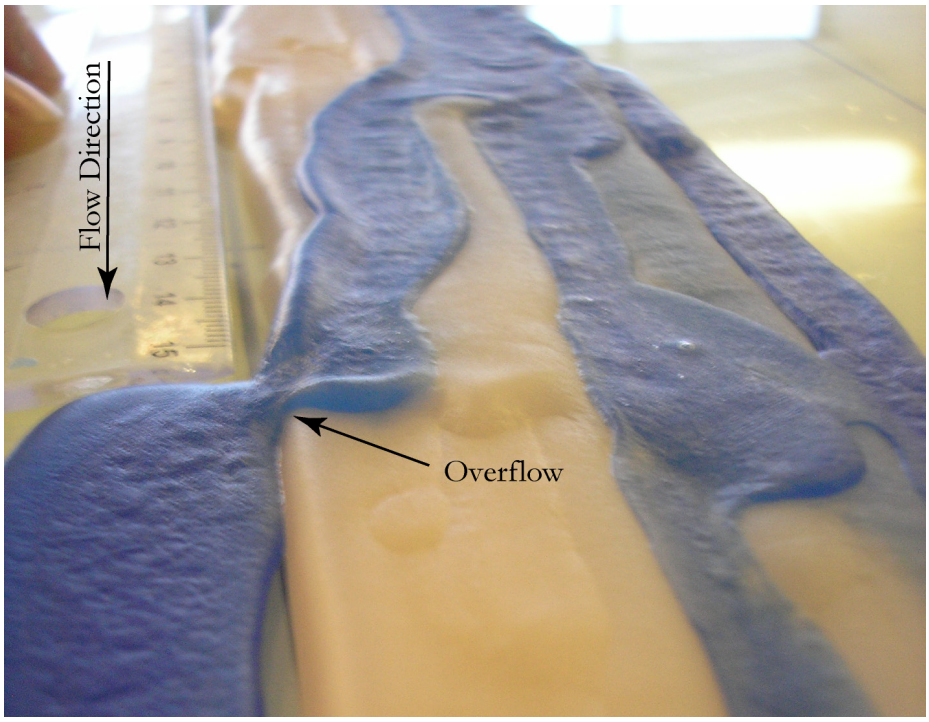

Figure 5.11 – Experiment 4.10 Volume 300 ml, Slope 8°. The blue wax can be seen overflowing the margin of the original channel in the pink wax. The flow narrows significantly as it flows over the side of the channel, widening again as it reaches the glass.

Breaches were the second mechanism by which breakouts formed and are differentiated from overflows by the mechanism by which they form. As flow volume increases, the shear pressure on the levees constraining that flow increases and overcomes the retaining strength of the levee causing it to breach (Figure 5.12, 5.13). Breaches occurred both individually and in clusters. Individual breaches resulted in a new flow becoming established at an angle of 10° and 40° to the slope. In some instances, breaches occurred in clusters which occurred simultaneously, in close proximity to each other. The majority of clusters formed small volume, short lived lobes and did not result in the formation of a new flow. However, it was observed that when clustered breaches did result in a new flow forming, only one of the breaches resulted in a flow and was the breach closest to the vent. Other breaches that were part of the cluster formed short lived lobes which became static

after they were cut off from supply as the breach up-channel, closest to the point of effusion, captured the flow. Breaches were also common where flow channels experienced curvature. In all cases breakouts originating from curving channels occurred on the outside bends of the curve.

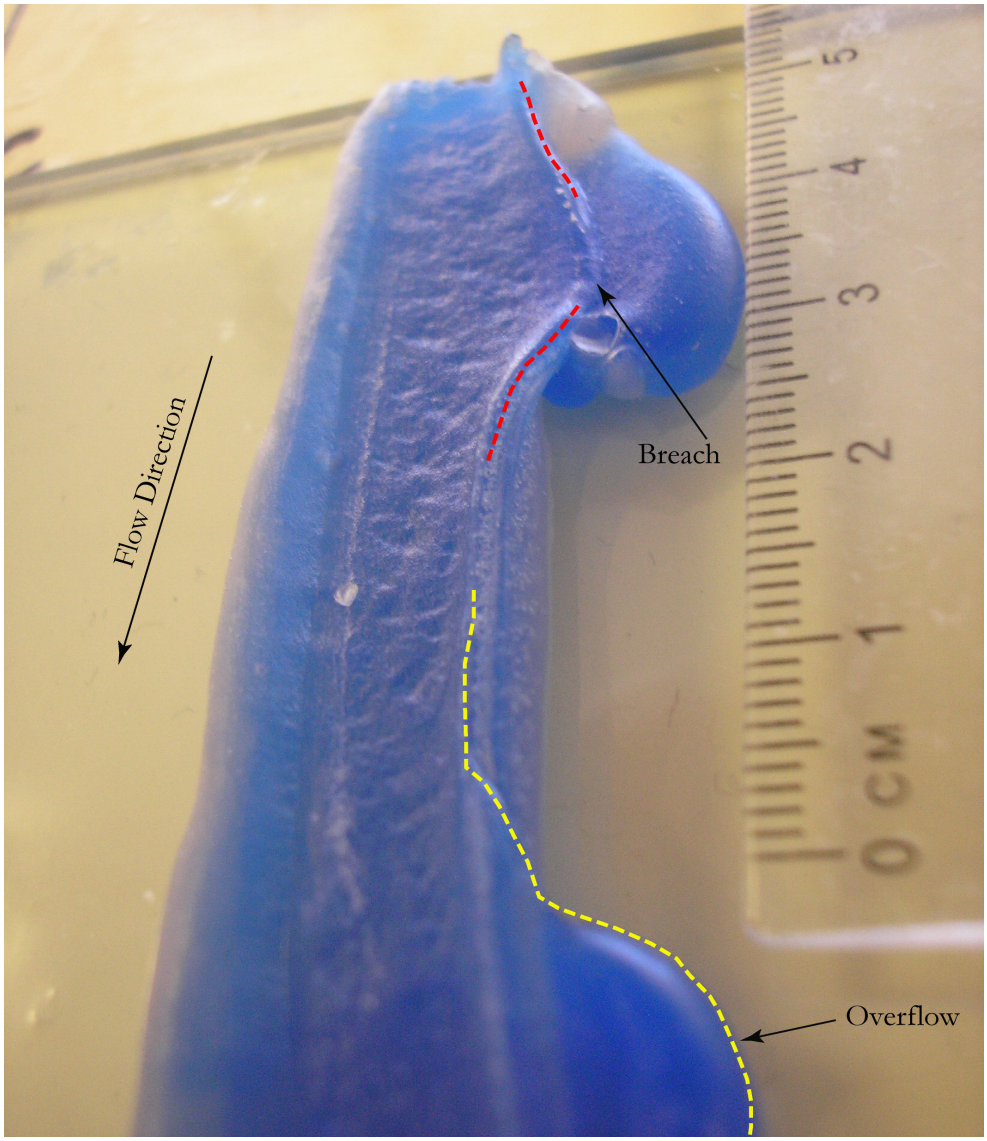

Figure 5.12 – Experiment 4.6 Volume 300 ml, Slope 8°. Flow showing both a small breach and an overflow close to the point of effusion, in the proximal section of the flow. The breach breaks through the levee, causing it to buckle outwards. In contrast, the overflow overtops the levee without altering its structure.

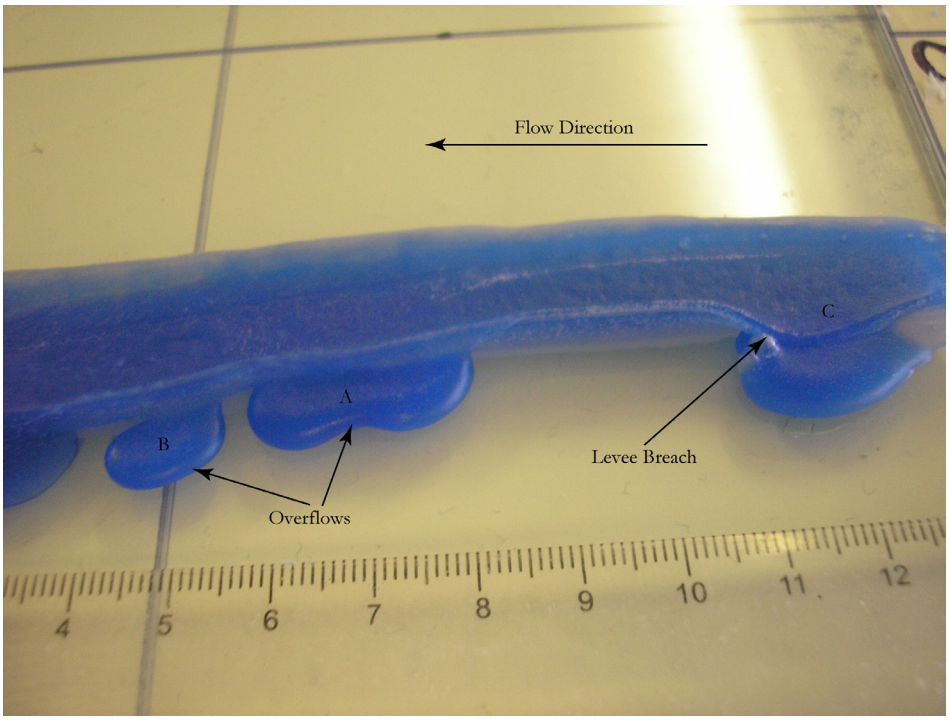

Figure 5.13 – Experiment 4.6, volume 300ml, Slope 8°. Overview of the proximal section of the flow-field containing a breach and two overflows. Both of the events did not result in the formation of new flows. At the breach the levees are buckled outwards while the overflow over the levee without altering its structure or orientation.

5.5.1.3 Angles of Secondary Flow Formation

The formation of secondary flows through breakouts was characterised by the angle at which the secondary flow forms with respect to its original channel. The angle ranged in values from 10° to 40° with 70% falling into the 25° – 35° bracket (Figure 5.14, 5.15) which is a direct correlation with what was observed in the field (Chapter 3, Section 3.2.2). At higher angles of slope the angle of formation decreases resulting in narrower flow-fields. New flows resulting from breakouts were observed to have, on average, the same width as the original flows regardless of the % of total flow volume captured by the new flow.

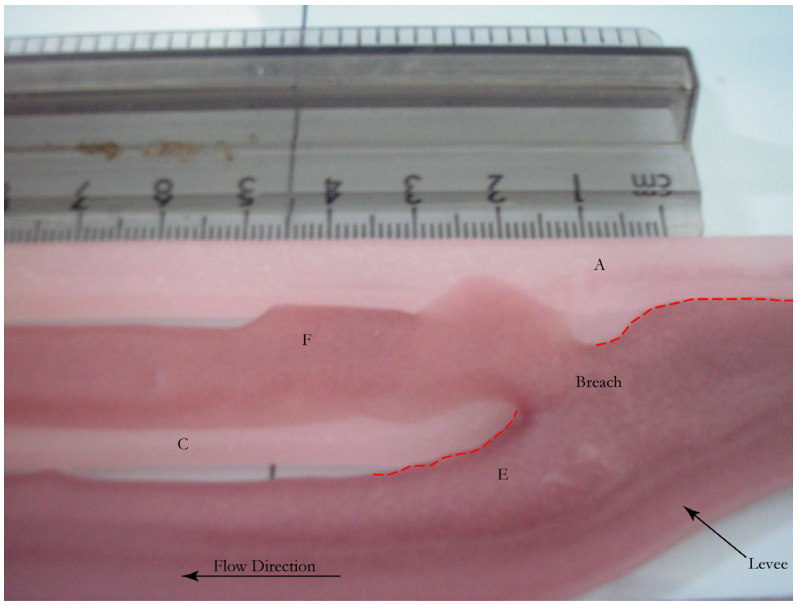

Figure 5.14 – Experiment 14 Volume 200 ml, Slope 10°. A new flow (F) formed from a breakout where Channel E experiences curvature. It was observed during the experimental suite that where channels experienced curvature, new flows originate from the outer bend. Arrow indicates flow direction.

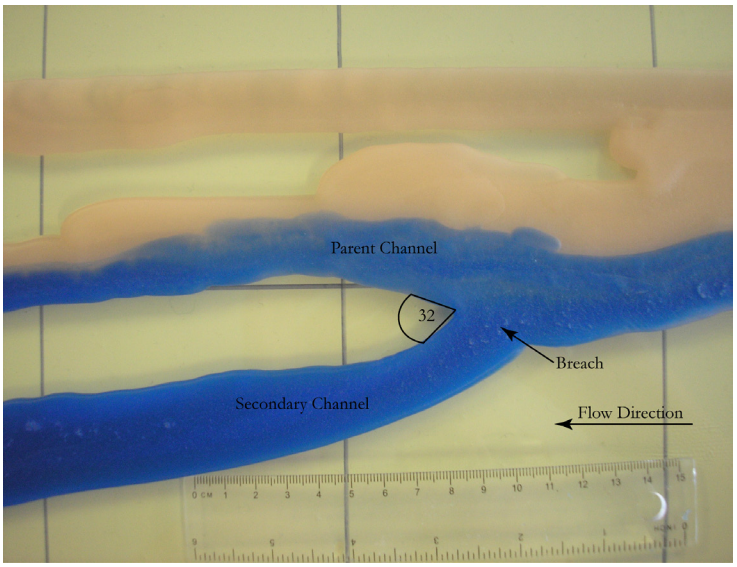

Figure 5.15 – Experiment 3.8 Volume 300 ml, Slope 6°. Secondary flow forms on the outer curve of the original or parent channel. The new flow formed at an angle of 32° to the original channel.

5.5.1.4 Levees

Levees were common to all experiments but were more frequently formed in experiments on slopes of 6^{o} or higher. As lava moved downslope a thermal boundary layer formed through cooling. At the onset, the material in this zone appeared to have a similar rheology as the material in the centre of the flow. Over time, the boundary layer material becomes more viscous and opaque, developing a yield strength and losing velocity, resulting in an outer band of wax that flowed slower that the interior of the flow. Given sufficient time for cooling, this layer solidified completely, passing though the ductile/brittle transition forming a levee. Levees initially formed at the final third of the proximal zone of the flow-field which was on average 10-15 cm long during the early stages of effusion and spread down flow. Levee development was also observed to move up-channel as the flow transitioned into the second stage – cooling controlled regime. Flows constrained by levees typically had uniform widths and thicknesses and were narrower than unconstrained flows in the same experiment. Due to the use of multi-coloured waxes, the growth of levees can be inferred through the contact relationships of the coloured wax. Lighter coloured waxes were used in the first stage of emplacement followed by a darker colour, the contrast between the two, providing a visual aid to flow evolution the darker wax contrasting with the solidified levees formed from the initial lighter wax. There was no mixing between the two wax colours, illustrating that the levees solidified soon after emplacement. However, levees were observed to contain both waxes showing that levee growth continued as long as the flow remained active (Figure 5.16). In addition to levee thickness increasing with time as material was added to the internal levee wall, the base of the flow also

became thicker, decreasing the carrying capacity of the channel. As a result, levees grew higher in order to accommodate the volume of material in the channel. In this way, channel morphology changes with time, becoming narrower and deeper.

Although fully solidified levees define a flows orientation and are responsible for either uniform or very gradually changing channel widths, localised areas of distension were observed in some experiments. Prior to passing into the brittle regime, levees were still ductile and could be forced outwards, without compromising their structural integrity to the point of failure, due to rapid changes in the volume of material in the channel. This was also observed during the field investigation (Section 3.2.1 Figure 3.8). Although the effusion rate was steady or even gradually decreasing towards the end of emplacement, pulses of material were not uncommon, resulting from the release of material pent up behind an obstacle, such as a piece of solidified wax, in the channel. The still ductile levees were forced to migrate outwards in order to increase the carrying capacity of the channel resulting in channel margins with irregular protuberances (Figure 5.17, 5.18)

Sets of levees either side of a flow were not always morphologically similar (Figure 5.16). Particularly in compound flows, which consist of a network of adjoining flows, levee morphology was heavily influenced by the contact relationship of the channel margin. Although levees had many different morphologies dependant on their emplacement and cooling histories, in general terms, levees formed by flows which have no contact relationship with other structures appeared convex on their outer wall. Where a new flow adjoined a channel, the existing structure provided a framework for the channel margin resulting in the development of levees with a concave or sheer profile (Figure 5.19).

Levee profiles were not uniform throughout the flow-field. In flows that experienced curvature, the levee on the outer most bend of the flow was observed to be thicker that its counterpart (Figure 5.20).

In multi-channel systems new flows became superimposed on existing flows, some of which were drained, leveed channels. Secondary flows were commonly observed to exploit the existing channel structure, flowing between the levees, mimicking the original channel's orientation and width (Figure 5.21, 5.22).

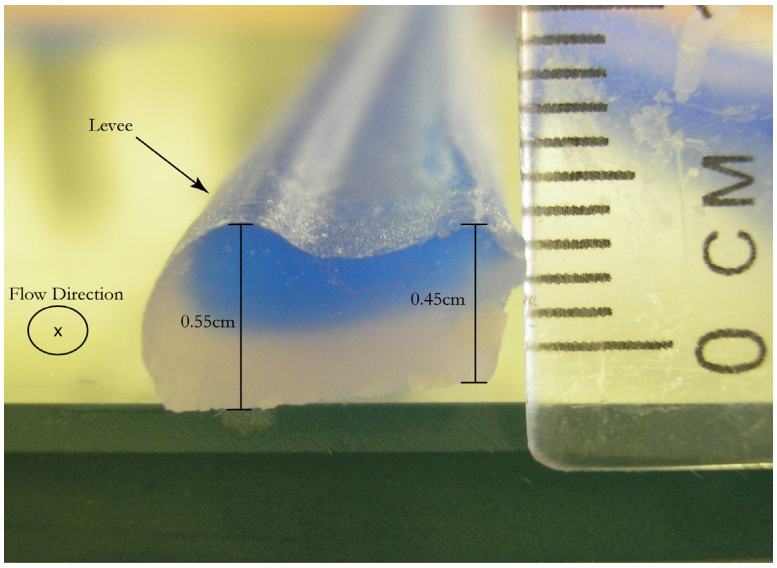

Figure 5.16 – Experiment 2.10 300 ml, Slope 4^0. The bicoloured wax illustrates the development of a levee over time. Levee height continues to grow with time as the level of fluid material in the channel rise due to thickening of the solidified flow floor.

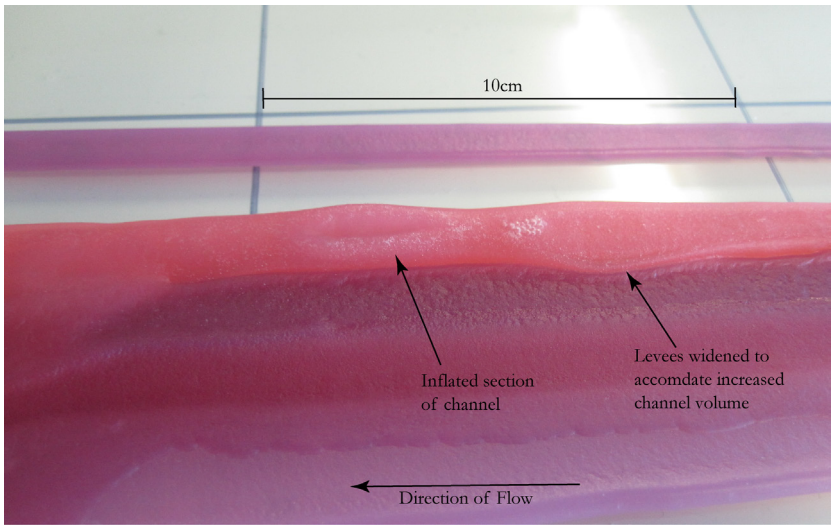

Figure 5.17 – Experiment 1.2 Volume 300 ml, Slope 2°. As the flow-front became stagnant due to the development of solidified crust, the flow experienced thickening and the levees migrated outwards to accommodate the increased volume of material.

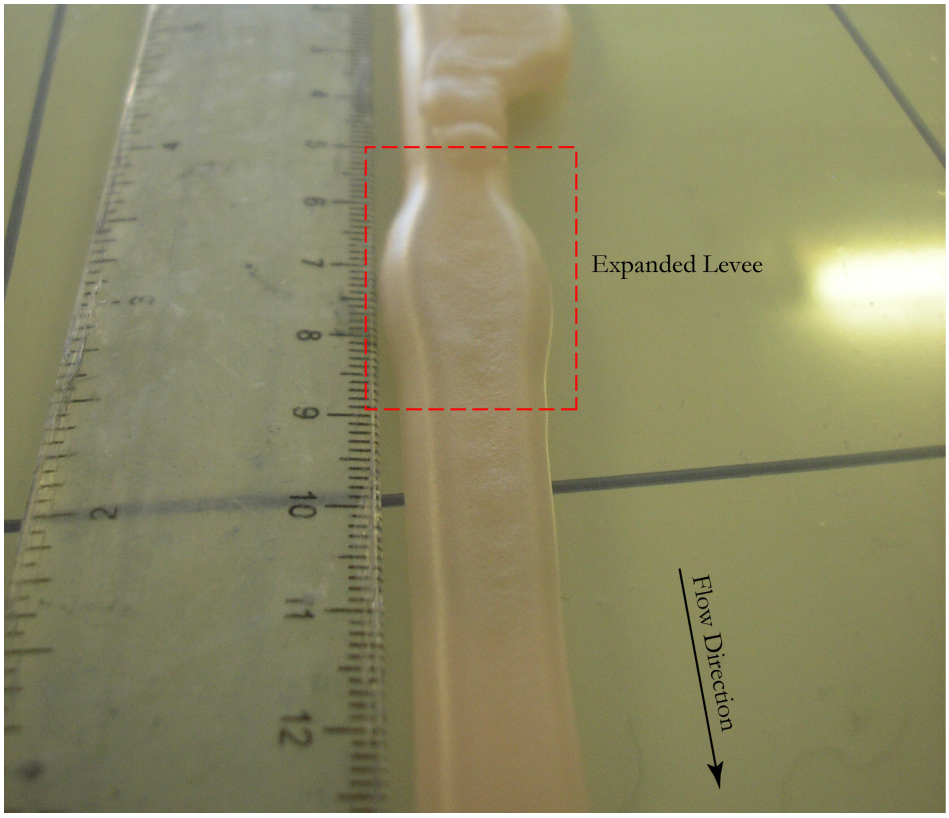

Figure 5.18 –Experiment 5.3 Volume 300 ml, Slope 10°. When the volume of material in a channel increases, the excess can result in either overflow or breach or if the levees are not fully solidified they can expand outwards increasing the carrying capacity of the channel.

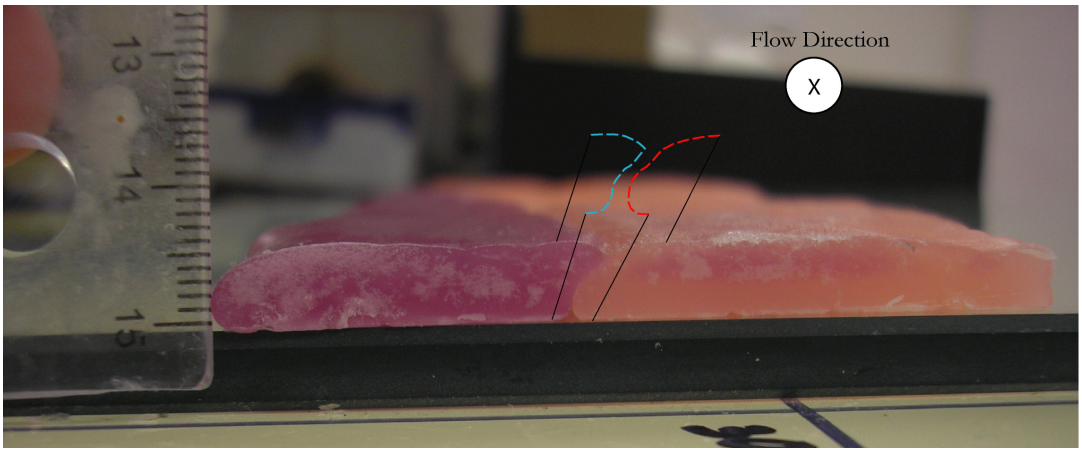

Figure 5.19 – The profile of the levee in the purple channel is represented by the blue dashed line and the profile of the levee in the pink wax channel is represented by the red dashed line. The pink channel was the first to form and the levee has the classic convex structure. The purple channel formed later alongside the existing levee which dictated the morphology of the purple channel margin.

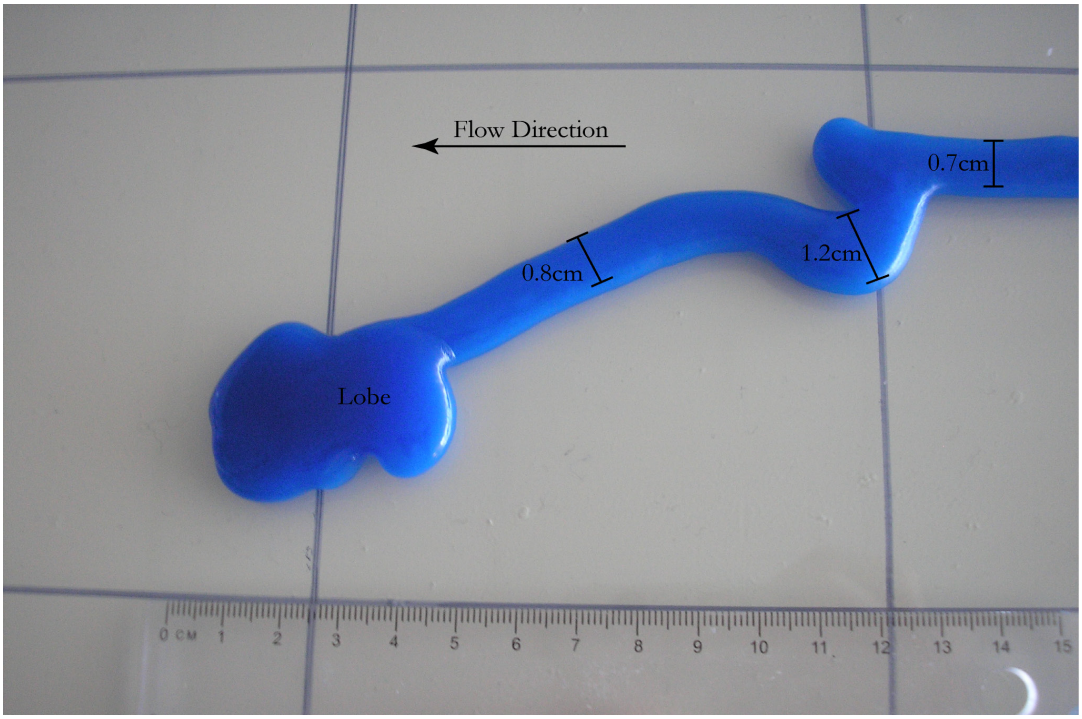

Figure 5.20 – Experiment 3.9 Volume 300 ml, Slope 6°. Flows experiencing curvature were found to be wider compared to flow widths before and after the bends.

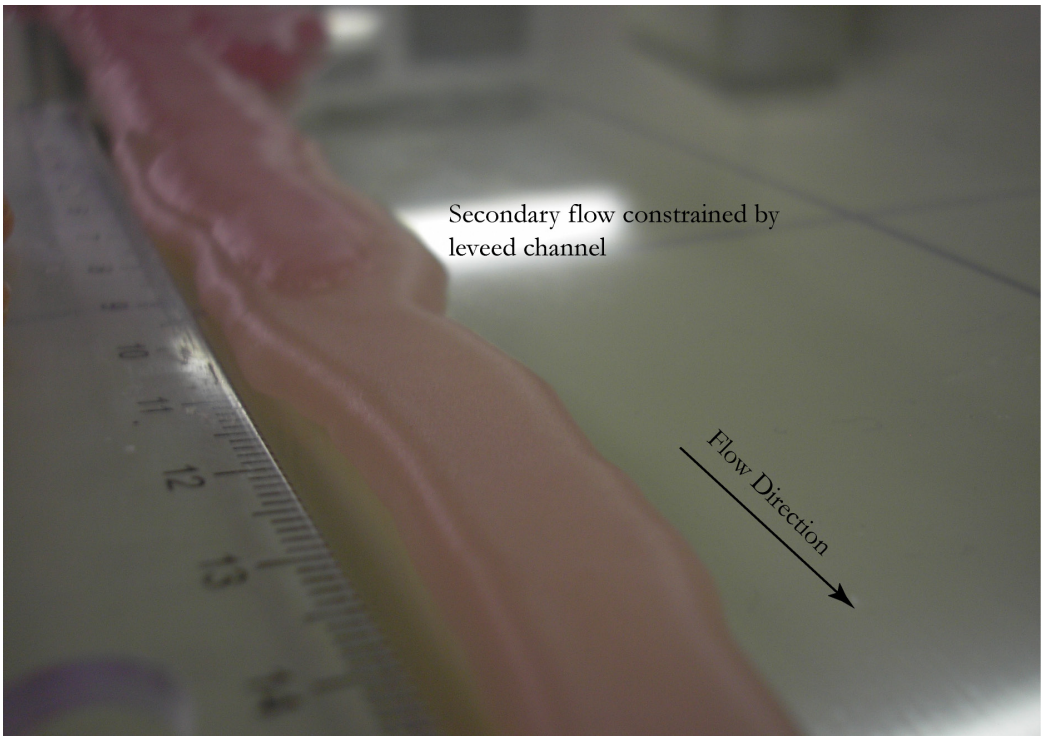

Figure 5.21 – Experiment 2.5 Volume 300 ml, Slope 4°. Secondary flow within an existing channel constrained by original channel levees.

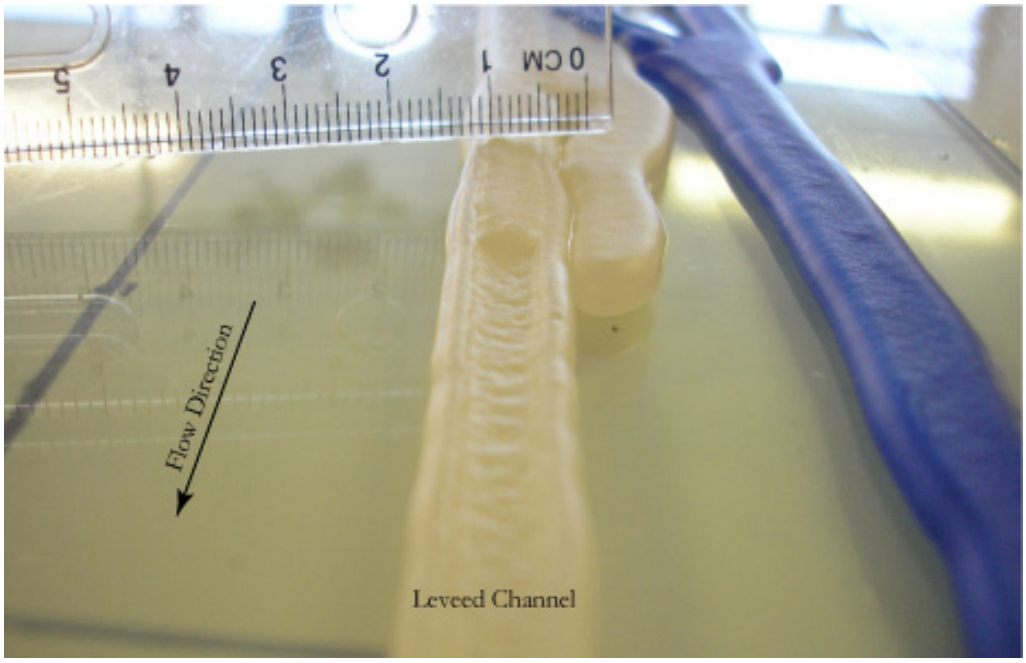

Figure 5.22 – Experiment 2.5 Volume 300 ml, Slope 4°. Secondary flow is constrained by the levees of an existing channel.

5.5.1.5 Tubes

Tubes were observed to form in all experiments but were more commonly formed in experiments on slopes of 8^{o} or less. Tube formation is linked to the combination of a development of a thermal boundary layer in addition to the development of surface crust. Tubes initially formed as levees, the mechanism starting with a thermal boundary layer as described in the previous section on levees. Cooling resulted in the formation of surface crust within the leveed flow, forming a continuous layer which eventually covered the entire top surface of the flow, effectively sealing the flow interior. Tubes were observed to stay active for longer periods of time than open channels due to the insulating effects of the tube. The addition of darker wax in the second stage of the experiment illustrated which tubes were still active as it was possible to see the wax flowing under the lighter coloured crust.

In some experiments, tube lengths reached to the end of the experimental sheet (>200 cm). In cases where the tube did not reach the end of the experimental sheet, cooling at the font of the tube eventually led to the development of crust of sufficient thickness to halt the rate of advance, causing the molten wax from the flow interior to pool under the crust, inflating it and forming a lobe. If the tube remained active and material continued to reach the lobe, the force of the confined material overcame the tensile strength of the lobe causing it to breach, allowing the wax to flow forming a new flow or lobe. When a breakout occurred from the lobe, the tube typically became drained, leaving a roughly circular void which can be traced to the point of origin (5.23). If no break-out occurs, then the material will

remain in the tube. In such cases the wax inside the tube remains semi-plastic for a longer period of time than in an open channel 5.24, 5.25).

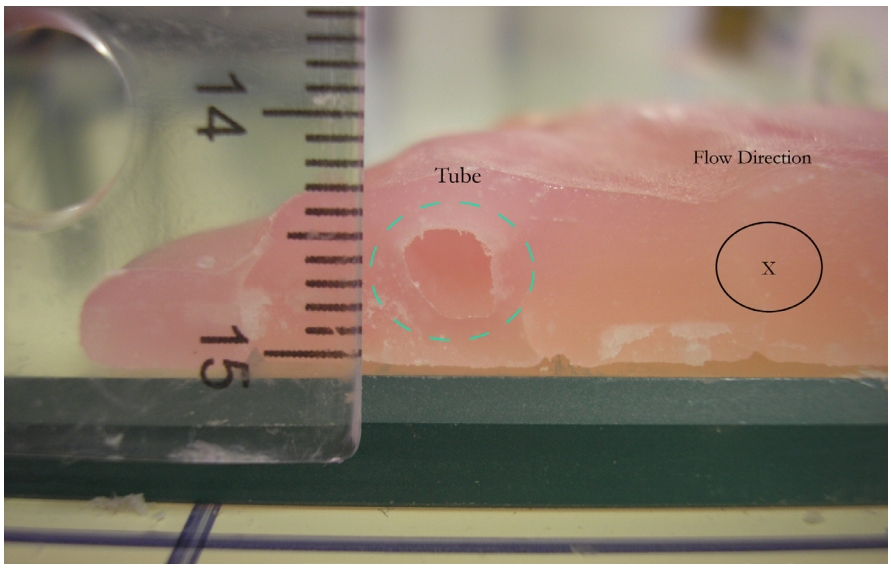

Figure 5.23 – Experiment 2.3 Volume 300 ml, Slope 4°. Drained tube. The tube formed in the first 50secs of effusion and became drained when a breakout up channel diverted the flowing wax into forming a new flow. As the flow-front was not yet solidified, the material in the tube flowed to the front and out of the tube.

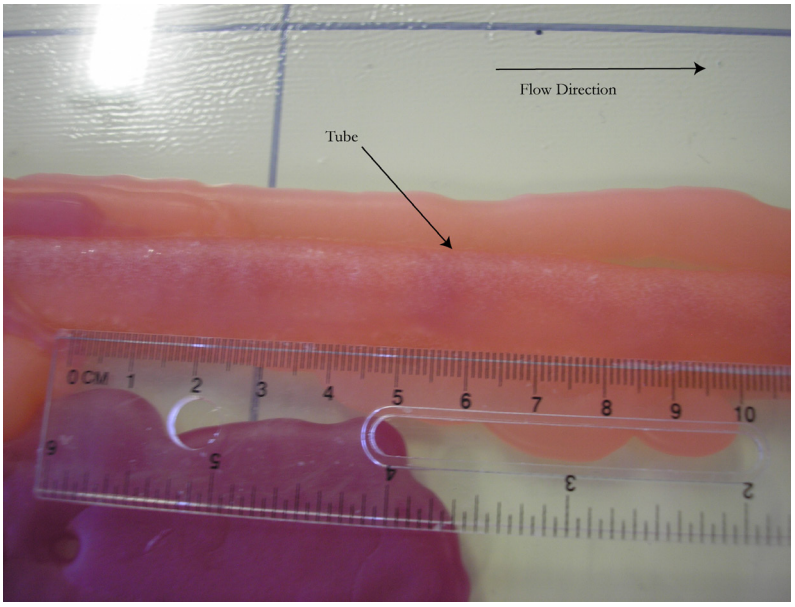

Figure 5.24 – Experiment 1.4 Volume 300 ml, Slope 2°. Tube formed in the proximal section of the flow-field closest to the vent. Darker purple wax from the second stage of effusion can be seen in the tube proving that it was active in the later stages of effusion.

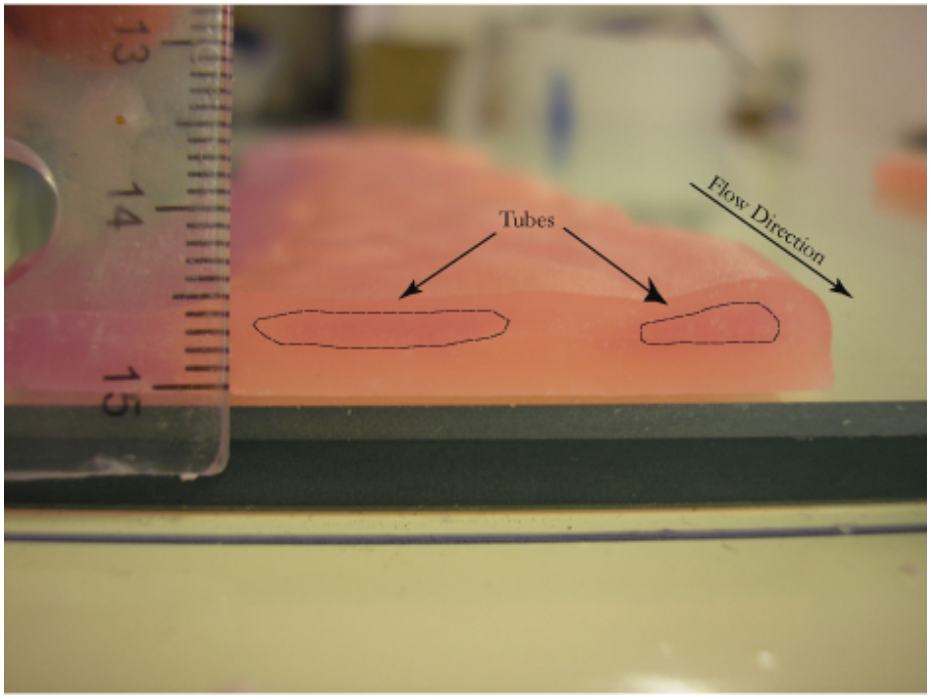

Figure 5.25 – Experiment 1.7 Volume 300 ml, Slope 2°. Solidified tubes containing darker purple wax from the second stage of effusion. The purple wax is surrounded by pink wax proving the tubes formed in the first stage of effusion and were still active when the purple wax was added.

5.5.1.6 Lobes

Lobes were seen to form in the latter stages of the majority experiments regardless of other emplacement parameters. Lobe formation was particularly common in experiments with lower V_{mean} and slope values. Initial flows were observed to have steady movement and uniform flow thickness. As the effusion continues, the advance of the flow became unsteady due to the retarding force of the developing surface crust. When the rate of wax input exceeded the rate of advance of the flow, molten material within the core of the flow accumulated in the flow interior, confined by the surface crust causing radial deformation called inflation. Inflation continued until the pressure of the fluid material moving under gravity overcame the tensile strength of the crust, breaching it to form a new flow.

The location of the breach within the lobe appeared to be independent of the area of maximum inflation. This is assumed to be due to the random distribution of micro-scale areas of weakness in the surface crust possibly resulting from impurities in the wax.

Successive chains of lobes were also observed where breakouts from lobes travel a short distance (1 to 5 cm) before forming a new lobe. This pattern could repeat itself until a chain of lobes formed in close proximity to each other (Figure 5.26, 5.27 & 5.28)

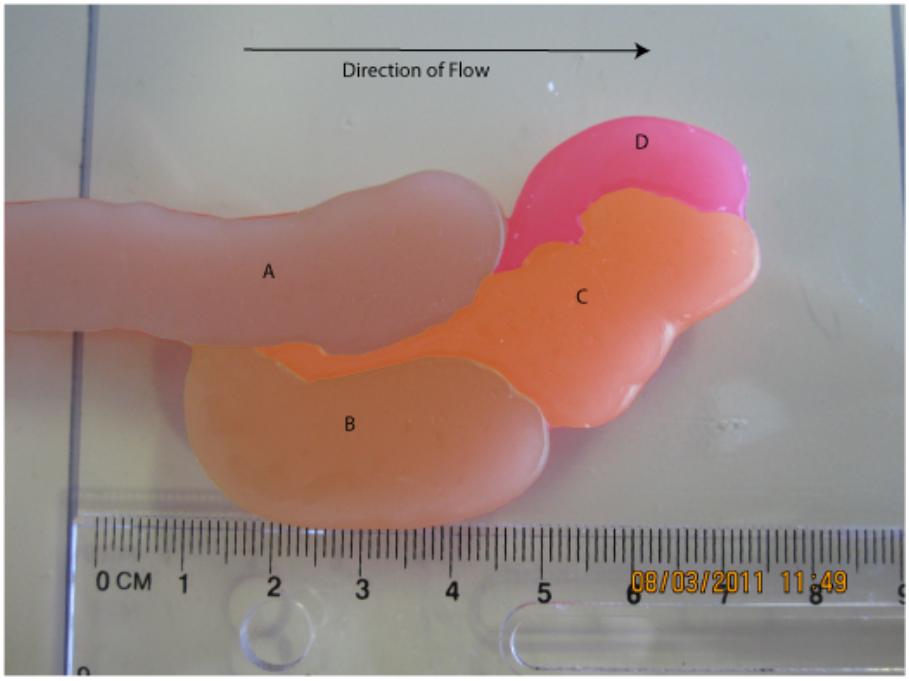

Figure 5.26 – Experiment 1.2 Volume 300 ml, Slope 2°. Sequence of lobes formed at the flow-front. By lifting the wax off the glass in one piece and turning it over so the surface in contact with the glass slope is uppermost, it is possible to see more clearly the age relations between lobes. The lobes are labelled A to D, oldest to youngest. The lobes in a sequence of inflation and breach. The site of the breach was independent of the area of maximum inflation.

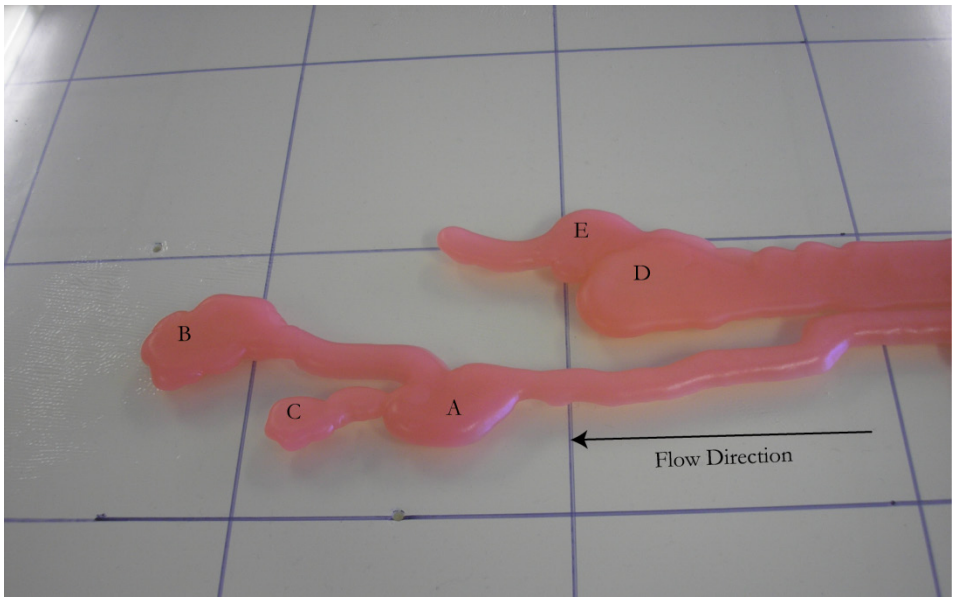

Figure 5.27 – Experiment 1.4 Volume 300 ml, Slope 2°. A sequence of lobes that formed in two flows the flow-field front. The lobes are labelled from oldest to youngest A to C in flow 1 and D to E in flow 2.

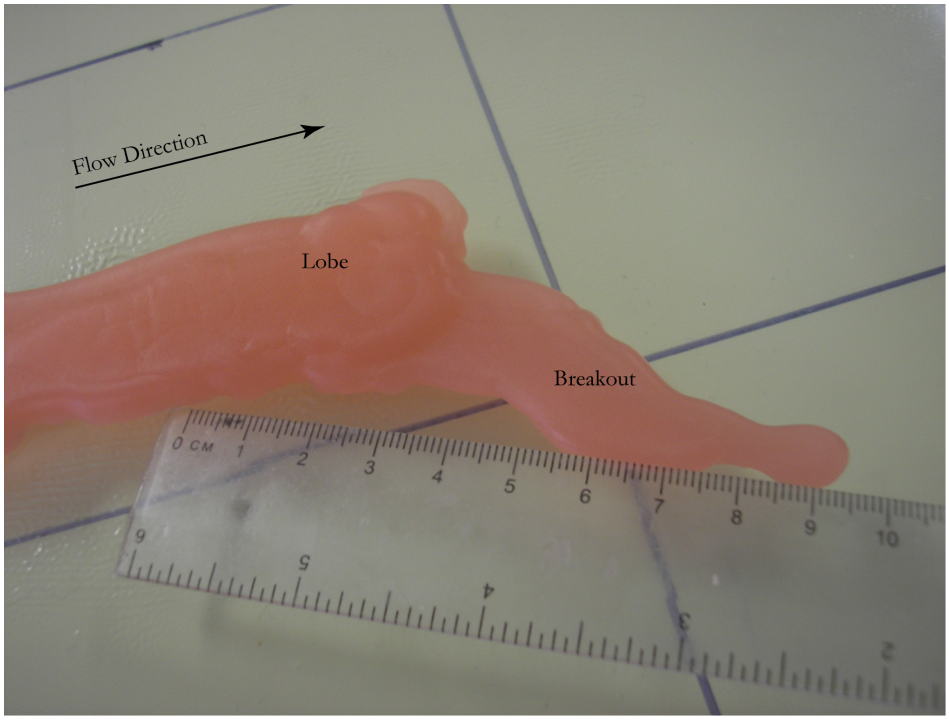

Figure 5.28 – Experiment 1.6 Volume 300 ml, Slope 2°. Breakout was observed to form from a breach within an inflated lobe. After the breach, the lobe became deflated as the excess volume formed a new toe.

Break-outs from lobes also formed new flows. The rates of advancement of these newly formed flows were observed to decrease in proportion with time for up to five seconds after the breakout occurred. The initial advance of the flow is thought to have a significantly higher velocity due to thickening prior to breaching. Once the accumulated material has dissipated, the driving force for flow advancement is once again, acceleration of fluid material due to gravity. In this way the observed acceleration in the rate of advance of a newly extruded flow immediately after breakout can be explained.

Not all lobes experienced breaches, in some experiments lobes were preserved intact due to a reduction in input rates (either exhaustion of the total experimental volume or some of the volume of material being redirected down a different flow) which translates into the build-up of pressure within the lobe achieving a steady state before it overcame the tensile strength of the crust to form a new flow (Figure 5.29).

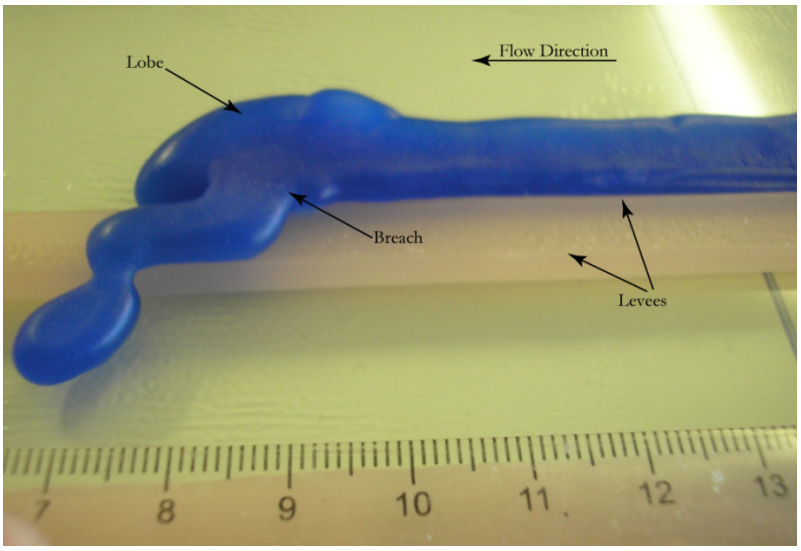

Figure 5.29 – Experiment 4.8 Volume 300 ml, Slope 8°. An inflated lobe formed in the blue flow which had a greater height than the adjacent channel. When the levee breached the wax escaping from the breach had enough momentum to cross the levees of the neighbouring channel.

5.5.2 Volume Variation

In order to investigate the effects of volume on flow-field morphology 11 experiments were run with a volume of 200 ml and 11 were run with a volume of 300 ml on variations of slope between 2^{o} and 12^{o} with otherwise identical emplacement mechanisms. The methodology used was as described above in the slope variation experiments. The methodology required the wax to flow under gravity. The wax was held in a reservoir (dropping funnel) which was placed above the inclined glass plane and the wax released via a tap at the base of the reservoir. The flow rate was dependent on the hydrostatic pressure in the dropping funnel. It was expected that the smaller 200 ml volume experiments would have a lower V_{mean} due to the smaller volume contained in the reservoir creating less hydrostatic pressure. As discussed in the slope variation results section, lower V_{mean} favours the growth of tubes over levees and results in smaller flow-field lengths. Therefore, it was hypothesised that decreasing the volume of material in the dropping funnel, would alter emplacement mechanisms, resulting the flow-fields that could be distinguished from each other morphologically. However, the V_{mean} and effusion rate for the 200 ml experiments remained consistent with those of the 300 ml (Figure 5.30). The smaller volume effusions did generate smaller flow-fields with fewer flows (5.31)

Figure 5.30 – The graph shows the average of all experiments. Effusion rates showed no appreciable change between the 200 ml and 300 ml experiments.

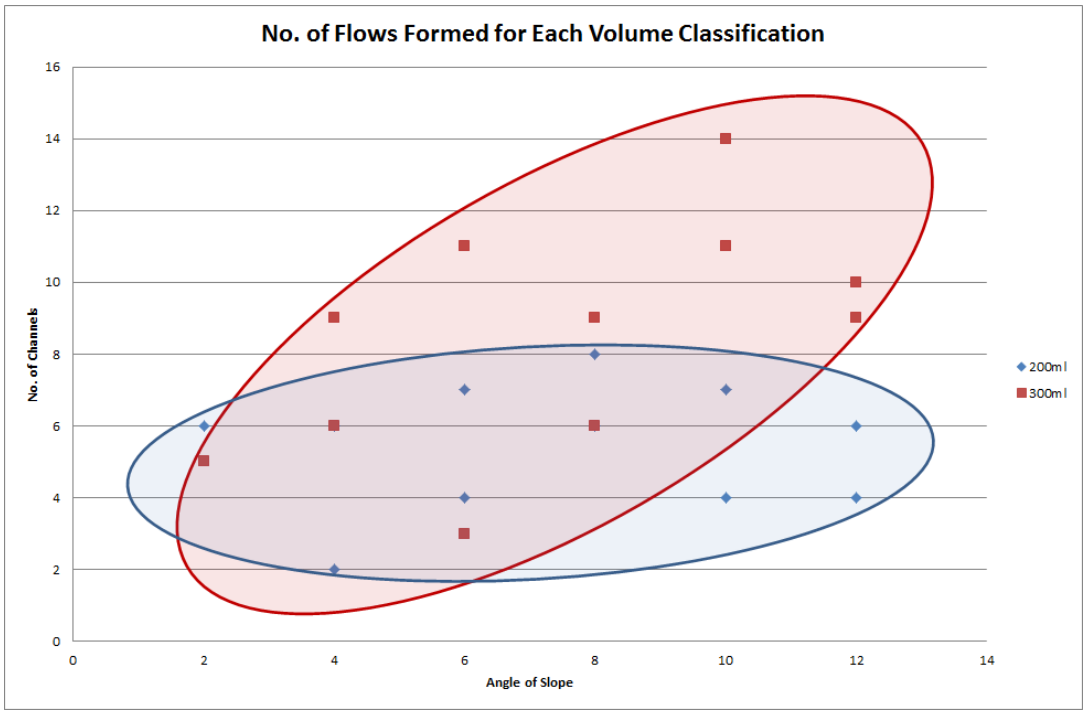

Figure 5.31 – The 300 ml experiments produced more flows at every degree of slope compared to the 200 ml experiments. At slopes above 8°, this trend is particularly pronounced with the 300 ml experiments producing >50% more flows that the 200 ml equivalent.

Although the flow-fields resulting from the 200 ml experiments may have been smaller, there was no appreciable difference between the flow or flow-field aspect ratios. Due to the smaller number of flows formed in the 200 ml experimental runs, the total number of lobes, channels and tubes formed was correspondingly lower but the ratio between slope and number of channels, lobes and tubes remained consistent between the different volume experiments. Flow behaviour and V_{mean} followed identical trends for both suites of experiments which were in line with the behaviour described in the slope variation section (Section 5.5.1). Emplacement mechanisms for flow structures was also in agreement with what was observed in the slope variation experiment suite with levee, tube and lobe growth following the same trends. The initial stages of emplacement were effusion rate controlled. In the slope variation experiments it was observed that emplacement rate increased with increasing slope and therefore structures associated with higher values of V_{mean} such as levees were more commonly found in experiments on higher slope angles. It was expected that 200 ml experiments would have a lower effusion rate ($E_{r)}$ than that of the 300 ml experiments due to the presumed lower hydrostatic pressure which would allow flow structures which were associated with lower V_{mean} such as tubes to appear on higher slopes than in 300 ml experiments. However, as there was no significant measured variation between E_r for an experiment of 200 ml and 300 ml on the same slope. The time taken for the flow emplacement regime to transition from being effusion rate controlled to cooling controlled with the development thermal boundary zones on the outer edges of the flow and growth of solidified crust on the surface of the wax also showed no difference between the two experimental suites. It was observed

that the third stage of emplacement which is normally characterised by thickening and lateral growth lasted for a shorter duration in the 200 ml experiments.

5.5.3 Effusion Rate Variation

In order to investigate the effect of effusion rate on flow-field morphology and the conditions under which flow structures develop, the effusion rate of experiments was varied and the resultant morphologies compared. The effusion rate experiments were carried out on all slope angles from 2^o to 12^o in 2^o increments. As the methodology called for the wax to flow under gravity using hydrostatic pressure, no pump was used in the apparatus. In order to vary the effusion rate, the degree to which the aperture of the dropping funnel was open was adjusted to produce different effusion rates. Effusion rates (E_r (m^3 s^{-1})) were measured using the equation for effusion rate described in the methodology and classified into three groups:

Low - ErL ($<8.23 \times 10^{-7} – 5.09 \times 10^{-6}$)

Medium - ErM ($>5.09 \times 10^{-6} – 9.59 \times 10^{-6}$)

High - ErH $>9.72 \times 10^{-6} – 3.50 \times 10^{-5}$)

Varying effusion rates produced strong and repeatable trends in flow-field evolution and the development of flow structures. As discussed in Section 5.51, the emplacement of the wax flow-fields occurred in three distinct stages – effusion rate controlled, cooling controlled and thickening and lateral growth. This was also true for the varied effusion rate experiments with all experiments following this

sequence. As with the slope variation experiments, varying the emplacement parameters had an effect on the time taken to transition from one stage to the next. At high effusion rates, the time taken to transition from effusion rate controlled to cooling controlled was longer with the first breakout forming at greater distances from vent. As discussed in Section 5.5.1 on slope variation, increasing the angle of slope resulted in an increase in effusion rate and a corresponding increase in distance from the vent to first breakout. This is illustrated again in the effusion rate experiments, although the high effusion rate experiments had the longest time elapsed to first breakout, there is a very definite trend with slope. For all effusion rate classifications, increasing the slope angle had the effect of increasing the time taken to first breakout. Although this trend was seen on all slopes, it decreased with increasing slope angle. For slopes of 2^{o}, time to first breakout increased by 50% from low to high effusion rates compared to 17% on slopes of 12^{o}. In the high effusion rate experiments on slopes of 12^{o} resulted in the largest value for time taken to breakout. The time taken for flow-fields to reach their maximum length showed no definite trend with increasing effusion rate contrary to our hypothesis.

During the high effusion rate experiments, the first stage of emplacement had the longest duration with the majority of wax effused during that time. Stage two - cooling and formation of flow structures, had the next longest duration whilst the last stage, thickening and lateral growth was the shortest and in some cases was difficult to distinguish from the second stage. Experiments carried out at low effusion rates evolved quickly from the effusion rate to cooling controlled stage, and this later stage had the longest duration. These experiments also had a well-defined third stage of thickening and lateral growth. For experiments with effusion

rates within the medium effusion classification, each stage was observed, with the time taken to transition between stages more uniform. For these experiments, the last stage, thickening and lateral growth was well defined, and had the most marked effect on overall flow-field morphology.

The variation in transitions times between stages for the three effusion rate classifications is reflected in the overall flow-field dimensions. High and medium effusion rates, which had the longest duration first stage of emplacement, had the longest flow-fields. There is also a strong correlation between flow-field length and angle of slope. For both medium and high effusion rate experiments, flow-field length increases with every 2^{o} increments of slope, the longest flow-fields occurring at the highest slope angle (12^{o}). For low effusion rate experiments the trend is not so clearly defined. At slope angle of between 6^{o} and 12^{o}, the length of the flow-field remains almost constant regardless of effusion rate but increases with slope (Figure 5.32).

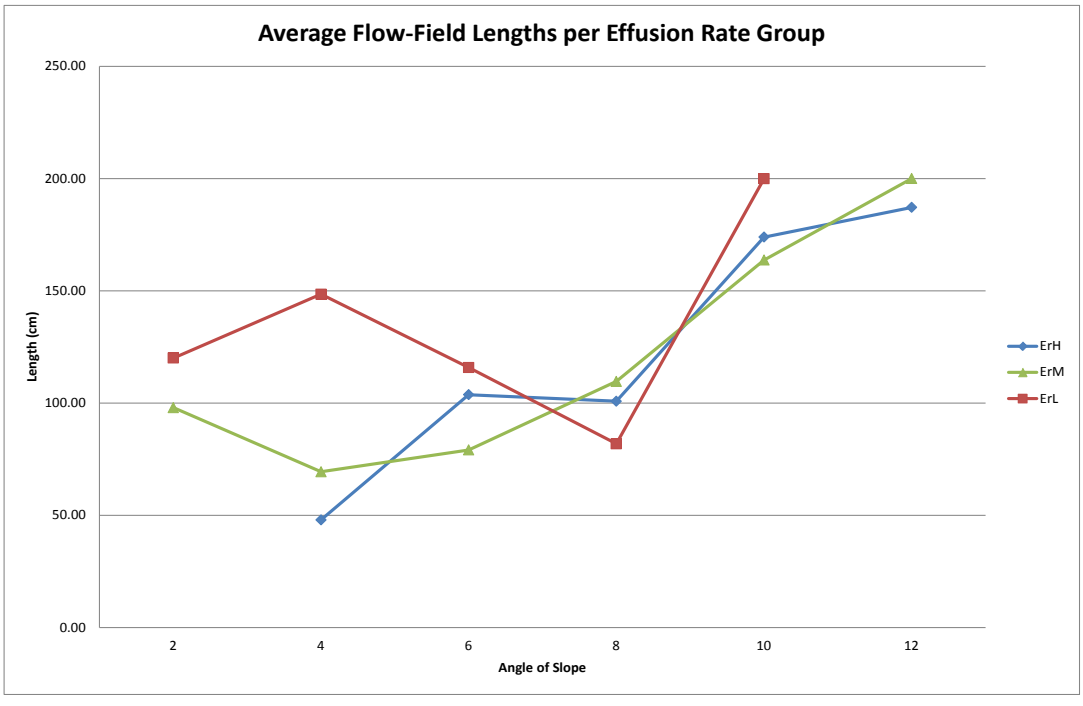

Figure 5.32 – At a given angle of slope overall flow-field length appears to be similar regardless of effusion rate classification. As the slope increased, the length of the flow-field also increased to the same degree in each effusion rate group. This trend is particularly pronounced at slope angles above 6^{o}.

A similar trend was observed with flow-field widths. During the slope variation experiments, it was observed that as slope increased, there was no strong trend in flow-field widths. What was unknown was if this was an effect only of slope or if other parameters apart from topography, also effect flow-field dimensions. All effusion rate experiments showed decreasing flow-field widths with increasing slope but what was also observed was that there was a clear distinction between the widths achieved by each effusion rate group, with the low effusion rate experiments consistently showing the lowest flow-field widths up to 8^{o}. On slopes of 10^{o} to 12^{o}, the high effusion rate group showed the narrowest widths. This group also had the biggest decrease in width from 2^{o} to 12^{o}, appearing to be more affected by the changing slope than the low and medium effusion rate experiments (Figures 5.33, 5.34).

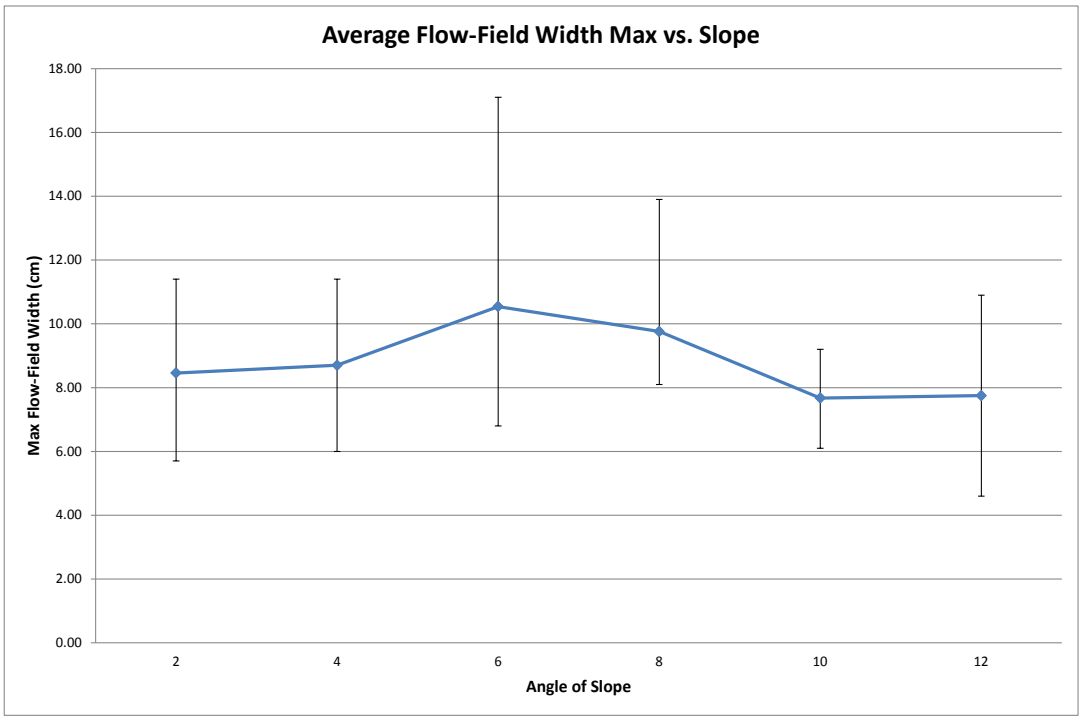

Figure 5.33 – There was no strong trend in average flow-field width with slope for the E_rH group.

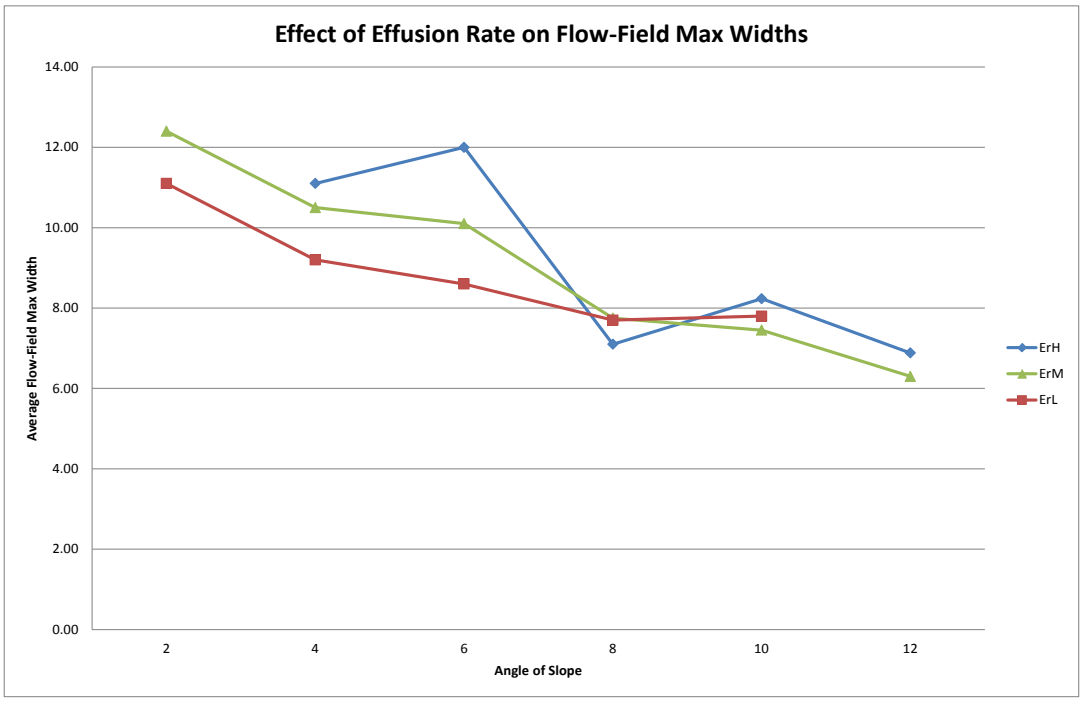

Figure 5.34 –Flow-field widths were observed to decrease with increasing slope angle. It was also observed that high effusion rate experiments, resulted in markedly lower max field widths.

In the slope variation experiments there was a minor trend between increasing slopes angles and increasing flow heights, in order to quantify whether this was as a result of slope or increasing effusion rate, the flow heights in the effusion rate experiments was also measured. The results show that the high effusion rate experiments have the largest flow heights at any given slope and that height decrease from high to medium to low effusion rate experiments. ErH showed no appreciable trend in flow height with slope. In the E_rL experiments, height increased with increasing slope but remained the smallest height at any given angle of slope in comparison with the other two experimental groups. E_rM showed a decreasing trend with increasing slope, contrary to the E_rL experiments (Figure 5.35).

For E_rM and E_rH, flow minimum widths decreased overall with increasing slope. E_rM showed the clearest trend, decreasing by 58% from 0.85 cm at slope 2^o to 0.50 cm at slope 6^o after which, flow minimum width stabilised. E_rH showed an overall decrease in width with increasing slope from 4^o to 12^o. However, the trend was not as strongly defined as with E_rM although for any given slope, E_rH widths were greater than those of E_rM. E_rL showed no trend with slope and no trend in width in regard to E_rM and E_rH (Figure 5.36).

As evidenced by the trends in flow heights and widths, flow-field aspect ratio also increased with increasing slope regardless of effusion rate classification. At any given angle of slope, the E_rH experiments had the highest aspect ratios, evidence of higher effusion rates producing higher, narrower flow-fields (Figure 5.37).

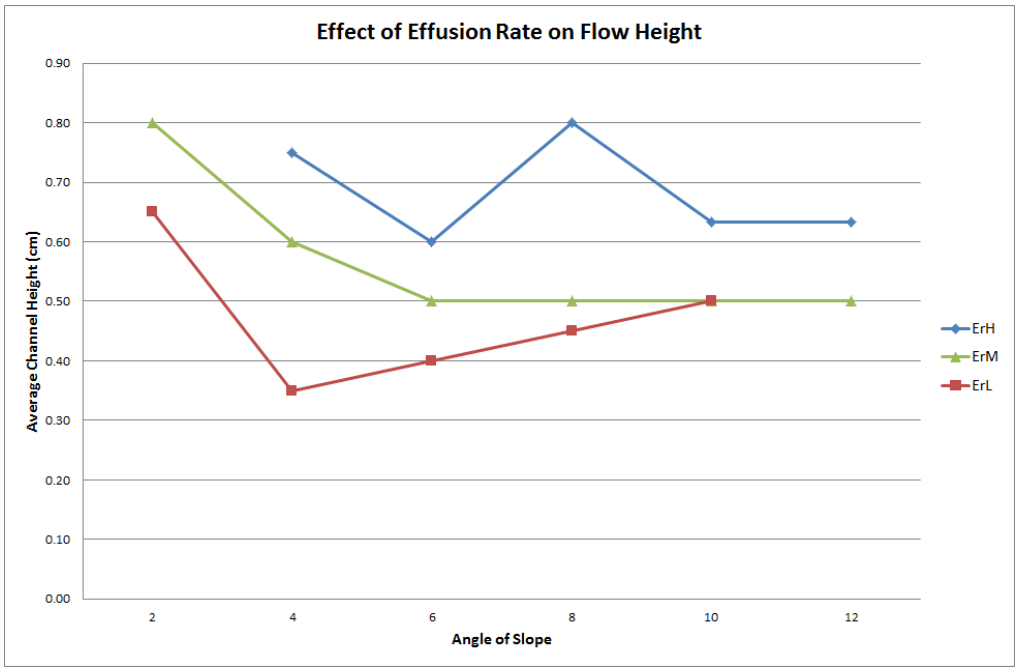

Figure 5.35 – For any given slope, higher E_r produced thicker flows. E_rL was the only experimental group which showed increasing flow thickness with increasing slope. E_rM decreased with increasing slope from 2^o – 6^o after which it remained stable.

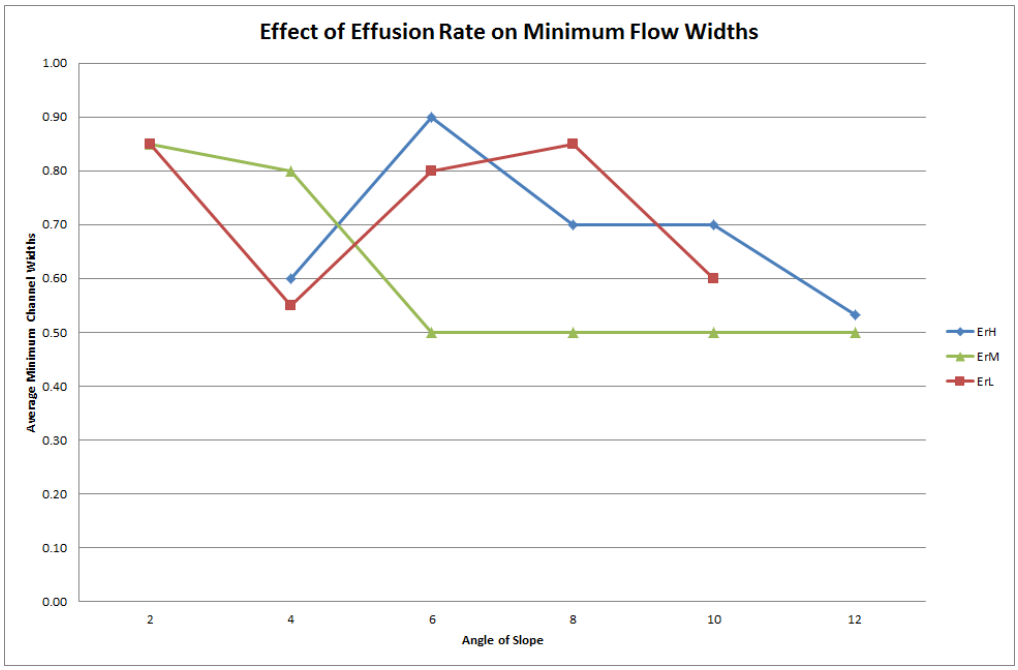

Figure 5.36 – At any given slope the high effusion rate experiments E_rH had on average, greater minimum flow widths that those of the E_rM experiments.

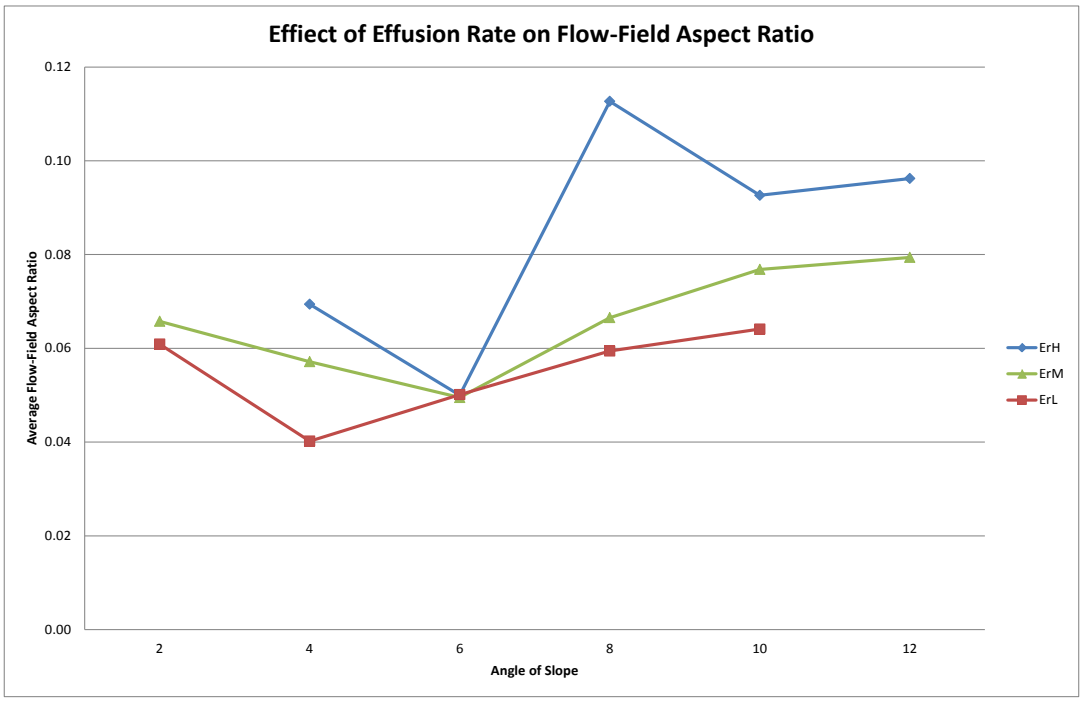

Figure 5.37 – At any given slope the high effusion experiments produced flows with the highest aspect ratio. This trend was also observed with increasing slope where, regardless of effusion rate classification, the aspect ratio of all experiments on average, increased with increasing slope.

The second stage of emplacement is also characterised by the development of flow structures such as secondary flows, levees, lobes and tubes. In the slope variation suite, the average number of flows formed, increased from 9 to 11 with increasing slope. The trend was not repeated in the effusion rate variation suite where there was a high degree of variability between slope and secondary flow formation and the highest average number of flows formed (Figure 5.38).

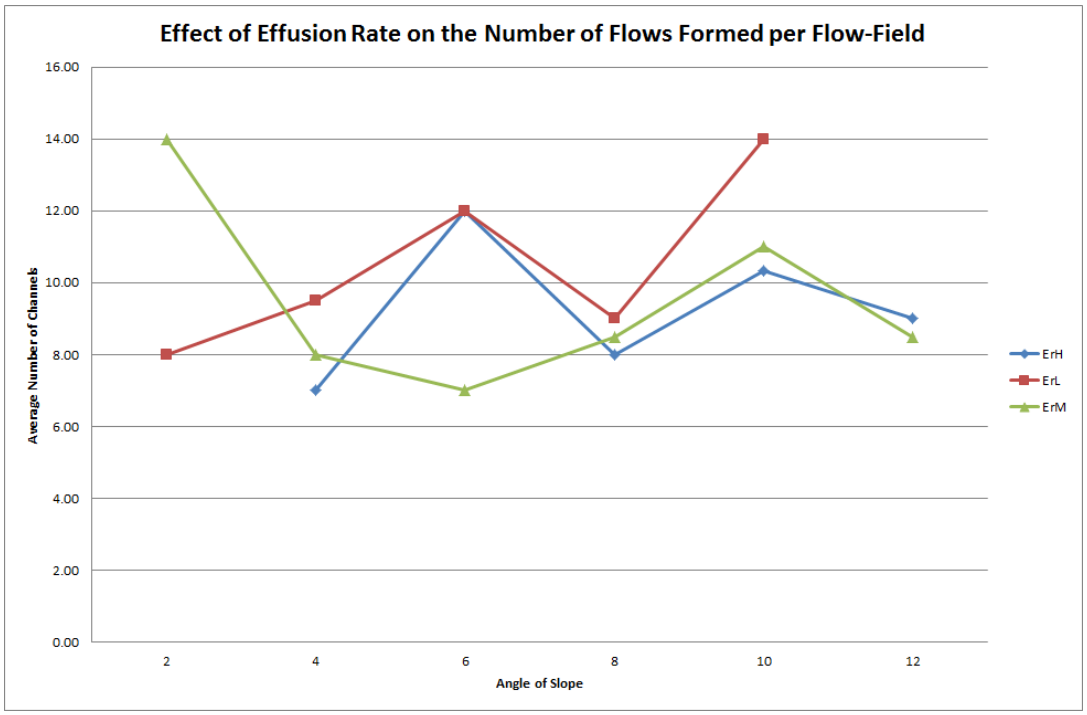

Figure 5.38 – The number of flows formed varied considerably at each angle of slope. There was also no trend between the effusion rate groups with the group with the highest number of flows formed varying for each angle of slope.

Lobe growth appeared to be independent of effusion rate while there was an overall trend of number of lobes decreasing with increasing slope in the slope variation experimental suite, this trend was not observed in the effusion rate experiments for E_rL. Lobe formation in the E_rM suite did decrease overall with increasing slope but show variability from slope angle to the next. The strongest trend was observed in the E_rH suite where lobe formation decreased steadily with increasing slope (Figure 5.39). It was thought that flow-fields with a greater number of flows would contain a greater number of lobes as cooling would act on the head of each flow, forming a solidified flow-front which would facilitate lobe growth. However this behaviour was not observed. In the multi-flow systems it was common for a flow to be suddenly and immediately drained if a breakout occurred up channel, capturing the material in the original channel and diverting it into a new

flow. This mechanism resulted in a drained channel, which halted, not because of cooling but because of a cease in supply. This meant that although there may be an increase in the number of flows formed during an experiment, not all will form lobes. Conversely, a flow-field with only a few flows can still form a large number of lobes as a succession of breakouts and new lobe formation build a network of lobes at the flow-front because of a higher effective feeding rate to each front..

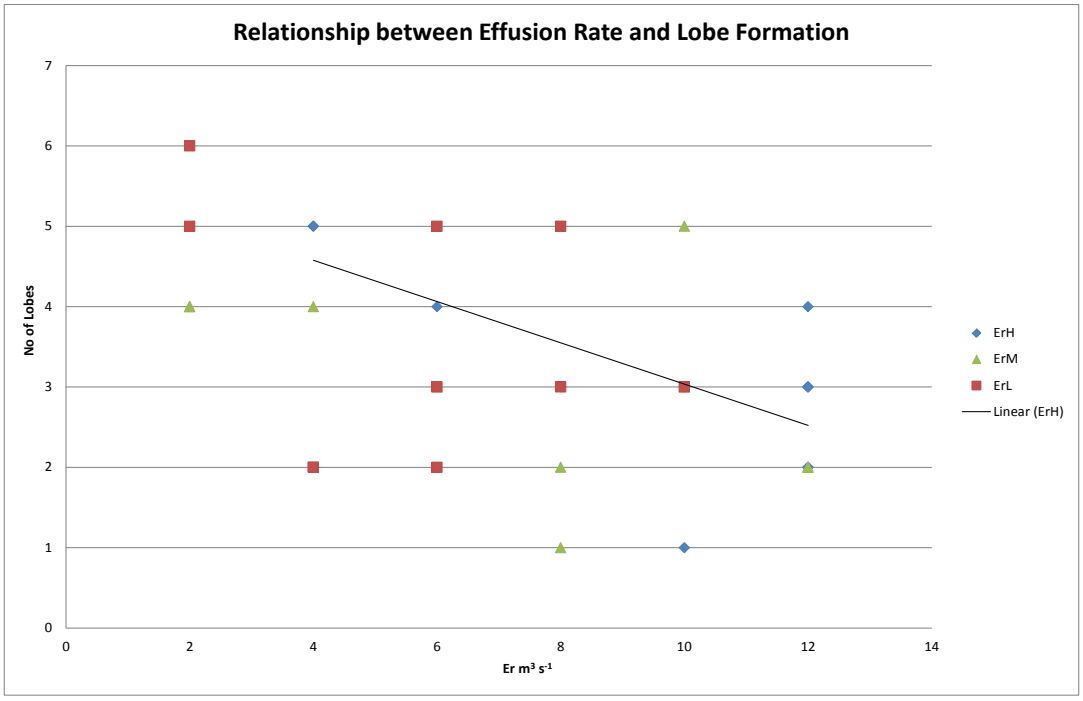

Figure 5.39 – Average of all effusion rate variation experiments. E_rH showed the strongest trend with lobe formation decreasing with increasing slope.

Tubes were observed to form more commonly in experiments on low angles of slope in the slope variation experimental suite, a trend which repeated itself in the effusion rate experiments (Figure 5.40). For all effusion rate groups, the number of tubes formed decreased overall with increasing slope. On angles of 2^o to 8^o for E_rL, the number of tubes increased with increasing slope from, on average, 0.5 to 2. On slopes higher than 8^o the number of tubes formed dropped by 50% to on average 1 per flow-field. E_rM showed the greatest variability in terms of slope vs. tube

formation. This group produced the most tubes per flow-field with an average of 3 at slopes of 4° and 8° degrees but also produced the lowest with experiments run on slopes 6° producing no tubes. E_rH showed a steady downward trend from 2.5 tubes on average per flow-field to 1 tube per flow-field for higher slopes.

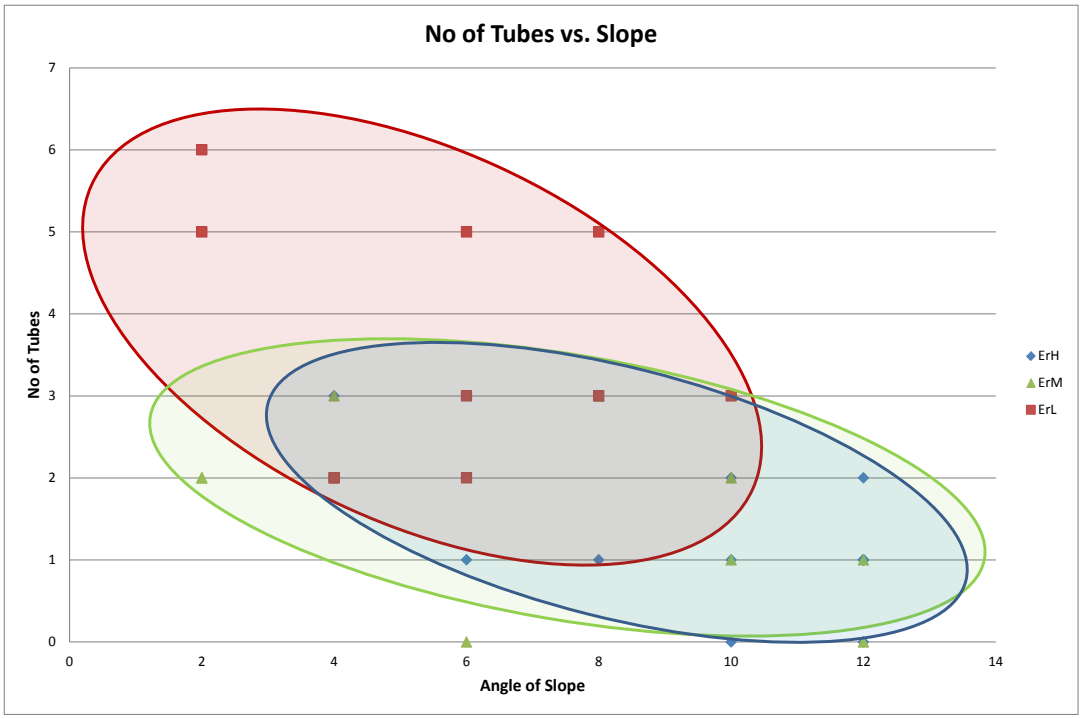

Figure 5.40 – For all experimental suites, the number of tubes formed decreased with increasing angle of slope. E_rL was the only experimental group to have at least one tube formed in every flow-field.

Leveed channels showed a very strong trend with slope. The slope variation suite showed an overall increase in number of levees formed with increasing slope (Figure 5.41). This trend was repeated in the effusion rate variation suite with the number of leveed channels increasing significantly with slope angle for E_rM and E_rH. Although the trend was seen in both experimental suites, there did appear to be a difference in the pattern of levee growth in the effusion rate experiments. The results showed that the trend is most stable for medium effusion rates, with number of leveed channels increasing with every 2° increments of slope. While the overall

trend for high effusion rates also supported this trend, there was some variation on an increment by increment basis. The E_rL experiments had, on average, the same number of levees form in each flow-field regardless of slope (Figure 5.42).

In the case of some very high effusion rates experiments, levees did not always form, resulting in unconfined flows whose widths were greater than their leveed counterparts with a lower aspect ratio. In these experiments, the material is moved so quickly down the slope that cooling played less of a role in channel formation and typically these flows were relatively featureless and either ended in a lobe or experienced a breakout which diverted material from the flow before any surface features could form.

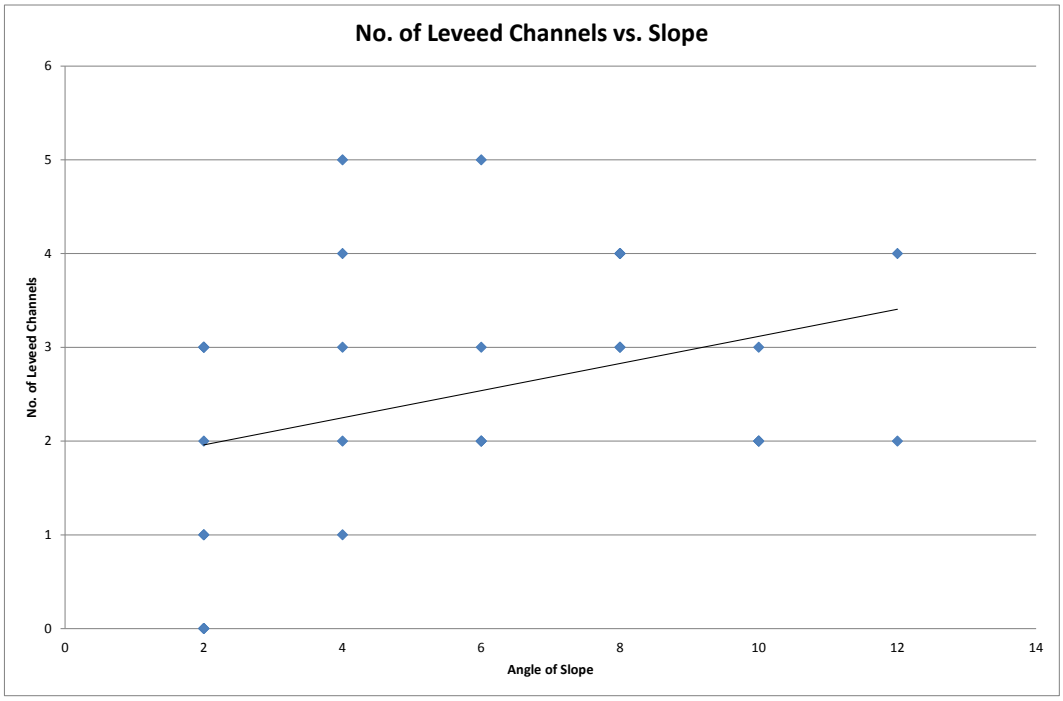

Figure 5.41 – Averaged number of levees formed vs. slope from the slope variation suite. Overall as slope increased, the number of levees formed also increased. There was also considerably less variation per degree of slope on higher slope angles.

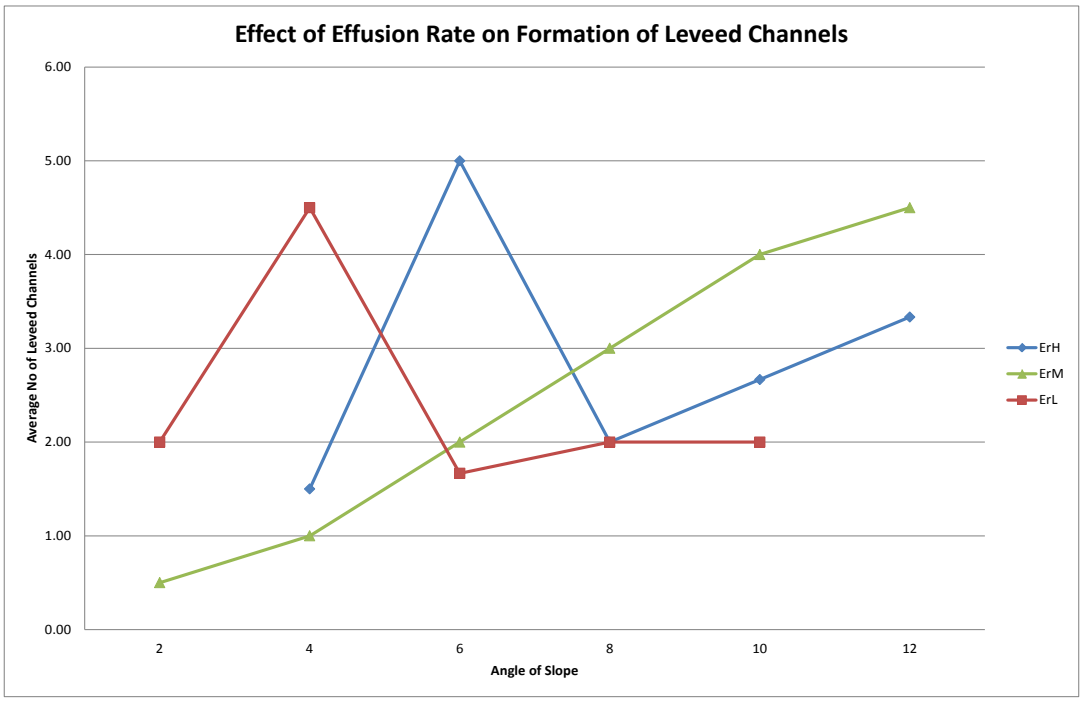

Figure 5.42 – Average of all effusion rate experiments. Strong trend between increasing slopes and the number of leveed flows formed. The medium effusion rate experiments resulted in the most stable trend and the highest number of leveed channels.

In the slope variation suite, the number of breaches observed per flow-field increased with increasing slope. This trend was not observed in the effusion rate variation suite. At any given angle of slope the effusion rate group with the highest number of breaches was varied although the E_rL suite showed the least amount of variability and was the only effusion rate group to show the same trend as the slope variation experiments with the number of breaches observed increasing with increasing slope (Figure 5.43)

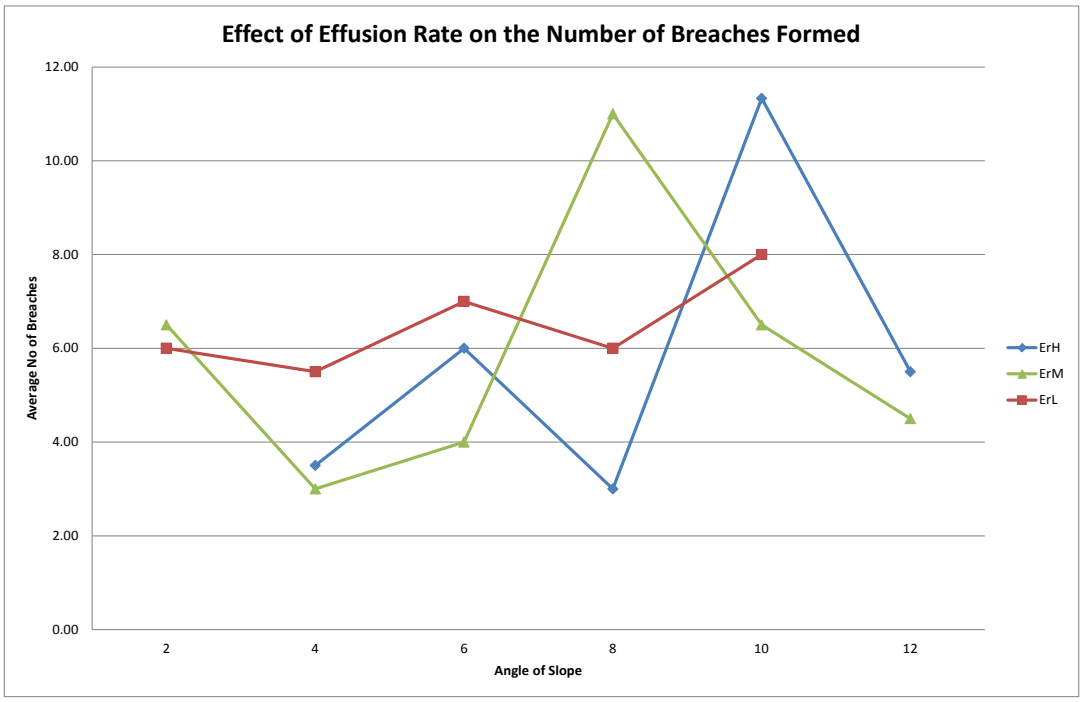

Figure 5.43 – E_rL was the only group to show a trend with increasing slope. As the slope increases, the number of breaches observed also increases, confirming the trend observed in the slope variation experimental suite. This trend disappears as the effusion rate increases with E_rH – the group with the highest effusion showing the greatest volatility.

Overflows, as a mechanism for secondary flow formation also showed an increase with increasing slope in the slope variation experiments, a trend which was repeated in the effusion rate variation suite. This trend was more pronounced in the ErM and E_rL groups which reached the highest number of overflows observed in at 10^o to 12^o degrees of slope. Although E_rL showed a steady increase of overflows with slope, fewer overflows overall were observed in this group. E_rH also had experiments with the lowest number of overflows recorded at 12^o. During these experiments, it was observed that the flows formed were wide and featureless, without levees or any other structures. These experiments typically had some of the highest effusion rates recorded for any experiment (Figure 5.44).

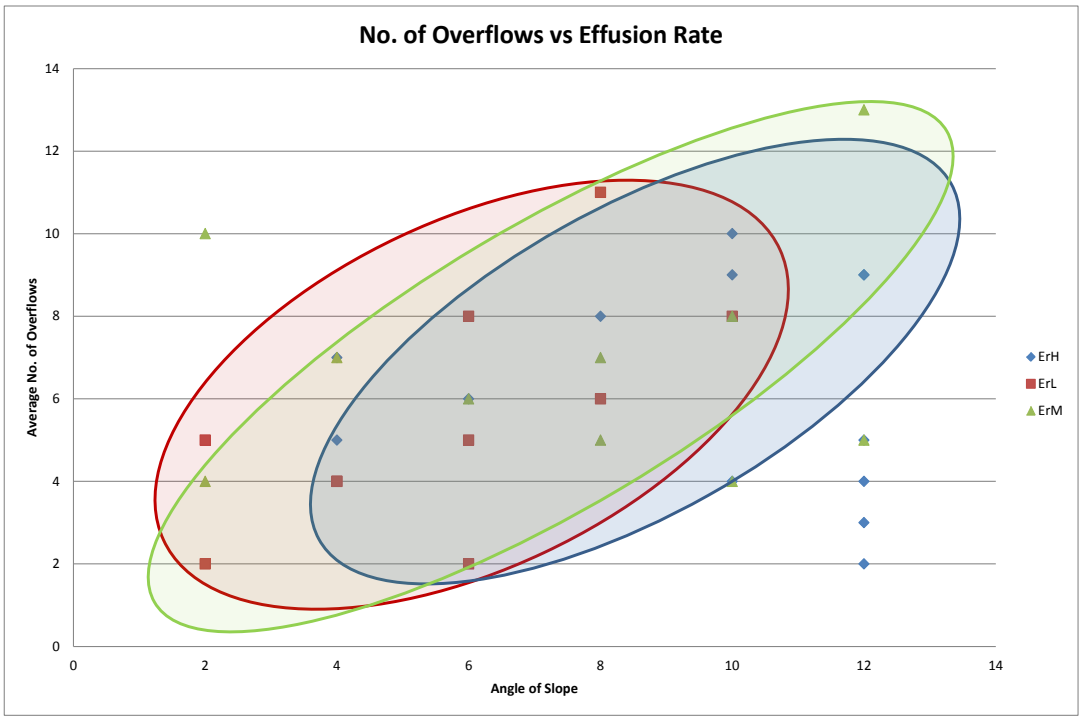

Figure 5.44 – The number of overflow observed in a flow-field increased with increasing slope. Although E_rL showed particularly good agreement with this trend, at any given slope angle, this group produced on average, less overflows than the other higher effusion rate groups.

When breaches or overflows resulted in the formation of secondary flows, it was observed that the flows formed at an angle to the original channel, contributing to the overall width of a flow-field. These angles ranged from 10^o to 40^o. For all experimental suites, this angle was observed to decrease with increasing slope with E_rM experiments producing the lowest angles of formation. At any given angle of slope, E_rM experiments produced smaller angles than those from E_rH experiments. The largest angles were produced in the low effusion rate suite E_rL at the lowest angle of slope (Figure 5.45).

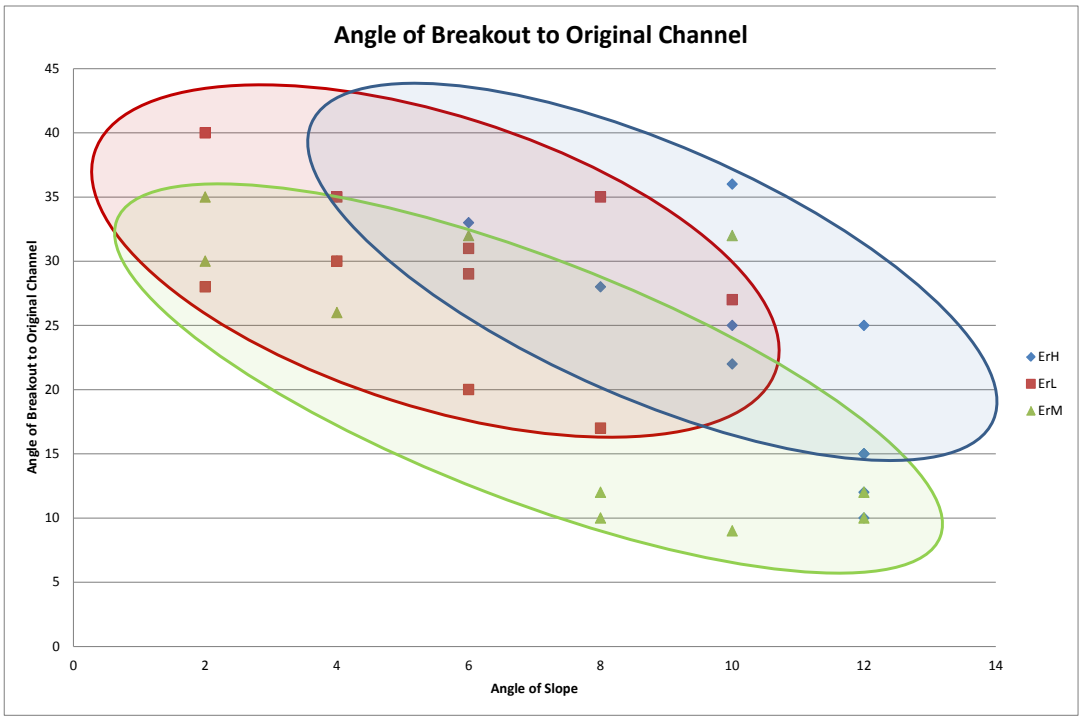

Figure 5.45 – For all effusion rate classifications, the angle at which secondary flow formed to the original channel decreased with increasing slope. E_rM recorded the lowest angles and at any given slope, E_rL produced smaller angles than E_rH.

5.6 Analysis

The qualitative description of the results presented in Section 5.5, show that all experimental suites followed the same general pattern of emplacement regardless of variations in emplacement parameters, slope, volume and effusion rate. It was observed that flow-field morphology is dependent on cooling and subsequently the development of flow structures. Varying the emplacement parameters illustrated the effect that the physical parameters of a flow with a temperature dependent viscosity affect cooling and therefore the overall flow behaviour and morphology. The emplacement history of the wax flows was divided into three distinct stages as previously described - lengthening, widening and

thickening. However, varying the emplacement parameters had the effect of varying the time taken to transition from one stage to the next.

5.6.1 Stage One – Lengthening

The first stage – lengthening, is characterised by the presence of no more than one or two flows which capture all the effused volume. In 70% of experiments (from all experimental suites), the first flow to form was the longest and in 86% of experiments flow-field maximum length was achieved during the first stage. All three experimental suites demonstrated that as the slope increased, so did the emplacement rate. For the slope variation and volume variation suites, the results showed an identical trend, with emplacement rate increasing with slope. All experiments in the suites were designed to have the same initial effusion rate. The emplacement rate increased from a maximum $8.60E^{-06}$ m^3 s^{-1} at slope 2^o to $9.59E^{-06}$ at slope 12^o which is a 111% increase (Figure 5.46).

The effusion variation experiments were designed to have variable starting effusion rates, grouped into three classifications: Low – E_rL, Medium – E_rM and High – E_rH. All three classifications showed increasing emplacement rates with slope, however, the lowest effusion rate group E_rL showed the weakest trend while E_rH showed the strongest. E_rL emplacement rates increased by 108% from 2^o to 10^o whilst E_rH increased by 249% from 4^o to 10^o (Figure 5.47). Therefore, increasing the slope clearly results in increased emplacement rates; however the degree to which, depends on the initial E_r with the effect becoming more pronounced at higher values of E_r.

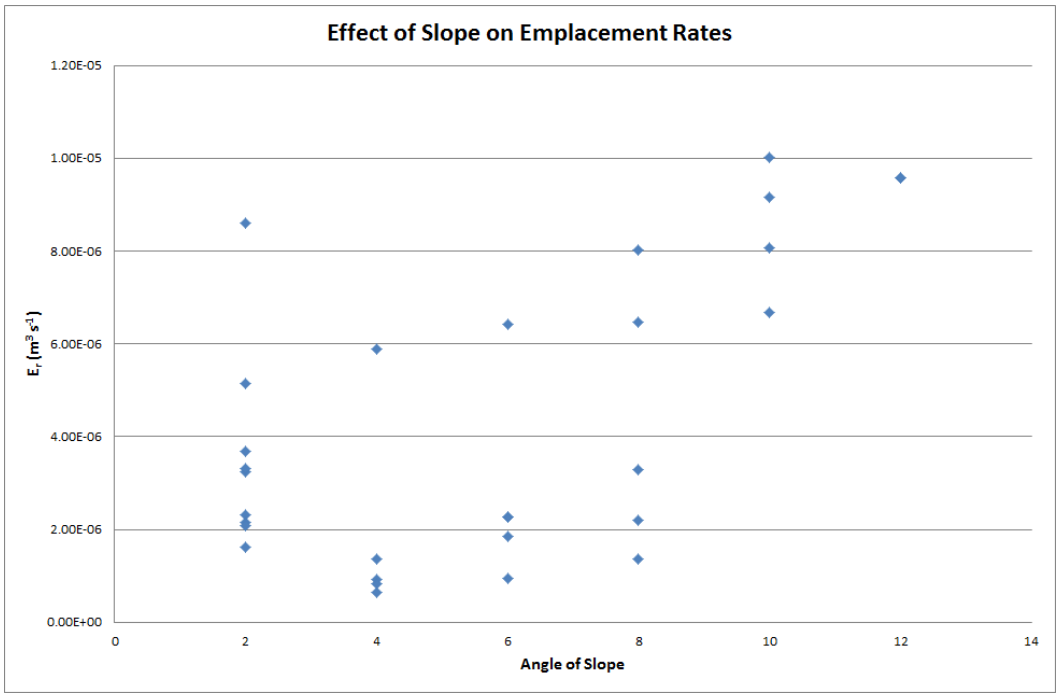

Figure 5.46 – Slope Variation Suite – All experiments were run with the same initial effusion rate. There is a clear trend between slope and emplacement rate, as the increasing slope provides the flow with momentum.

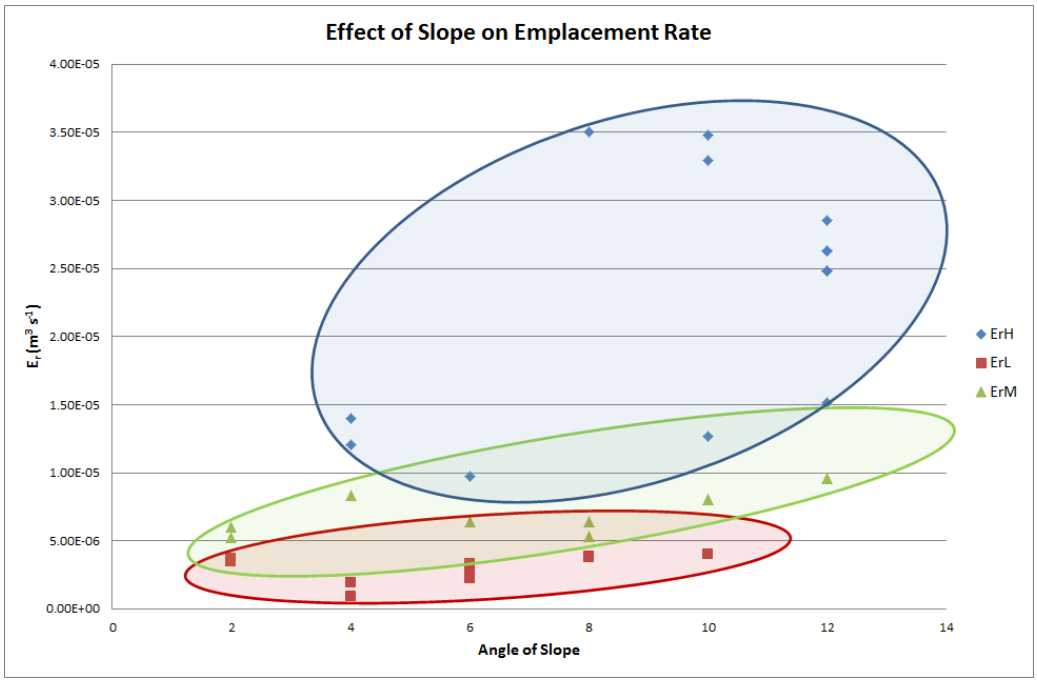

Figure 5.47 – Effusion Rate Variation Suite. Regardless effusion rate, as slope increased so did the emplacement rate. E_rH effusion rates were particularly affected by the changing slope. On slopes >

8° emplacement rates increased by up to 28% to 6°. The experimental results show that the faster the initial effusion rate, the greater the impact changing slope has on the overall emplacement rate.

All experimental suite results showed that flow-field lengths increased with increasing slope whilst the time taken for flow-fields to reach their maximum length decreased (Figures 5.48, 5.49).

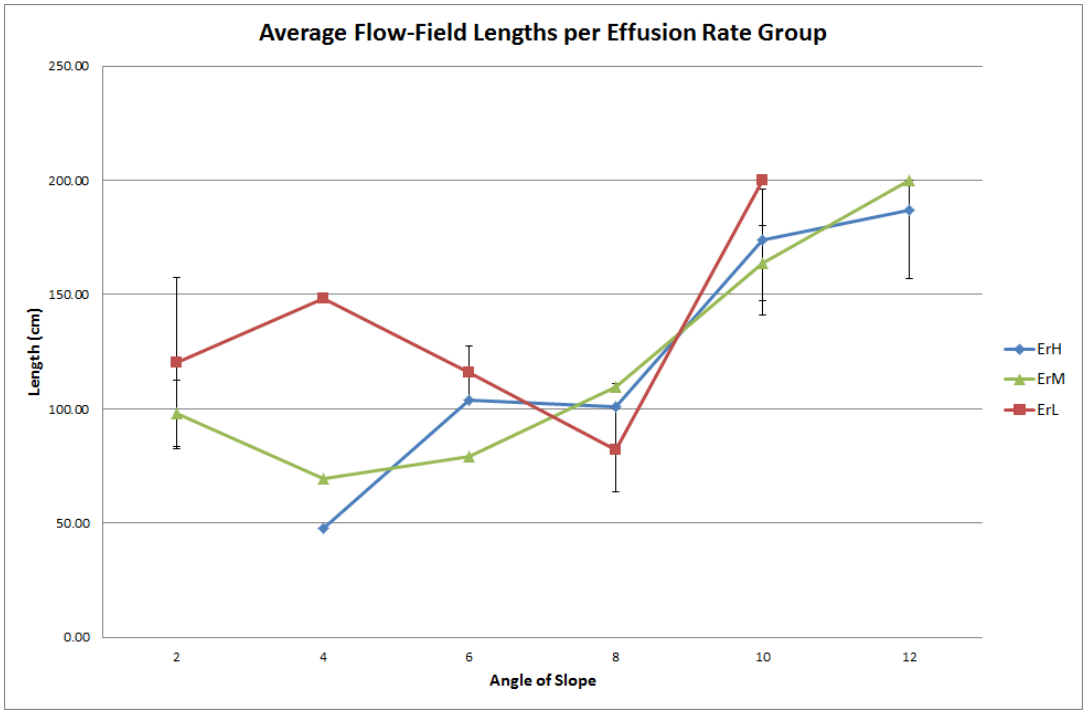

Figure 5.48 – Effusion Rate Variation Experimental Suite - In all effusion rate classifications, the maximum flow-field length increased with increasing slope. At lower angles of slope (≤ 6°) there was a distinct difference in flow-field lengths between the three effusion rate groups. At slopes of > 8° flow-field lengths become very similar, regardless of starting effusion rate.

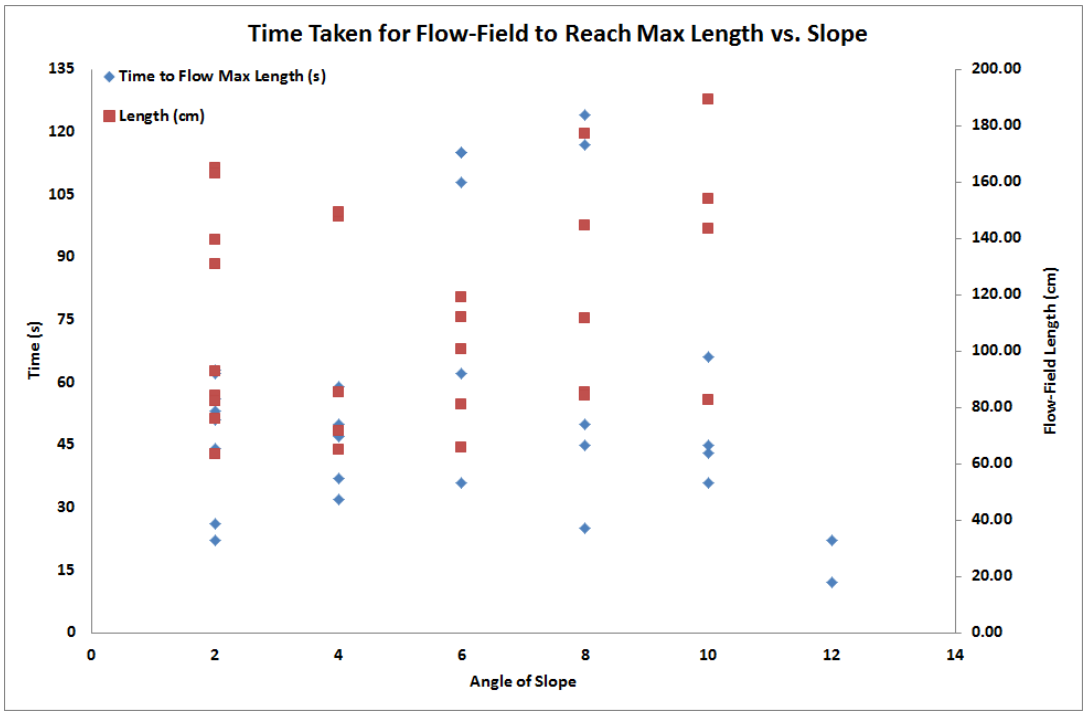

Figure 5.49 – Slope Variation Experimental Suite – The time taken for flows-fields to reach their maximum length decreased with increasing angle of slope, whilst flow-field length increased.

As can be seen in in Figure 5.48, at lower angles of slope ($\leq 6^{o}$) there was a distinct difference in flow-field lengths between the three effusion rate groups. E_rL had, on average the longest flow-fields, whilst E_rH had the shortest. At slopes of $>8^{o}$ flow-field lengths become very similar, regardless of starting effusion rate suggesting that the rise in slope angle, increased the emplacement rate sufficiently to produce flows of similar lengths. This, combined with the data showing that low angles of slope, from 2^{o}- 4^{o}, reproduced on average the longest flow-fields, suggests that the angle of slope may have a greater control on flow length than effusion rate and that increasing slope is responsible for increased length whilst the increase in effusion rate may be responsible for the decrease in time taken to achieve maximum flow-field length.

The development of thermal boundary zones and the occurrence of breakouts was an indicator that flow emplacement was transitioning from stage one,

to stage two. The occurrence of the first breakout therefore, could and was used to pinpoint the transition from one regime to the next. In the slope variation experimental suite, the time taken for a breakout to occur increased with increasing angle of slope, however there was a high degree of variability between the times recorded for any given angle of slope. (Figure 5.50). As discussed above, flow-field length and effusion rate increased with increasing slope while the time taken for maximum length to be achieved decreased. The majority of flow-fields reached their maximum lengths prior to the formation of breakouts, lengths which were achieved more quickly on higher slopes, in direct contrast to the time to first breakout which increased with increasing slope and effusion rate. This would suggest that not only were flows longer on higher slope angles but also that they were more stable and resistant to breakouts.

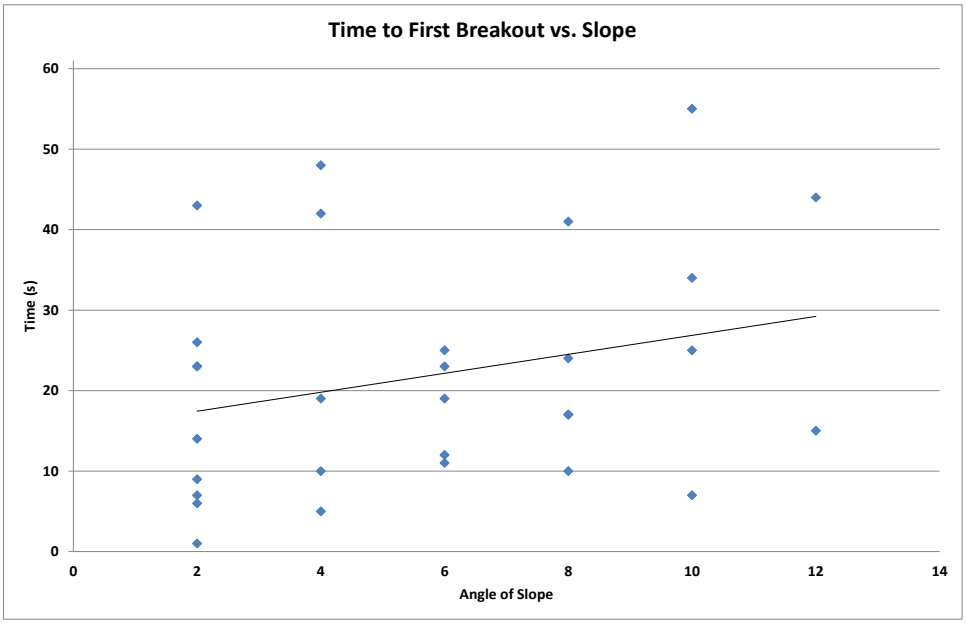

Figure 5.50 – Time taken for the first breakout to occur decreased with increasing slope. However there was a degree of variability between times for any given angle of slope, suggesting that slope angle was not the only parameter influence the timings of breakouts.

In the effusion rate variation experimental suite, there was also a high degree of variability for an effusion rate group at any given slope angle. However the E_rH experiments at 12° of slope produced the greatest degree of variability, showing both the highest and one of the lowest values for time in the experimental suites (Figure 5.51). It was observed during the experimental run that with the highest effusion rates, the wax is moving too fast to form any kind of levee or thermal boundary layer, resulting in relatively wide, free flowing flows of fluid wax. The width of these unconstrained flows means that they are better equipped to cope with fluctuations in the volume of material in the flow, making them more stable and less likely to result in a breakout. Evidence also shows that flows formed at high angles of slope with fast effusion rates result in high narrow flows with well-developed levees more resistant to breaching. These structures and mechanisms will be discussed in more detail in Section 5.6.2 Widening.

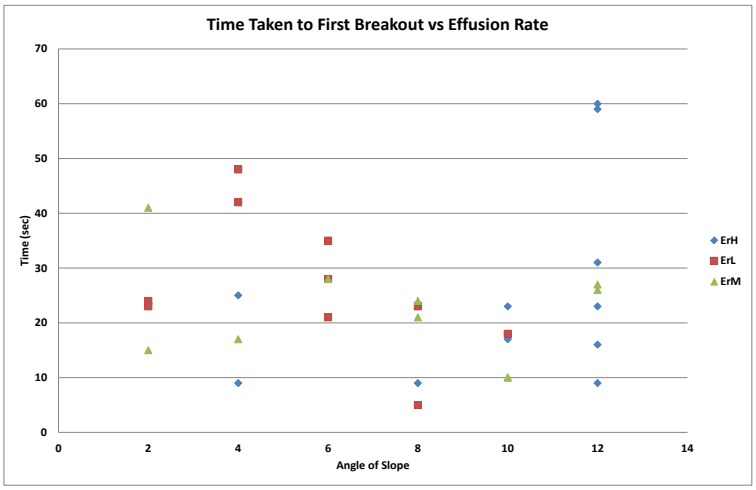

Figure 5.51 – Effusion Rate Variation Suite. For any given slope angle there was a large degree of variability in time taken for a breakout to occur. This was particularly true for the E_rH experiments at 12° which resulted in one of the lowest and highest values for time taken. It was observed during the experimental run that flows formed on high slope angles and high effusion rates where often wide and structureless, with a large carrying capacity increasing the flows ability to adapt to changes in volumes which in other, more well constrained flows would have resulted in a breakout.

High angles of slope produced flows with greater velocity, which achieved flow-fields with the greatest lengths before cooling resulted in the formation of a solidified flow-front and the formation of secondary flows through breakouts. High effusion rates produced flows that required less time to achieve maximum length. Therefore, for a flow with a temperature dependent viscosity, increasing the rate of emplacement either at the point of effusion or by the angle of slope will result in flows of greater lengths.

5.6.2 Stage Two – Widening

The transition to the second stage of emplacement is marked by the appearance of secondary flows, widening the flow-field or the formation of thermal boundary zones on the edges of the preliminary channel and the subsequent development of flow structures, increasing flow-field complexity.

5.6.2.1 Flow-Field Width

The effusion rate experiments all showed a decrease in flow-field width with slope. For a given value of slope, E_rH on average consistently produced the widest flow-fields, with E_rL producing the narrowest. As the slope increases the difference between the effusion rate groups reduces, while still maintaining the trend (Figure 5.52)

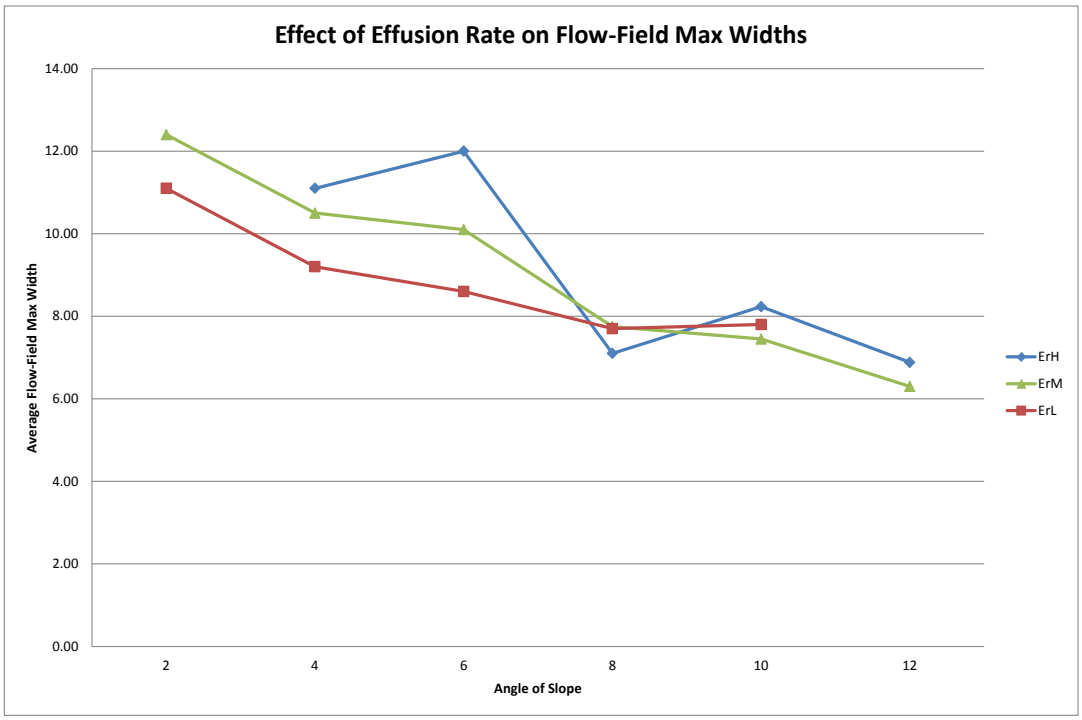

Figure 5.52 – Each effusion rate classification showed a decreasing in flow-field width with slope. At any given slope, E_rH had on average, the greatest widths while E_rL had the lowest apart from at 8^o. This change in trend is caused by one experiment and could be consider anomalous.

As discussed in the previous section, the time to first breakout and flow lengths both increase with increasing effusion rate. All slope and effusion rate experiments were run with a set volume of 300 ml. The greater the distance the initial flow reaches the greater the percentage of the total volume of wax that will be emplaced in first one or two flows resulting in a smaller remaining volume to be effused in secondary flows. The same is true for flow-fields with the largest value for time to first breakout. The longer the first stage of emplacement lasts, the less volume will be available for the formation of secondary flows. The volume variation experiments support this theory as a clear trend can be seen in the smaller 200 ml experiments. As slope and therefore emplacement rate increases, flow-field width decreases. The 300 ml results are more variable with no clear trend in flow-field width, mirroring the results of the slope variation experiments which were also

carried out with 300 ml of wax (Figure 5.53). During the 200 ml experiments, it was observed that the total volume of wax was typically effused during stage one and two of emplacement and therefore stage three – thickening was never realised. This was not true for the 300 ml experiments in both the volume and slope variation experimental suite which experienced lateral growth in both the second and third stages of emplacement.

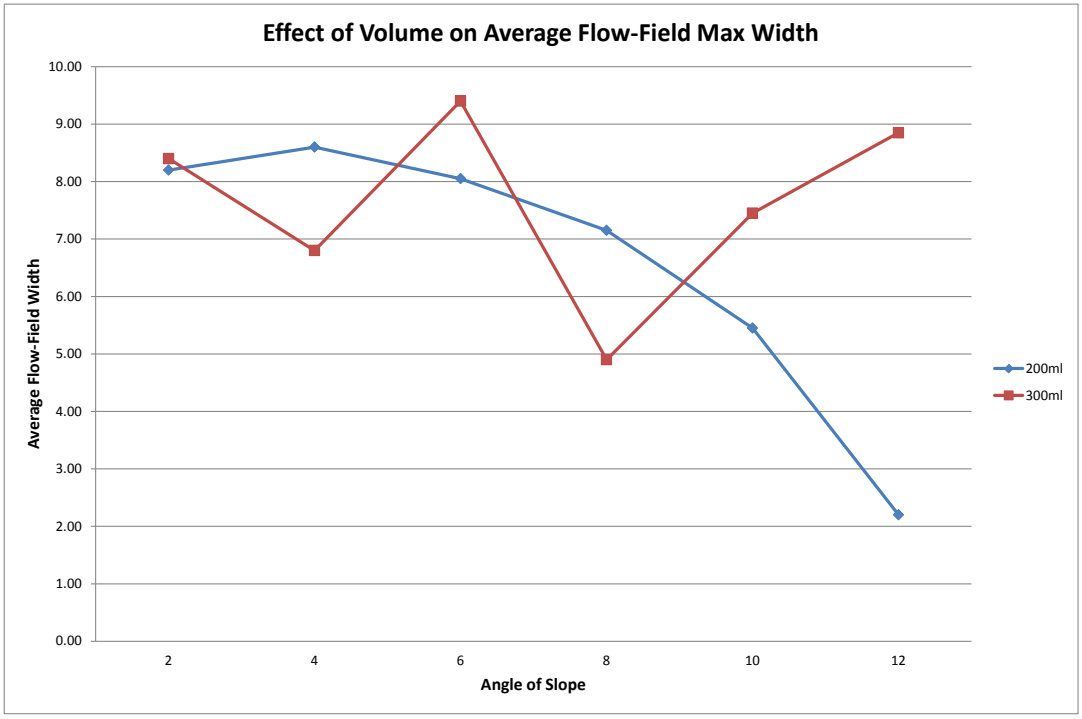

Figure 5.53 – In the 200 ml experimental suite there was a clear trend between increasing slope and increasing effusion rates. The same trend was not present in the 300 ml experiments.

Flow widths also follow the same trend as overall flow-field widths with minimum flow widths decreasing with increasing slope. On average, minimum flow widths of experiments carried out at 12^{o} were 58% smaller than those carried out at 2^{o} (Figure 5.54). Although the effusion rate experimental suite also showed the same trend with increasing slope, the degree to which the minimum flow width was affect varied with effusion rate classification. For the E_rL experimental group,

flow width decreased by 30% on average from 2° to 12° slopes while E_rH experimental group showed only an 11% decrease (Figure 5.55).

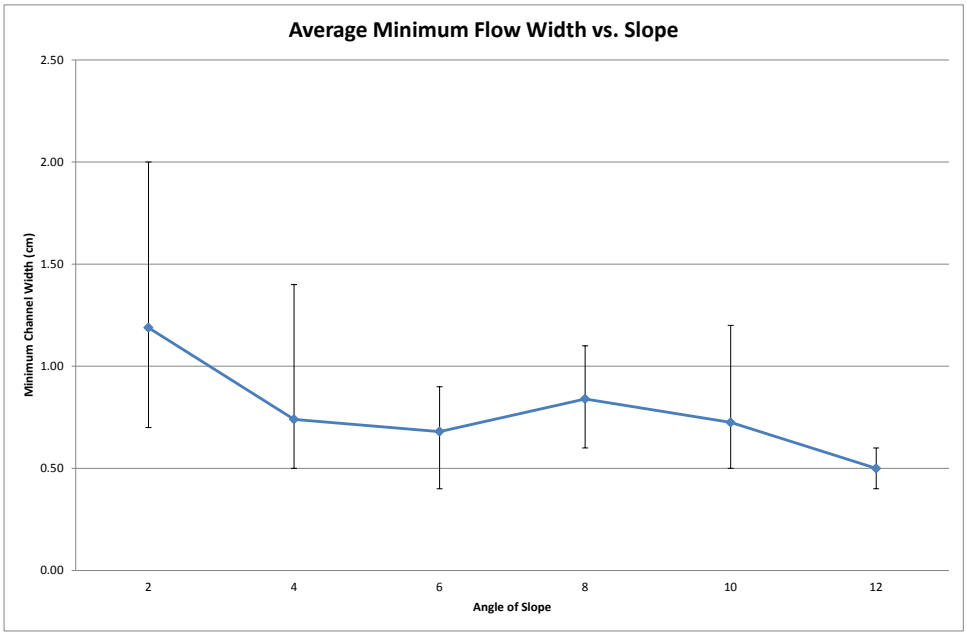

Figure 5.54 –Slope Variation Experimental Suite. On average, minimum flow widths decreased by 58% from experiments carried out 2° to 12°.

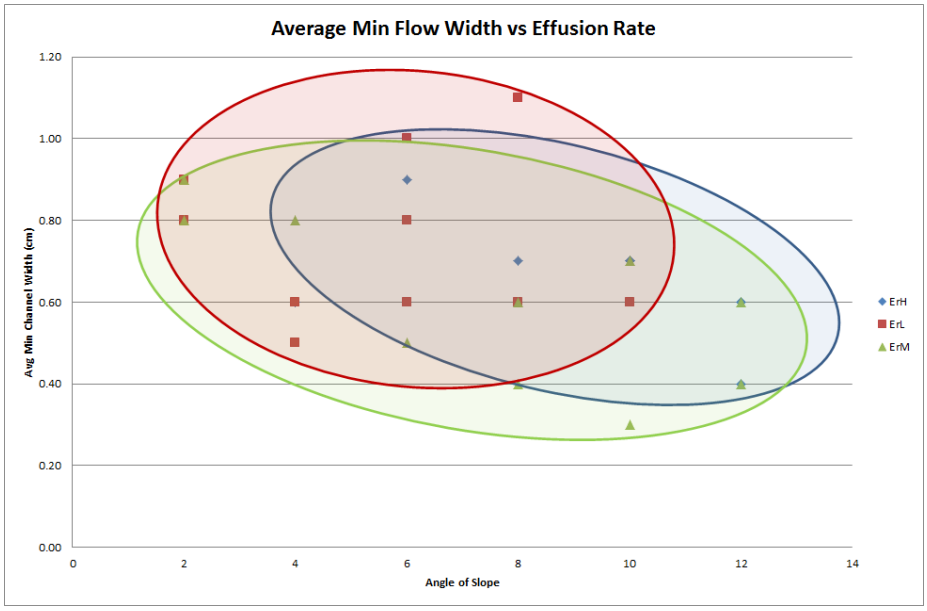

Figure 5.55 – Effusion Rate Variation Experimental Suite. E_rL on average showed a 30% decrease in minimum flow widths in experiments carried out on slopes of 12° compared to those carried out on slope of 2°. E_rH group showed an 11% decrease under the same conditions.

These results support the work of Gregg & Fink (2000) who observed that flow widths decrease with increasing slope which is behaviour typical of a Newtonian fluid. Gregg and Fink also observed that although flow width decreases with slope, for any given slope value, increasing the effusion rate results in wider flows, trend which is also represented in the effusion rate variation suite where the change in flow minimum widths with increasing slope is 30% of E_rL compared with 11% for E_rH.

In addition to flows becoming wider with increasing effusion rate, their height also increases. As can be seen in Figure 5.56 for any given value of slope, the higher the effusion rate, the larger the flow height. E_rL has the lowest height, whilst E_rH has the largest. These results follow the observations of Stasiuk et al., (1993) who state that increasing the effusion rate for a given viscosity leads to a thicker flow.

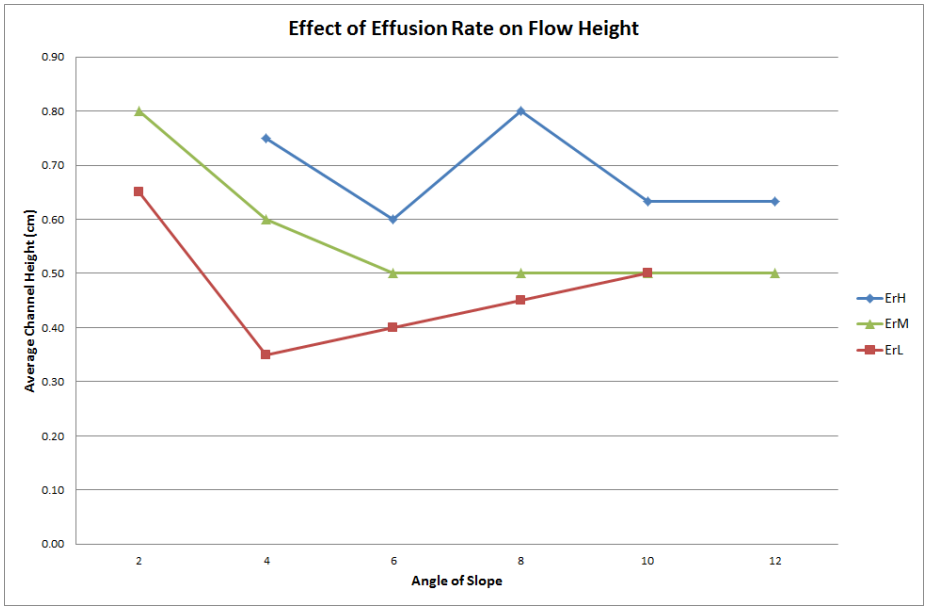

Figure 5.56 – For a given angle of slope, E_rH consistently produced flows that had on average, greater heights than those of E_rM and E_rL.

Secondary flows formed at an angle to the original channel, which contributes to the overall increase in flow-field width which correlates with measurements taken during the field investigation (Section 3.2.2) The angles ranged in values from 10^{o} to 40^{o} with 70% falling into the 25^{o} – 35^{o} bracket. In the slope variation suite, on average the angle of breakout decreased with increasing slope. However, there was a large degree of variability in the angles recorded at lower slopes of between 2^{o} and 4^{o} (Figure 5.57). The same trend was confirmed in the effusion rate variation experimental suites. At any given angle of slope, E_rM experiments produced smaller angles than those from E_rH experiments. The largest angles were produced in the low effusion rate suite E_rL at the lowest angle of slope (Figure 5.58).

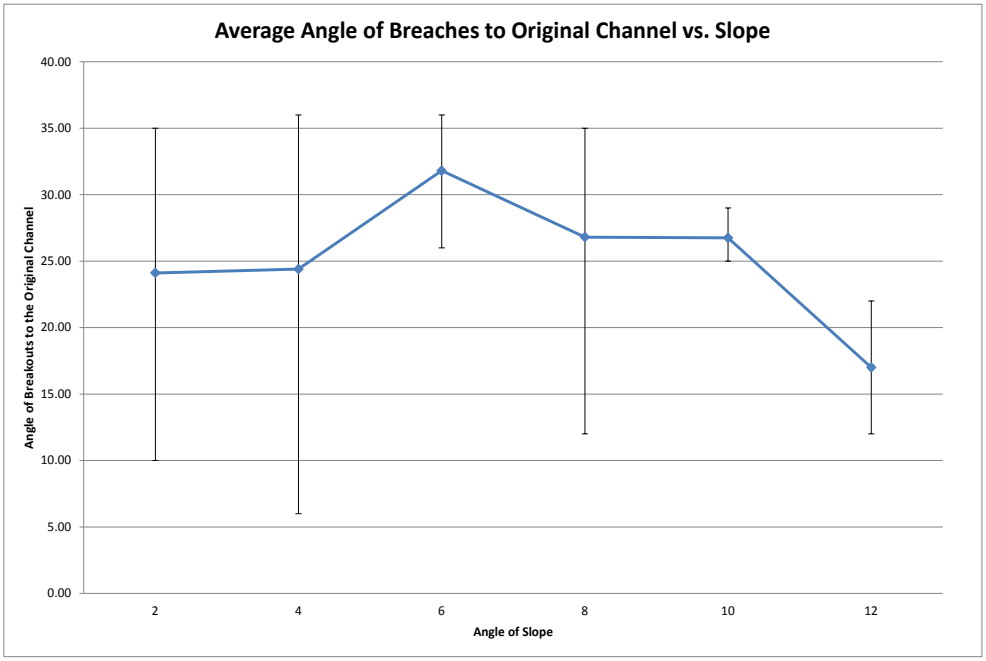

Figure 5.57 – Slope Variation Experimental Suite. The angle at which secondary flows form to the original channel on average decreased with increasing angle of slope. However the experiments run at lower angles of slope 2^{o} – 4^{o} showed a greater degree of variability compared to that of the higher slope angles.

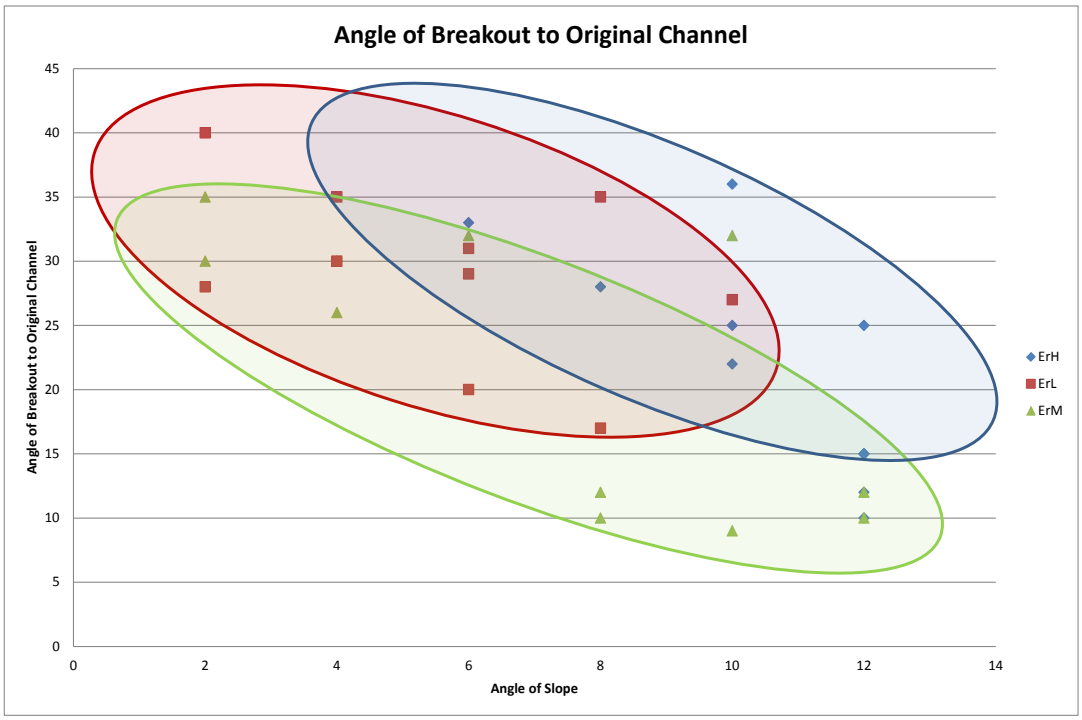

Figure 5.58 – For all effusion rate classifications, the angle at which secondary flow formed to the original channel decreased with increasing slope. E_rM recorded the lowest angles and at any given slope, E_rL produced smaller angles than E_rH.

Given that E_rM produced the lowest angles of breakout in these experiments, slope was not the only controlling factor on the size of the angle of breakout. During the experimental runs, a number of different behaviours of secondary flow formation were observed. For all experimental suites, it was observed that immediately as a secondary flow forms, its initial velocity is greater than that of the overall flow-field. This is due to pressure of material building up in the channel being released quickly. This initial burst of speed, propels the wax almost laterally across the surface of the glass plane before that energy is lost and the new flow begins to lose momentum to flow downslope under gravity. Gentler slope angles exert less influence on the initial burst of fluid material, allowing the lateral movement greater influence. This means that for experiments carried out on low angles of slope, the angle of breakout is greater.

For the E_rH experimental suite, it can be theorised that the high effusion rate of the flowing material adds impetus to the initial burst of the breakout, forcing the angle out wider initially. However on higher slope angles, gravity exerts a greater influence on the newly formed flow to move downslope resulting in smaller angles of formation.

Flow-field widths decreased with increasing slope despite total volume emplaced remaining constant and very little variance in the number of flows formed with increasing slope or varying effusion rate except on slopes of 12° where the number of flows was seen to decline (Figure 5.59). Therefore the decreasing flow-field width can be attributed to a combined influence of narrower flow widths and smaller angles of breakout for secondary flows with increasing slope. Although higher effusion rates resulted in wider flows, the effect of slope proved to be the biggest control on flow widths and subsequently flow-field widths.

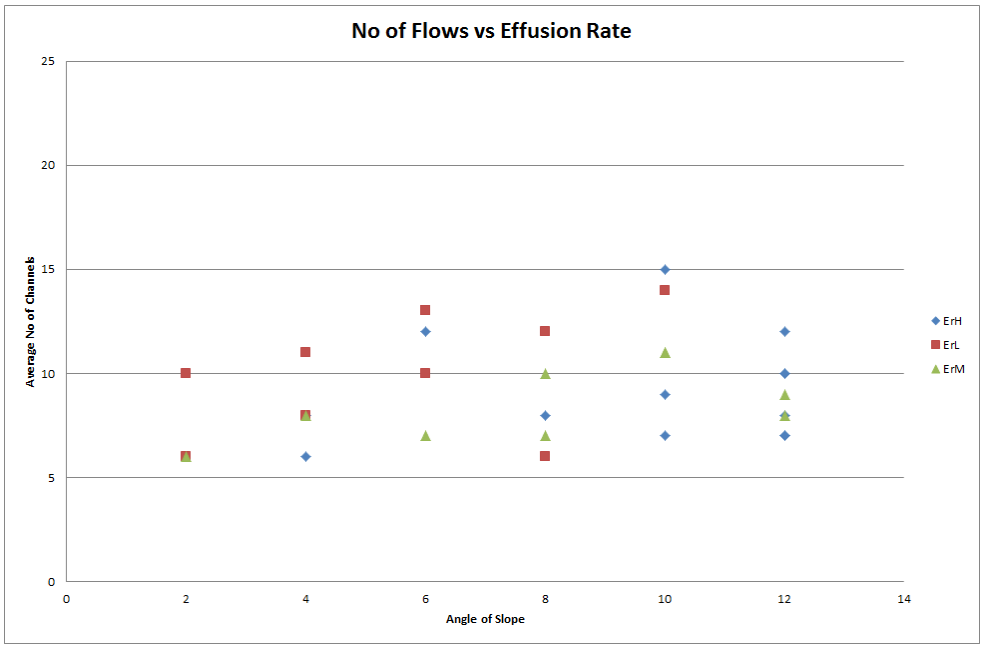

Figure 5.59 – Effusion Rate Variation Suite. The number of flows formed during emplacement showed very little variation with slope in all experimental suites.

5.6.2.2 Breakouts – Breaches and Overflows

Secondary flows formed through breakouts and are classified into two categories – breaches and overflows. As described in the Section 5.5, breaches and overflows are differentiated by their mechanism of formation. Both mechanisms result from material build up behind a cooled flow-front or obstacle. Overflows flow up and over a levee or channel margin without altering its internal structure. Breaches occur when the channel levee is either wholly or partially broken down, allowing the wax to flow out of the channel.

The slope variation experiments showed that the occurrence of breaches increases with increasing slope (Figure 5.60). The low value for breaches at 8^{o} corresponds to a peak in the number of overflows recorded for the same value of slope (Figure 5.62). As previously stated, the number of secondary flows emplaced showed very little variation with slope or between the various experimental suites. Therefore a decrease in one mechanism of secondary flow formation should correspond to an increase in the other. The effusion rate variation suites also showed an increase in the number of breaches with increasing slope from 2o to 10^{o}. At slopes of 12^{o}, the number of breaches decreases significantly (Figure 5.61). The trend for E_rL was the closest match to the slope variation experiments, showing a continuous growth in the number of breaches formed against slope. The trends for E_rM and E_rH had a higher degree of variability at any given angle of slope, showing that high effusion rates affect the occurrence of breakouts.

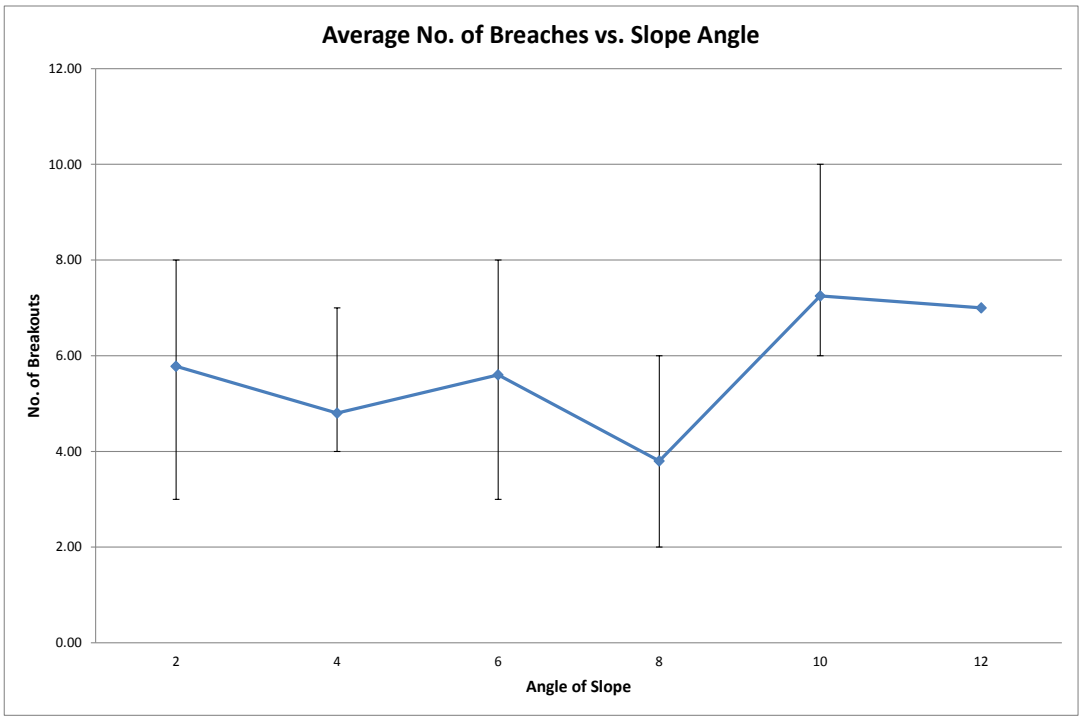

Figure 5.60 – Slope Variation Experimental Suite. The average number of breaches recorded decreases with increasing slopes of up to 8°. For slopes >8°, the number of breaches recorded increases significantly.

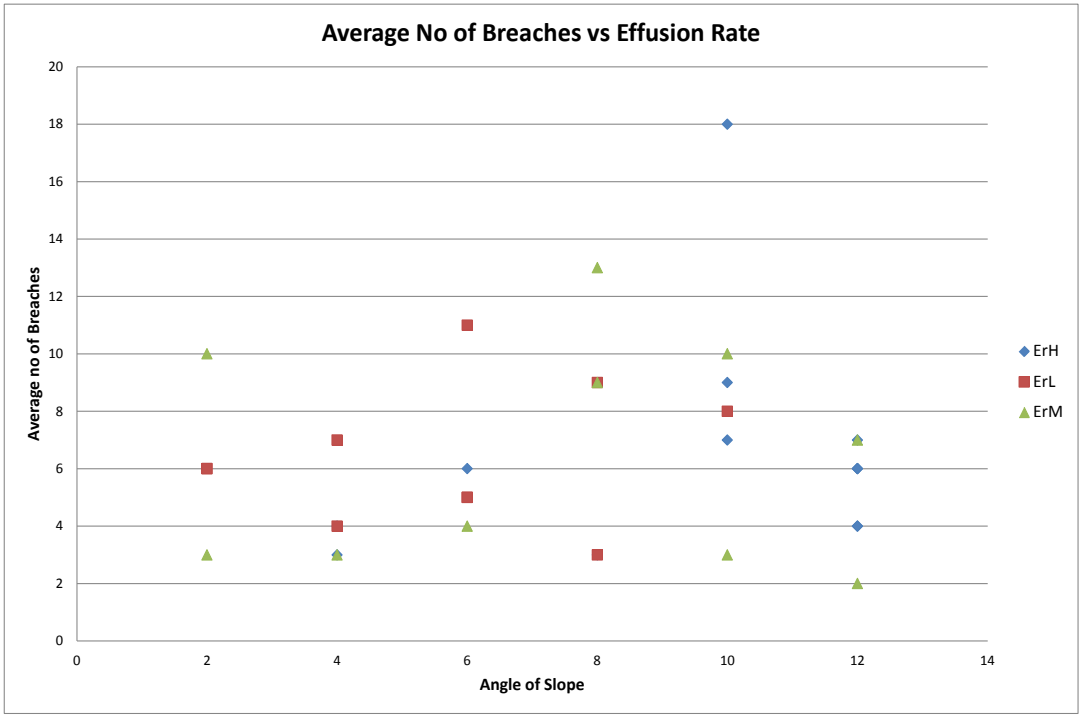

Figure 5.61 – Effusion Rate Variation Suite. All three effusion rate groups show the number of breaches increasing with slopes to 10°. At slopes of 12° the number of breaches decreases.

A similar trend was observed with overflows. The slope variation and effusion rate variation suite both showed increasing occurrence of overflows with increasing slopes up to 10^o and then a clear decline at 12^o (Figures 5.62, 5.63). E_rH experiments resulted in the lowest value for overflows at 12^o, the opposite trend as was observed with breaches. The overflows were observed to be relatively short lived with almost none forming secondary arterial flows, a direct correlation with what was observed in the field (Section 3.2.2)

The slope variation experiments showed that, on average, the number of secondary flows formed increased with increasing slope whilst the effusion rate variation experiments showed very little variation in the number of secondary flows formed with slope up to 10^o and a decline at 12^o. Qualitative observations of the experiments showed that the experiments with the highest effusion rates – E_rH slope 12^o formed flow-fields with wide structureless flows where the wax retained a low viscosity for longer. The aspect ratio of the flows, wide and thick, meant that the development of flow-fronts was delayed and therefore the volume of material in the flows remain constant and flowing, reducing the occurrence of breaches and overflows. Therefore the optimum conditions for the occurrence of breaches and overflows are low angles of slope, between 2^o and 10^o and medium to low effusion rates. Qualitative evidence also demonstrates that the location of breakouts, breaches or overflows, migrates up channel with time as result of cooling moving the flow-front back towards to point source of effusion.

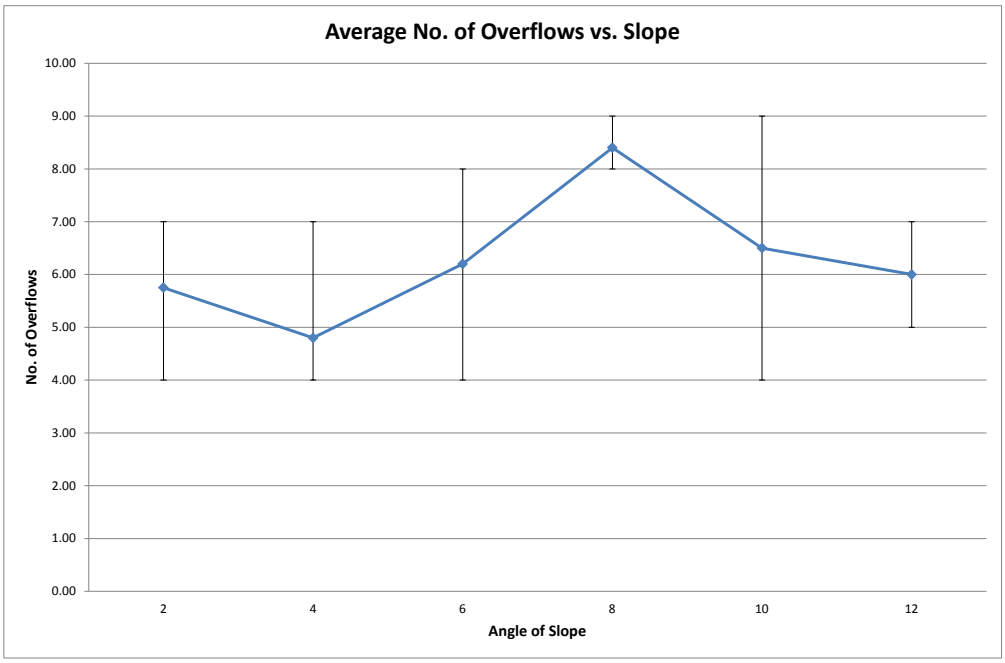

Figure 5.62 – Slope Variation Experimental Suite. The average number of overflows increased with increasing slope from 2° to10°. At slopes >10° the number of overflows recorded declined significantly.

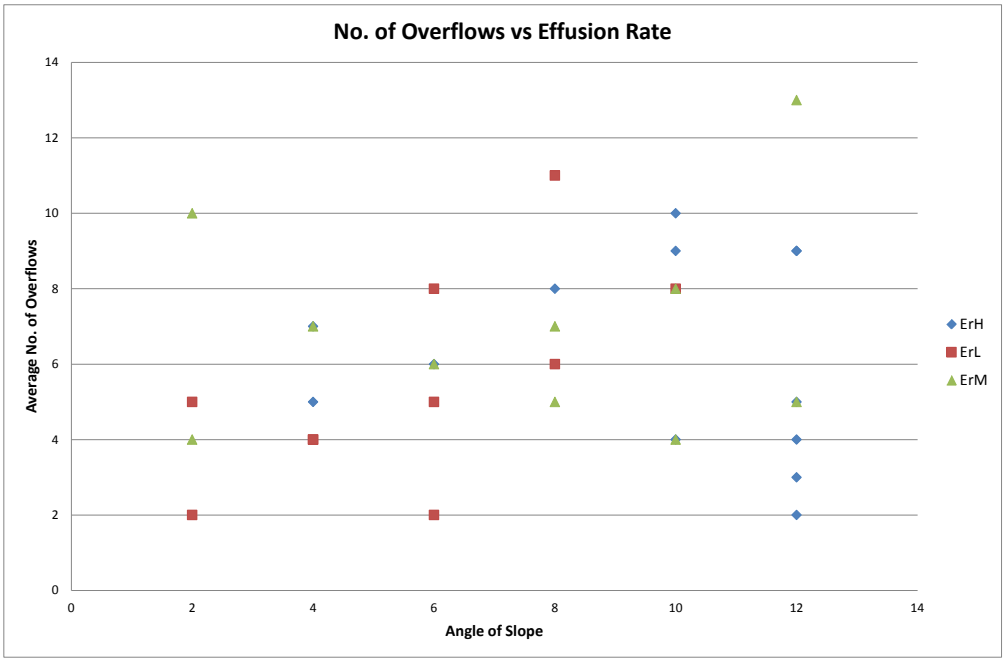

Figure 5.63 – Effusion Rate Variation Suite. All effusion rate groups presented with increasing occurrence of overflows with increasing slopes up to 10°. On slopes of 12°, particularly for group E_rH, the number of overflows declined sharply.

5.6.2.3 Flow Structures – Levees, Tubes and Lobes

In the slope variation suite all experiments produced leveed channels with the number of levees formed growing with increasing slope from 2^o to 8^o. There was however a large degree of variability in the number of levees formed for a given value of slope except on slopes $>8^o$, there was less variability as well as an overall decrease in levee occurrence (Figure 5.64).This supports the findings of Gregg & Fink (2000) who stated that sufficiently high effusion rates result in flows without levees as the fast effusion rate off-sets the effects cooling hindering the formation of thermal boundary zones, which are the precursors to levee growth. The effusion rate variability experiments followed the same trend in the E_rL and E_rH groups. The E_rM group however produced a smooth trend with increasing slope values although some variability begins to show at slopes $>6^o$ (Figures 5.65, 5.66). From these results it can be surmised that increasing slopes and stable effusion rates in the range of the E_rM group ($>5.09 \times 10^{-6} – 9.59 \times 10^{-6}$) promote levee growth. For all three effusion rate groups and the slope variability suite, slopes $>8^o$ produced a change in levee formation behaviour. E_rL and E_rH groups and the slope variation experiments showed a decrease in the number of levees formed whilst E_rM produced a greater degree of variability for a given angle of slope. As discussed previously, increasing the angle of slope at the effect of increasing the emplacement rate. This meant that an experiment in the E_rH group may produce the same number of leveed channels at 6^o slope as an experiment in the E_rM group produces at 10^o. From the evidence, it is clear that there is an optimal set of conditions for levee growth and that both slope and effusion rate are controlling parameters on formation.

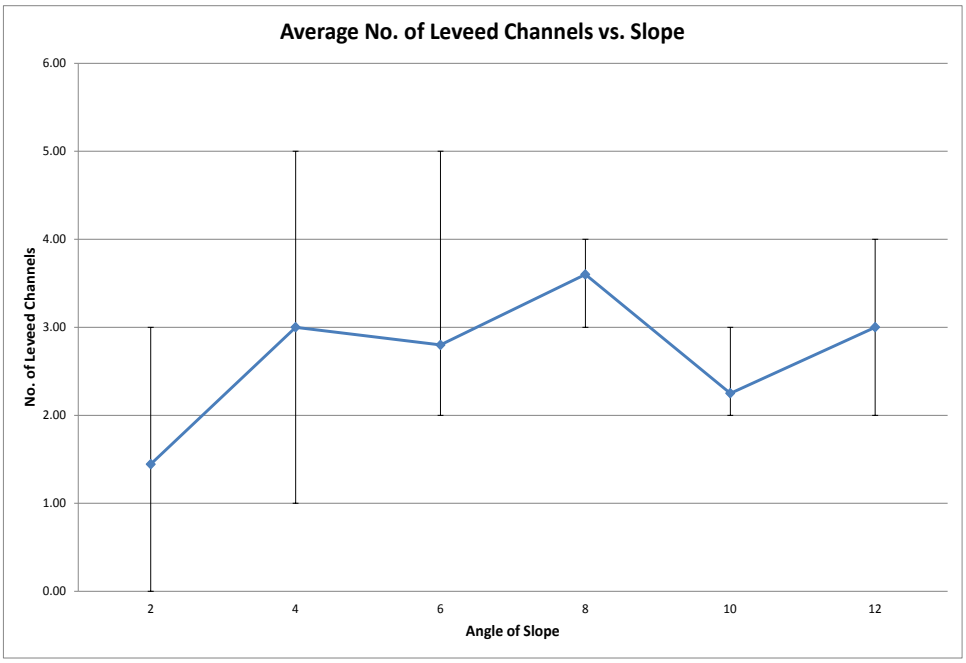

Figure 5.64 – Slope Variation Experimental Suite. On average the number of levees formed increased with slope from 2° to 8°. On slopes of >8° the number of levees formed becomes less variable but an average smaller than for lower slopes.

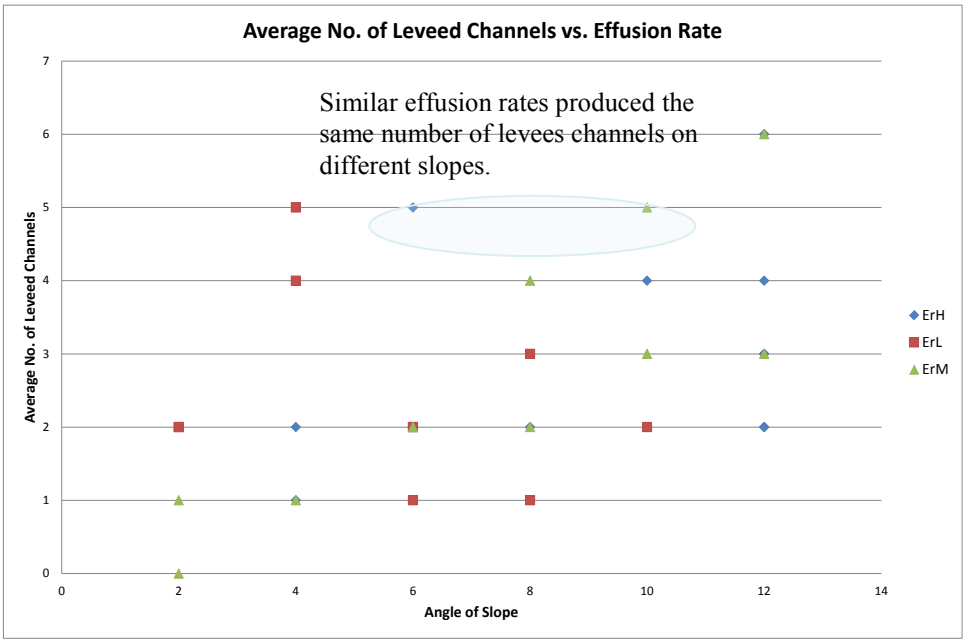

Figure 5.65 – Effusion Rate Variation Suite. E_rL and E_rH experiments both showed a high degree of variability in the number of levees formed for a given value of slope. The E_rM group showed a more stable trend. Experiments in different effusion rate groups produced the same number of levees at similar effusion rates on different angle of slope.

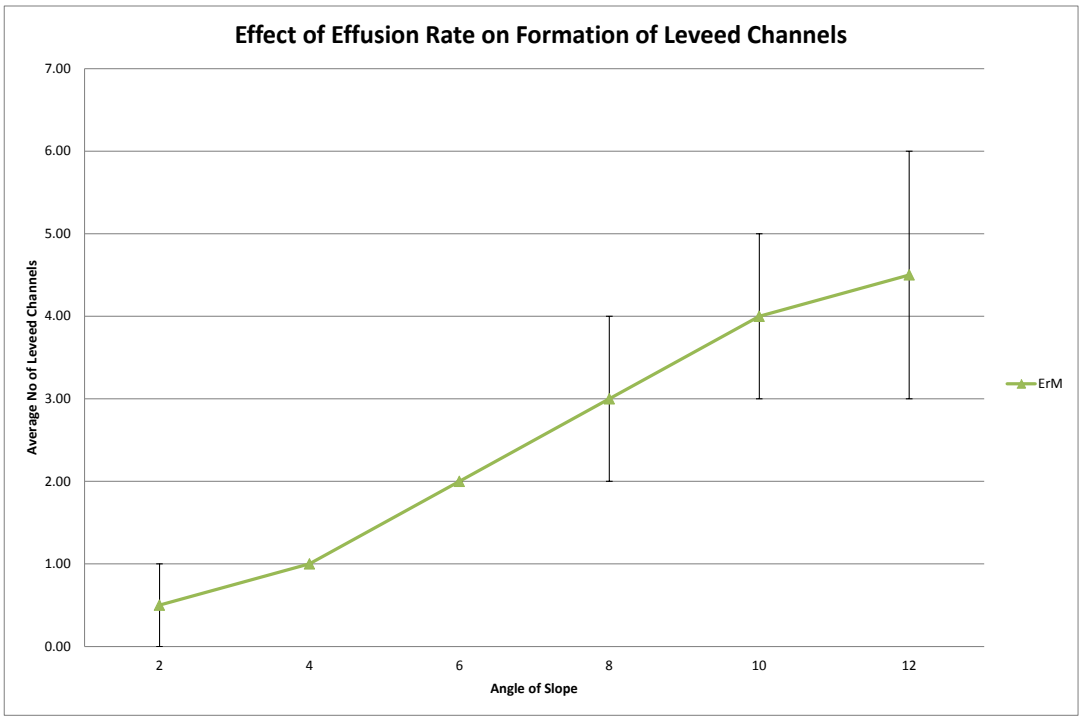

Figure 5.66 – Effusion Rate Variation Suite. Average number of levees formed by slope for E_rM group. This group was the only one to produce a stable trend with slope. On slopes >6° some variability occurs in the number of levees formed.

There was also correlation between the existence of leveed channels and the occurrence of overflows. As demonstrated in Figure 5.67, increased numbers of leveed flows resulted in a rise in the number of overflows. Qualitative observations showed that channels with well-defined and stable levees experienced overflows more often than breaching whilst channels with small, unsolidified levees experienced both mechanisms for breakouts. This relationship could be explained by the levees having an inherent yield strength which is missing in flows which are not constrained by levees. As a result the path of least resistance for the wax was to overflow the channel as opposed to breaching the wall. The exception to this observation was for channels that experienced curvature. Breakouts from these channels typically occurred on the outer bend of the flow in the form of breaches. It can be inferred from these trends that the angle of shear pressure that the fluid,

moving wax applies to the levee is an important consideration for the mechanism of breaching and levee failure, a topic that will be discussed further in Chapter 6.

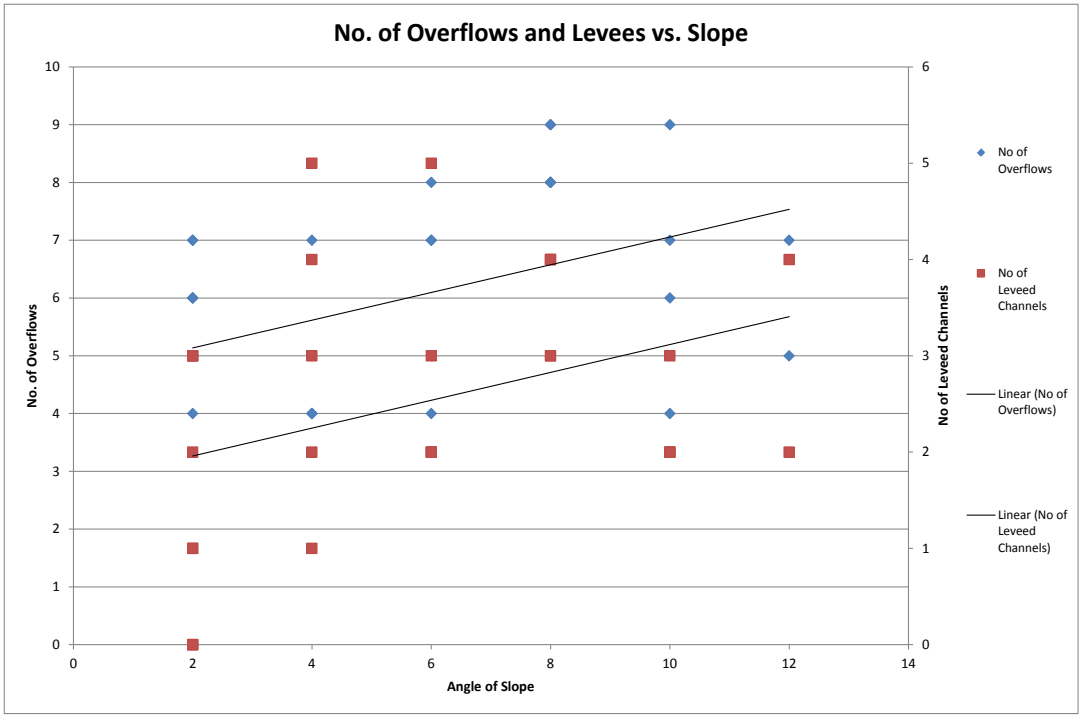

Figure 5.67– Slope Variation Suite. Correlation between the number of leveed channels and the occurrence of overflows.

The formation of levees is an important precursor to tube growth and their mechanism of formation is described in Section 5.5.1.4. The slope variation experimental results show that low angles of slope c. 2° favour the growth of tubes (Figure 5.68). The effusion rate experiments corroborate this trend and show that low effusion rates and low angles of slope combine to favour tube growth (Figure 5.69). Qualitative analysis on tube formation showed that high emplacement rates, resulting from either a high effusion rate or from higher slope angles are a limiting factor in the development of tubes. Tube formation is dependent on the formation of cooled crust on the surface of the flow which grows into the levees, enclosing the flow in a crust of solidified stationary material. High effusion rates mean that the

fluid within the channel is flowing at a higher velocity, exerting a greater amount of shear pressure on the solidifying surface crust, breaking it up and pulling it down flow before it can form a unified layer. Therefore tubes are more commonly found at conditions where cooling and the development of solidified crust are dominate parameters, facilitating the growth of solidified crust and where effusion rates are sufficiently low to reduce the shear stress on the surface crust.

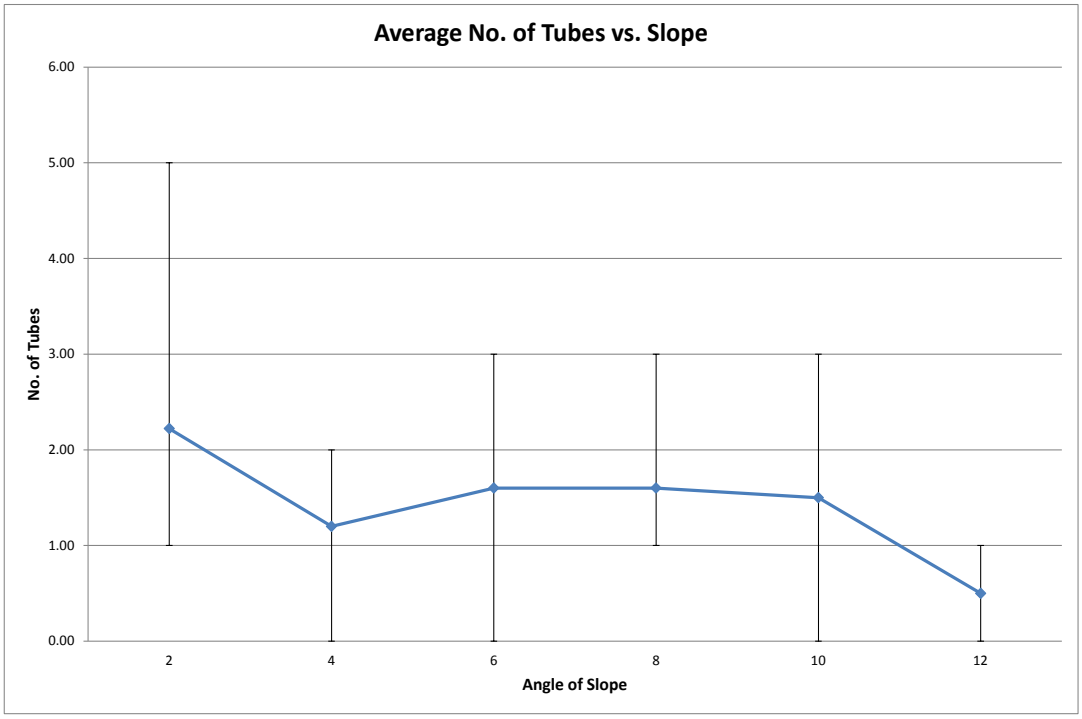

Figure 5.68 – Slope Variation Suite. On average tubes were most commonly found at very low angles of slope **c.** 2°.

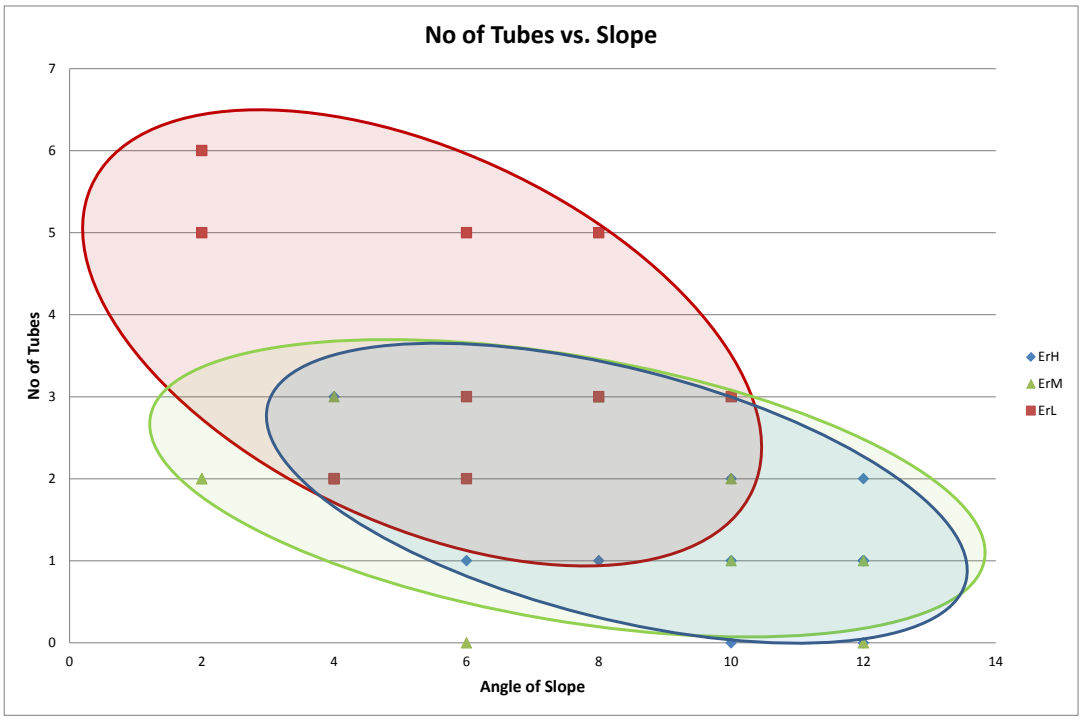

Figure 5.69 – The existence of tubes was recorded for all E_r groups at all values for slope, however, low effusion rates and low angles of slope 2^o – 6^o are the most ideal conditions for tube growth.

Lobes typically formed at the end of a flow due to the development of a solidified front. The development of lobes and subsequent reduction in flow advancement signify the transition from stage two of flow-field emplacement to stage three. The slope variation experiments show that lobes form at all angles of slope but are more common on slopes of $\leq 6^o$ (Figure 5.70).

The effusion rate variation experimental suite results show that low angles of slope and low effusion rates result in increased lobe formation. E_rL at slopes $\leq 8^o$ result in the most favourable conditions for lobe growth (Figure 5.71). Contrary to this trend, E_rH resulted in more lobes than E_rM. This was due to the development of leveed channels in the E_rM experiments. The leveed channels remained active for longer and although some did develop lobes at their flow-fronts, not all did. The finite amount of wax used in the experiment combined with the insulating effect of

the levees, off-set the effects of cooling, meaning that in some cases the total amount of wax was effused before the flow developed a crusted front.

The number of lobes formed for groups E_rM and E_rH is also affected by the higher occurrence of breakouts – overflows and breaches which occur in these groups. Qualitative evidence showed that, breakouts and the development of secondary flows, diverts fluid from the original channel before it reaches the front, leaving behind a drained channel.

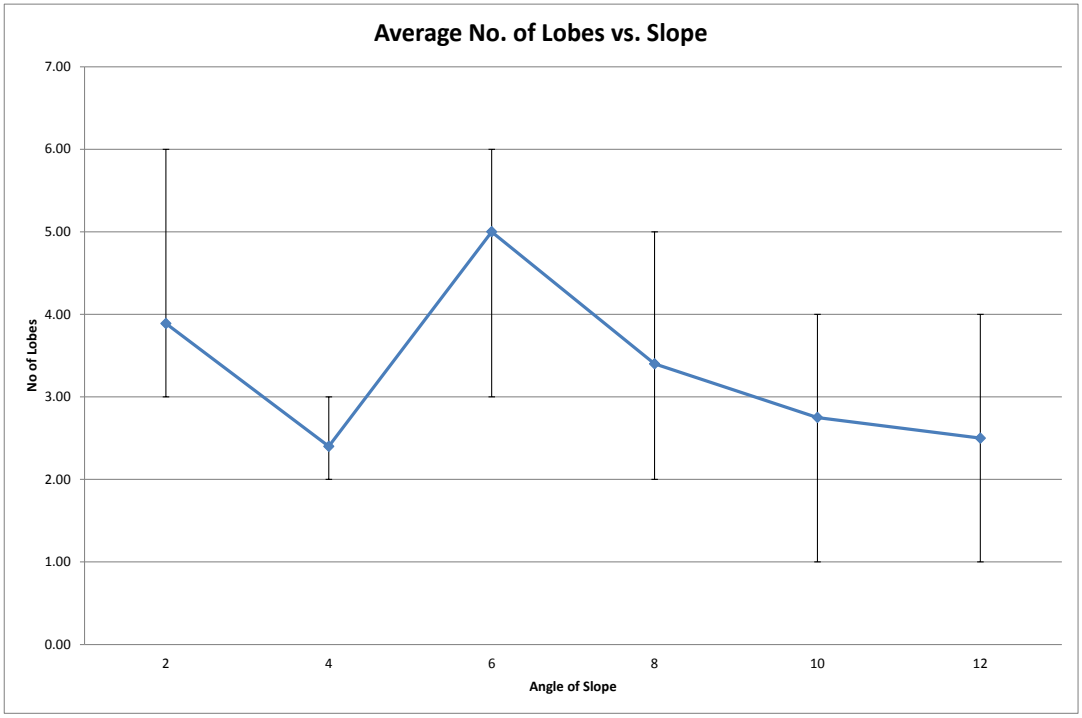

Figure 5.70 – Slope Variation Suite. On average, lobes are more commonly found at slopes ≤ 6° but did form under all experimental conditions.

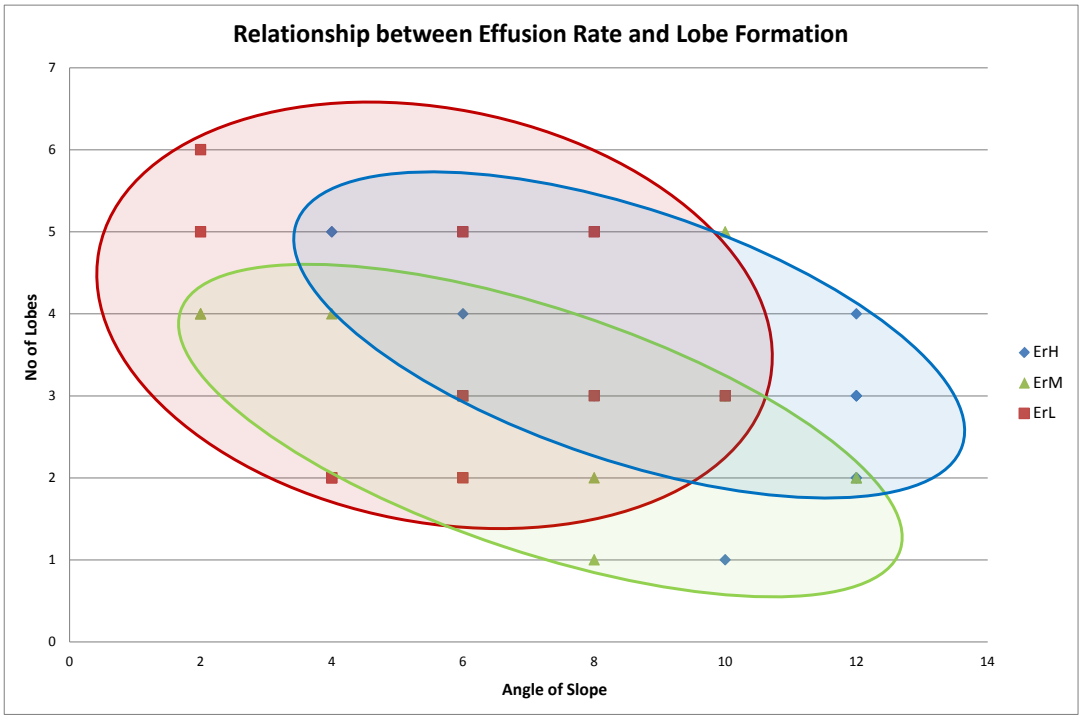

Figure 5.71 – Effusion Rate Variation Suite. While lobes formed in each experiment regardless of E_r grouping or angle of slope, they formed in the greatest numbers at low angles of slope and low effusion rates, group E_rL.

Lobes did experience breakouts and the formation of short lived flows which formed subsequent lobes in a chain as long as the flow-front was active. Breakouts from lobes were frequently observed to have a much higher initial velocity that the rest of the active flows within the flow-field. These observations corroborate similar observations made by Miyamoto & Crown (2006) in their study on the lateral growth of lobes. They assumed that the pressure build-up in the lobe ($\Delta\rho$) was a function of increased thickness (Δh) in that particular section of a flow, assuming no change in channel flow before or after inflation. They expressed this theory as:

$$\Delta\rho \sim \rho g \Delta h \qquad \text{Eq. 5.5}$$

Where Δp is overpressure, ρ is density, g is acceleration due to gravity and Δh is thickness difference.

Using this equation it can be assumed that new flows result from a lobe when Δp exceeds the tensile strength of the crust causing it to fail. Therefore Miyamoto & Crown (2006) show that the thickness needed to form a breakout can be expressed as Δh with respect to the tensile strength of the crust divided by acceleration due to gravity combined with the channel radius and the density of the fluid:

$$\Delta h \sim \frac{\sigma \delta}{D \rho g} \qquad \text{Eq. 5.6}$$

Where σ is tensile strength, δ is thickness of surface crust and D is radius.

The laboratory experiments assume a uniform tensile strength for the crust which holds relatively true for wax but cannot be assumed in a natural system where crystallisation, local differences in crustal thickness and vesiculation result in surface crusts with variable tensile strengths (Gregg & Keszthelyi, 2004).

The second stage of emplacement is where flow-fields gain complexity and is characterised by the formation of secondary flows and flow structures. The majority of growth in this stage is lateral, flow-field length having been mostly achieved in the first stage. This stage typically has the longest duration of the three stages, particularly for experiments with low to medium values for E_r as the moderate effusion rate allows time for cooling to become the dominate controlling

parameter in emplacement. The emplacement history of a flow-field can be inferred from the variety and frequency of structures present with tubes and lobes favouring low effusion rate, low underlying slope conditions and levees and overflows more commonly found at higher angles of slope and/or effusion rate.

5.6.3 Stage Three – Thickening

The third stage of emplacement is characterised by flow-field thickening. Typically when a flow-field reached this stage, effusion rates were dropping and the overall flow-field length and width had been achieved. Cooling has been sufficient to halt all flow advance and any remaining flowing material was emplaced in lobes or in semi-plastic flows, increasing their thickness. This stage was not was not observed in every experiment; in the effusion rate variation suite, the high effusion rate/high slope angle experiments typically did not achieve this stage as the total amount of wax available had been effused in the first and second stages of emplacement. Flow-fields which did achieve this stage were typically emplaced on low slope angles with low effusion rates which allowed the effects of cooling to be observed more quickly.

5.7 Summary

This model presents flow emplacement in three stages – lengthening, widening and thickening. The duration and significance of each of these stages in overall flow-field growth is dependent on how emplacement parameters vary the effects of cooling. Overall flow-field morphology is dependent on the complex interactions of a number of different parameters. Flows with higher angles of

underlying slope, high effusion rates or a high value for V_{mean} result in the longest flow-fields with the material reaching greater distances before cooling produces a crusted front. The first stage of emplacement is the most dominant for these types of flows and the resultant flow-fields are typically long and narrow. Flows with moderate to high effusion rates on all slope angles will form wider flows characterised by the presence of leveed channels. Flow-field will be narrower with increasing slope. Flows with moderate to low effusion rates will transition more quickly into the second and third stage of emplacement and are more likely to form the widest, thickest fields with a network of tubes and lobes.

6 Rock Mechanics

6.1 Strength Analysis of Lavas

In order to be able to forecast the locations of levee failure, a comprehensive understanding of their mechanical properties is vital. The scarce rock mechanics experiments available for volcanic rocks have focused on the massive cores of basaltic lava flows both from the point of view of their general properties (Ryan & Sammis, 1981) and applying data on both brittle and ductile failure of volcanic rocks and fracture maps to illustrate the interactions between stress, strain rate and temperature in lava flows (Rocchi et al., 2004). Basaltic lava flows are considered to be generally homogenous in terms of their bulk composition but analysis of hand samples and thin sections shows that rock textures such as crystal and vesicle size and distribution can vary significantly throughout a flow. Porosity is of particular interest as it has been shown to be a control on whether the rock fails in a ductile or brittle manner (Rutter & Hadizadeh, 1991) with the brittle/ductile transition occurring at approximately 7% porosity (Shimada, Ito, & Cho, 1989).

Howarth & Rowlands (1987) showed that fracture modes in basalts were intra-granular and that crack propagation was highly influenced by textural variations in the rock. Crystal content, vesicle distribution and other micro and macro heterogeneities within a unit are known to cause areas of localised variability in the mechanical properties of the rock (Herd & Pinkerton, 1997; Apuani et al., 2005; Adelinet et al., 2013) which is illustrated by the fact that smaller samples typically have higher strengths than large samples due to the greater probability of micro or macro flaws being present in larger samples.

This is especially true of levees. Although it could be logical to assume that the behaviour of lava deciphered from cores of flows and that of the lava forming the levees to be the same, the different formation and cooling histories of levees compared to the flows they are constraining mean that their properties may vary substantially from that of a flow. Therefore, it is essential to test the strength of samples from levees themselves and not use recorded strengths from previous studies of basaltic lava flows. In previous studies of basalt strength, the main concern with sample picking was to choose samples which were representative of the bulk strength of the flow regardless of localised variance in vesicle and crystal content. For this study where the factors controlling the location of breakouts were of interest, it was important to quantify the effect micro and macro flaws and other planes of weakness have on rock strength and therefore samples were chosen that represented the levee as a whole, including areas of localised heterogeneity.

The conditions governing the location of breaches and overflows from levees are not well understood and may be constrained by other factors than just the presence of micro and macro flaws. Field analysis of the location of levee breaches on Mount Etna, Sicily and Mount Teide in Tenerife showed that breaches occur more frequently on the outer bend of curved flows (Chapter 3, Section 3.2.4) which could mean that the orientation of applied pressure in addition to localised variations in rock strength are controlling factors in the location of breaches. A methodology was needed which investigated the effect not only of heterogeneity in basalt composition but also variance in the angle of applied stress had on sample strength. Therefore samples were chosen which encompass variance in vesicle size and distribution, phenocrysts and grain size to constrain the upper and lower limits of the strength of the samples. Some of these were identified at a macro level

during fieldwork and others were discovered once the samples were cored in preparation for testing. Cores were also taken from homogenous, core flow material as control samples for the bulk strength of a particular flow. This was done to understand what structures reduced the strength of the material and if any structure increased the strength of the material.

Preliminary rock mechanic tests on levee samples showed that the alignment of crystals and vesicles in relation to the direction of the applied pressure has a significant negative impact on the inherent strength of a sample (Nolan, 2006). A similar result was obtained by Rocchi et al., (2003) for lava cores, but the former study also seems to indicate that levee strength varies substantially between levee types. However, the initial study took samples at random orientations and it was therefore difficult to quantify the result in relation to their position in the levee.

Fixed, massive lava levees, were identified as the levee morphology with the closest characteristic to that of massive lava (Nolan, 2006) and so will have tensile and compressional strengths (at sub-solidus temperatures) of ~1-10 and 40-130 MPa respectively. However, 'a'a flows have typical thicknesses of ~1-10 m, and so are associated with static pressures on their margins of ~0.1 MPa, implying that stress alone could not cause levee failure: internal structure and planes of weakness within a levee must therefore influence susceptibility to failure. Moreover, preliminary field observations on Etna's 1983 and 2001 flows suggest that morphological factors that influence dynamic pressure on levees such as curvature of the levee also have an influence on levee failure: lava levees are more likely to breach where lava channels and tubes experience certain degree of curvature (Nolan, 2006).

6.2 Tests

A total of 210 uniaxial compression tests, 191 dry density test, 191 porosity tests and 29 vesicle analysis tests were carried out on a total of 44 samples of basalt levees and flows (21 samples collected from Mount Etna and 23 samples collected from Tenerife).

6.2.1 Uniaxial Tests

One of the main focuses of this study was to understand the mechanisms of levee breaching and the conditions required for a levee to fail. To achieve this, the mechanical properties of levees need to be constrained. Levees solidify at atmospheric pressures and therefore uniaxial (unconstrained) tests were required. In order to understand the behaviour of morphologically different levees and also to test the strength of levees from different angles of applied stress, it was decided that samples were to be taken from a number of different levees at field sites on Tenerife and Mt. Etna, Sicily. As levees are orientated near vertical, samples were marked with top, bottom and flow direction. Cores were taken normal, parallel and oblique (30^{o}-45^{o}) to the flow direction using a Meddings 10 speed drill with a 25 mm diameter diamond tipped core barrel attached.

The cores had a height to diameter ratio of between 1.99 – 2.06 and were tested in a uniaxial compression machine with a proving ring constant of 218.8 N/div at room temperature. The compressive stress (MPa) was logged to failure and the mode of failure recorded and photographed.

6.2.2 Density and Porosity Tests

The density and porosity of 191 of the 210 samples was calculated using the saturation and buoyancy technique as described by the International Society of Rock Mechanics Commission on Standardisation of Laboratory and Field Tests. This method was chosen because it was suitable for use on regular and irregular shaped samples. The decision to carry out density tests was taken part-way though the research program after some samples had already been cored, tested and shattered. For those samples that had already been tested, where possible, remnant off-cuts from coring were used. For all subsequent samples collected, the cores for uniaxial testing were used prior to testing.

The methodology uses samples with a mass greater that 50g or a minimum dimension ≥ 10 times the maximum grain size. The samples are submersed in water overnight, and then transferred underwater to a wire basket completely submerged in a bucket of water. The wire basket was suspended in the bucket using a thread attached to the stirrup of a balance which recorded the saturated submerged mass (M_{sub}) of the sample and basket and of the basket alone.

The sample was removed from the bath and the surface water removed by blotting with a damp cloth. The sample was then weighed and the saturated-surface-dry mass (M_{sat}) recorded. Samples were placed in an oven at 105^{o}C overnight to be dried to constant mass. Samples were cooled in a desiccator and then weighed to calculate the grain weight (M_s).

The porosity and dry density were calculated using the follow equations:

Bulk Volume:

$$V = \frac{M_{sat} - M_{sub}}{\rho_w} \quad \text{Eq. 6.1}$$

Pore Volume:

$$V_v = \frac{M_{sat} - M_s}{\rho_w} \quad \text{Eq. 6.2}$$

Porosity:

$$n = \frac{100V_v}{V}\% \quad \text{Eq. 6.3}$$

Dry density of rock:

$$\rho_d = \frac{M_s}{V} \quad \text{Eq. 6.4}$$

6.2.3 Vesicle Analysis

During sample collection and processing it was noted that there were significant differences in vesicle content and size between the samples and these differences may affect the mode of failure of the sample. In order to quantify the variations in vesicle concentration, slices were taken from the samples cored for uniaxial compression tests in the same orientation as the cores – normal, parallel and oblique to the flow direction. The slices were made through representative portions of the rock. The samples were then overlain with a 5 cm by 5 cm square divided into a 1 cm by 1 cm grid and an inventory of the number of vesicles within the grid squares was taken. In order to include the variation in vesicle size in the analysis the vesicles were grouped in to three categories: <1 mm, 2-10 mm and >1

cm. It was also noted if there appeared to be any lineation or preferred orientation within the vesicle population.

6.3 Petrology

Samples were taken from a variety of locations within field-sites on Mount Etna, Sicily and Tenerife, Canary Islands. A list of sampling localities can be found in Appendix A. As the focus of this study is to understand the factors controlling levee breaching and to constrain a range of strengths representative of different levee types, samples were taken from a number of different levee types. Particular attention was paid to collecting samples on or close to breaches in a levee. Where samples were taken on or close to a breach, a further sample was taken from the same levee but at a distance from the breach in order to understand if the mechanical properties of the levee varied in and around the location of the breach.

Samples were also taken from the interior of a massive flow on Mount Etna in order to quantify the difference in strength between flow and levee material. In both field locations, samples were taken from levees constraining basaltic 'a'a flows. A full account of the sampling procedure can be found in Chapter 3, Section 3.3.

6.3.1 Mount Etna

Samples were collected from the 1983, 2001 and 2003 flow-fields on Mount Etna. The samples consisted of a dark grey crystalline trachybasalt containing phenocrysts of olivine (<1%), pyroxene (<5%) and feldspar (<15%). The samples had a porosity of between 4 – 8%. Although the vast majority of vesicles were < 5 mm in size, the samples did also contain vesicles larger than 1 cm in size.

Figure 6.1 – Picture taken in the 1983 flow-field of Mount Etna showing the presence of large >1 cm vesicles in levee material.

6.3.2 Tenerife

Samples were taken from the Arafo, Chinyero and Garachico flows on Tenerife. These samples were basaltic and taken from 'a'a flows. The samples consisted of a fine grained porphyritic basalt with between 4 and 12% porosity. The Arafo samples were distinct from those of the Chinero and Garachico flows due to the presence of olivine phenocrysts up to 5 mm in size.

6.4 Results

6.4.1 Uniaxial Compression Tests

210 uniaxial compression tests were carried out at ambient temperature and pressure and with a constant strain rate of $1x10^{-3}s^{-1}$ on samples taken from flows on Mount Etna and Tenerife, please see Table C.1, Appendix C for a full list of test results. The results of the uniaxial tests showed a number of clear trends with

changing porosity and / or angle at which the core was taken from the levee relative to the direction of flow.

For each location, where possible, cores were taken parallel, 90^o and 45^o to the flow direction. Cores taken 90^o to the flow direction are hereafter referred to as C_{90} group, cores drilled 45^o to the flow direction are referred to as the C_{45} group and cores taken parallel will be referred to as the C_{par} group. Before testing, the textural features of each core which could have an effect on rock strength were documented, such as fractures or vesicle / crystal concentration and orientation. In addition to measuring the maximum compressive strength of the sample, it was important to understand if the core underwent brittle or ductile failure. Once testing was complete, the samples were carefully removed from the machine and their mode of failure photographed. These analyses, along with plots of the axial strain were used to understand the mode of failure for the sample. Brittle failure was characterised by high angle, clear, macroscopic fractures and sharply declining axial strain lines.

Although the samples from different locations on Mount Etna and Tenerife were morphologically different in terms of composition, crystal & vesicle content and grain size, the first analysis was to arrange all samples in to three broad groups regardless of location picked - C_{90}, C45 and C_{par} by field site. The maximum compressive strengths of all cores were compared at this level to identify any global trends in strength with direction of applied stress.

Although the maximum strength of cores taken from field-sites on both Etna and Tenerife varied greatly, results showed that on average, the C_{par} group had the highest maximum compressive strengths. On average, the C_{45} cores had the lowest max compressive strengths (Figures 6.2 & 6.3).

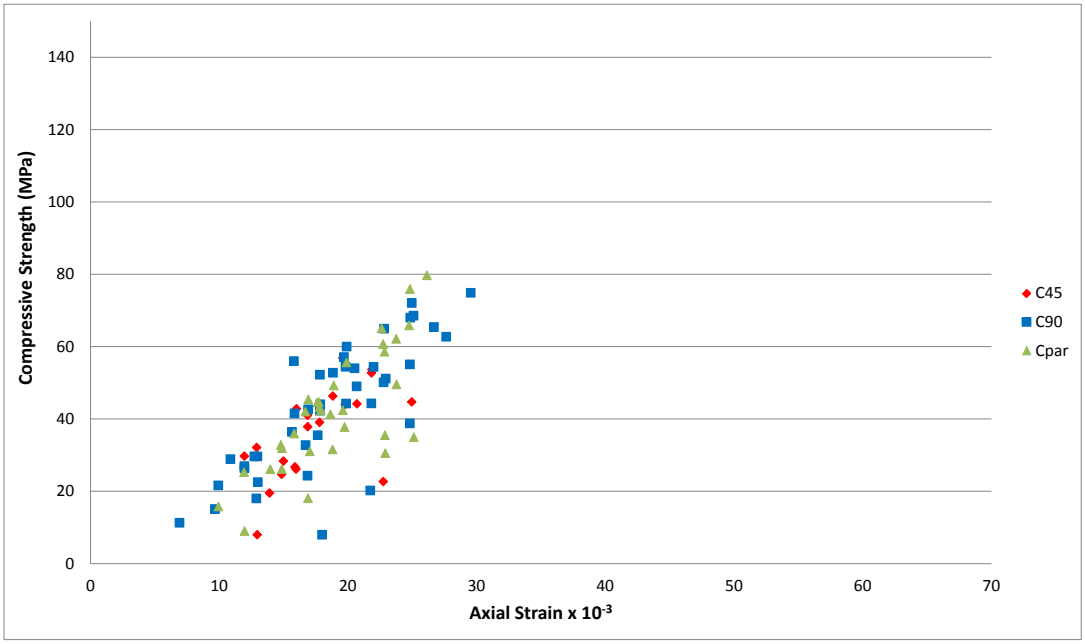

Figure 6.2 – Maximum compressive strength of cores taken from various flows on Mount Etna, Sicily. Group C_{par} globally had the highest compressive strengths whilst the group C_{45} had the lowest.

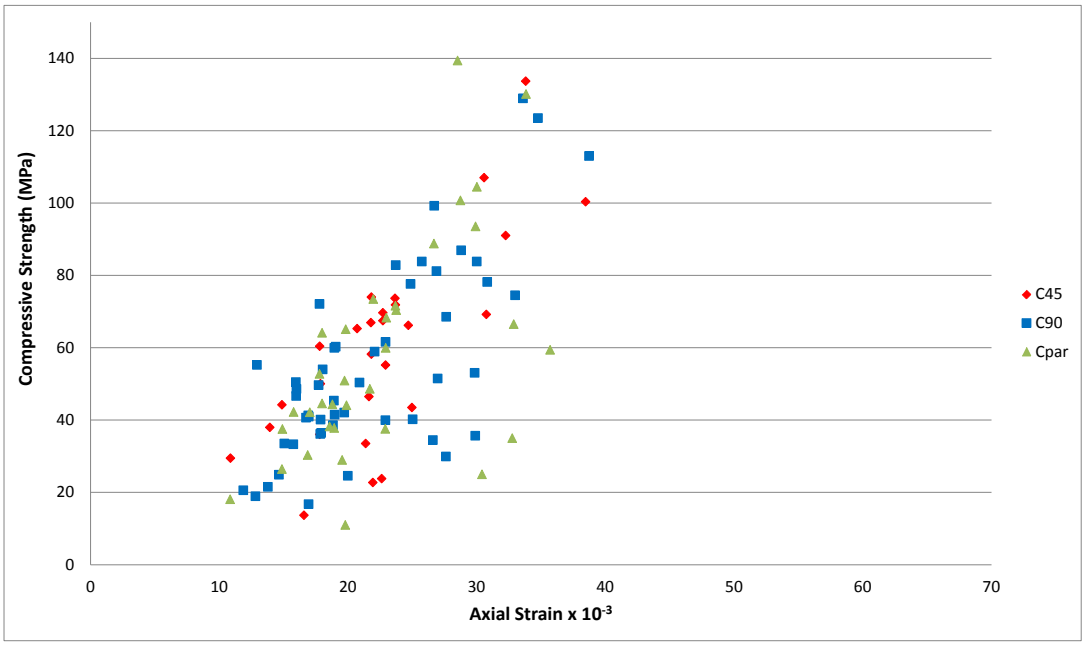

Figure 6.3 – Maximum compressive strength of cores taken from a number of different flows on Tenerife. These samples also showed that the C_{par} group had the highest compressive strengths.

The global analysis showed that, although on average, the C_{par} cores had the highest maximum compressive strengths, there was a great degree of variability within the sample population due to the variance in morphologies between cores taken from levees of different ages and compositions. When the three core groups from the same sample are compared, the results show that the C_{par} group have distinctly higher compressive strengths that the C_{45} and C_{90} groups (Figure 6.4). It was not possible to get parallel cores from all samples and for those groups where only groups C_{45} and C_{90} were tested, the majority of the C_{90} cores were shown to have higher compressive strengths (Figure 6.5).

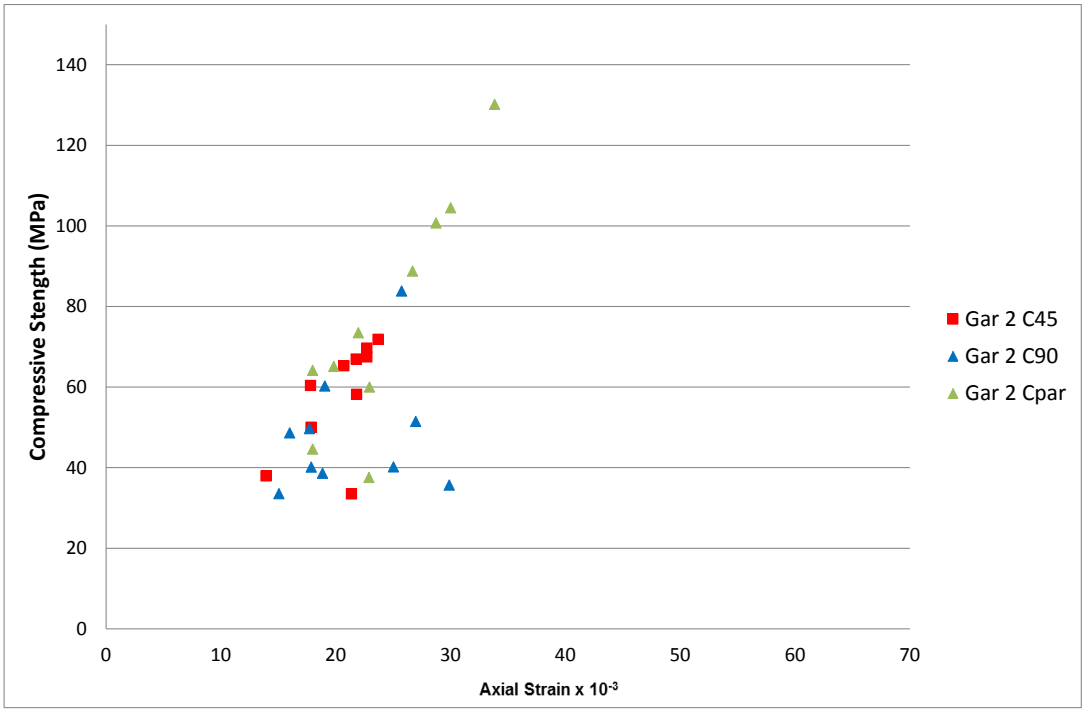

Figure 6.4 – Maximum compressive strength of cores taken from the Garachico flow in Tenerife. The cores that were taken parallel to the flow direction (green triangles) showed the highest values for maximum compressive stress whilst the cores taken at 45° to the direction of flow (red squares) had, on average, the lowest compressive strengths.

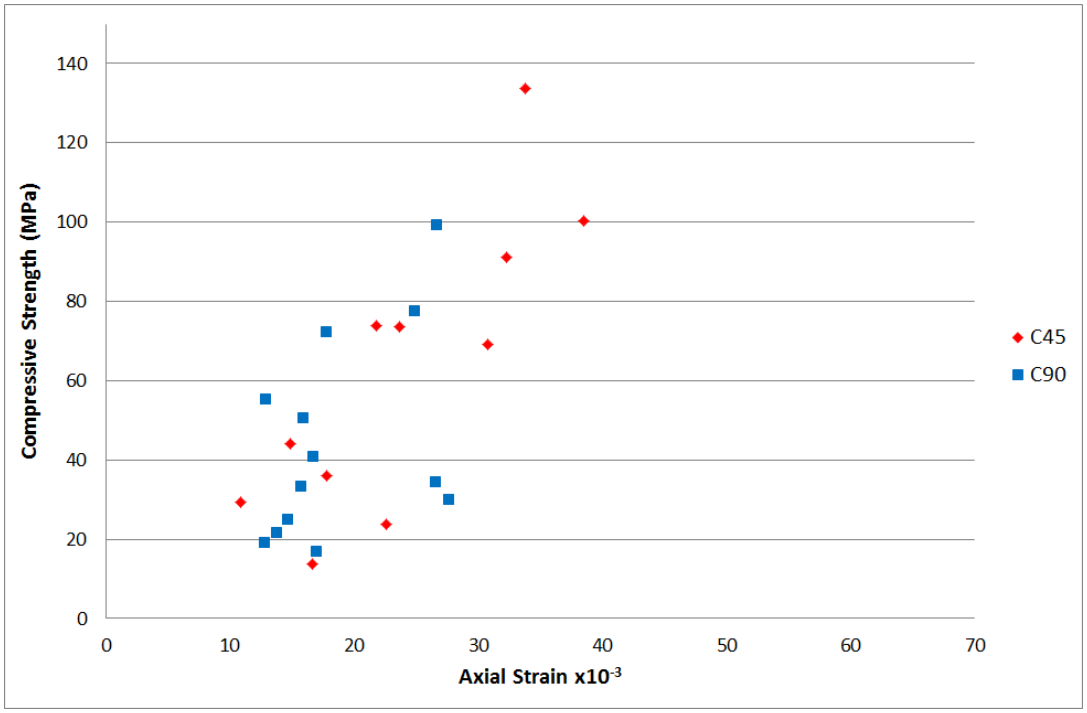

Figure 6.5 – Maximum compressive strengths of cores taken from the Arafo flow, Tenerife. The cores drilled 45° on average had higher maximum strengths that the 90° cores.

The cores taken from the massive, central part of a number of lava samples were also tested to understand the difference in mechanical properties between massive lava and levee material and were also found to follow the same trend with the C_{par} group having the highest compressive strengths (Figure 6.6). Massive lava samples were taken only from Mount Etna and when compared to the samples taken from Etnean levees, the lava samples had much high compressive strengths (Figure 6.7)

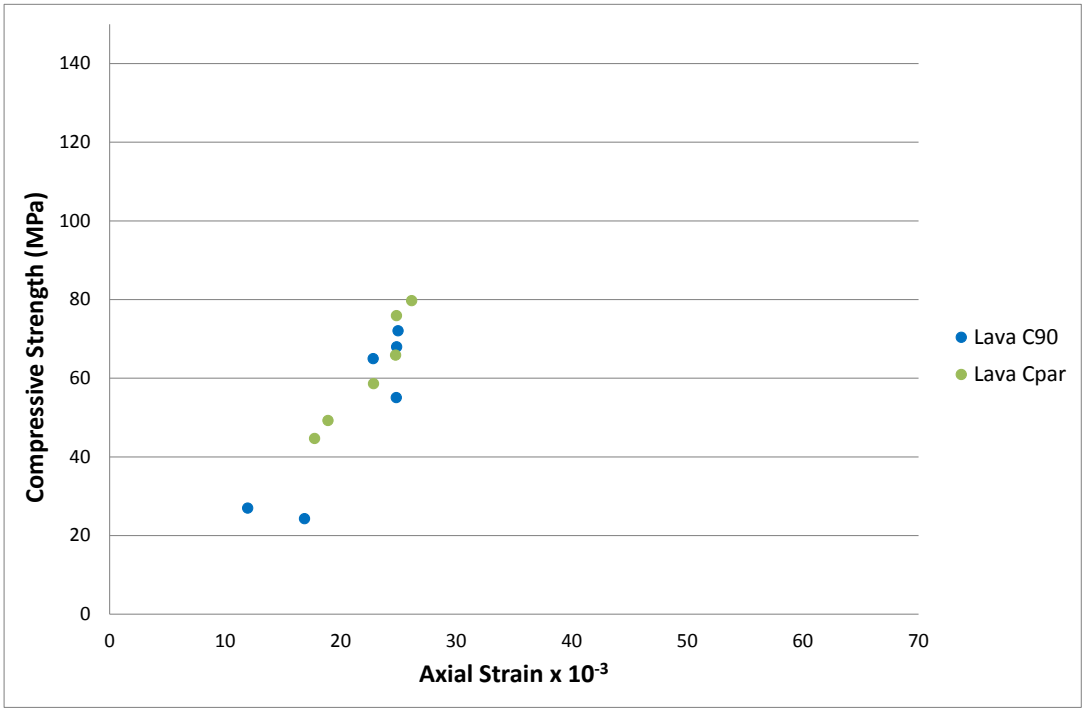

Figure 6.6 – The maximum compressive strengths of cores taken from the interior of a massive flow unit also show the same trend with angle of applied pressure at the cores from levee samples.

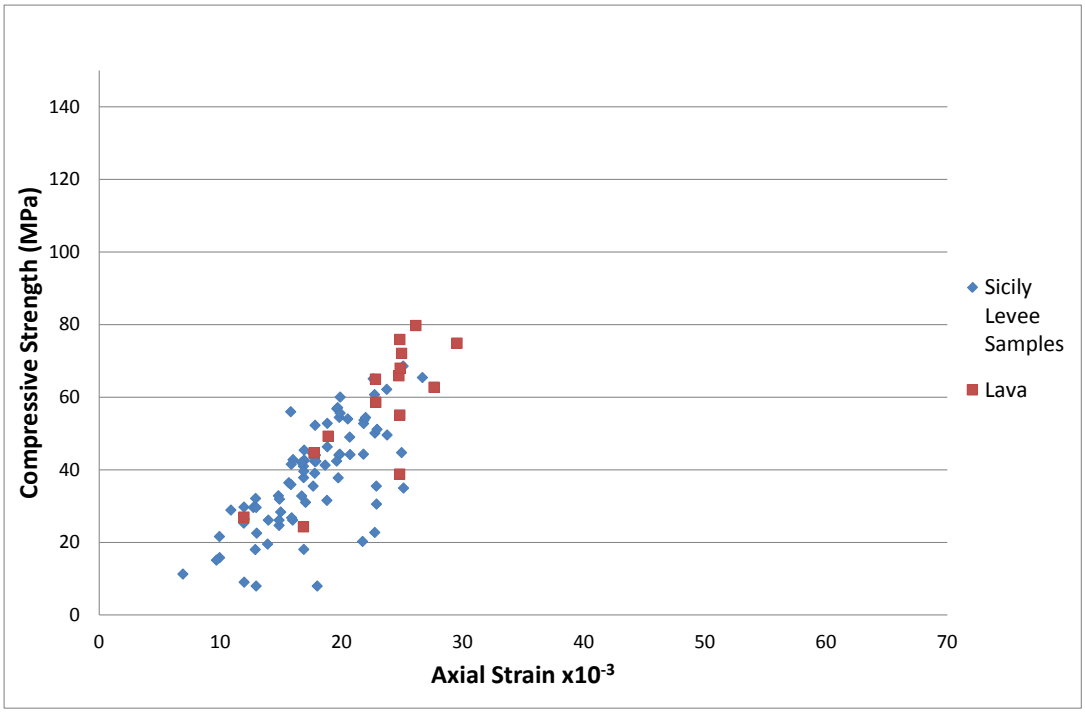

Figure 6.7 – The maximum compressive strengths of cores taken from the massive flow material had, on average, higher compressive strengths than the cores taken from levees on Mount Etna.

The C_{par} cores clearly had the strongest compressive strength but the trend with the C_{45} and C_{90} cores was not as clear and in a few cases, no trend was observed. In order to understand why the C_{par} cores had the highest compressive strengths and the C_{45} and C_{90} groups had variable strength ranges, the axial strain lines and angle of failure of the samples were examined for mode of failure. The uniaxial compression test results were then also compared with the results of the porosity and dry density tests to quantify the effect these factors had on overall strength and mode of failure.

For the samples that followed the global trend with strength, the axial strain plots showed that C_{45} groups underwent brittle fracture in the majority of tests. The C_{90} and C_{par} groups showed many results for ductile and staggered failure (Figure 6.8).

Samples from the 2003 flow on Mount Etna and one set of samples from the Garachico flow on Tenerife, did not follow the global trend with C_{par} showing the largest compressive strengths and C_{45} showing the weakest. The strength of the 2003 Etnean cores appeared independent of direction of applied stress. Cores from the same sample displayed a range of values with no particular orientation in any one sample showing greater values for strength (Figure 6.9). Despite the change in trend, from the axial strain plots (Figure 6.10) it can be seen that in accordance with the other sample groups, the C_{45} cores underwent brittle failure while some of the C_{90} and the majority of the C_{par} groups underwent ductile failure.

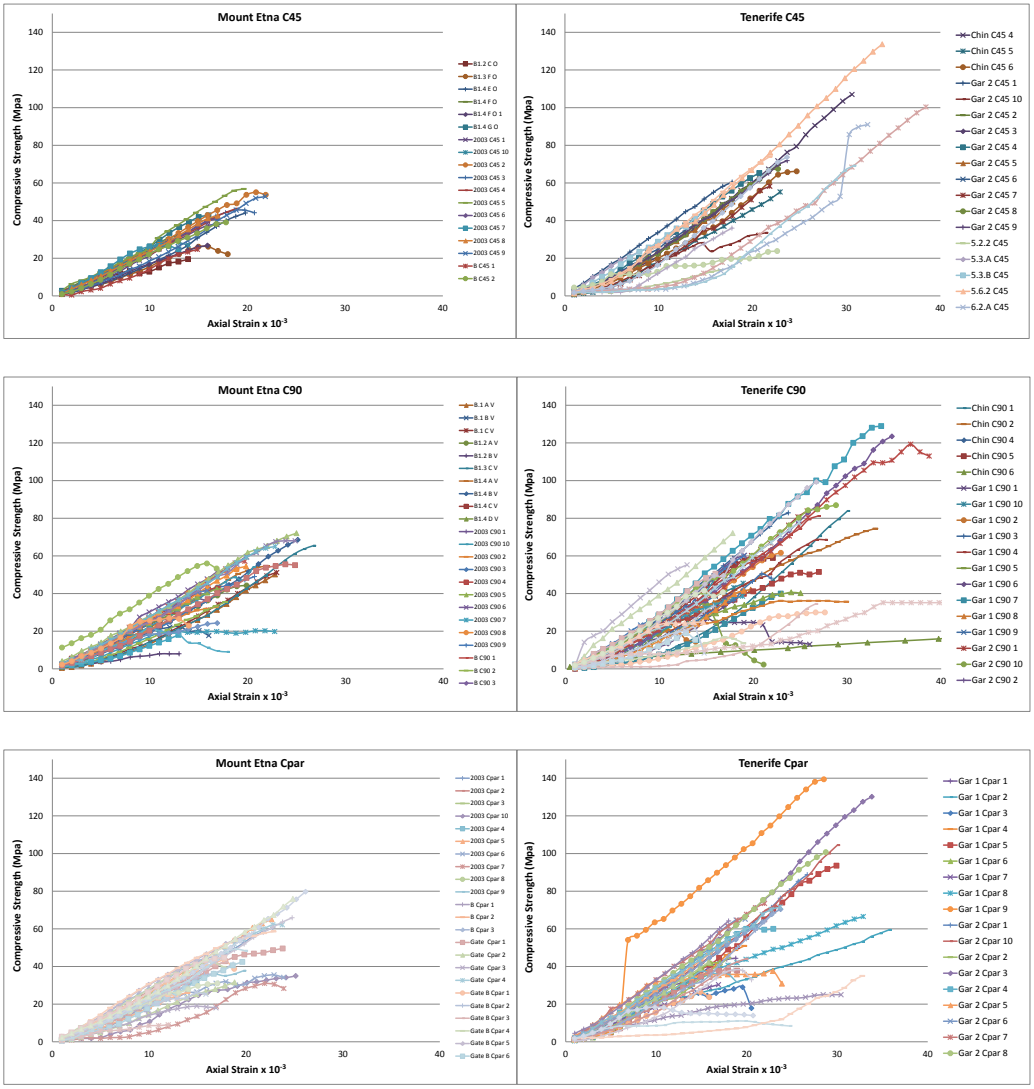

Figure 6.8 – Stress-Strain graphs for the samples from Etna and Tenerife grouped by orientation. The graphs on the left represent the Etnean samples whilst the graphs on the right display the results from the Tenerife samples. The C_{45} group in both field sites show smooth constant strain rates and brittle fracture. The C_{90} and C_{par} groups both show a variety of behaviours with brittle and ductile fracture.

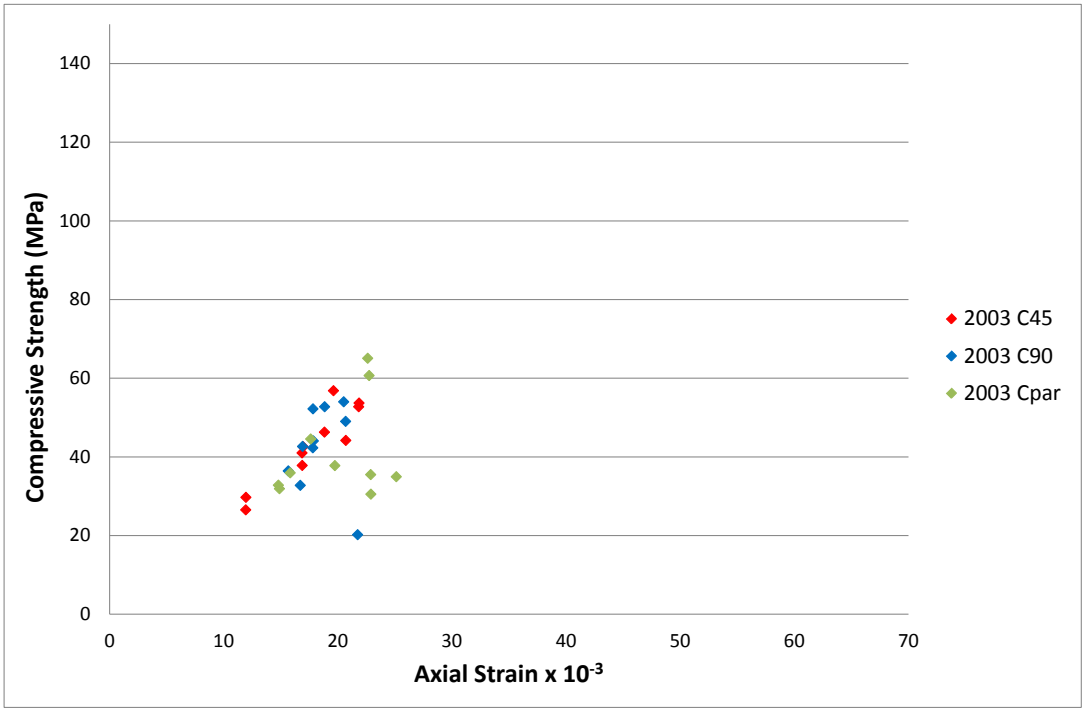

Figure 6.9 – Maximum compressive strengths for samples from the 2003 flow-field on Mount Etna. Unlike the other basaltic levee samples collected, these cores did not display any trend in strength with angle of applied pressure.

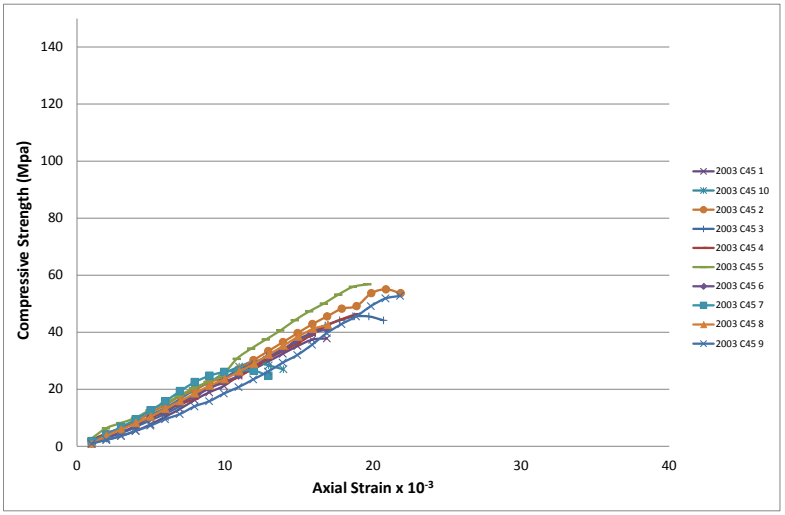

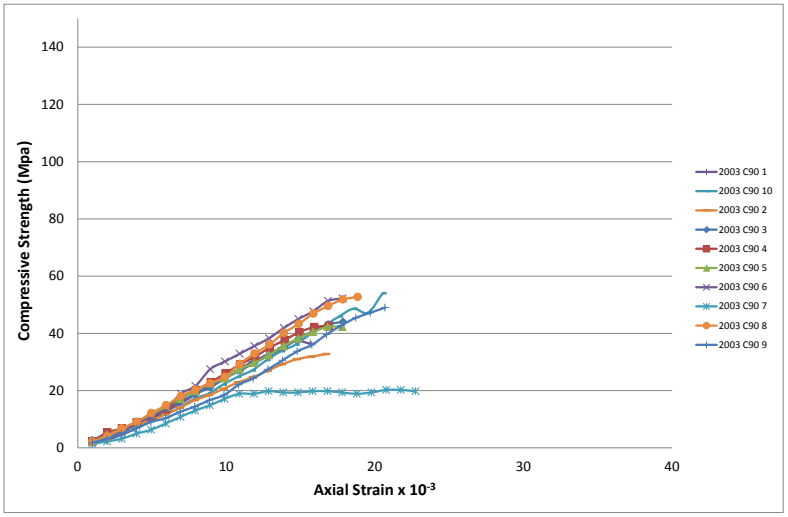

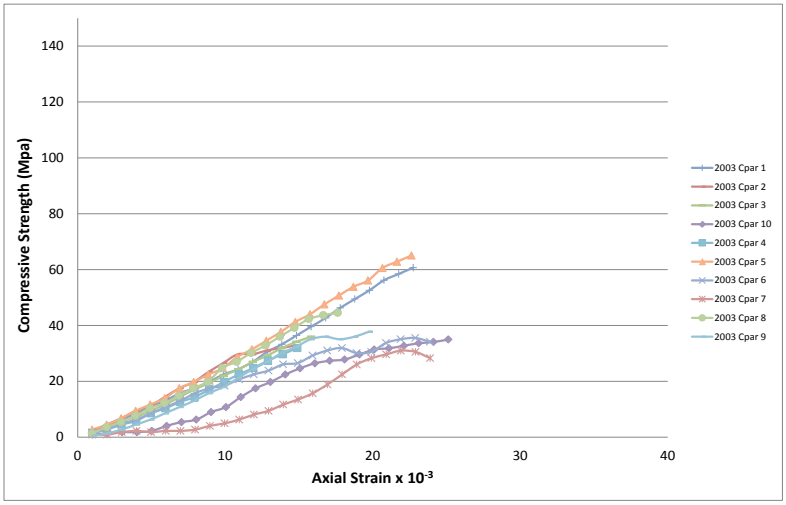

Figure 6.10 –In contrast to the global trend, the majority of the cores in the C_{par} group underwent ductile fracture and failed in a series of stages. In contrast, the entire C_{45} group experienced brittle failure characterised by high failure angles and clear macroscopic fractures on the tested cores and sharp sudden ends to the axial strain line.

One set of cores (Gar 3) did display a trend with core direction but it was the opposite of the global trend. The C_{90} group were, on average stronger than the C_{par} (Figure 6.11). The axial strain plots showed that the C_{90} group were characterised by a sharp drop in the strain rate and although the samples failed with multiple fractures, the fractures were high angle and macroscopic, suggesting that the samples underwent brittle failure (Figure 6.12). The cores drilled parallel to the flow direction were overall weaker and had shallowly sloping axial strain lines or had staggered strain lines showing that the sample went through multiple stages of failure (Figure 6.13).

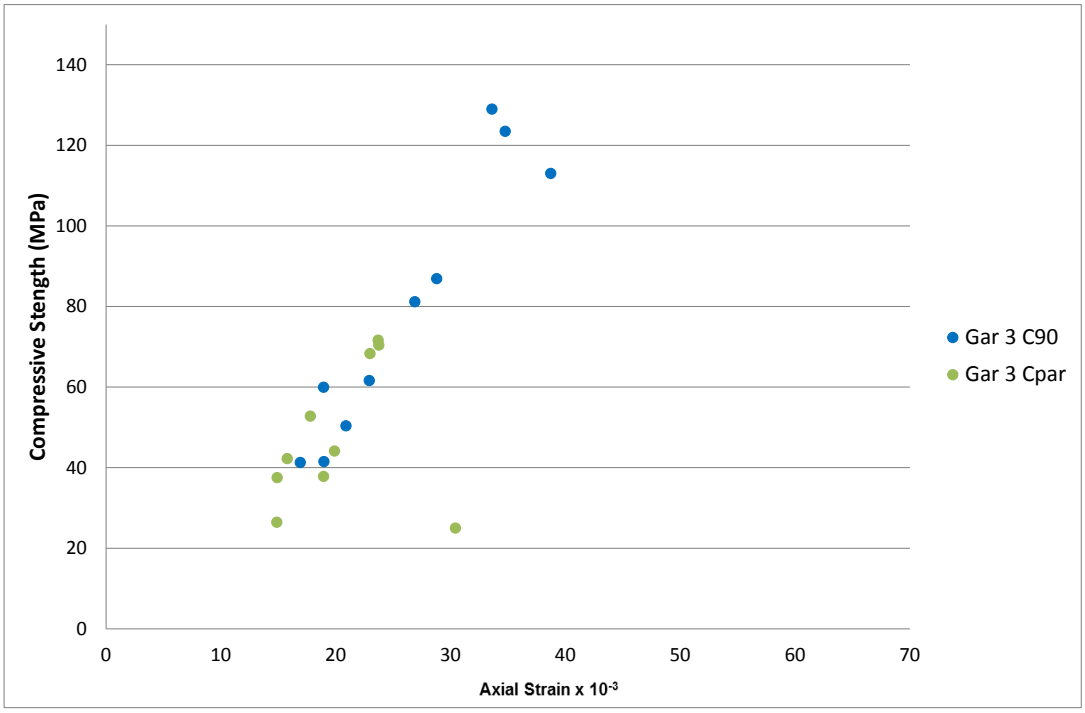

Figure 6.11 – Samples taken from the Garachico flow on Tenerife show the opposite trend to all other samples taken from that flow or from other flows on Tenerife with the cores drill parallel to the flow direction showing smaller maximum compressive strengths than the cores drill at 90°.

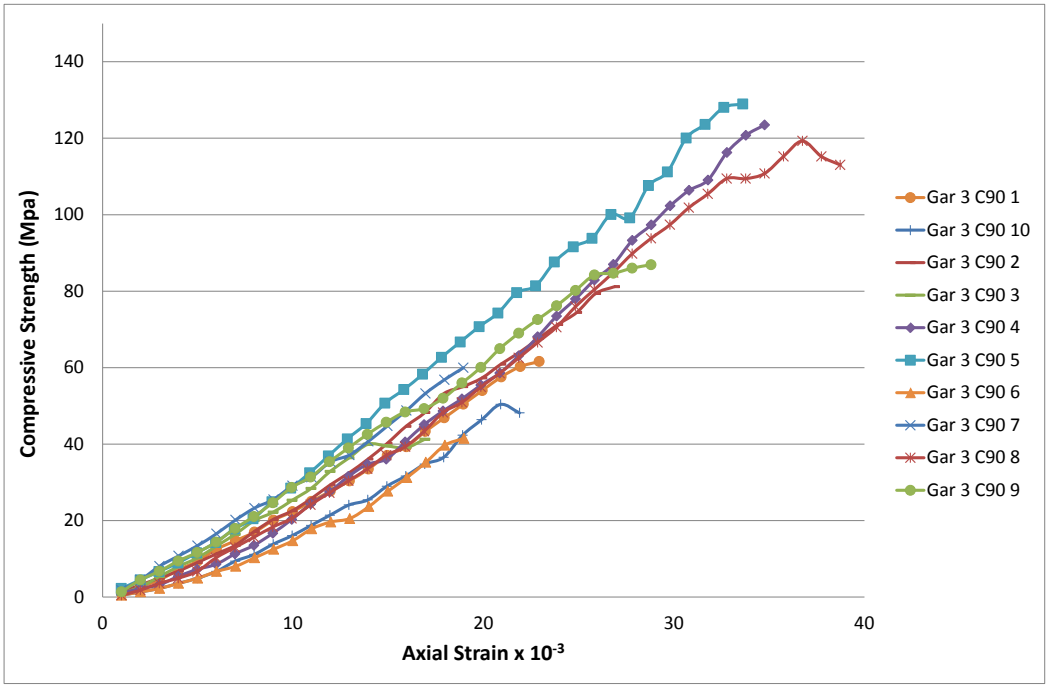

Figure 6.12 – The samples that were drilled 90° to the flow direction overall had higher maximum compressive strengths with steep and uniform axial strain rates with sharp drop off showing that the samples underwent brittle failure.

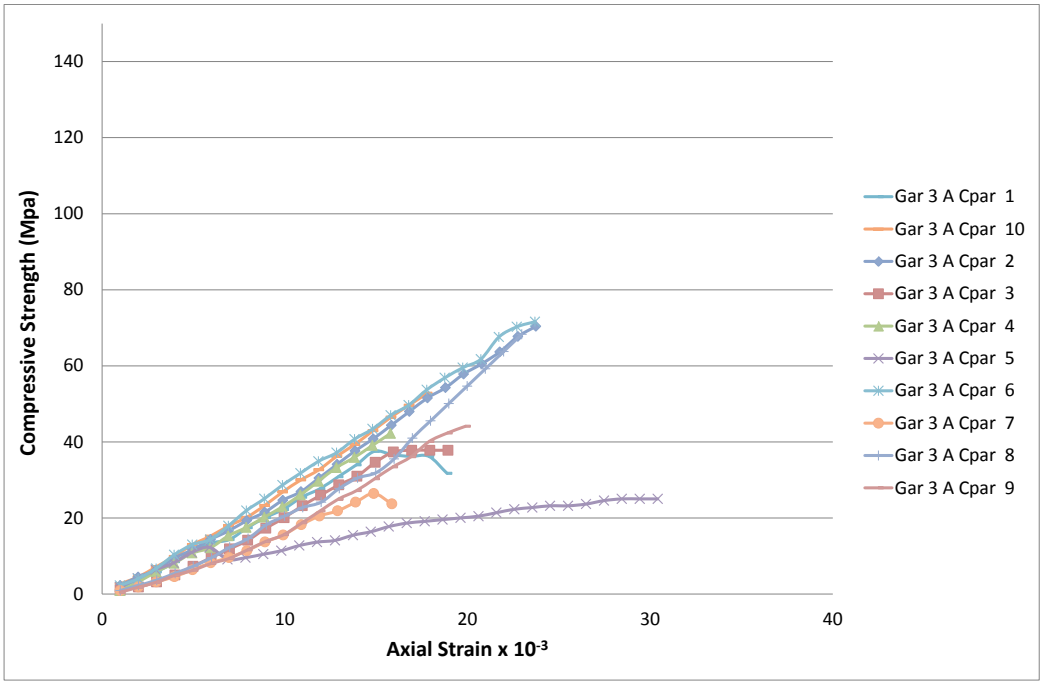

Figure 6.13 – Results of the uniaxial compression tests on the Gar 3 samples cored parallel to the flow direction. Overall these samples were weaker. The stain lines also show that the sample underwent ductile failure.

It is likely that some local variability in the sample set that resulted in the reversed trend in strength for these samples. The un-shattered cores showed a number of fractures running through the samples in different orientations to the vesicle alignment (Figure 6.14).

Figure 6.14 – A sample of the Gar 3 cores showing the presence of fractures in random orientations. This type of fracturing was not present in the other sample groups.

6.4.2 Porosity Tests

The mechanical properties of basalts have been documented in previous studies (Benson et al., 2007; Fortin et al., 2011). However, these studies focused on basalts with low porosities which therefore failed in a brittle manner. In order to investigate the effects of porosity on rock strength and mode of failure, the porosity of 191 of the 210 samples was calculated using the saturation and buoyancy technique as described by the International Society of Rock Mechanics Commission on Standardisation of Laboratory and Field Tests. A full list of results is given in Table C.2, Appendix C. Porosities ranged from 0.41% for the samples taken from the massive, interior part of a lava flow to 17.32% for cores taken from a levee in the Arafo flow-field on Tenerife. In order to identify global trends in the effect of porosity on rock strength in relation to the angle of applied stress, the maximum compressive strengths of all samples were plotted against porosity.

The results for the group C_{par} show a very strong trend between increasing porosity and decreasing compressive strength. The C_{45} group also displayed this trend though not as strongly. The compressive strength of cores from the C_{90} group appeared to be only weakly dependent on porosity as there appeared to be almost no correlation for these cores between increasing porosity and decreasing uniaxial compressive strength (Figure 6.15).

Overall the results show a strong trend between increasing porosity and decreasing strength.

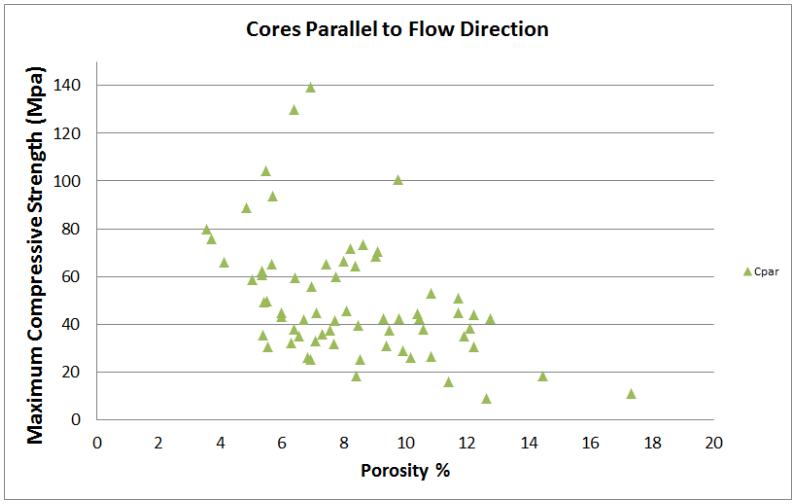

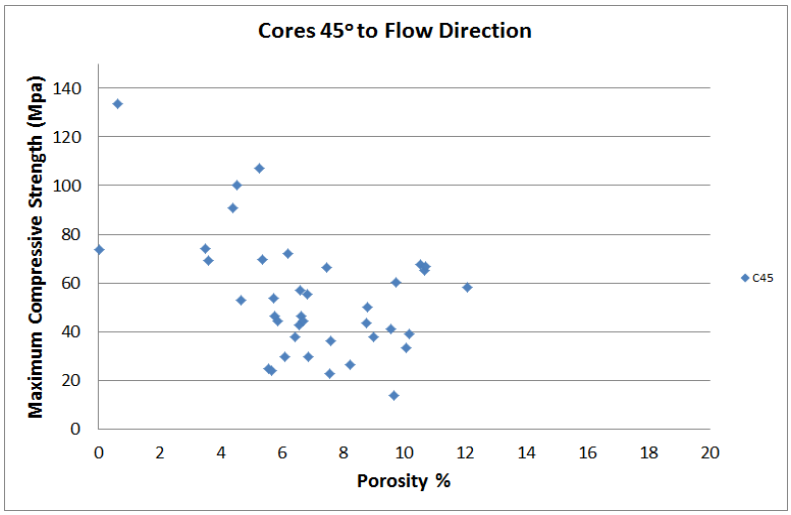

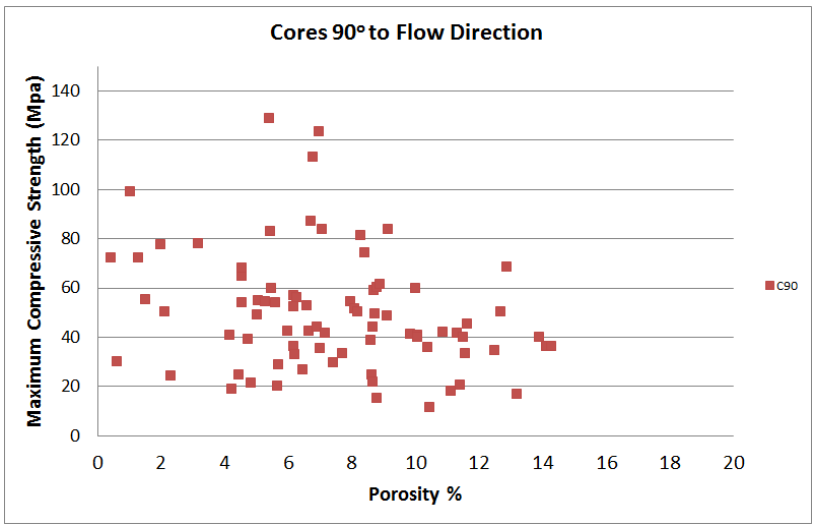

Figure 6.15 – The maximum compressive strengths for all 191 cores were plotted against porosity by angle of core to the flow direction. The cores where the direction of applied stress is parallel or 45^{o} showed a strong relationship between increasing porosity and decreasing strength.

Both C_{par} groups from Tenerife and Etna, displayed the strongest trend with increasing porosity. The Tenerife sample groups in particular showed a very distinct trend between the angle at which the cores were drilled relative to the flow direction and the effect of porosity on core strength. The porosity of the Tenereife samples was 8.15% compared to 7.07% for the Etnean samples. The C_{par} group strengths were the most affected by increasing porosity with the effect lessing as the core direction changes from 45^{o} to 90^{o} (Figure 6.16).

In contradiction to the trend seen in the global analysis and Tenerife samples, the C_{90} group of cores from Sicily also showed a strong trend between increasing porosity and decreasing strength with the C_{45} group showing the weakest trend. However, the C_{45} group had the smallest sample population which may be skewing the results (Figure 6.17). The global trend is even clearer when the strength results for the three cores groups from the same sample are plotted against porosity (Figure 6.18).

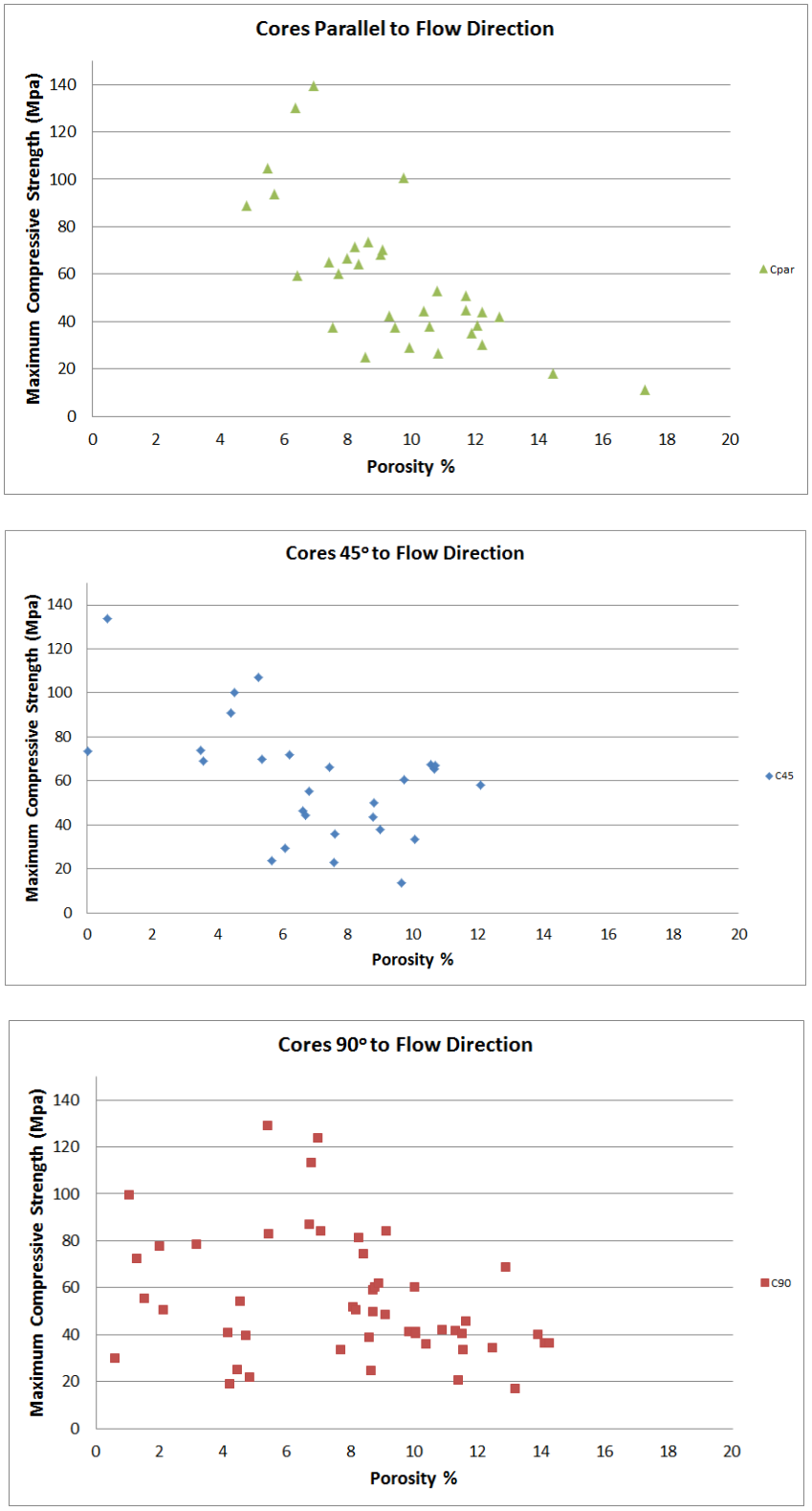

Figure 6.16 – Compressive Strength vs. Porosity. The samples from Tenerife showed a strong trend between increasing porosity and decreasing strength for C_{par} group. The results for the C_{45} and C_{90} groups also showed that compressive strength decreases with increasing porosity but the extent to which porosity affects strength deceases as core direction changes from parallel, through 45° to 90°.

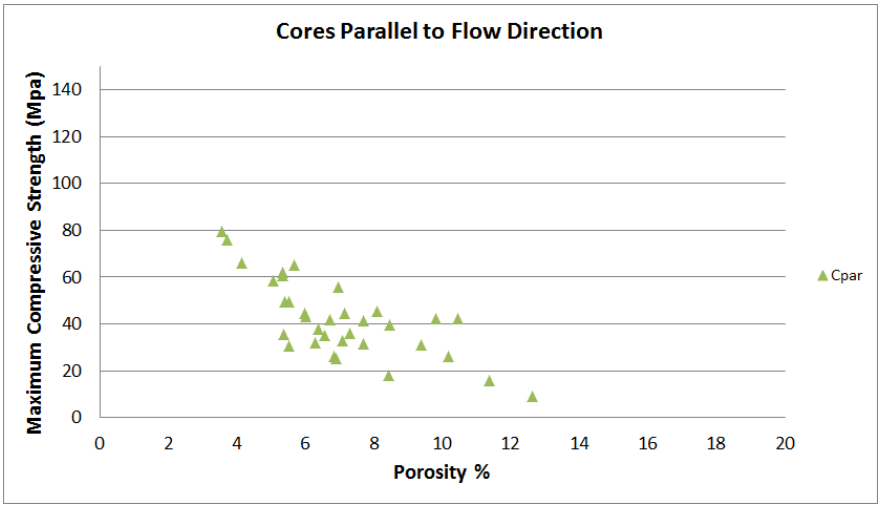

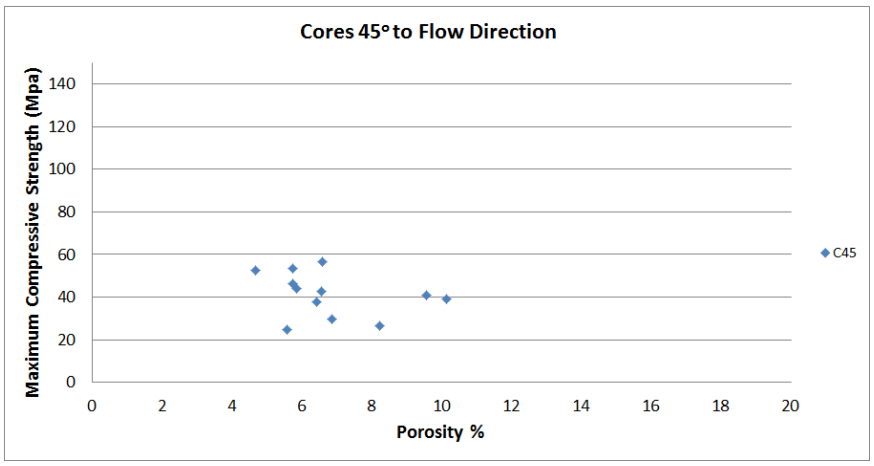

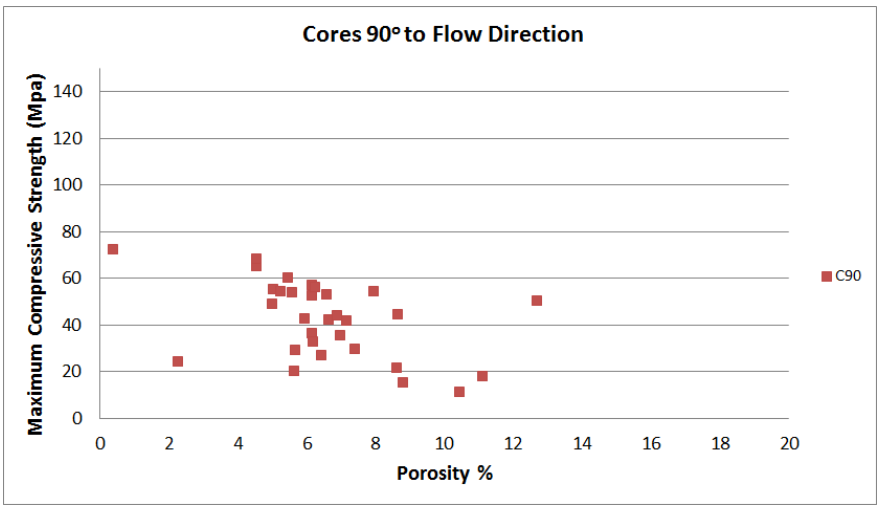

Figure 6.17 – The set of cores from Etna showed the same trend as seen in the Tenerife sample set with those cores which were taken parallel to the direction of flow showing a strong trend between increasing porosity and decreasing strength. In contrast to the Tenerife samples, the 90° samples and 45° samples showed very little variance between the two groups in the magnitude to which porosity affected rock strength with the 90° showing a marginally stronger trend.

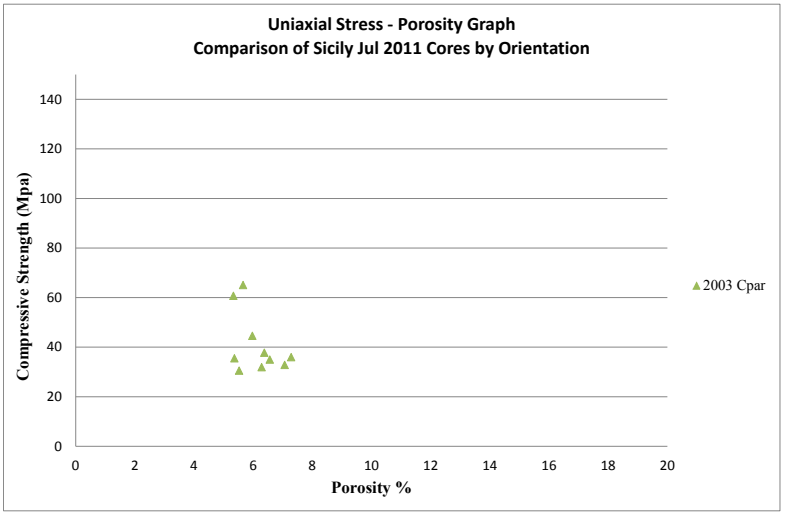

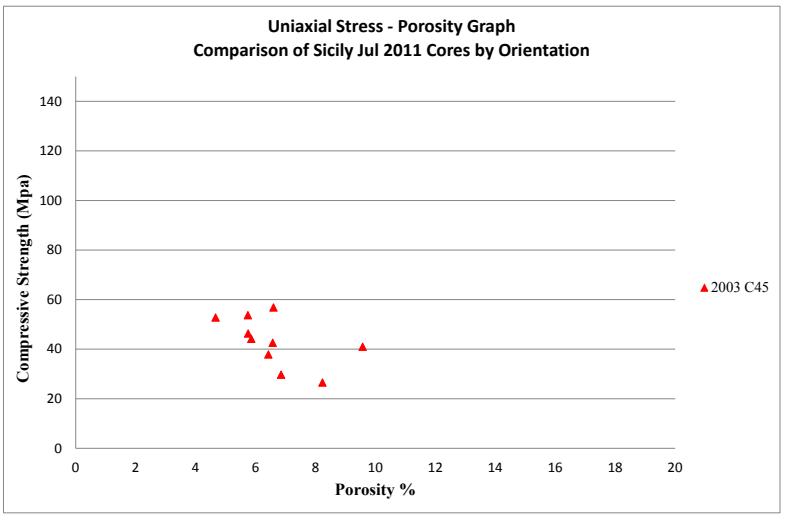

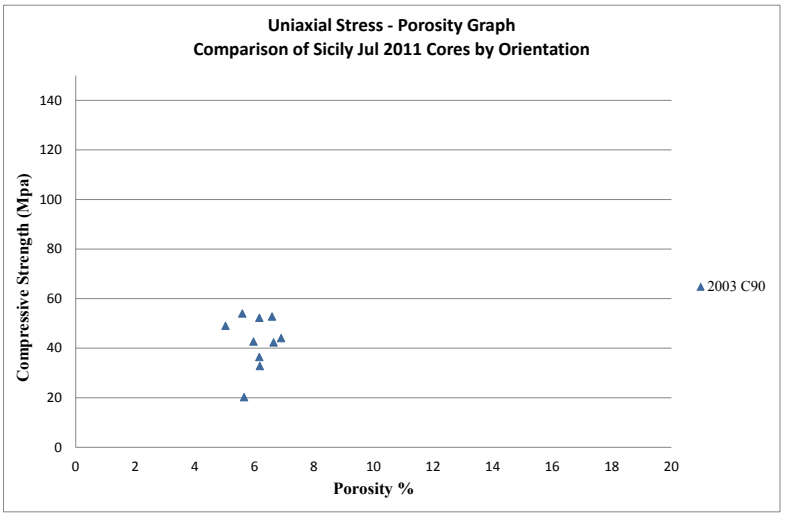

Figure 6.18 – The cores represented in these graphs were taken from the 2003 flow-field on Mount Etna. The C_{par} and C_{45} groups show the same trend with decreasing strength and increasing porosity. The C_{90} group results show that the strength of the cores is independent of porosity.

Cores were also drilled from a sample of the interior of a massive flow unit as a control to examine the difference in the mechanical properties between flow material and levees. The porosity of the lava material was calculated and plotted against max compressive strength to see if the same trends emerged between increasing porosity and strength. The cores taken from the lava samples also showed the rock strength decreased with increasing porosity. However, the trend was not as pronounced as in the C_{par} cores from the levee samples. There was also very little difference in the porosity/strength relationship between the C_{par} and C_{90} sample groups in contrast to the results of the levee samples (Figure 6.19). The one anomalous data point within the 90^{o} group was attributed to local macroscopic fractures within that core which resulted in a comparatively low maximum compressive strength for the core.

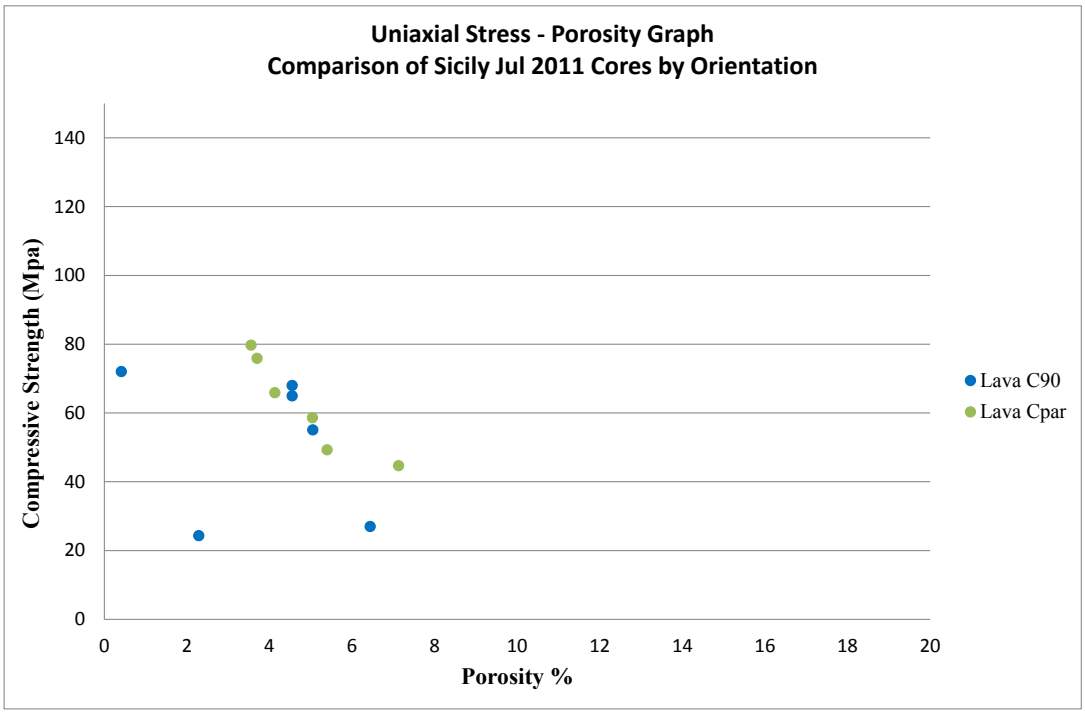

Figure 6.19 – Cores taken from the interior of a massive lava flow were also tested to quantify the mechanical differences between levee and flow material. The lava cores also showed a trend between increasing porosity and decreasing compressive strength but to a lesser extent that the C_{par} cores from levee samples.

6.4.3 Density Tests

The dry density for the samples was calculated to quantify the effects of density on the mechanical behaviour of the cores. For a full list of results please see Table C.2, Appendix C. As expected, it was observed that as density increased, the compressive strength of the rock also increased. The cores from the flow material had the greatest densities and also the greatest compressive strengths. This trend was true for all samples from both Tenerife and Etna (Figure 6.20 & 6.21).

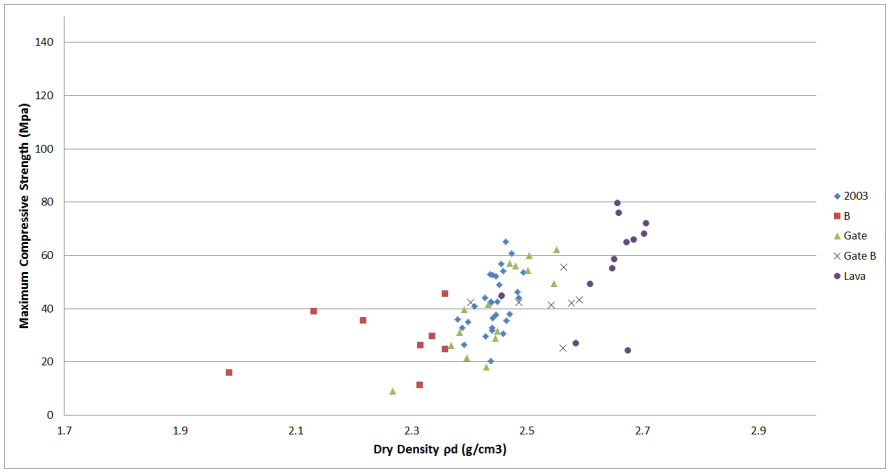

Figure 6.20 –Maximum strength of cores taken from the 2003 and 1983 flow-fields on Mount Etna plotted against density. As expected – as density increases, the maximum compressive strength of basalt also increases.

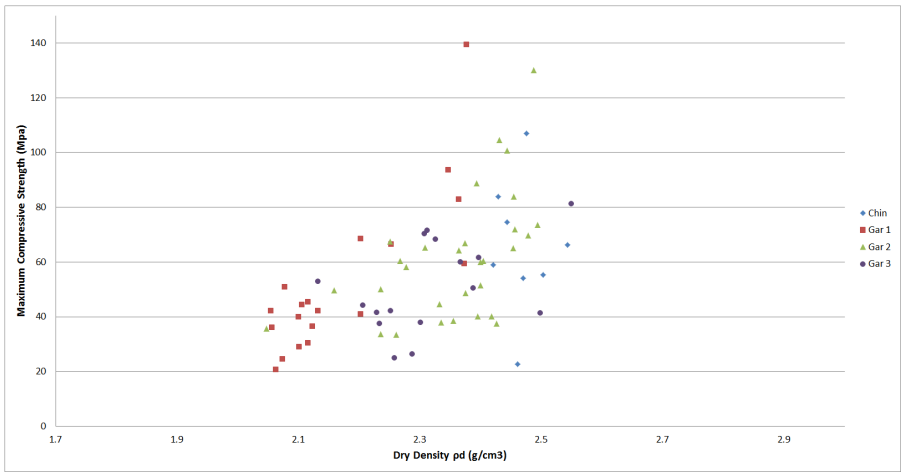

Figure 6.21 – Maximum compressive strength vs. density of the cores taken from Tenerife also showing the trend that strength increases with density.

6.4.4 Vesicle Analysis

Vesicles in basalts typically show a large range of sizes and heterogeneous placement (Smith, 2002; Shea et al., 2010). Hand specimen petrology showed that the samples taken in this study contained a broad spectrum of % vesiculation.

Vesicle analysis was carried out using random sampling principles. A cut surface from one specimen within each sample group from Etna and Tenerife was selected and then overlaid with a clear grid measuring 5 cm by 5 cm divided into 1 cm by 1 cm squares and the number of vesicles within pre-defined size ranges was counted. A full list of results is available in Table 6.1

The Etna samples had the biggest range in vesicle sizes with 58% of vesicles in the <1 mm range and 36% of vesicles in the 1-5 mm range and 5% of vesicles in the >10 mm range, compared to the Tenerife samples which had 86% of all vesicles in the <1 mm range, 18% in the 1-5 mm range and no vesicles >10 mm. The vesicle distribution was compared to the average maximum compressive strength for that samples group and the results show that on average, those samples with more vesicles within the 1-5 mm range had smaller compressive strengths than their counterparts. Samples with greater concentrations of vesicles within the <1 mm range also showed the same trend with compressive strength but it was less distinct. Overall in the majority of cases, samples from the same group but with a larger concentration of vesicles had, on average, lower maximum compressive strengths regardless of vesicle size.

In the case of the B1.2 samples group from Sicily. The sample with the highest vesicle concentration had the lowest maximum compressive strength. This was due to the presence of very large >10 mm vesicles in the cores which did not

appear in the random sampling face. The failure of the core was clearly in-line with the orientation of these large vesicles and therefore the low compressive strength of this group can be considered anomalous and the result of local textures in the cores and not representative of the sample overall.

The Tenerife and Etna samples all displayed the trend that increasing vesicle content resulted in lower compressive strengths. However, although overall the samples from Tenerife were more vesiculated, Etnean samples had lower compressive strengths. Therefore % vesiculation, although an important factor in rock strength, is not the only control. The only difference in Etnean to Tenerife vesiculation is that the Etnean samples contained a much greater quantity of vesicles >1 mm in size indicating that vesicle size rather than % vesicularity has a greater control over rock strength.

Table 6.1 – Results of the vesicle analysis carried out on representative samples from each sampling site on Tenerife and Sicily. The Sicilian samples displayed a great distribution in sample size, however when comparing the average maximum compressive strength for the samples group with the number of vesicles, it was found that in the majority of cases, samples with the largest number of vesicles, regardless of vesicle size, had the lowest compressive strengths.

	% of Vesicles			
	<1mm	1-5mm	5-10mm	>10mm
Etna	58%	36%	5%	1%
Tenerife	81%	18%	1%	0%

			No. of Vesicles Recorded by Size					
Field Site	**Group**	**Sample No.**	**<1mm**	**1-5mm**	**5-10mm**	**>10mm**	**Total No. of Vesicles**	**Average Max Compressive Strength (MPa)**
Sicily	B1.3	B1.3 C90	46	62	7	0	115	41.59
Sicily		B1.3 C45	53	46	12	7	118	39.81
Sicily	**B1.3 Total**		**99**	**108**	**19**	**7**	**233**	
Sicily	B1.4	B1.4 C90	86	47	16	4	153	44.71
Sicily		B1.4 C45	85	76	13	2	176	33.67
Sicily	**B1.4 Total**		**171**	**123**	**29**	**6**	**329**	
Sicily		2003 Cpar	211	55	2	0	268	40.97
Sicily	2003	2003 C45	303	24	7	0	334	43.13
Sicily		2003 C90	316	22	0	0	338	42.63
Sicily	**2003 Total**		**830**	**101**	**9**	**0**	**940**	
Sicily		B C45	193	80	14	2	289	31.85
Sicily		B Cpar	135	161	18	5	319	29.11
Sicily	B	B C90	108	204	28	8	348	23.60
Sicily	**B Total**		**436**	**445**	**60**	**15**	**956**	
Sicily		B1 C45	57	57	10	0	124	28.35
Sicily	B1	B1 C90	86	155	6	0	247	41.25
Sicily	**B1 Total**		**143**	**212**	**16**	**0**	**371**	
Sicily		B1.2 C45	73	60	7	2	142	13.73
Sicily	B1.2	B1.2 C90	57	81	6	2	146	26.11
Sicily	**B1.2 Total**		**130**	**141**	**13**	**4**	**288**	

			No. of Vesicles Recorded by Size					
Field Site	**Group**	**Sample No.**	**<1mm**	**1-5mm**	**5-10mm**	**>10mm**	**Total No. of Vesicles**	**Average Max Compressive Strength (MPa)**
Tenerife	6.6	6.6 C90	279	112	13	0	404	39.31
Tenerife		6.6 C45	457	81	14	0	552	29.91
Tenerife	**6.6 Total**		**736**	**193**	**27**	**0**	**956**	
Tenerife		7.2 C45	117	56	2	0	175	72.29
Tenerife	7.2	7.2 C90	390	40	0	0	430	40.67
Tenerife	**7.2 Total**		**507**	**96**	**2**	**0**	**605**	
Tenerife		Gar 1 Cpar	358	63	3	0	424	61.72
Tenerife	Gar 1	Gar 1 C90	591	39	14	0	644	43.76
Tenerife	**Gar 1 Total**		**949**	**102**	**17**	**0**	**1,068**	
Tenerife	Gar 2	Gar 2 C45	190	109	3	5	307	58.12
Tenerife		Gar 2 Cpar	424	89	1	0	514	76.89
Tenerife		Gar 2 C90	566	85	0	0	651	48.19
Tenerife	**Gar 2 Total**		**1,180**	**283**	**4**	**5**	**1,472**	
Tenerife	4.6	4.6 C90	50	34	1	0	85	32.56
Tenerife	5.3	5.3 C45	110	75	11	2	198	36.83
Tenerife	6.3	6.3 C45	227	156	12	0	395	21.77
Tenerife	6.2	6.2 C45	471	74	3	0	548	51.89
Tenerife	4.1	4.1 C90	574	52	4	0	630	63.87

6.5 Analysis

In order to explain the observations of trends in rock strength made in this chapter, this section will focus on combining the results from the uniaxial, porosity and density tests and vesicle analysis to quantify the effect of intrinsic variables such as porosity, vesicle size and orientation, density and crystal content have on overall rock strength.

6.5.1 Angle of Applied Stress in Relation to Rock Textures

As the results of the strength analysis show, regardless of overall compressive strength of a sample, the cores taken parallel to the flow direction or C_{par} consistently have the highest compressive strengths compared to cores from the

same sample taken 45° or 90° to the flow direction (C_{45} & C_{90} groups), in both the Tenerife and Etnean samples sets. In addition, the C_{45} group consistently proved to be weakest samples showing that the angle of applied stress relative to some characteristic of the core linked to flow direction must be a control on rock strength. This observation correlates well with trends observed in sedimentary rocks where samples containing micro-structures also failed at lower compressive strengths when the angle of applied stress is 45° to structure (Mogi 2007).

Prior to testing, the samples were examined for textures such as crystal or vesicle alignment or existing fractures. The majority of samples had a significant % of vesiculation of between 4-8%. Analysis of the failed cores showed that the samples in which the vesicles were roughly 45° to the angle of applied stress – in the majority of cases within the C_{45} group – the line of fracture runs from vesicle to vesicle resulting in shearing of the vesicles. The vesicles continue to be clearly visible after failure with fracture lines passing diagonally through the vesicle. In the samples where the vesicles are orientated parallel or perpendicular to the direction of applied stress, analysis of the failed cores showed that the vesicles appeared compressed. This correlates with the findings of Loaiza et al., (2012) who show that basalts with a high % porosity (~18%) fail in a ductile manner with compaction prior to failure, the result of compression of aligned pores in a direction perpendicular to the main compression axis. Plotting the stress/strain graphs showed that where the majority of samples within the C_{45} group underwent brittle failure represented by a smooth axial strain line and sharp drop off and the C_{90} and C_{par} groups which underwent ductile deformation prior to sample failure as represented by staggered axial strain lines (Figure 6.22 & 6.8). Comparing the axial strain lines, max compressive strengths, orientation of applied stress and mode of

failure of the sample, showed that whilst the C_{par} group had the highest compressive strengths, this group was also more likely to undergo ductile deformation and the C_{45} group, which had the lowest compressive strengths, was more likely to fail in a brittle fashion.

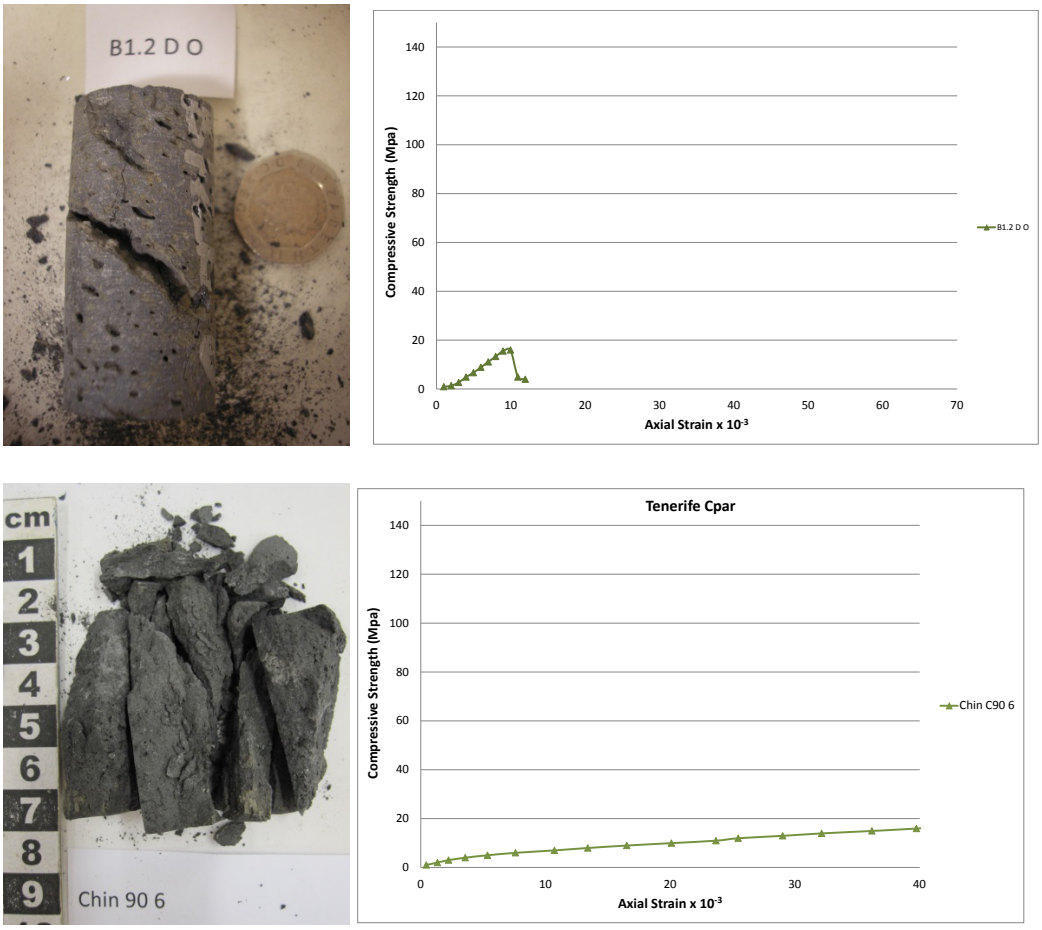

Figure 6.22 – The top images show the mode of fracture and axial strain line for a C_{45} core from the 1983 flow-field on Mount Etna, Sicily. The shattered core shows that the angle of fracture followed the alignment of the vesicles. The axial strain plot shows that the sample failed in a brittle fashion. The bottom images are of a core from Tenerife in the C_{90} group. The shatter core has no definite angle of failure and the axial strain line shows that the sample underwent ductile failure. Closer analysis of the failed core shows some compression of vesicles.

The Extended Griffith Crack Theory presented by Digby & Murrell (1976) states that elliptical factures may close under high compressive stress, ten times the

uniaxial strength of the rock and that frictional stress resulting from the sides of the closed crack coming into contact with one another may actually increase the strength of the rock. In the C_{par} group, the majority of cores which displayed vesicle alignment showed that the vesicles were aligned in the direction of flow. The same was true for the C_{90} and C_{45} groups where vesicles were aligned in the direction of flow. The angle of applied stress during the uniaxial compression tests can be illustrated by Figure 6.23.

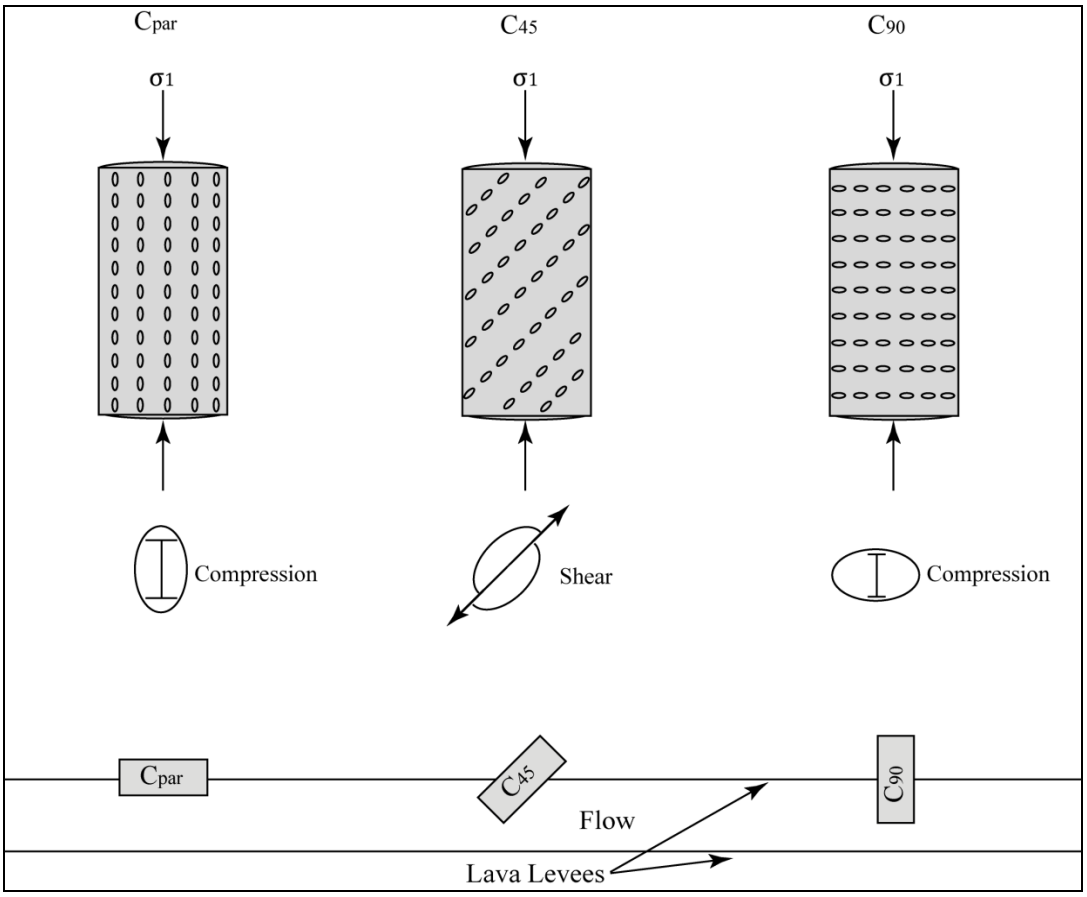

Figure 6.23 – Graphic shows vesicle orientation in relation to σ_1 in each C group – C_{par}, C_{45} and C_{90} and the possible mechanism for vesicle closure under uniaxial compression. The C_{par} and C_{90} cores exhibited ductile deformation as shown through the axial strain lines pointing towards vesicle closure due to compression. The C_{45} group underwent brittle failure and analysis of failed samples showed that the vesicles were being sheared during failure.

Given that the C_{par} and C_{90} groups were shown to undergo ductile deformation prior to failure and were on average stronger than the C_{45} group, it can be assumed that compression resulted in the closure of some vesicles, bring the sides of the vesicle into contact with each other, briefly increasing the strength of the sample. The C_{45} group were shown to fail in a brittle fashion and the shattered cores showed no significant compression of vesicles.

6.5.2 Strength Trends with Porosity

The porosity and density tests showed that the Tenerife samples overall had a higher porosity and lower density than the Etnean samples in addition to having a larger range of porosities (Figures 6.25 & 6.26). These factors would logically mean that the Tenerife samples should have the lower compressive strengths of the two groups. However, the results of the uniaxial compression tests showed that the samples from Tenerife had, on average, higher maximum compressive strengths than the samples from Etna.

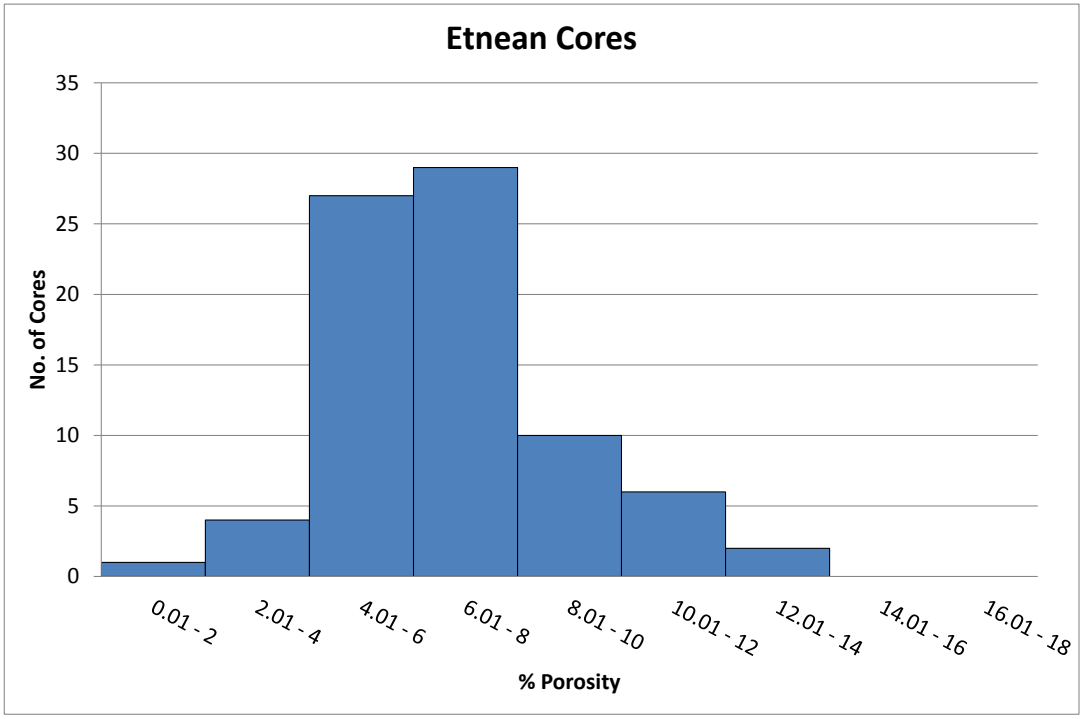

Figure 6.24 – The Etnean cores show that 71% of the 79 cores tested had porosities of between 4 and 8%.

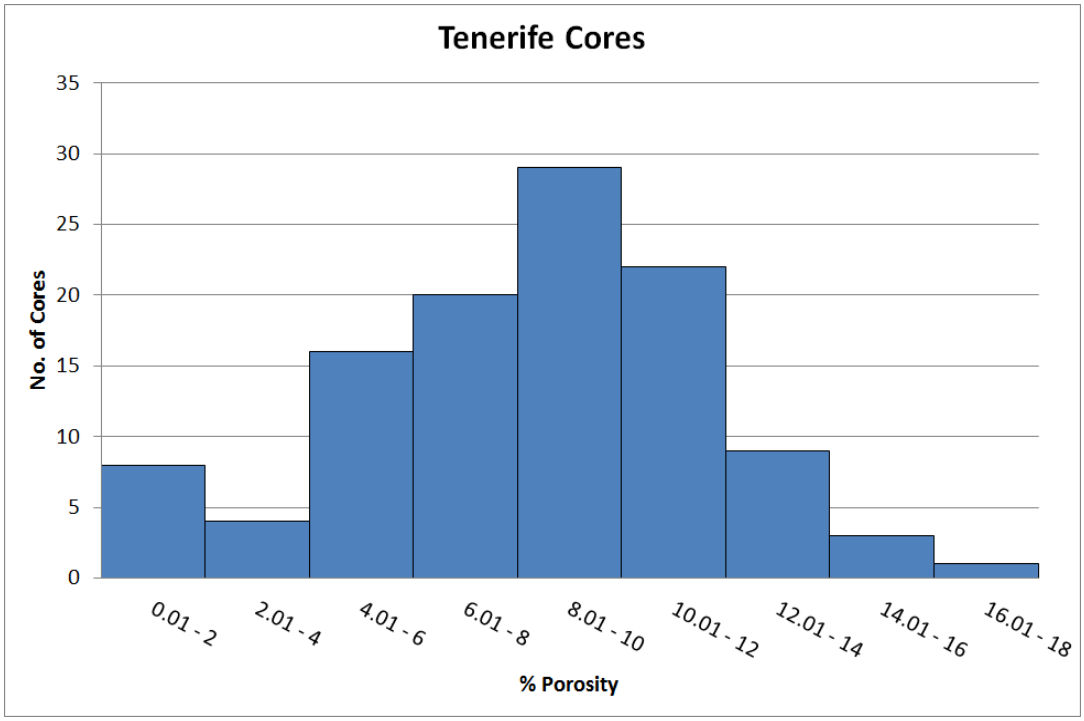

Figure 6.25 – The results of the porosity tests for the Tenerife samples show that the core displayed a much larger range of porosities that the Etnean samples with only 32% plotting in the 4 – 8% porosity range (which accounts for the majority of Etnean samples).

The orientation of vesicles in relation to the angle of principal stress has already been shown as a controlling factor in rock strength. Prior to testing, the samples were examined for textures such as fracture patterns or vesicle/crystal alignment. As a result, the samples were also classified by anisotropy into three groups. 1). Cores which showed vesicles with no particular orientation which were roughly spherical with no elongation. 2). Cores showing elongated vesicles orientated in the direction of flow. 3). Cores which show elongated vesicle with a defined orientation but not in the direction of flow (direction of flow here means the direction of flow of the lava channel that the levees were bounding).

In both sample sets from Tenerife and Etna, taking the maximum values for all samples only, the cores drilled parallel to the flow direction (C_{par}) had the highest maximum compressive strengths. When the density and porosity of the samples with the largest compressive strengths was compared to the weaker samples, no trend with density and porosity was found. The strongest samples were not those with the lowest porosity and highest density (Table 6.2). For example – a comparison between the % vesicularity and compressive strengths of the Tenerife C_{45} group and the Etnean C_{45} group shows that the Etnean samples are significantly weaker than their counterparts from Tenerife despite being denser and with a lower % porosity. Given that the 210 samples display a range of values for porosity, density and vesicle size and orientation, it can be argued that these parameters do not determine (or are not key to) the strength of these rocks.

However, the strength of the cores was also shown not to be completely independent of these factors. As stated previously, plotting the max strengths against porosity clearly illustrates that as the porosity increases, compressive strength decreases. When comparing the trends between increasing porosity and

max strength, it is clear that as porosity increases, strength decreases. This is especially true for the C_{par} and C_{45} groups. The C_{90} group results showed that strength is only weakly affected by porosity. This trend is true of both sets of samples from Tenerife and Etna. However, when the two field sites are plotted separately, it can be seen that the samples from Etna show a stronger trend with increasing porosity and decreasing strength than the samples from Tenerife despite the Tenerife samples having the highest % porosity and also a much greater range of porosities (Figures 6.26 & 6.27).

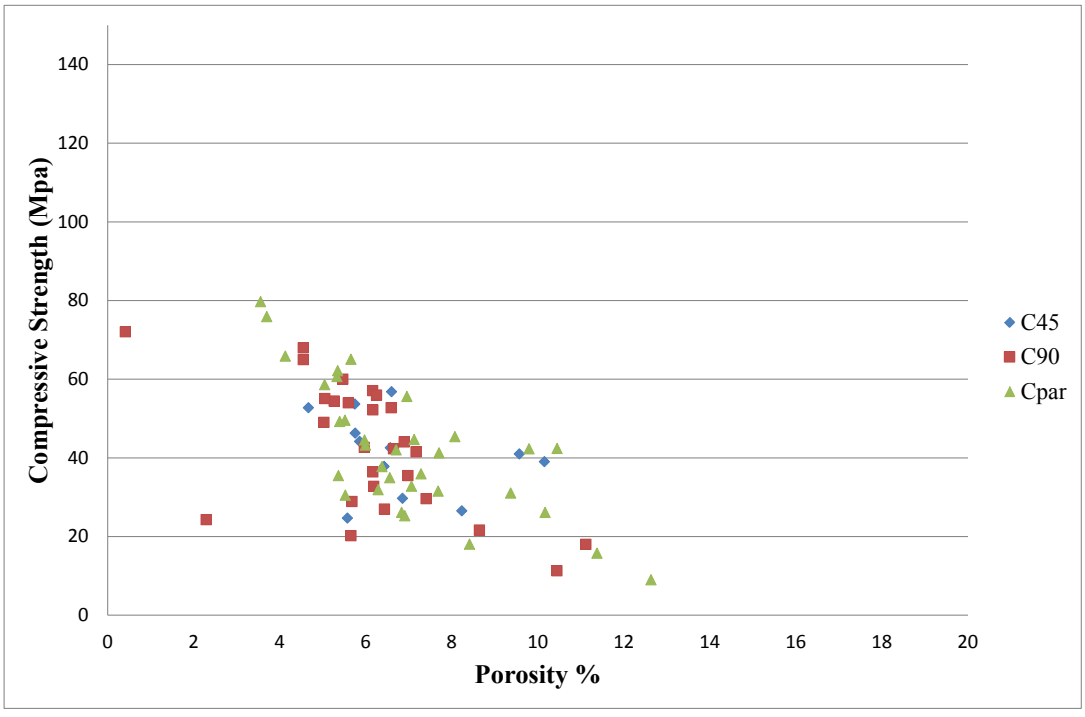

Figure 6.26 – Etnean samples. Cores show a strong trend between increasing porosity and decreasing compressive strengths.

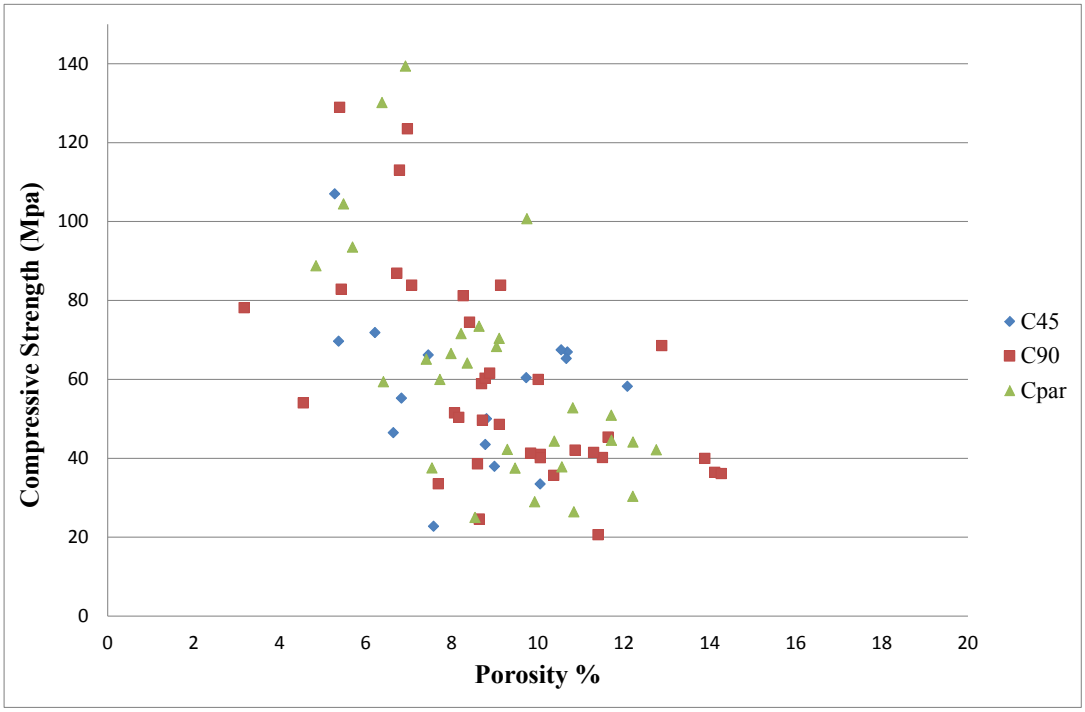

Figure 6.27 – Tenerife samples. The strength of the cores showed a smaller degree of dependency on porosity.

Table 6.2 – Maximum compressive strength by core group for all 210 samples taken. For both field sites, C_{par} group had the sample with the highest compressive strength. There was no parallel trend with density and porosity however, the core with the highest strength did not have a correspondingly low value for porosity or higher value for density as expected.

Field Site	Core Direction	Max Compressive Strength	Porosity %	Density (g/cm^3)
Sicily	C_{45}	56.80	6.83	2.42
Sicily	C_{90}	74.85	7.19	2.48
Sicily	C_{par}	79.70	7.02	2.47
Tenerife	C_{45}	133.68	6.97	2.40
Tenerife	C_{90}	128.95	7.79	2.39
Tenerife	C_{par}	139.40	9.63	2.30

Taking the average of all of the cores taken from Etna, the porosity, density and max compressive strength of the samples was 7.07%, 2.47 g/cm^3 and 79.70 MPa respectively compared to the average for the Tenerife samples which is 8.15%, 2.37 g/cm^3 and 139.40 MPa. The results of the vesicle analysis (Table 6.1)

show that 36% of the Etna samples had vesicles in the 1-5 mm range and 5% of vesicles in the 5-10 mm range compared to the Tenerife samples which had just 18% in the 1-5 mm range and 1% in the 5-10 mm range. Therefore, although the Etna samples had lower % porosity, they had a greater % of vesicles with sizes above 1 mm. During testing it was observed that the macro-fractures resulting from the failure of the sample ran from vesicle to vesicle on the Etnean samples with large (>1 mm) vesicles resulting in a high degree of variability in the angle of failure. The Etnean and Tenerife samples with no large vesicles in contrast had either the steep angles of failure with clear macro-fractures typical of brittle failure or multiple high angle fracture with compressed vesicles (Figure 6.28). Both of the cores shown in Figure 6.28 were taken from the same sample block taken from a levee in the 1983 flow. The first core – B $C_{par}1$ had a high % of vesicles over 1 mm in size (porosity 11.38%). The core failed at 15.78 MPa and had multiple fractures which ran in a zig-zag pattern from vesicle to vesicle. In contrast the core B $C_{par}3$ (bottom set of pictures) was taken from the same sample but had much fewer large vesicles (porosity 8.07%). This core failed at 45.41 MPa along one angle of failure which is typical of brittle fracture. The failed core also showed signs of vesicle compression which was absent from the B $C_{par}1$ core.

These cores also had some of the highest max compressive strengths (Figures 6.8 & 6.22). Therefore it is logical to assume that the size rather than the quantity of vesicles is a controlling factor in rock strength.

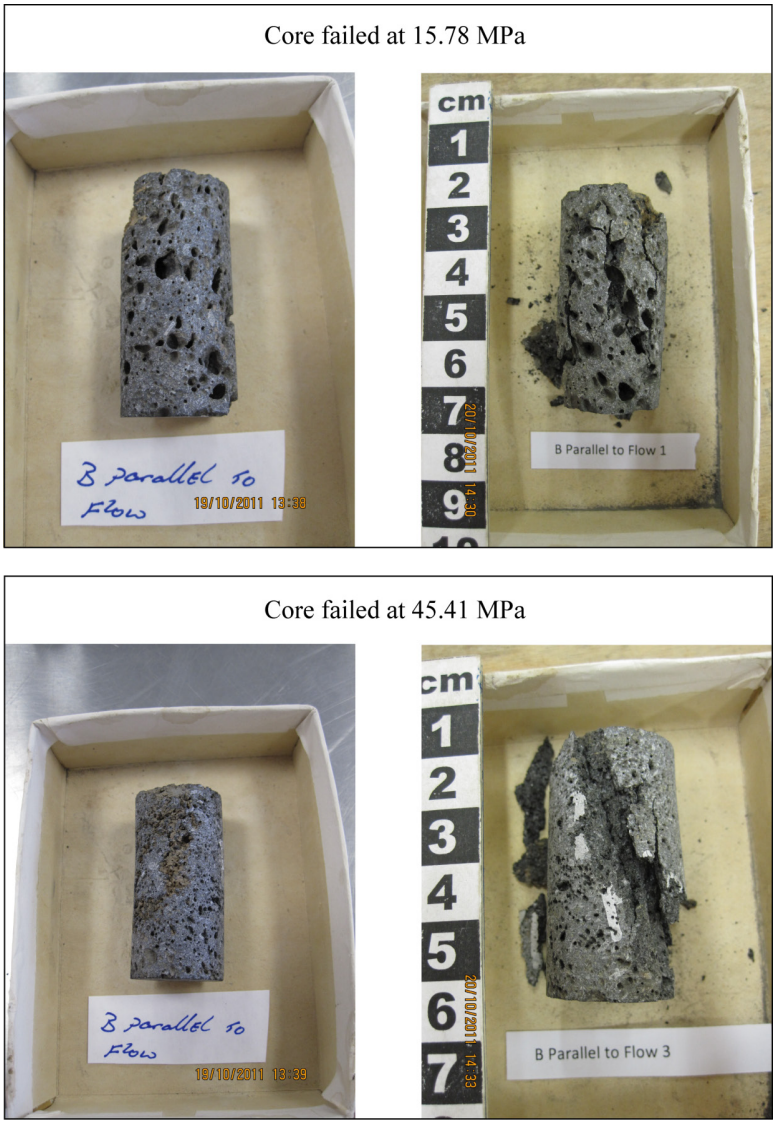

Figure 6.28 – The Etna cores with large vesicles often showed multiple lines of fracture which zig-zagged from vesicle to vesicle and often had low compressive strengths.

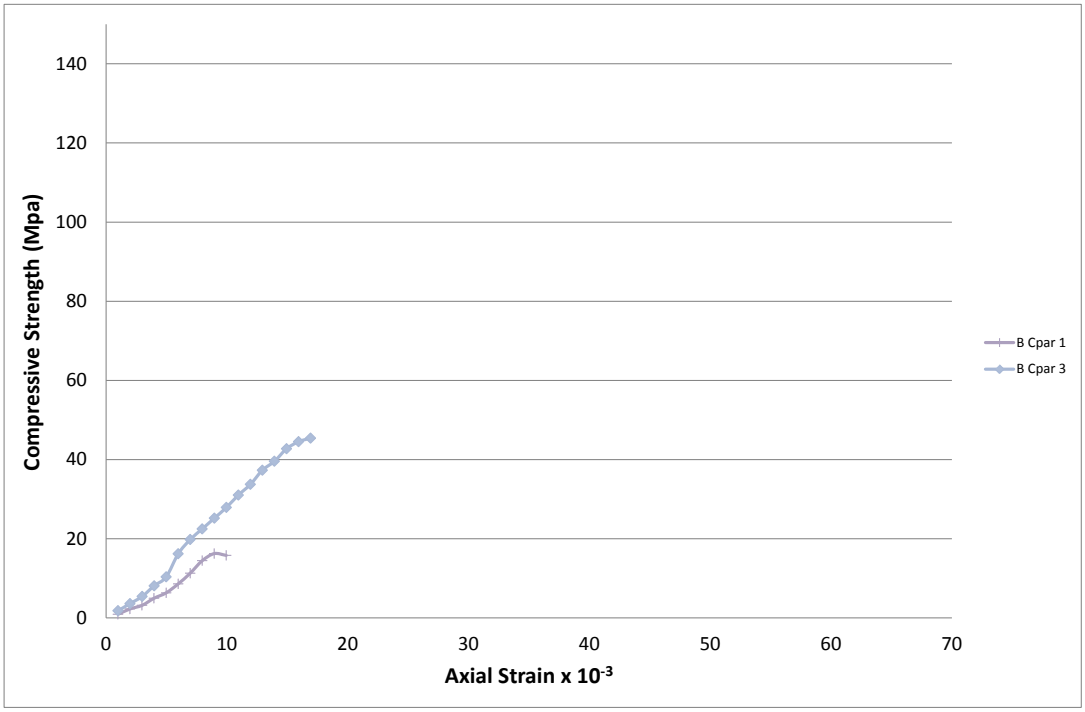

Figure 6.29 – Axial strain line plots for cores B parallel to flow (C_{par}) 1 and 3. C_{par} 1 was much weaker than the C_{par} 3 sample despite having been taken from the same sample block. The only morphological difference between the two samples was the size of the vesicles.

The axial strain plots were compared with porosity to assess the mode of failure of the samples. It was thought that all samples with a high vesicularity would have staggered axial trend lines representing ductile deformation relating to vesicles collapse due to the compression however the mode of failure of the cores – brittle or ductile was independent of porosity. However, as discussed in Section 6.4.1, when arranged into groups by core direction, the graphs (Figure 6.8) show that the C_{90} and C_{par} groups had the most samples that failed with a staggered axial strain line showing that the sample was deforming in stages before failure while the C_{45} almost always underwent brittle fracture. When comparing the cores that underwent ductile deformation with hand specimen petrology of the samples, there was no correlation between % porosity and ductile failure meaning that the transition from ductile to brittle failure was somehow dependent on the orientation

of applied stress. As previously discussed in Section 6.5.1 and illustrated in Figure 6.23, changing the direction of applied stress in relation to orientation of the vesicles resulted in different methods of failure of the samples. For the C_{par} and C_{90} groups, the vesicles appeared to be undergoing compression during loading resulting in ductile failure whilst the C_{45} group appear sheared with no compression prior to failure. Therefore the strength of the core changes with direction according to the orientation, distribution and size of the vesicles and appears to be either independent or only weakly dependent on the % vesicularity.

6.5.3 Deviations From The Trend

There were some core samples which deviated from the trends described previously. One of these groups was Gar 2 samples from the Garachico flows in Tenerife. In this group, the majority of the C_{par} samples had max compressive strengths of greater than 65 Mpa and were on average 25% stronger than the C_{45} group and 40% stronger than the C_{90} group. The C_{90} samples had, on average, the lowest max compressive strength in direct contrast with the majority of other samples groups from the Garachico flow in Tenerife, other flows on Tenerife and the samples from Mount Etna where the C_{45} group was the weakest (Table 6.3). When the stress-strain curves were plotted, it was observed that the axial strain lines were still in accordance with the global trend with the C_{par} and C_{90} groups displaying a tendency towards ductile failure and the C_{45} group showing brittle failure in the majority (Figure 6.30).

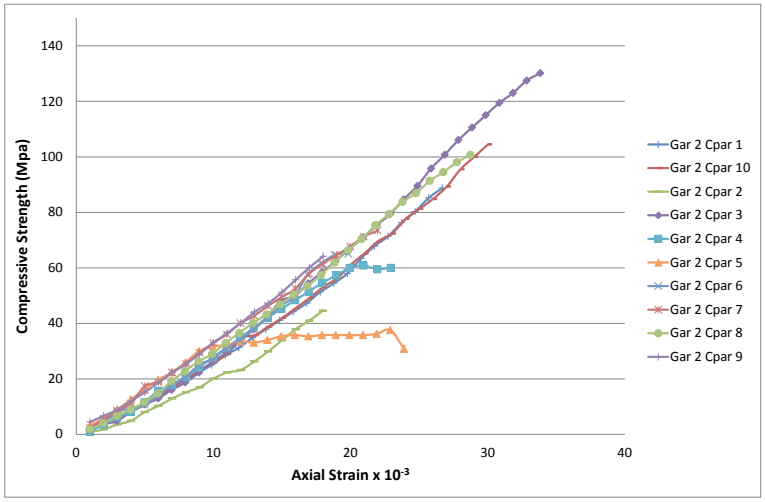

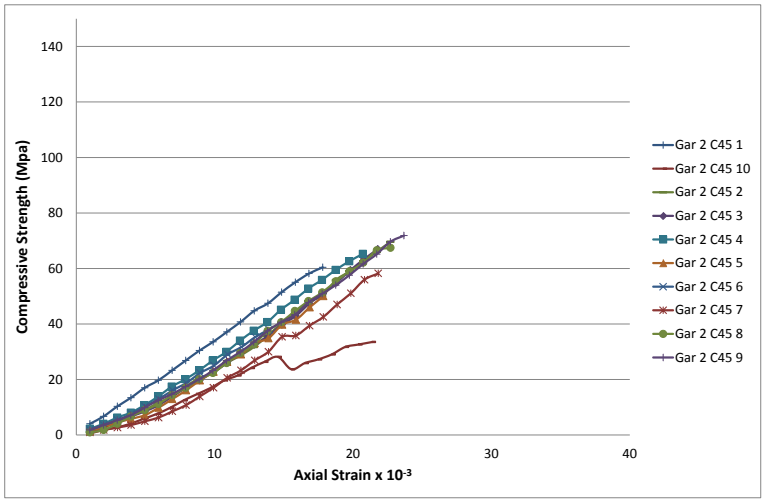

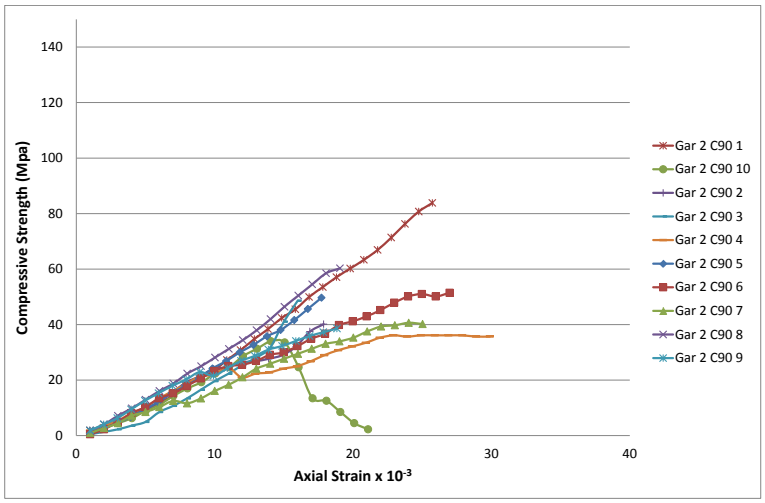

Figure 6.30 – The three graphs show the axial strain rates for cores from the same sample from Garachico, Tenerife, drilled at three different angles relative to flow direction. The first graph shows the results for C_{par} group which was the strongest, the second graph show results for the C_{45} and the third graph shows results for the C_{90} group.

Table 6.3 – Table shows the average max compressive stress, porosity and dry density of the samples from the Garachico 2 sample.

Field Trip	Group	Core Direction	Average Max Compressive Stress (Mpa)	Average of Porosity (n) %	Average of Dry Density (g/cm3)
Tenerife Aug 2011	Gar 2	45	58.12	9.31	2.32
Tenerife Aug 2011	Gar 2	90	48.19	9.20	2.32
Tenerife Aug 2011	Gar 2	Parallel	76.89	7.78	2.42

Table 6.3 shows that the samples drilled parallel to the flow direction had the highest max compressive strength, the lowest % porosity and the highest dry density which are all factors expected from the strongest sample. However, it can also be seen that the weakest samples, the ones drilled 90^o to the flow direction did not have the highest % porosity and had a density equal to that of the sample drilled 45^o to the flow direction. In order to understand the reason that the trend was reversed for this sample group, despite having similar characteristics to that of the other Garachico samples, the orientation of the vesicles relative the angle of applied stress was examined. The samples drilled 90^o to the flow direction were found to contain aligned vesicles. However, in contrast to other samples in the C_{90} group, these vesicles were not aligned in the direction of flow but rather approximately 45^o to the angle of applied stress and direction of flow. The vesicles in the Gar 2 45^o samples were found to be either steeply oblique to the angle of applied stress or without elongation or alignment. The vesicles in the samples drilled parallel to the flow direction were either aligned in the direction of flow or completely spherical, making alignment difficult to judge within the cored sample (Figure 6.31).

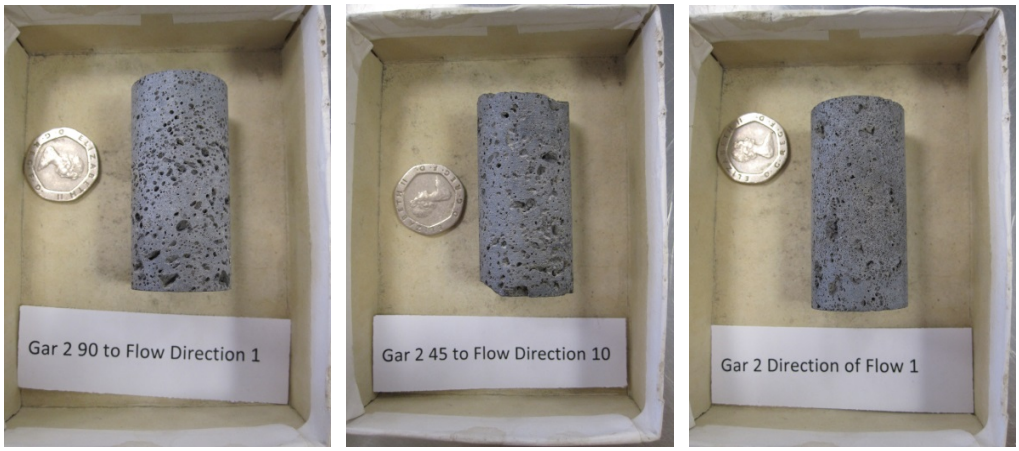

Figure 6.31 – Representative samples of cores from the same sample which were drilled at different orientations to the direction of flow. As can be seen from these cores, the angle of coring resulted in the vesicles being in different orientations relative to angle of applied stress in a uniaxial compression test.

From these results, it would appear that again, it is the angle of principal stress in relation to the orientation of aligned vesicles within a core, regardless of the cores orientation with respect to flow direction that has the greatest control on rock strength as shown previously in Section 4.5.2.

It was observed during the field investigation that although the vesicles in levees are predominantly orientated in the direction of flow it is possible to have areas within the levee where vesicle alignment is contra to the flow direction. Therefore for any core, regardless of orientation to the overall flow direction if the local vesicle alignment is oblique to the direction of applied stress the result will be lower compressive strength.

6.6 Summary

The angle of principal stress in relation to vesicle alignment is clearly a key controlling factor in the rock strength of vesiculated basalts. Strength analysis on cores taken at different orientations (parallel, 90^{o} and 45^{o}) to the flow directions

showed that the C_{par} cores had the highest maximum compressive strengths and that C_{45} cores had the lowest. However, investigations into deviations from the trend showed that it was the alignment of vesicles in relation to the direction of applied stress that exerted the greatest control on rock strength regardless of the orientation of the core, with vesicle alignment oblique (approximately 45^{o} to the orientation of applied stress) resulting in the lowest compressive strengths.

The size distribution of the vesicles rather than the overall percentage porosity was also shown to have a significant effect on rock strength with samples with a higher percentage of vesicles in the >1 mm range showing lower compressive strengths.

7 Results Interpretation

The aim of this study was to further the understanding of lava flow-field growth by using a multi-disciplinary approach involving fieldwork, rock mechanics and analogue modelling in order to support lava hazard management. In order to achieve the aims listed in Chapter 1, Section 1.2 a number of hypotheses were identified. These hypotheses could be arranged into two groups, the first group referred to the role of levee failure in flow-field development and how external factors such as topography and levee curvature influence levee failure. The second set of hypotheses were concern with the mechanisms of levee failure and the mechanical properties of the levee affecting strength.

This chapter will combine and interpret the results outlined in chapters three, five and six of the different methodologies, to modify the current classifications of flow emplacement into three stages, lengthening, widening and thickening and to validate the hypotheses of this study listed in Chapter 1, Section 1.2.1.

7.1 Stages of Flow Emplacement

The results of the field investigation and the analogue modelling experiments Chapter 2 Section 2.3.1 and Chapter 5, Section 5.6.1, have provided the basis for the classification of the growth of flow-fields emplaced on slopes. The first stage of emplacement of a flow-field is characterised by lengthening. In this stage, the flow typically consists of no more than one or two arterial flows which carry the majority of the effused material (Figure 7.1). The end of this stage occurs when cooling has resulted in the development of crust which is sufficiently thick to retard the forward movement of the flow.

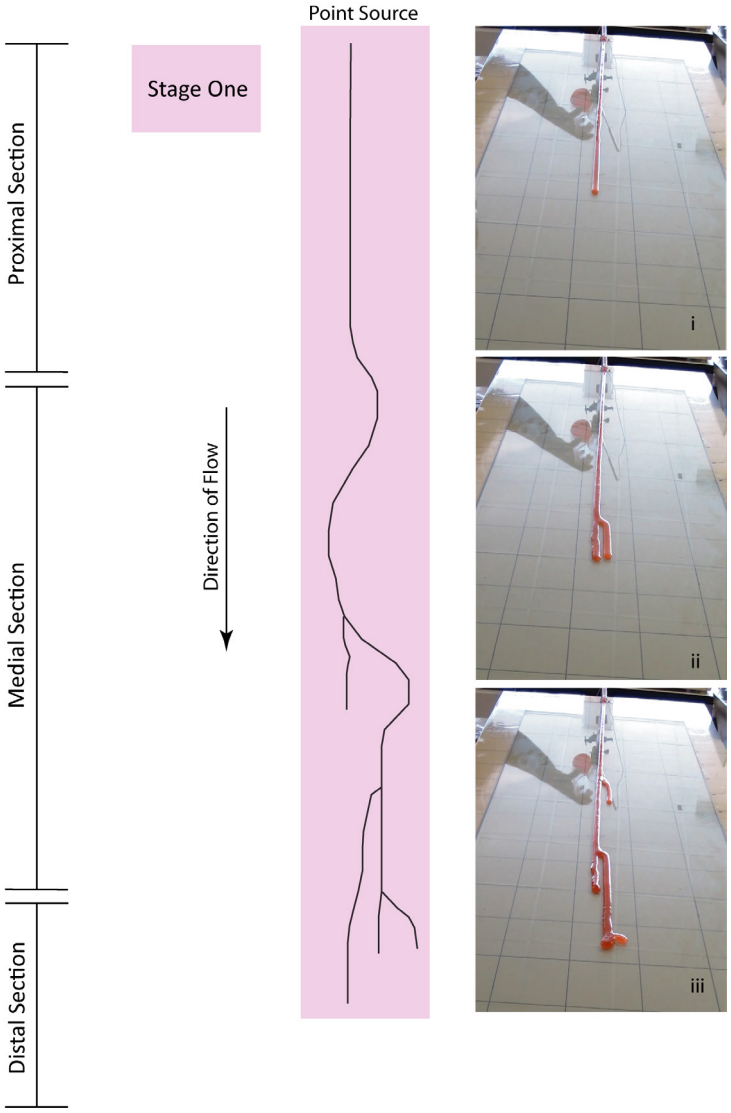

Figure 7.1 – Schematic shows a stylised representation of the first stage of flow-field development. The majority of flow-field length is achieved in this stage of emplacement. The inset pictures show an analogue modelling experiment carried out on 2^0 degrees of slope. The photographs are inserted chronologically, timeline runs from i to iii. In this stage, the 87% of overall flow-field length was reached. As can be seen from the pictures, the flow consists of only two arterial flows and 2 small secondary flows during this stage.

Stage two of emplacement is characterised by widening through the development of breakouts in the form of breaches or overflows and the growth of secondary flows. These processes have been linked to cooling which is therefore the dominant controlling parameter of this stage of emplacement, assuming uninterrupted supply from the vent (Figure 7.2).

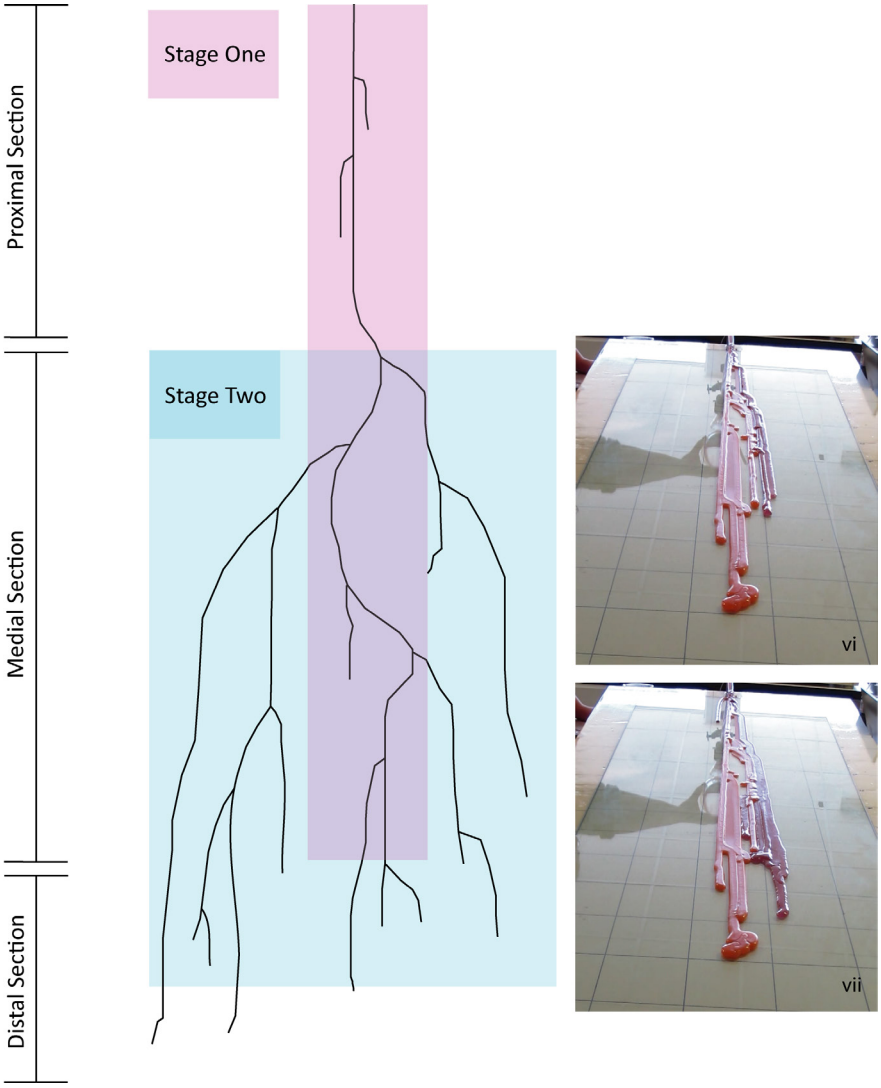

Figure 7.2 - Schematic shows a stylised representation of the second stage of flow-field development. In this stage, flow-field growth is dominated by widening through breakouts from the arterial flows through breaching or overflow and the formation of secondary flows. The inset photographs show the same experiment carried out on a 2^{o} slope as shown in figure 5.1. These photographs are also inserted chronologically from vi – vii and show that the flow-field widened through the formation of secondary flows.

The third stage of emplacement takes place when cooling has halted the advance of the entire flow-field and the only growth is in terms of inflation or thickening. Typically when a flow-field reached this stage, effusion rates have dropped and the overall flow-field length and width have been achieved. Any remaining fluid material is emplaced as squeeze-outs from the flow-front or inflation of existing lobes (Figure 7.3)

This last stage is not observed in every eruption, and it is missing particularly in those which are high effusion rate and small volume, where the entire supply of lava is emplaced before cooling has resulted in sufficiently thick crust to restrict all forward movement or breaching/ secondary flow generation. Flow-fields which did realize this stage were typically emplaced on low slope angles with low effusion rates.

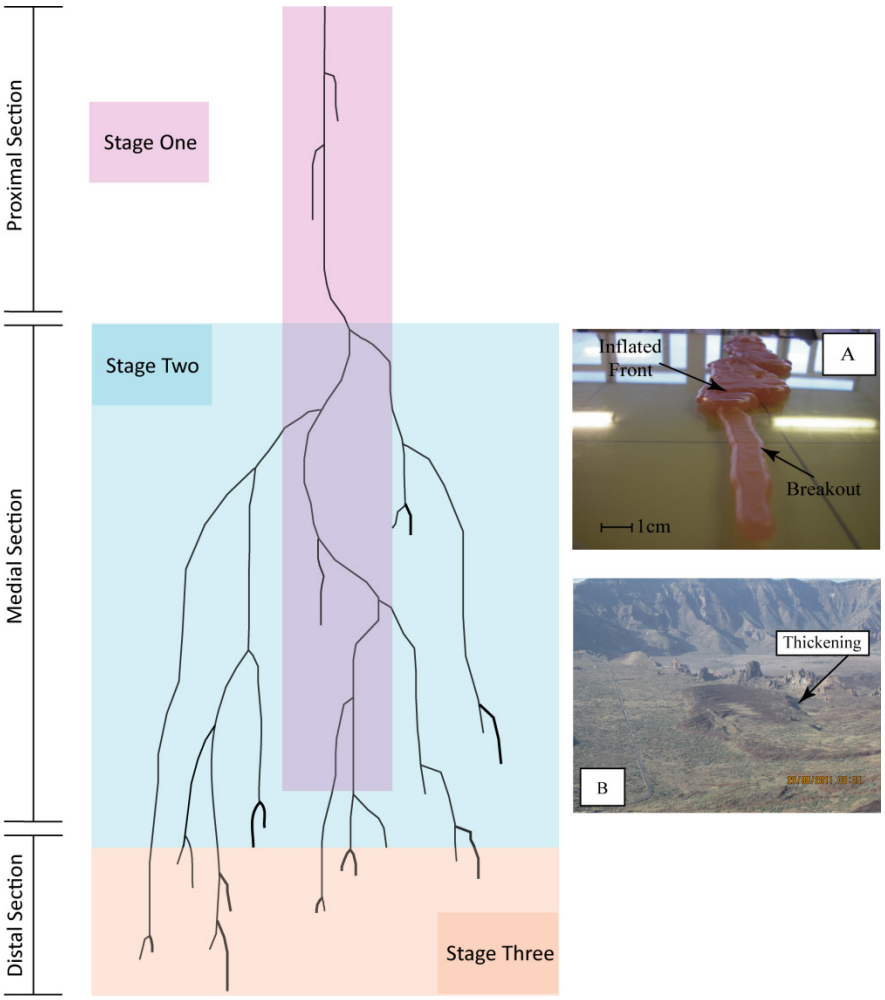

Figure 7.3 - Schematic representation of the third stage of flow emplacement which is dominated by thickening. Thickening of the active flows is shown by the thicker lines in the cartoon schematic. Inset picture A shows a flow-front from an experiment carried out at 2°. An inflated front can be seen in the middle background of the photograph and a small breakout from that front in the middle foreground. The difference in thickness of the front compared to the breakout shows the effects of thickening on flow height. Inset photograph B shows a thickened flow-front in the Teide caldera in Tenerife.

This classification of the stages of flow emplacement is a modification of classification of Kilburn & Lopes (1988) which described an evolutionary trend from lengthening to widening over time due to cooling. The authors also described the systematic development of secondary flows as a product of cooling. The stages outline above follow the same essential pattern where flow emplacement is first dominated by lengthening then widening and then thickening as the effects of cooling and therefore solidification and the development of crust become the dominate control on flow emplacement.

7.1.1 Development of Flow-field Morphology

The first set of hypotheses for this study were related to the role levee failure plays in flow-field development and the external factors affecting failure. The results of the analogue modelling and field study confirm our hypothesis that the formation and breaching of levees leading to the growth of secondary flows is vital to flow-field development. The formation of these secondary flows and their location and orientation, defines the final dimensions of a flow-field and therefore the area potentially requiring hazard management. The processes governing the formation of secondary flows are not fully understood and little research has been carried out which focuses on defining the factors controlling the location and timings of overflows and breaches.

The results of the analogue modelling (Chapter 5, Section 5.2.2 Volume Variation) supports Pinkerton & Wilson's (1994) refutation of Malin's (1980) hypothesis of volume as the key control in flow-field development. Experiments were carried out where all other parameters were equal but the volume was varied from 200 cm^3 to 300 cm^3. The results showed no significant difference in the flow

lengths achieved in the 200 cm^3 compared to the 300 cm^3 flows. However, what was observed in the results of the analogue model, was that volume does have an effect on overall flow-field width. Smaller volume eruptions produce fewer secondary flows which correspondingly produce narrower flow-fields. This was also identified in the field by Guest et al., (1987)

The results of the analogue modelling experiments on effusion rate (Chapter 5 Section 5.5.3) showed qualitatively that for all effusion rate groups; Low, Medium and High there was no significant difference in the lengths of the resultant flow-fields but that the time taken for flows to reach their maximum length decreased with increasing effusion rate. The results also showed that overall the number of secondary flows formed decreased with increasing effusion rate.

The analogue modelling results also suggested that slope angle may be a significant control on flow dimensions. Experimental results showed that at all angles of slope, the first stage of emplacement was dominated by lengthening but there were significant deviations in the average lengths of the flow-fields with changing underlying angle of slope as all other flow parameters were identical. The lengths of the initial flows were controlled by the time taken for cooling to result in the formation of a static flow-front which effectively halted advance. Increasing the angle of slope also increased the overall length of the flow-field and decreased the time taken for flows to reach their maximum length, showing that emplacement rates were also being affected by the angle of slope. Therefore increasing the angle of slope and correspondingly the rate of emplacement, somewhat negates the effects of cooling allowing the flow to reach greater distances before a static flow-front is formed.

Although on average increasing the slope resulted in longer flow-fields, the effusion rate variation experiments showed that the low effusion rate flows resulted, on average, in longer flow-fields than the medium or high effusion rate experiments.

Flows on shallower slopes with lower rates of emplacement more commonly formed tubes than flows with faster emplacement rates (Chapter 5, Section 5.6.2.3). A similar correlation can be found in the natural system with slower moving pahoehoe flows forming tubes more commonly than faster moving 'a'a flows. The development of tubes in the analogue modelling was thought to be a result of decreasing the energy supplied by the movement of the lava on the developing surface crust as the flows were moving more slowly, facilitating the development of a continuous crust which indicated the transition from a Newtonian to Bingham rheology.

The results of the analogue model, in conjunction with the emplacement behaviour inferred from extant flows or the field by other researchers, show that flows reach their maximum length during the first stage of emplacement and that effusion rate has a significant control on that length. It is extremely challenging to measure the effusion rate of a flow and studies (Walker et al., 1973; Frazzetta & Romano, 1984; Guest et al., 1987; Anderson et al., 1999; Griffiths, 2000) have shown that effusion rate can vary widely over the duration of emplacement. However, the rate of emplacement and angle of slope will have an effect on the flows ability to overcome the effects of cooling and the development of solidified crust which halts flow advance and signals the transition from stage one to stage two. From this, it can be inferred that although the majority of flow-length is achieved in the first stage of emplacement, flow-field length and time taken to transition from

one stage to the next is heavily influenced by parameters which either support or limit the effects of cooling – i.e. effusion rate.

Other studies (Walker, 1971; Walker et al., 1973; Wadge, 1978; Pieri & Baloga, 1986; Guest et al., 1987; Kilburn & Lopes, 1988; Kilburn, 1990, 1996; Kilburn & Guest, 1993; Pinkerton & Wilson, 1994; Baloga & Spudis, 1995; Calvari & Pinkerton, 1998; Calvari et al., 2003) also support effusion rate as the most important parameter in flow-field length. Guest et al., (1987) describe two very different eruptions – the 1981 and 1983 flows on Mount Etna and the effect of effusion rate on flow-field length. The authors use these eruptions to propose that high effusion rate events result in simple flow-fields containing just one or two arterial flows, which reach their maximum lengths quickly and are likely to be volume controlled, with the majority of total volume effusion emplaced in stage one. Lower effusion rates result in complex multi-channel flow-fields where the length of each flow is limited by the occurrence of breakouts up-channel, which form new arterial flows, starving the initial flow and limiting its length. Therefore it is reasonable to assume that in low effusion rate eruptions, in terms of overall flow-field growth, stage two is the dominant stage.

7.2 Breaching and Secondary Flow Formation

The second set of hypotheses for this study concerned the mechanical properties of levees and the mechanisms of levee failure. The results of the analogue model in this study can be used qualitatively to describe a general chronology for the occurrence of breakouts.

1. The first stage of emplacement is characterised by a simple flow-field with only one or two arterial flows.

2. Levees develop behind the flow-front in the main arterial flow as it moves forward
3. The first indication that the flow is transitioning into the second stage of emplacement is that the flow-front begins to slow down.
4. Inflation is observed in the flow behind the front
5. Overflows or breaches form along the flow margins
6. Secondary flows form from the breach or overflow, some of which result in only short lived flows, others form secondary arterial flows
7. The initial arterial flows may become completely stagnant if the material in the channel becomes diverted into the new flow
8. Cycle repeats in the secondary flows, forming compound flow-fields

The development of the analogue modelling flow-fields is documented chronologically in Figure 3.8 in Section 3.7.1.

Cooling and the formation of near stagnant flow-fronts is clearly a precursor to overflows and breaches and the subsequent formation of secondary flows which concentrates the majority of flow-field growth laterally in the second stage of emplacement. Although lengthening still takes place during this stage, widening dominates. The factors influencing the locations of breakouts and the mechanisms of failure of levees are still not well understood.

7.2.1 Locations of Breaching

Patterns in the locations of breaches were observed in both the field and the analogue model which would seem to indicate some locations are inherently weaker than others and that the location of breaches may be somewhat systematic. These

identified patterns suggest a number of locations where breaching is more likely to occur.

Field data shows that breaches occurred immediately after a change in slope (Chapter 3, Section 3.2.1) when the channel either became more narrow (increasing slope) or underwent widening or curvature (decreasing slope). In both the natural system and the analogue model, it was observed that where a channel experienced sinuosity, breaches were commonly seen from the outer bend of the curved channel (Figure 7.4 & 7.5).

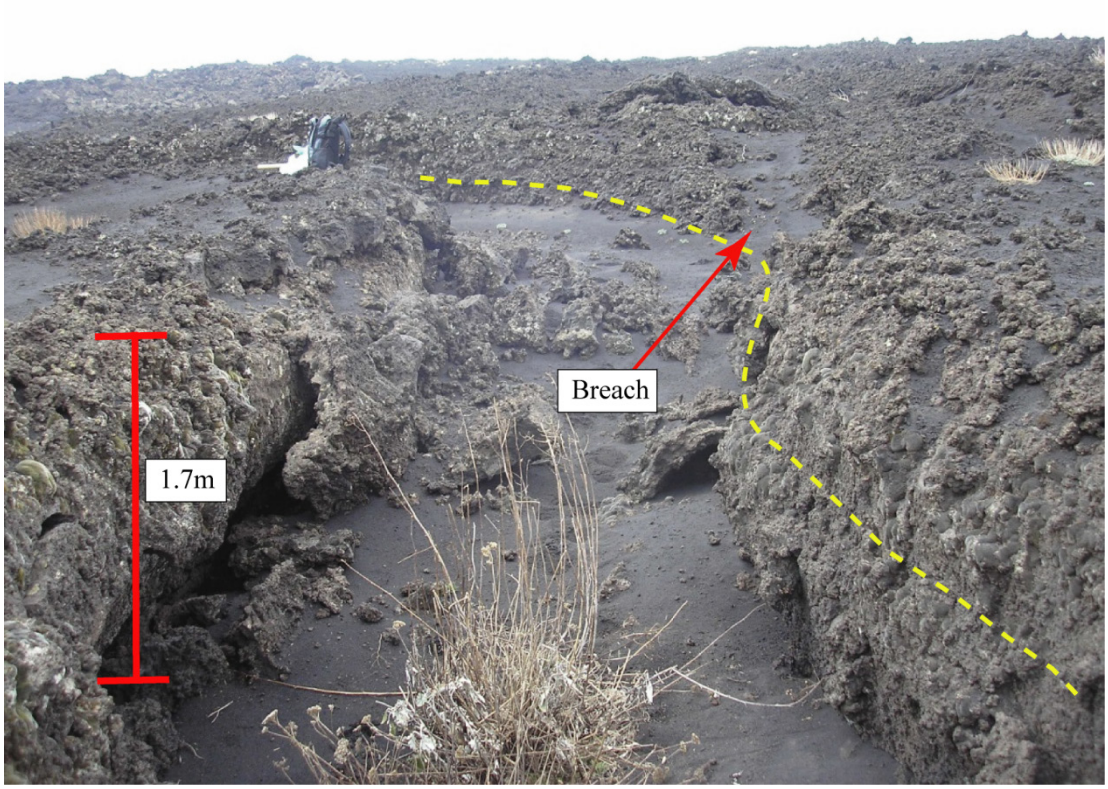

Figure 7.4 – Drained channel in the 1983 flow-field on Mount Etna. A breach and new channel can be seen in the upper middle ground of the photograph, marked with a red arrow. This breach formed in the outer curve of the channel.

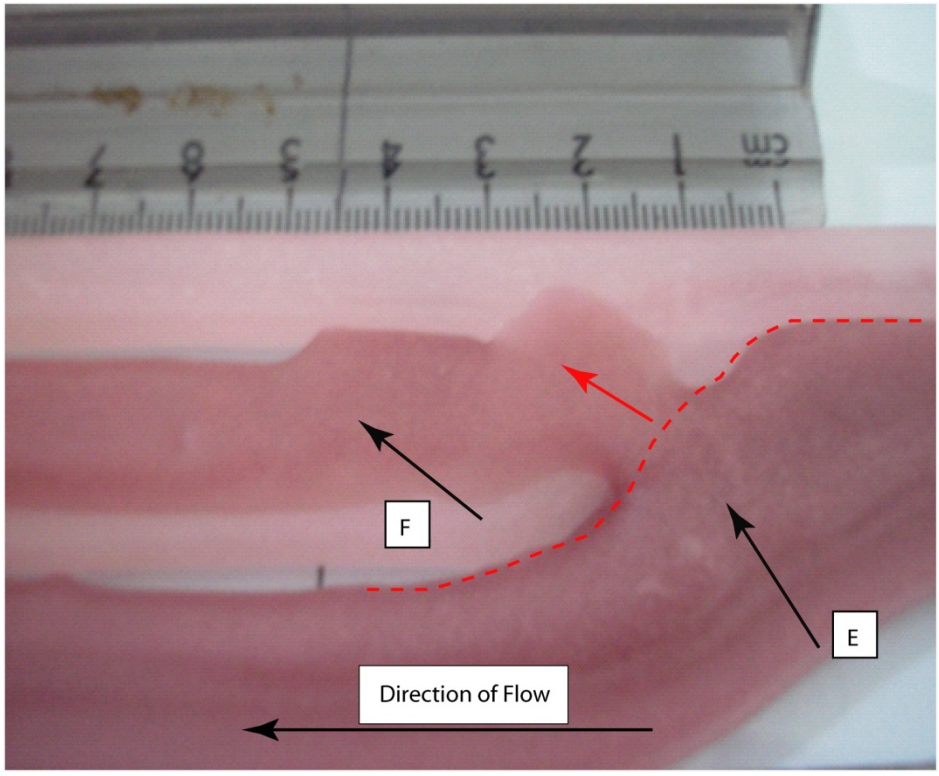

Figure 7.5 – Experiment 1.4: (Slope 2°). A new channel (F) formed from a breakout which occurred on the outer bend of a curve in channel E. This correlates with an observation made during the fieldwork portion of this study – that breaches are more common where flow channels experience curvature.

It was also observed during the 2002 eruption of Mount Etna that a barrier which was built to protect the Refugio Sapienza caused the flow to curve and that an overflow originated on the outer bend of the lava flow (Sonia Calvari pers. comm.). Therefore curvature and the occurrence of breaches is not only a consideration for hazard assessment and prediction of the location of breaches but also for civil protection when planning lava flow diversions.

The formation of secondary flows through breaching and overflow has been documented by many studies describing flow-field development (Walker et al., 1973; Pinkerton & Sparks, 1976; Sparks et al., 1976; Guest et al., 1987; Kilburn & Lopes, 1988, 1991; Borgia & Linneman, 1990; Kilburn & Guest, 1993; Kerr et al., 2006; Riker et al., 2009; Applegarth et al., 2010; Robertson & Kerr, 2010; James et

al., 2011; Robertson & Kerr, 2012). However, these studies have mostly focused on describing specific flows and mechanical precursors to breaching rather than identifying possible locations of breaches. Guest et al., (1987) did observe two precursors to breaching that indicated possible locations. The first was that secondary arterial flows in the 1983 flow-field formed at changes in slope in the medial and distal sections of the flow-field and secondly that prior to breaching, large occlusions were observed in the channel. For both of these precursors, the conditions described resulted in inflation in the channel either through reducing the gradient and therefore the velocity of the flow-front or inflation behind a blockage in the channel.

A secondary result from the analogue modelling experiments was the observation that breaching moved up-channel towards the point source of effusion over time. This was thought to be due to cooling. This correlates with a similar observation made by Guest et al., (1987) during the 1983 eruption of Mount Etna.

7.2.2 Mechanical Aspects of Breaching

The results of the uniaxial compression tests and field studies have identified four mechanisms for breaching (Chapter 3, Figure 3.17) in addition to patterns in the mechanical properties of levees which may increase the probability of a breach occurring. The results of the uniaxial compression tests showed that the strength of the levee samples changed with direction according to the size, distribution and orientation of vesicles and that samples were more susceptible to failure when the angle of applied stress was oblique to the orientation of the vesicles (Chapter 6, Section 6.5.1).

There is very little in the literature linking the strength of a rock sample to the orientation of applied stress in relation to vesicle alignment and therefore the results of this study represent a new, unique perspective. It had been initially thought that the morphology of the levee and its generation would affect its overall strength. However, the results of the uniaxial compression tests showed that while there were variances in rock strength from sample to sample, it was the angle of applied stress in relation to textures such as vesicle alignment which seemed to have the greatest control on rock strength.

Regardless of overall compressive strength of a sample and the morphology of the levee it originated from, the cores taken parallel to the flow direction (C_{par}) consistently had the highest compressive strengths and the C_{45} group (cores taken oblique to the flow direction) consistently had the lowest. Analysis of the mode of failure of the shattered cores showed that for the C_{45} samples, the line of fracture runs from vesicle to vesicle and that the vesicles themselves were sheared. In the C_{par} and C_{90} shattered cores, vesicles appeared to be compressed and the fractures were independent of the vesicles (Chapter 6, Section 6.5.1). The axial strain lines showed that the majority of samples within the C_{45} group underwent brittle failure represented by a smooth axial strain line and sharp drop off and the C_{90} and C_{par} groups which underwent ductile deformation prior to sample failure as represented by staggered axial strain lines, indicative of compression prior to failure.

As previously discussed, the field study and analogue modelling results showed that breakouts were commonly observed from the outer bends of curved channels. As a flow moves though a curved channel, the material in the channel is pushing against the outer curve, in much the same way as stress and friction is concentrated on the outer bends of a meander in a river system as evidenced by

erosion. This represents a change in the angle of applied stress between the flow and the levee than in those parts of the flow which are relatively straight. Given the results of the uniaxial compression tests which indicate that when the angle of applied stress is oblique to the textures within the core (such as vesicle alignment), the core is weaker, this could at least partially explain the propensity to failure of levees on the outer curves of sinuous channels.

Therefore, it may not be the morphology of the levee that indicates its propensity to failure but the angle of applied stress in relation to the orientation of the vesicles that should be the basis for classification. The combination of the patterns in the locations breached identified from the analogue modelling and field studies and the results of the uniaxial test results, give a new insight on the controls on the mechanical aspects of breaching.

Kilburn & Lopes (1988) state that breaching is restricted by the development of crust and that in order for a breach to occur, the stress driving the lava forward must exceed the crustal retaining strength. Given that inflation was a precursor to almost all breaches observed during the analogue modelling, it would seem that increasing the thickness of the material in the channel increases the stress acting on the levees sufficiently to overcome their retaining strength.

These different precursors to failure also mean different failure mechanisms for the levees. As discussed in (Chapter 3, Section 3.2.4) for flows undergoing inflation, Push Translational, Swing or Toppling - where the levee is being pushed outwards by the increased volume of material in the channel and topples either forwards or backwards - are the likely mechanisms for failure (Figure 3.17, Mechanism A, D, C1 & C2).

For breakouts from a curved flow, the mechanism for failure is more likely to be a Trapdoor effect where a fracture forms in the levee that widens as material flows against the gap, gradually pushing a section of the levee outwards at an angle to the channel (Figure 3.17 Mechanism B) as seen in the Chinyero flow-field on Tenerife.

The results of the analogue modelling and field work carried out in this study correlate well with the existing observations in the literature that cooling, the development of stagnant flow-fronts and subsequent inflation in the channel are precursors to breakouts and the formation of secondary flows. These processes mostly take place in the medial or distal section of the flow-field during stage two of emplacement and concentrate the growth of the flow-field laterally.

7.2.3 Vesicularity

The results of the rock mechanics tests combined with the porosity and density tests show that the samples containing larger vesicles (>1 mm) which were elongate in the direction of flow were weaker than those samples which had a higher % vesiculation but overall smaller vesicles (approx. <1 mm) Chapter 6, Section 6.4.4.

Both suites of samples from Tenerife and Etna underwent density and porosity tests in addition to cataloguing of the vesicle size and distribution. The Tenerife samples overall had higher porosity, lower density and higher compressive strengths than the Etnean samples. However, in both sample sets, taking the maximum values for all samples only, the cores drilled parallel to the flow direction (C_{par}) had the highest maximum compressive strengths independent of density and porosity. Given that the 210 samples display a range of values for porosity, density

and vesicle size and orientation, if the strength of the cores was strongly dependent only on porosity and density, the results would show that the core with the lowest porosity and highest density would have the highest compressive strength regardless of the orientation of applied stress, which they do not.

The size and distribution of vesicles in the samples was catalogued and it became apparent that the Etna samples had a much higher % of vesicles in the >1 mm range (41%). When the mode of fracture of the shattered cores was assessed, it was observed that the fractures in the Etnean cores ran from vesicle to vesicle with the result that the angle of failure was highly variable. The samples which predominately had vesicles <1 mm had either the steep angles of failure with clear macro-fractures typical of brittle failure or multiple high angle fracture with compressed vesicles. These cores also had some of the highest max compressive strengths.

The effect of vesicle size and alignment on mode of failure was not equal for all sample groups. The axial strain plots for the three sample groups showed that the C_{90} and C_{par} groups had the most samples that failed with a staggered axial strain line showing that the sample was deforming in stages before failure even if said samples contained a significant % of vesicle >1 mm. In contrast the C_{45} almost always underwent brittle fracture regardless of location of collection or porosity. For this it can be inferred that the angle of applied stress in relation to flow textures such as vesicle alignment influences the strength and mode of failure of the sample.

7.2.4 Angle of Secondary Flows to Flow-Fields

The growth of secondary flows is intrinsically linked to overall flow-field dimensions and in particular the width of the flow-field. However, field studies and

the results of the analogue model have indicated that there are two factors influencing the final width of a flow-field: the final width of the new flow, but also the angle at which it forms to the initial channel.

Although the orientation and widths of secondary flows are often reported in the literature describing the development of a flow-field, almost none of these studies have described the angle the secondary flow forms in relation to the initial channel and none have attempted to identify any patterns in these angles.

The results of the analogue modelling experiments showed that secondary flows consistently formed at angles of between 10 and 40^{o} to the levee they originated from with 70% falling into the 25^{o} – 35^{o} bracket. The angle at which the secondary flows formed decreased with increasing angle of underlying slope, but given that the analogue modelling experiments were carried out on a completely smooth surface and that the angle of formation was consistent for a given angle of slope, this points to some systematic process governing the angle of emplacement (Chapter 5, Section 5.5.1.3).

Field data collected during this study both from in situ measurement and measurements taken from Google Earth images (Chapter 3, Section 3.2.2) also shows that secondary flows, be they short lived breakouts from the flow margin or the generation of secondary arterial flows through breaching, form at an angle of between 30 and 50^{o} to their parent channel. This angle of formation substantially adds to the overall width of a flow-field. It is difficult to account for the effect local topography had on the angle of formation but there is at least some degree of correlation to the analogue model.

The reason for this angle of formation is unknown but some qualitative observations of the analogue model show that breaching or overflow is often as a

result of inflation in the channel, meaning that there is a build-up of pressure behind the levee. Once the levee is breached or overtopped then that accumulated pressure is released, causing the material in the channel to shoot out of the breach in the same orientation as the breach has been created for a short time until the effect of gravity forces it to flow down the steepest slope angle. Should the levee breach in the trapdoor motion (previously described in Section 3.2.4, Figure 3.17) then is likely that the angle of the trapdoor would cause the material leaving the channel to flow at an angle in respect to the remobilised section of levee.

For the secondary flow originating from the outer curve of a sinuous channel, the original channel is curving away from the outer bend, immediately resulting in a difference in orientation between the secondary flow and its progenitor.

Regardless of the factors controlling the emplacement orientation of the secondary flows, the angles at which these flows make to the originating channel contribute significantly to overall flow-field width and must be taken into account when defining the areas of possible inundation by lava during hazard planning.

7.3 Summary of Timings and Locations of Break-Outs

This study, in conjunction with existing observations in the literature, has identified some broad trends in flow-field propagation in terms of timing and location. Given the current impossibility to predict exactly when or where a breakout will occur, in order to support hazard management, a generalised guideline to precursors and trends in secondary flow formation has been developed.

As discussed, the first stage of emplacement is likely to occur rapidly leaving very little time to implement counter measures to inundation by lava (Solana & Aparicio, 1999). Therefore, it will be very difficult to influence the orientation or

length of the initial flow-field. The second stage of emplacement and associated flow-field widening will occur more slowly allowing time to pin point possible locations for breaches to occur. The formation of secondary flows will most likely occur in the medial section of the flow-field at an angle of between 30-50^{o} to the original channel. The likelihood of a breakout and secondary flow forming is increased after one or more of the following conditions are met:

1. The flow-front has slowed down and become stagnant and effusion continues at the source
2. Inflation in the flow behind the front is observed
3. Blockages have formed in an arterial flow
4. Inflation has occurred behind the blockage
5. One or more of the active arterial flows have become sinuous.
6. Major changes in slope
7. Deformation is observed on the levee

The location of the breach is dependent on the morphology of the initial channel and the locations of areas of inflation in that channel. Should the inflation occur behind a blockage, the breakout will occur above the blockage. Where flows experience sinuosity, the breakout will most likely occur on the outer margin of that flow. If the flow is relatively straight and inflation is occurring behind a stagnant flow-front, then a breach may form at a break in slope or where a levee is adjacent to a gross change in topography making it unstable.

Other factors that affected levee strength such as the orientation and size of vesicles in relation to the stress imposed on a levee by the lava flowing in the channel would be almost impossible to measure in the field during an active eruption. However, vesicle size distribution can be measured in laboratory on

collected samples, and this information, added to direct observations of the lava flow, might suggest the presence of magma still rich in gas, and thus more prone to levee failure.

7.4 Consequences and Implications

The implications of this study are that hazard remediation agencies should focus their attention, in addition to the advance of the flow-front, on managing the width of flow-field as there is likely to be sufficient time to react and implement hazard management measures. The trends identified in this study could help pin point areas of potential weakness which could then be reinforced with barriers preventing breaches or at least angled barriers to try and control the orientation of the secondary flows, as done during the 2002 Etna flows near the Refugio Sapienza.

In cases where an existing flow is following an undesirable orientation, these same areas of weakness could be used to identify locations where blasting to create an artificial breach is more likely to be successful.

8 Conclusions

The aim of this research was to use a multidisciplinary methodology to investigate the significance of levee breaching in 'a'a flow-field development and to identify the conditions and locations under which levee failure is likely to occur.

An analogue model was developed capable of investigating the development of extended flows and the formation of channels and flow-fields by breaching or overflow of levees by the systematic alteration of emplacement parameters slope, effusion rate and volume. Field sites were chosen on Mount Etna and Tenerife to investigate the locations and mechanisms for levee failure. Uniaxial compression tests, density and porosity measurement and analyses of vesicle size and distribution were carried out on 210 samples taken from levees in the 'a'a flow-fields of Mount Etna and Tenerife to create a database on the mechanical properties of levees.

The following summarises the main findings of this study:

- From the study of extant 'a'a flow-fields on Mount Etna and Tenerife, four mechanisms for levee breaching have been identified: push translational, swing, trapdoor and toppling. The mechanism name refers to the direction of movement of the remobilised section of levee. This represents a new classification system for the mode of levee failure.
- Field investigation and the results of the analogue modelling show that where a flow becomes curved either due to a decrease in slope or around a topographic high, breaches commonly form in the levee constraining the outer curve of the flow.

- Breaching in the flow-fields generated by the analogue model was observed to migrate up-channel towards the source of the flow over time. Where the breach resulted in a new secondary flow, material was diverted out of the main arterial channel and into the new flow. Consequently, secondary flows down channel became partially or completely starved of supply of wax, halting their advance. A similar process was observed by Guest et al., (1987) during the 1983 eruption of Mount Etna.
- Analysis of the field and analogue modelling data showed that secondary flows consistently formed at an angle tangential to the original flow. This was observed to be between 30 – 50^{o} in the field and 10-40^{o} in the analogue model, significantly contributing to the overall width of the flow-field.
- Investigation into the mechanical properties of levees through the uniaxial compression tests, porosity and density measurements and the vesicle analysis showed that the strength of the levee changes with direction according to the orientation, size and distribution of the vesicles. Samples in which vesicle alignment was oblique to the direction of principal stress (C_{45} samples) were consistently the weakest and failed in a brittle manner with fractures running from vesicle to vesicle with the vesicles themselves appearing sheared. In contrast, samples where vesicle alignment was parallel or perpendicular to the direction of principal stress (C_{par} and C_{90}) failed in a more ductile manner with the vesicles appearing compressed in the failed core.
- The shape and size distribution of vesicles was shown to have a greater control on rock strength than the overall percentage of vesiculation with

samples containing a higher percentage of vesicles in the >1 mm range being significantly weaker.

- The results of the analogue modelling and the field investigation were used to define the three stages of flow-field development: Lengthening, widening and thickening with each stage being defined by its growth mechanisms. This represents a modification of the classification of flow-field growth by Kilburn and Lopes (1988) who described an evolutionary trend from lengthening to widening over time due to cooling and the development of crust.
- The results of all three methodologies were combined to identify precursors and trends in levee breaching. From these a set of guidelines to the likely locations and conditions necessary for breaching and secondary flow formation have been created. The guidelines identify flow behaviours, topographic constrains and levee morphologies where breaching is most likely to occur, which could be used to support lava hazard management activities.

8.1 Future Work

This study highlighted a number of different trends in flow-field development which could prove interesting and fruitful ground for more in-depth study. Although four mechanisms for levee failure have been identified, further investigation into the particular conditions leading to each type of breaching is required to accurately forecast the mode of failure as this could have implications in the field of lava hazard management, making the technique of reinforcing levees to prevent breaching more effective.

Further work is needed to properly quantify the effect of vesicles on levee strength. There has been very little previous work in this area. The rock mechanics tests highlighted a number of interesting trends in relation to the variability of levee strength with direction in relation to the size and orientation of vesicles which could significantly contribute to our understanding of levee failure.

The angle at which secondary flow formed in relation to the original channel also warrants further investigation including a systematic measurement of formation angles in a number of different flow-field which had different emplacement mechanisms to investigate the parameters controlling the angle of formation.

References

Adelinet, M., Fortin, J., Schubnel, A., & Guéguen, Y. (2013). Deformation modes in an Icelandic basalt: From brittle failure to localized deformation bands. *Journal of Volcanology and Geothermal Research, 255*, 15-25.

Allard, P., Behncke, B., D'Amico, S., Neri, M., & Gambino, S. (2006). Mount Etna 1993–2005: Anatomy of an evolving eruptive cycle. *Earth-Science Reviews, 78*(1-2), 85-114.

Allen, J. (1966). Note on the use of plaster of paris in flow visualization, and some geological applications. *Journal of Fluid Dynamics, 25,* 331-335.

Anderson, S. W., Stofan, E. R., Smrekar, S. E., Guest, J. E., & Wood, B. (1999). Pulsed inflation of pahoehoe lava flows: implications for flood basalt emplacement. *Earth and Planetary Science Letters, 168* (1–2), 7-18.

Applegarth, L. J., Pinkerton, H., James, M. R., & Calvari, S. (2010). Lava flow superposition: The reactivation of flow units in compound 'a'ā flows. *Journal of Volcanology and Geothermal Research, 194*(4), 100-106.

Apuani, T., Corazzato, C., Cancelli, A., & Tibaldi, A. (2005). Physical and mechanical properties of rock masses at Stromboli: a dataset for volcano instability evaluation. *Bulletin of Engineering Geology and the Environment, 64*(4), 419-431.

Avolio, M., Lupiano, V., Mazzanti, P., & Gregorio, S. (2008). Modelling Combined Subaerial-Subaqueous Flow-Like Landslides by Cellular Automata. In H. Umeo, S. Morishita, K. Nishinari, T. Komatsuzaki & S. Bandini (Eds.), *Cellular Automata* (Vol. 5191, pp. 329-336): Springer Berlin Heidelberg.

Avolio, M. V., Crisci, G. M., Di Gregorio, S., Rongo, R., Spataro, W., & Trunfio, G. A. (2006). SCIARA γ2: An improved cellular automata model for lava flows and applications to the 2002 Etnean crisis. *Computers & Geosciences, 32*(7), 876-889.

Bagdassarov, N., & Pinkerton, H. (2004). Transient phenomena in vesicular lava flows based on laboratory experiments with analogue materials. *Journal of Volcanology and Geothermal Research, 132*(2-3), 115-136.

Bailey, J., Harris, A., Dehn, J., Calvari, S., & Rowland, S. (2006). The changing morphology of an open lava channel on Mt. Etna. *Bulletin of Volcanology, 68*(6), 497-515.

Baloga, S., & Spudis, P. D. (1995). The dynamics of rapidly eraplaced terrestrial lava flows and implications for planetary volcanism. *Journal of geophysical research, 100*(B12), 24,509-524,519.

Barberi, F., Brondi, F., Carapezza, M. L., Cavarra, L., & Murgia, C. (2003). Earthen barriers to control lava flows in the 2001 eruption of Mt. Etna. *Journal of Volcanology and Geothermal Research, 123*(1-2), 231-243.

Barberi, F., Carapezza, M. L., Valenza, M., & Villari, L. (1993). The control of lava flow during the 1991–1992 eruption of Mt. Etna. *Journal of Volcanology and Geothermal Research, 56*(1-2), 1-34.

Barca, D., Crisci, G. M., Di Gregorio, S., & Nicoletta, F. P. (1993). *Active lavas : monitoring and modelling*. London: U. C. L. Press.

Barca, D., Crisci, G. M., Gregorio, S. D., & Nicoletta, F. (1994). Cellular automata for simulating lava flows: A method and examples of the Etnean eruptions. *Transport Theory and Statistical Physics, 23*(1-3), 195-232.

Behncke, B., & Neri, M. (2003). The July–August 2001 eruption of Mt. Etna (Sicily). *Bulletin of Volcanology, 65*(7), 461-476.

Benson, P. M., Thompson, B. D., Meredith, P. G., Vinciguerra, S., & Young, R. P. (2007). Imaging slow failure in triaxially deformed Etna basalt using 3D acoustic-emission location and X-ray computed tomography. *Geophysical Research Letters, 34*(3).

Blake, S., & Bruno, B. C. (2000). Modelling the emplacement of compound lava flows. *Earth and Planetary Science Letters, 184*(1), 181-197.

Booth, B., & Self, S. (1973). Rheological features of the 1971 Mount Etna lavas. *Philosophical Transactions of the Royal Society of London. Series A, Mathematical and Physical Sciences, 274*(1238), 99-106.

Booth, B., Sparks, R., & Walker, G. (1975). Notes on the eruption of Etna in April 1975. *United Kingdom Research on Mount Etna. The Royal Society, London*, 69-71.

Borgia, A., & Linneman, S. (1990). On the mechanisms of lava flow emplacement and volcano growth: Arenal, Costa Rica.

Burkhard, D. J. (2003). Thermal interaction between lava lobes. *Bulletin of Volcanology, 65*(2-3), 136-143.

Calvari, S., Neri, M., & Pinkerton, H. (2003). Effusion rate estimations during the 1999 summit eruption on Mount Etna, and growth of two distinct lava flow fields. *Journal of Volcanology and Geothermal Research, 119*(1-4), 107-123.

Calvari, S., & Pinkerton, H. (1998). Formation of lava tubes and extensive flow field during the 1991 & 1993 eruption of Mount Etna. *J. Geophys. Res., 103*(B11), 27291-27301.

Calvari, S., & Pinkerton, H. (1999). Lava tube morphology on Etna and evidence for lava flow emplacement mechanisms. *Journal of Volcanology and Geothermal Research, 90*(3-4), 263-280.

Calvari, S., & Pinkerton, H. (2002). Instabilities in the summit region of Mount Etna during the 1999 eruption. *Bulletin of Volcanology, 63*(8), 526-535.

Castruccio, A., Rust A. C., (2010). Rheology and flow of crystal bearing lavas: Insights from analogue gravity currents. *Earth and Planetary Science Letters 297*, 471-480.

Clague, D. A., Moore, J. G., & Reynolds, J. R. (2000). Formation of submarine flat-topped volcanic cones in Hawai'i. *Bulletin of Volcanology, 62*(3), 214-233.

Cloos, E. (1955). Experimental Analysis of Fracture Patterns. *Bulletin of the Geological Society of America, 66*, 241.

Coltelli, M., Marsella, M., Proietti, C., Scifoni, S. (2012). The case of the 1981 eruption of Mount Etna, an example of very fast moving lava flows. *Geochemistry Geophysics Geosystems, 13,* 1, Q01004.

Crisci, G. M., Di Gregorio, S., Rongo, R., Scarpelli, M., Spataro, W., & Calvari, S. (2003). Revisiting the 1669 Etnean eruptive crisis using a cellular automata model and implications for volcanic hazard in the Catania area. *Journal of Volcanology and Geothermal Research, 123*(1-2), 211-230.

Crisci, G. M., Rongo, R., Di Gregorio, S., & Spataro, W. (2004). The simulation model SCIARA: the 1991 and 2001 lava flows at Mount Etna. *Journal of Volcanology and Geothermal Research, 132*(2-3), 253-267.

Damiani, M. L., Groppelli, G., Norini, G., Bertino, E., Gigliuto, A., & Nucita, A. (2006). A lava flow simulation model for the development of volcanic

hazard maps for Mount Etna (Italy). *Computers & Geosciences, 32*(4), 512-526.

Del Negro, C., Cappello, A., Neri, M., Bilotta, G., Herault, A., Ganci, G., (2013). Lava flow hazards at Mount Etna: constraints imposed by eruptive history and numerical simulations. *Scientific Reports, 3,* 1-8.

Digby, P. J., & Murrell, S. A. F. (1976). The deformation of flat ellipsoidal cavities under large confining pressures. *Bulletin of the Seismological Society of America, 66*(2), 425-431.

Dragoni, M., Bonafede, M., & Boschi, E. (1986). Downslope flow models of a Bingham liquid: Implications for lava flows. *Journal of Volcanology and Geothermal Research, 30*(3–4), 305-325.

Dragoni, M., D'Onza, F., & Tallarico, A. (2002). Temperature distribution inside and around a lava tube. *Journal of Volcanology and Geothermal Research, 115*(1–2), 43-51.

Dragoni, M., & Tallarico, A. (1996). A model for the opening of ephemeral vents in a stationary lava flow. *Journal of Volcanology and Geothermal Research, 74*(1–2), 39-47.

Dutton, C. E. (1884). Hawaiian Volcanoes. *U.S. Geological Survey Annual Report 1882-1883*, 75-219.

Favalli, M., Harris, A., Fornaciai, A., Pareschi, M., & Mazzarini, F. (2010). The distal segment of Etna's 2001 basaltic lava flow. *Bulletin of Volcanology, 72*(1), 119-127.

Favalli, M., Fornaciai, A., Mazzarini, F., Harris, A.J.L., Neri, M., Behncke, B., Pareschi, M.T., Tarquini, S., Boschi, E. (2010). Evolution of an active lava flow field using a multi-temporal LIDAR acquisition. *Journal of Geophysical Research, 115*, B11203.

Felpeto, A., Araña, V., Ortiz, R., Astiz, M., & García, A. (2001). Assessment and Modelling of Lava Flow Hazard on Lanzarote (Canary Islands). *Natural Hazards, 23*(2-3), 247-257.

Fink, J., & Zimbelman, J. (1986). Rheology of the 1983 Royal Gardens basalt flows, Kilauea Volcano, Hawaii. *Bulletin of Volcanology, 48*(2-3), 87-96.

Fink, J. H., & Griffiths, R. W. (1990). Radial spreading of viscous-gravity currents with solidifying crust. *Journal of Fluid Mechanics, 221*, 485-509.

Fink, J. H., & Griffiths, R. W. (1992). A laboratory analog study of the surface morphology of lava flows extruded from point and line sources. *Journal of Volcanology and Geothermal Research, 54*(1), 19-32.

Fink, J. H., & Griffiths, R. W. (1998). Morphology, eruption rates, and rheology of lava domes: Insights from laboratory models. *Journal of Geophysical Research: Solid Earth, 103*(B1), 527-545.

Fortin, J., Stanchits, S., Vinciguerra, S., & Guéguen, Y. (2011). Influence of thermal and mechanical cracks on permeability and elastic wave velocities in a basalt from Mt. Etna volcano subjected to elevated pressure. *Tectonophysics, 503*(1), 60-74.

Frazzetta, G., & Romano, R. (1984). The 1983 Etna eruption: event chronology and morphological evolution of the lava flow. *Bulletin Volcanologique, 47*(4), 1079-1096.

Ganci, G., Vicari, A., Cappello, A., Del Negro, C. (2012), An emergent strategy for volcano hazard assessment: From thermal satellite monitoring to lava flow modeling, *Remote Sensing of Environment, 119,* 197-207.

Garry, W. B., Gregg, T. K. P., Soule, S. A., & Fornari, D. J. (2006). Formation of submarine lava channel textures: Insights from laboratory simulations. *Journal of Geophysical Research: Solid Earth, 111*(B3), B03104.

Gregg, T. K. P., & Fink, J. H. (1995). Quantification of submarine lava flow morphology through analog experiments. *Geology, 23*, 73-76.

Gregg, T. K. P., & Fink, J. H. (2000). A laboratory investigation into the effects of slope on lava flow morphology. *Journal of Volcanology and Geothermal Research, 96*(3-4), 145-159.

Gregg, T. P., & Keszthelyi, L. (2004). The emplacement of pahoehoe toes: field observations and comparison to laboratory simulations. *Bulletin of Volcanology, 66*(5), 381-391.

Griffiths, R. W. (2000). The dynamics of lava flows. *Annual review of fluid mechanics, 32*, 477-518.

Griffiths, R. W., & Fink, J. H. (1992a). Solidification and morphology of submarine lavas: A dependence on extrusion rate. *Journal of Geophysical Research: Solid Earth, 97*(B13), 19729-19737.

Griffiths, R. W., & Fink, J. H. (1992b). The morphology of lava flows in planetary environments: Predictions from analog experiments. *Journal of Geophysical Research: Solid Earth, 97*(B13), 19739-19748.

Griffiths, R. W., & Fink, J. H. (1993). Effects of surface cooling on the spreading of lava flows and domes. *Journal of Fluid Mechanics, 252*, 667-702.

Guest, J. E., Kilburn, C. R. J., Pinkerton, H., & Duncan, A. M. (1987). The evolution of lava flow-fields: observations of the 1981 and 1983 eruptions of Mount Etna, Sicily. *Bulletin of Volcanology, 49*(3), 527-540.

Gómez-Fernández, F. (2000). Application of a GIS algorithm to delimit the areas protected against basic lava flow invasion on Tenerife Island. *Journal of Volcanology and Geothermal Research, 103*(1–4), 409-423.

Hallworth, M., Huppert, H., & Sparks, R. (1987). A laboratory simulation of basaltic lava flows. *Mod. Geol, 11*, 93-107.

Harris, A. J. L., Favalli, M., Mazzarini, F., & W., H. C. (2009). Construction dynamics of a lava channel. *Bulletion of Volcanology, 71*, 459-474.

Herd, R. A., & Pinkerton, H. (1997). Bubble coalescence in basaltic lava: Its impact on the evolution of bubble populations. *Journal of Volcanology and Geothermal Research, 75*(1-2), 137-157.

Hodgson, G. W. (1969). An experimental investigation of simulated lava flows using carbowax materials. Diss. Air Force Institute of Technology, Air University, Ohio. 1969.

Howarth, D. F., & Rowlands, J. C. (1987). Quantitative assessment of rock texture and correlation with drillability and strength properties. *Rock Mechanics and Rock Engineering, 20*(1), 57-85.

Hulme, G. (1974). The Interpretation of Lava Flow Morphology. *Geophysical Journal International, 39*(2), 361-383.

Hulme, G., & Fielder, G. (1977). Effusion rates and rheology of lunar lavas. *Philosophical Transactions of the Royal Society of London. Series A, Mathematical and Physical Sciences, 285*(1327), 227-234.

Huppert, H. E., Shepherd, J. B., Haraldur Sigurdsson, R., & Sparks, S. J. (1982). On lava dome growth, with application to the 1979 lava extrusion of the soufrière of St. Vincent. *Journal of Volcanology and Geothermal Research, 14*(3-4), 199-222.

Ishihara, K., Iguchi, M., & Kamo, K. (1989). LAVA FLOWS AND DOMES. *IAVCEI PROCEEDINGS IN VOLCANOLOGY*.

Jaggar, T. (1930). Distinction between pahoehoe and aa or block lava. *Volcano Lett, 281*, 1-4.

James, M., Applegarth, L., & Pinkerton, H. (2011). Lava channel roofing, overflows, breaches and switching: insights from the 2008–2009 eruption of Mt. Etna. *Bulletin of Volcanology*, 1-11.

James, M. R., Pinkerton, H., & Robson, S. (2007). Image-based measurement of flux variation in distal regions of active lava flows. *Geochemistry, Geophysics, Geosystems, 8*(3).

Jeffreys, H. (1925). The flow of water in an inclined channel of rectangular section. *The London, Edinburgh, and Dublin Philosophical Magazine and Journal of Science, 49*(293), 793-807.

Kerr, R. C., Griffiths, R. W., & Cashman, K. V. (2006). Formation of channelized lava flows on an unconfined slope. *Journal of Geophysical Research: Solid Earth, 111*(B10), B10206.

Kilburn, C. (1996). Patterns and predictability in the emplacment of subaerial lava flows and flow fields. In C. Scarpa & R. Tilling (Eds.), *Monitoring and mitigation of volcano hazards* (pp. 491-537). Berlin: Springer.

Kilburn, C., & Luongo, G. (1993). *Active lavas : monitoring and modelling*. London: U. C. L. Press.

Kilburn, C., & McGuire, W. (1997). Mount Etna: its evolution and hazards.

Kilburn, C. R., & Guest, J. E. (1993). *Active lavas: monitoring and modelling*: Taylor & Francis.

Kilburn, C. R. J. (1981). Pahoehoe and aa lavas: a discussion and continuation of the model of Peterson and Tilling. *Journal of Volcanology and Geothermal Research, 11*(2-4), 373-382.

Kilburn, C. R. J. (1990). Surfaces of aa flow-fields on Mount Etna, Sicily: morphology, rheology, crystallization and scaling phenomena. In J. H. Fink (Ed.), *Lava flows and domes* (pp. 129–156). Berlin: Springer.

Kilburn, C. R. J. (2000). Encyclopedia of Volcanoes. In B. Houghton, H. Rymer, J. Stix & S. McNutt (Eds.), *Eos Trans. AGU* (Vol. 81, pp. 291-305): AGU.

Kilburn, C. R. J. (2004). Fracturing as a quantitative indicator of lava flow dynamics. *Journal of Volcanology and Geothermal Research, 132*(2-3), 209-224.

Kilburn, C. R. J., & Lopes, R. M. C. (1988). The growth of aa lava flow fields on Mount Etna, Sicily. *J. Geophys. Res., 93*(B12), 14759-14772.

Kilburn, C. R. J., & Lopes, R. M. C. (1991). General Patterns of Flow Field Growth: Aa and Blocky Lavas. *J. Geophys. Res., 96*(B12), 19721-19732.

Koyi, H. (1997). Analogue modelling: From a qualitative to a quantitative technique - a historical outline. *Journal of Petroleum Geology, 20*(2), 223-238.

Lipman, P. W., & Banks, N. (1987). Aa flow dynamics, Mauna Loa 1984. *US Geol Surv Prof Pap, 1350*, 1527-1567.

Loaiza, S., Fortin, J., Schubnel, A., Gueguen, Y., Vinciguerra, S., & Moreira, M. (2012). Mechanical behavior and localized failure modes in a porous basalt from the Azores. *Geophysical Research Letters, 39*(19).

Lopes, R., & Guest, J. E. (1982). Lava flows on Etna, a morphometric study *The comparative study of the planets* (pp. 441-458): Springer.

Lopes, R. M. C., & Kilburn, C. R. J. (1990). Emplacement of Lava Flow Fields: Application of Terrestrial Studies to Alba Patera, Mars. *J. Geophys. Res., 95*(B9), 14383-14397.

Lyman, A. W., Koenig, E., & Fink, J. H. (2004). Predicting yield strengths and effusion rates of lava domes from morphology and underlying topography. *Journal of Volcanology and Geothermal Research, 129*(1-3), 125-138.

Macdonald, G. A. (1953). Pahoehoe, aa, and block lava. *American Journal of Science, 251*, 169-191.

Mader, H. M., Manga, M., & Koyaguchi, T. (2004). The role of laboratory experiments in volcanology. *Journal of Volcanology and Geothermal Research, 129*(1-3), 1-5.

Malin, M. C. (1980). Lengths of Hawaiian lava flows. *Geology, 8*(7), 306.

Mazzarini, F., Pareschi, M.T., Favalli, M., Isola, I., Tarquini, S., Boschi, E. (2005). Morphology of basaltic lava channels during the Mt. Etna September 2004 eruption from airborne laser altimeter data. *Geophysical Research Letters, 32,* L04305.

Merle, O. (2000). Numerical modelling of strain in lava tubes. *Bulletin of Volcanology, 62*(1), 53-58.

Miyamoto, H., Kogure, J., Tosaka, H., Tokunaga, T., Fukui, K. (2001). Experimental Studies on Non-Newtonian Fluid Flows as Analogues of Lava Flows: Toward a Numerical Model with a Cooling Crust. *Theoretical Applied Mechanics, 50*, 351-356.

Miyamoto, H., & Crown, D. A. (2006). A simplified two-component model for the lateral growth of pahoehoe lobes. *Journal of Volcanology and Geothermal Research, 157*(4), 331-342.

Mogi, K., (2007). Experimental rock mechanics. *CRC Press,* 361.

Murase, T., & McBirney, A. R. (1973). Properties of Some Common Igneous Rocks and Their Melts at High Temperatures. *Geological Society of America Bulletin, 84*(11), 3563-3592.

Naranjo, J. L., Sigurdsson, H., Carey, S. N., & Fritz, W. (1986). Eruption of the nevado del ruiz volcano, Colombia, on 13 november 1985: tephra fall and lahars. *Science (New York, N.Y.), 233*(4767), 961-963.

Nolan, M. (2006). *Analogue Modelling of Lava Flow Morphologies: Implications for Hazard Assessment on Mount Etna.* Unpublished MSc, University of Portsmouth, Portsmouth.

Papadopoulos, G. (1990). Deterministic and stochastic models of the seismic and volcanic events in the Santorini Volcano. *Thera and the Aegean World III. The Thera Foundation, London, 2*, 151-159.

Pieri, D. C., & Baloga, S. M. (1986). Eruption rate, area, and length relationships for some Hawaiian lava flows. *Journal of Volcanology and Geothermal Research, 30*(1-2), 29-45.

Pierson, T. C., Janda, R. J., Thouret, J.-C., & Borrero, C. A. (1990). Perturbation and melting of snow and ice by the 13 November 1985 eruption of Nevado del Ruiz, Colombia, and consequent mobilization, flow and deposition of lahars. *Journal of Volcanology and Geothermal Research, 41*(1–4), 17-66.

Pinkerton, H., & Sparks, R. S. J. (1976). The 1975 sub-terminal lavas, mount etna: a case history of the formation of a compound lava field. *Journal of Volcanology and Geothermal Research, 1*(2), 167-182.

Pinkerton, H., & Wilson, L. (1994). Factors controlling the lengths of channel-fed lava flows. *Bulletin of Volcanology, 56*(2), 108-120.

Polacci, M., & Papale, P. (1997). The evolution of lava flows from ephemeral vents at Mount Etna: Insights from vesicle distribution and morphological studies. *Journal of Volcanology and Geothermal Research, 76*(1-2), 1-17.

Quareni, F., Tallarico, A., & Dragoni, M. (2004). Modeling of the steady-state temperature field in lava flow levées. *Journal of Volcanology and Geothermal Research, 132*(2-3), 241-251.

Riker, J. M., Cashman, K. V., Kauahikaua, J. P., & Montierth, C. M. (2009). The length of channelized lava flows: Insight from the 1859 eruption of Mauna Loa Volcano, Hawai‘i. *Journal of Volcanology and Geothermal Research, 183*(3-4), 139-156.

Robertson, J., & Kerr, R. (2010). Rheological controls on the dynamics of channeled lava flows.

Robertson, J. C., & Kerr, R. C. (2012). Solidification dynamics in channeled viscoplastic lava flows. *Journal of Geophysical Research: Solid Earth, 117*(B7), B07206.

Robson, G. (1967). Thickness of Etnean lavas.

Rocchi, V., Sammonds, P. R., & Kilburn, C. R. J. (2003). Flow and fracture maps for basaltic rock deformation at high temperatures. *Journal of Volcanology and Geothermal Research, 120*(1-2), 25-42.

Rocchi, V., Sammonds, P. R., & Kilburn, C. R. J. (2004). Fracturing of Etnean and Vesuvian rocks at high temperatures and low pressures. *Journal of Volcanology and Geothermal Research, 132*(2-3), 137-157.

Rongo, R., Spataro, W., D'Ambrosio, D., Vittoria Avolio, M., Trunfio, G. A., & Di Gregorio, S. (2008). Lava Flow Hazard Evaluation Through Cellular Automata and Genetic Algorithms: an Application to Mt Etna Volcano. *Fundamenta Informaticae, 87*(2), 247-267.

Rossetti, F., Ranalli, G., & Faccenna, C. (1999). Rheological properties of paraffin as an analogue material for viscous crustal deformation. *Journal of Structural Geology, 21*(4), 413-417.

Rossi, M. J. (1997). Morphology of the 1984 open-channel lava flow at Krafla volcano, northern Iceland. *Geomorphology, 20*(1-2), 95-112.

Rutter, E., & Hadizadeh, J. (1991). On the influence of porosity on the low-temperature brittle—Ductile transition in siliciclastic rocks. *Journal of Structural Geology, 13*(5), 609-614.

Ryan, M. P., & Sammis, C. G. (1981). The Glass Transition in Basalt. *J. Geophys. Res., 86*(B10), 9519-9535.

Sakimoto, S. E. H., & Gregg, T. K. P. (2001). Channeled flow: Analytic solutions, laboratory experiments, and applications to lava flows. *Journal of Geophysical Research: Solid Earth, 106*(B5), 8629-8644.

Shaw, H. R. (1969). Rheology of Basalt in the Melting Range. *Journal of Petrology, 10*(3), 510-535.

Shaw, H. R., Wright, T. L., Peck, D. L., & Okamura, R. (1968). The viscosity of basaltic magma; an analysis of field measurements in Makaopuhi lava lake, Hawaii. *American Journal of Science, 266*(4), 225-264.

Shea, T., Houghton, B. F., Gurioli, L., Cashman, K. V., Hammer, J. E., & Hobden, B. J. (2010). Textural studies of vesicles in volcanic rocks: an integrated methodology. *Journal of Volcanology and Geothermal Research, 190*(3), 271-289.

Sheets, P. D., & Grayson, D. K. (1979). *Volcanic Activity and Human Ecology*: Academic Press.

Shimada, M., Ito, K., & Cho, A. (1989). Ductile behavior of a fine-grained porous basalt at room temperature and pressures to 3 GPa. *Physics of the earth and planetary interiors, 55*(3), 361-373.

Small, C., & Naumann, T. (2001). The global distribution of human population and recent volcanism. *Global Environmental Change Part B: Environmental Hazards, 3*(3–4), 93-109.

Smith, J. V. (2002). Structural analysis of flow-related textures in lavas. *Earth-Science Reviews, 57*(3), 279-297.

Solana, M., Kilburn, C., Rodriguez Badiola, E., & Aparicio, A. (2004). Fast emplacement of extensive pahoehoe flow-fields: the case of the 1736 flows from Montana de las Nueces, Lanzarote. *Journal of Volcanology and Geothermal Research, 132*(2), 189-207.

Solana, M. C. (2012). Development of unconfined historic lava flow fields in Tenerife: implications for the mitigation of risk from a future eruption. *Bulletin of Volcanology, 74*(10), 2397-2413.

Solana, M. C., & Aparicio, A. (1999). Reconstruction of the 1706 Montaña Negra eruption. Emergency procedures for Garachico and El Tanque, Tenerife,

Canary Islands. *Geological Society, London, Special Publications, 161*(1), 209-216.

Soule, S. A., & Cashman, K. V. (2004). The mechanical properties of solidified polyethylene glycol 600, an analog for lava crust. *Journal of Volcanology and Geothermal Research, 129*(1-3), 139-153.

Soule, S. A., Cashman, K. V., & Kauahikaua, J. P. (2004). Examining flow emplacement through the surface morphology of three rapidly emplaced, solidified lava flows, Kīlauea Volcano, Hawai'i. *Bulletin of Volcanology, 66*(1), 1-14.

Sparks, R. S. J., Pinkerton, H., & Hulme, G. (1976). Classification and formation of lava levees on Mount Etna, Sicily. *Geology, 4*, 269-271.

Sparks, R. S. J., Pinkerton, H., & Hulme, G. (1976). Classification and formation of lava levees on Mount Etna, Sicily. *Geology, 4*(5), 269-271.

Stasiuk, M. V., Jaupart, C., Stephen, R., & Sparks, J. (1993). Influence of cooling on lava-flow dynamics. *Geology, 21*(4), 335-338.

Stevens, N. F., Murray, J. B., & Wadge, G. (1997). The volume and shape of the 1991–1993 lava flow field at Mount Etna, Sicily. *Bulletin of Volcanology, 58*(6), 449-454.

Tarquini, S., Favalli, M., Mazzarini, F., Isola, I., Fornaciai, A. (2013), Morphometric analysis of lava flow units: Case study over LIDAR-derived topography at Mount Etna, Italy. *Journal of Volcanology and Geothermal Research, 11-22,* 235-236.

Vicari, A., Bilotta, G., Bonfiglio, S., Cappello, A., Ganci, G., Hérault, A., Rustico, E., Gallo, G., Del Negro, C., (2011), LAV@ HAZARD: a web-GIS interface for volcanic hazard assessment. *Annals of Geophysics, 54 (5),* 662-670.

Vicari, A., Ganci, G., Behncke, B., Cappello, A., Neri, M., and Del Negro, C., (2011), Near real time forecasting of lava flow hazards during the 12–13 January 2011 Etna eruption. *Geophysical. Research Letters. 38*, L13317.

Voight, B. (1990). The 1985 Nevado del Ruiz volcano catastrophe: anatomy and retrospection. *Journal of Volcanology and Geothermal Research, 42*(1–2), 151-188.

Wadge, G. (1978). Effusion rate and the shape of aa lava flow-fields on Mount Etna. *Geology, 6*(8), 503-506.

Wadge, G., & Lopes, R. (1991). The lobes of lava flows on Earth and Olympus Mons, Mars. *Bulletin of Volcanology, 54*(1), 10-24.

Wadge, G., Young, P. A. V., & McKendrick, I. J. (1994). Mapping lava flow hazards using computer simulation. *Journal of Geophysical Research: Solid Earth, 99*(B1), 489-504.

Walker, G. (1971). Compound and simple lava flows and flood basalts. *Bulletin of Volcanology, 35*(3), 579-590.

Walker, G., Huntingdon, A., Sanders, A., & Dinsdale, J. (1973). Lengths of Lava Flows [and Discussion]. *Philosophical Transactions of the Royal Society of London. Series A, Mathematical and Physical Sciences, 274*(1238), 107-118.

Watt, G. (1804). Observations on Basalt, and on the Transition from the Vitreous to the Stony Texture, Which Occurs in the Gradual Refrigeration of Melted Basalt; With Some Geological Remarks. *Philosophical Transactions of the Royal Society of London, 94*(ArticleType: research-article / Full publication date: 1804 /), 279-314.

Zhu, W., Smith, D. K., & Montési, L. G. J. (2003). Effects of regional slope on viscous flows: a preliminary study of lava terrace emplacement at submarine volcanic rift zones. *Journal of Volcanology and Geothermal Research, 119*(1–4), 145-159.

Appendix A

Table A.0.1 – List of the locations of samples taken for the rock mechanics tests

Site	Group	Latitude (N)	Longitude (E)
Etna	B.1	37°40'53.46"	14°59'6.73"
Etna	B1.2	37°40'53.79"	14°59'53.79"
Etna	B1.3	37°40'53.47"	14o59'5.74"
Etna	B1.4	37°40'52.30"	14°59'61.71"
Etna	B	37°40'52.95"	14°59'6.41"
Etna	2003	37°47'52.2"	15°3'36.00"
Etna	Lava	37°40'52.91"	14°59'5.96"
Etna	Gate	37°40'33.78"	14°59'17.1
Etna	Gate B	37°40'31.93"	14°59'16.97"
Chinyero, Tenerife	Chin	28°16'28.56"	16°44'35.06"
Garachico, Tenerife	Gar 1	28°19'52.67"	16°46'18.69"
Garachico, Tenerife	Gar 2	28°19'49.16"	16°46'7.79"
Garachico, Tenerife	Gar 3	28°19'49.79"	16°46'5.69"
Arenas, Tenerife	4.1	28°19'58.2"	16°25'59.9"
Arenas, Tenerife	4.6	28°19'49.2"	16°25'49.3"
Arenas, Tenerife	5.2	28°19'59.3"	16°25'38.0"
Arenas, Tenerife	5.3	28°19'54.9"	16°25'36.6"
Arenas, Tenerife	5.6	28°19'40.2"	16°25'25.5"
Arenas, Tenerife	6.2	28°19'44.26"	16°26'14.56
Arenas, Tenerife	6.3	28°19'43.25"	16°26'11.26"
Arenas, Tenerife	6.6	28°19'52.61"	16°25'57.47"
Arenas, Tenerife	7.2	28°19'47.6"	16°26'25.9"

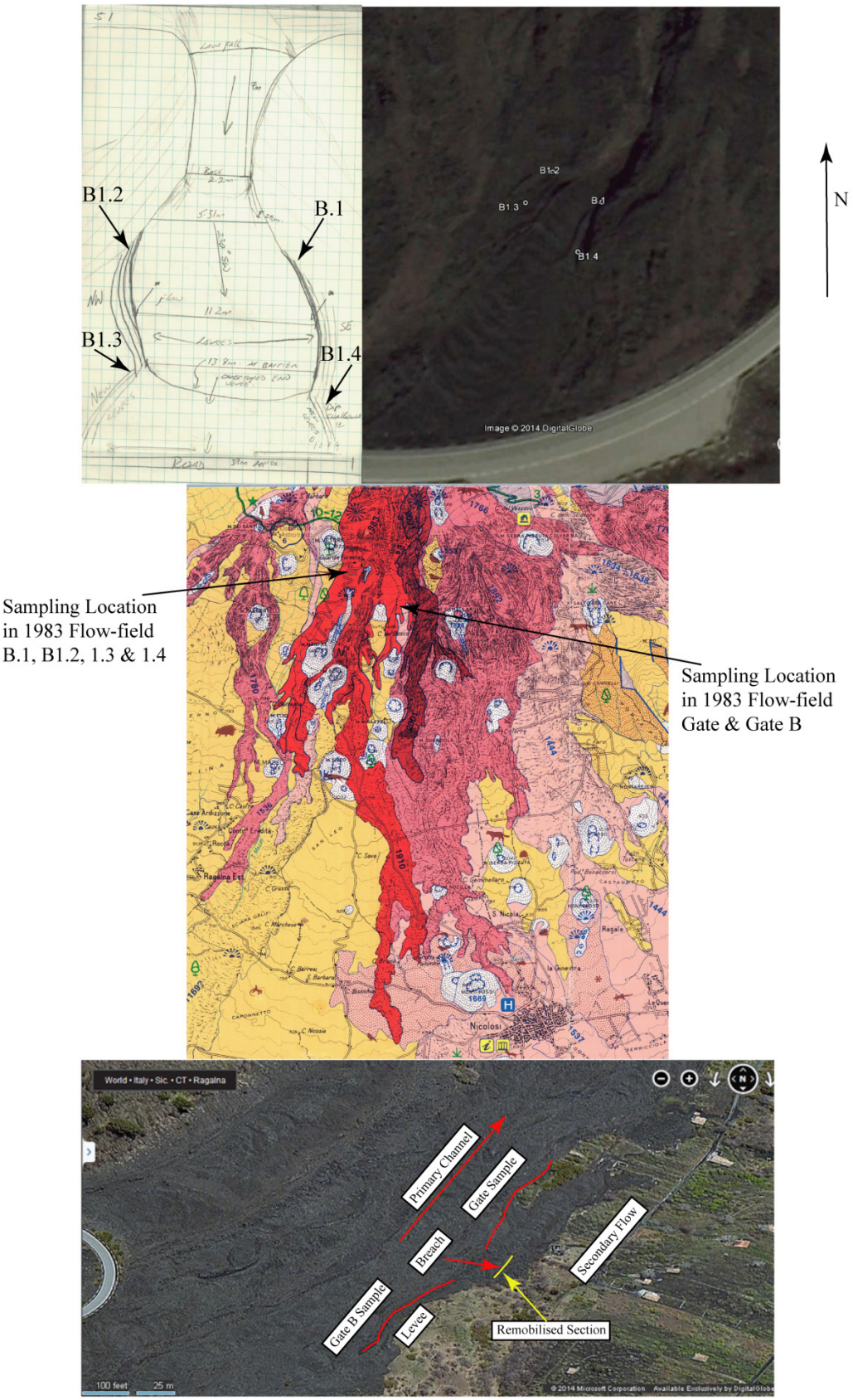

Figure A.0.1 – Locations of samples taken from the 1983 flow-field on Mount Etna for the rock mechanics tests. The exact coordinates are given in Table A.0.1. Samples were taken from levees either side of breaches or changes in morphology.

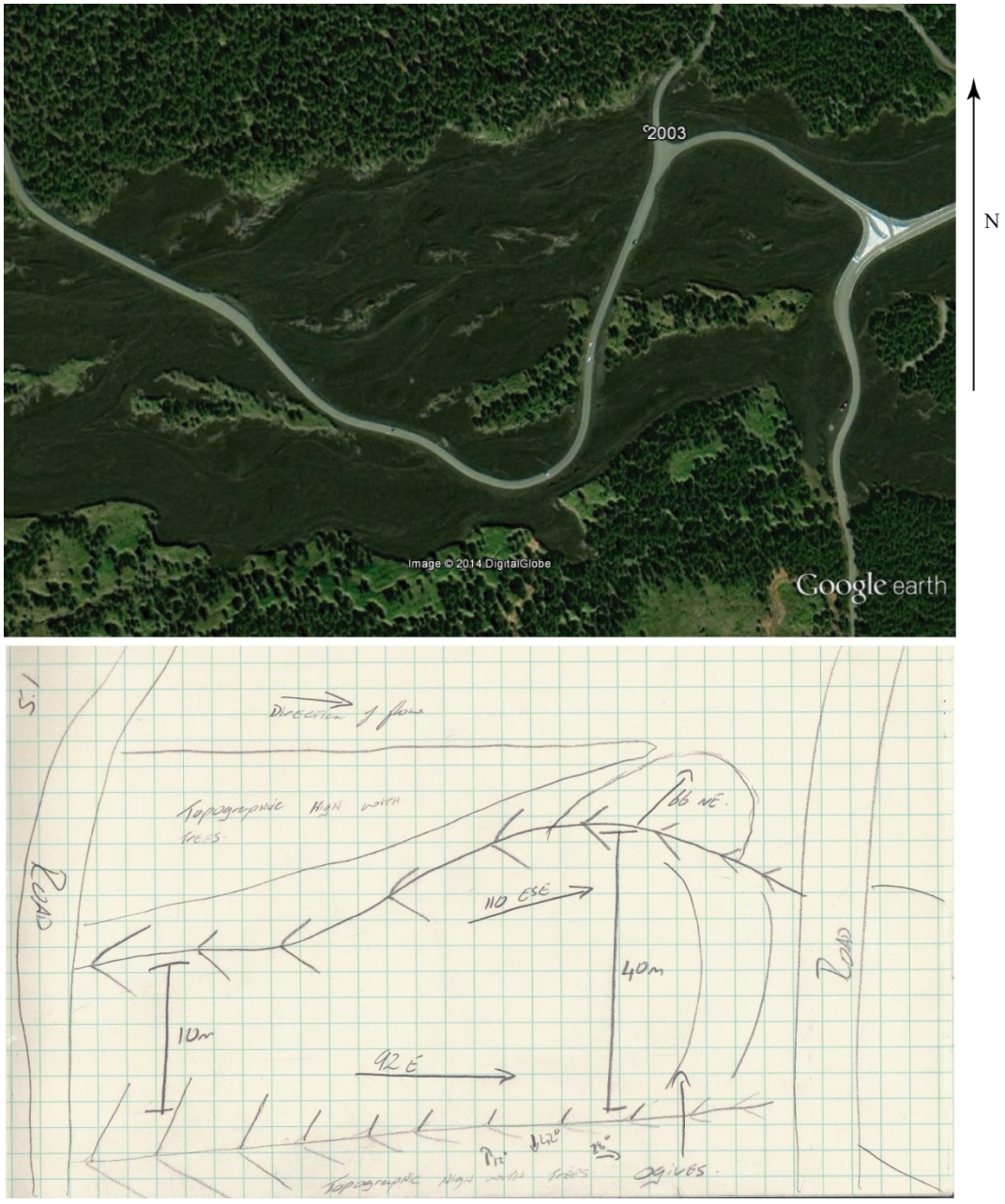

Figure A.0.2 – The location of the samples taken from the 2003 flow-field on Mount Etna. Samples were taken from a levee which contained a small breach which resulted in a small (<10 m) secondary flow shown in the field sketch.

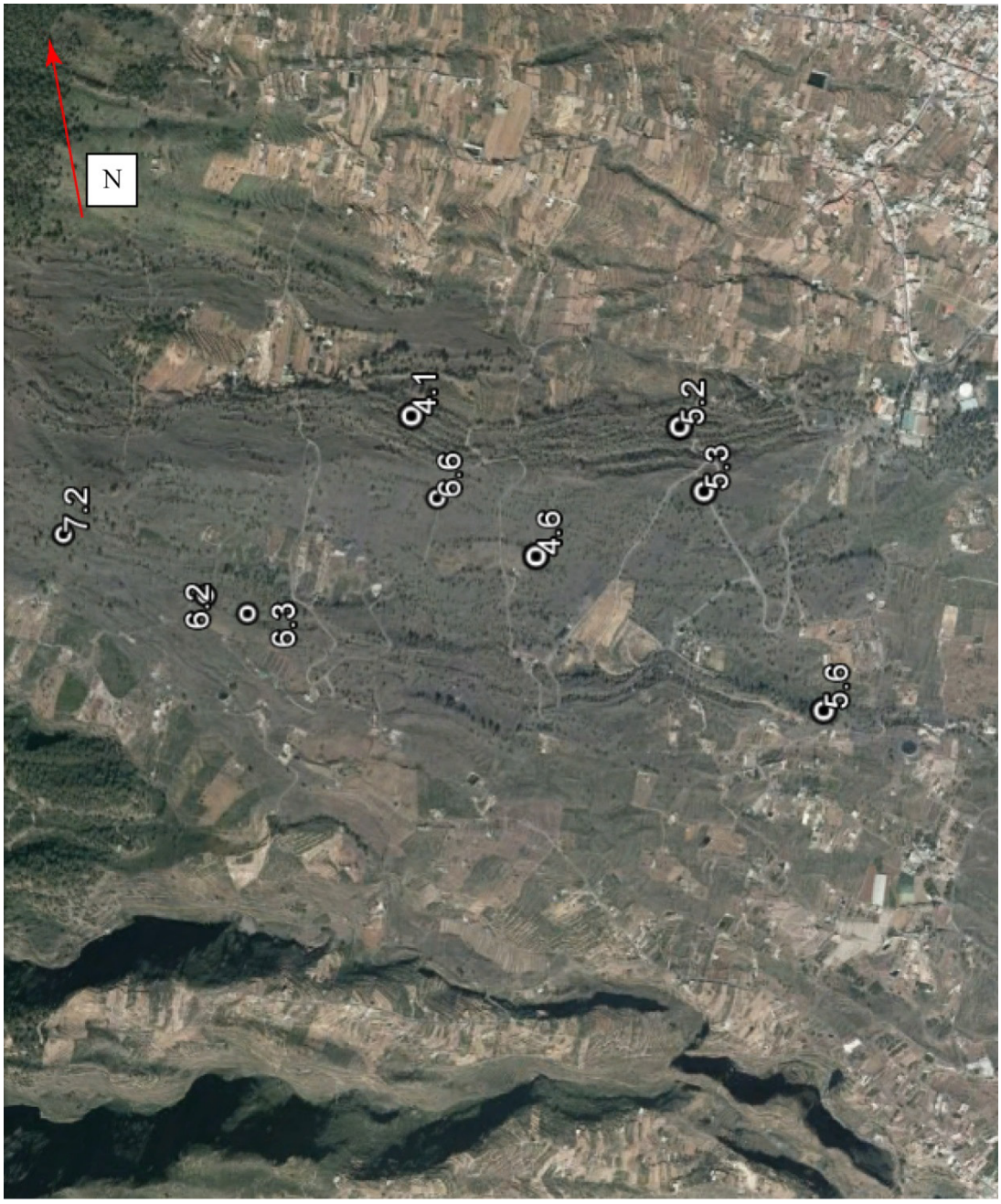

Figure A.0.3 – Image taken from Google Earth which shows the locations of the samples listed in Table A.0.1, taken for the rock mechanic tests from the Arenas flow, Tenerife.

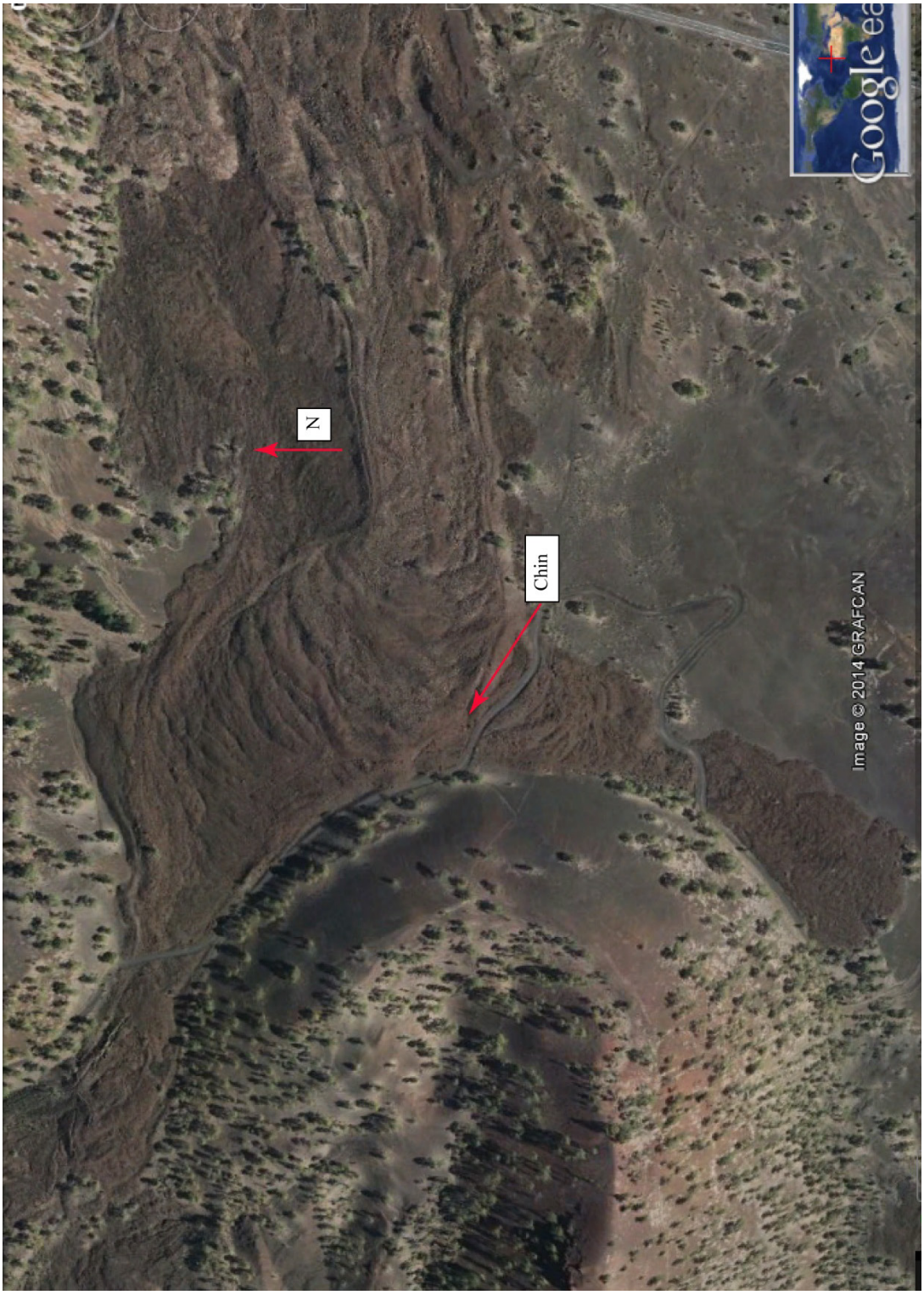

Figure A.0.4 – Image taken from Google Earth showing the location of the samples taken from the Chinyero flow-field on Tenerife for rock mechanics testing. The flow can be seen bi-furcating around a cinder cone. The samples were taken from around a breach in the levee marked by the red arrow.

Figure A.0.5 – Image taken from Google Earth shows the locations of samples taken from the Garachico flow on Tenerife for rock mechanics testing.

Appendix B

Table B.0.1 – Results of the slope variation suite of the analogue modelling experiments.

Exp. No.	Angle of Slope	Volume (cm^3)	Length (cm)	Height (cm)	Field Width Max (cm)	Time to First Break Out (sec)	Time to Flow Max Length (s)	No of Flows	No of Tubes	No of Leveed Flows	No of Lobes	Max Flow Width (cm)	Min Flow Width (cm)	Angle of Breaches to Original Channel	No of Breaches	No of Over Flows	Flow Field Aspect ratio (cm)	Flow Aspect Ratio (cm)	E_r (m^3 s^{-1})
1.5	2	300	165.00	0.6	8.70	14	22	12	4	0	3	1.40	1.60	10	5	7	0.07	0.43	3.24E-06
1.7	2	300	84.20	0.6	7.60	1	62	7	1	3	3	1.00	0.90	25	3	7	0.08	0.60	2.32E-06
1.4	2	300	63.50	0.5	8.10	6	53	10	1	0	6	1.60	0.90	15	5	7?	0.06	0.31	2.15E-06
1.8	2	300	92.80	0.6	11.40	7	63	7	1	1	3	0.90	1.10	30	8	6	0.05	0.67	2.09E-06
1.3	2	300	163.00	0.5	5.70	43	26	8	2	3	5	1.20	2.00	35	8	6	0.09	0.42	1.61E-06
1.2	2	400	139.50	0.7	9.70	23	44	11	5	3	4	1.00	1.90	30	7	4	0.07	0.70	3.68E-06
1.1	2	300	130.90	0.7	8.40	26	121	14	3	1	5	1.40	0.70	35	8	5	0.08	0.50	5.15E-06
1.1	2	400	82.00	0.9	6.62	23	56	4	2	2	3	1.10	0.80	15	3	5	0.14	0.82	8.60E-06
1.1	2	300	75.70	0.7	9.90	9	51	6	1	0	3	0.90	0.80	22	5	6	0.07	0.78	3.31E-06
2.8	4	300	147.80	0.3	10.80	48	37	11	2	5	2	1.60	0.50	35	7	4	0.03	0.19	9.26E-07
2.1	4	300	149.20	0.4	7.60	42	47	8	0	4	2	0.60	1.40	30	4	4	0.05	0.67	8.23E-07
2.9	4	300	85.50	0.3	7.70	19	59	12	2	3	3	1.10	0.70	15	4	7	0.04	0.27	6.37E-07
2.1	4	300	64.80	0.5	11.40	5	50	10	2	1	3	2.20	0.50	36	4	5	0.04	0.23	5.90E-06
2.7	4	300	71.70	0.4	6.00	10	32	8	0	2	2	1.00	0.60	6	5	4	0.07	0.40	1.37E-06
3.5	6	300	100.60	0.4	8.60	25	115	7	1	3	3	1.10	0.60	31	3	8	0.05	0.36	2.26E-06
3.9	6	300	119.10	0.4	17.10	19	115	12	3	2	6	1.10	0.90	36	8	4	0.02	0.36	2.26E-06
3.7	6	300	111.90	0.4	7.90	11	148	12	3	2	5	0.90	0.40	26	5	7	0.05	0.44	1.85E-06
3.1	6	300	65.70	0.3	12.30	12	62	9	1	5	6	1.10	0.90	32	6	5	0.02	0.27	9.54E-07

Table B.0.1 (cont.)

Exp. No.	Angle of Slope	Volume (cm^3)	Length (cm)	Height (cm)	Field Width Max (cm)	Time to First Break Out (sec)	Time to Flow Max Length (s)	No of Flows	No of Tubes	No of Leveed Flows	No of Lobes	Max Flow Width (cm)	Min Flow Width (cm)	Angle of Breaches to Original Channel	No of Breaches	No of Over Flows	Flow Field Aspect ratio (cm)	Flow Aspect Ratio (cm)	E_r (m^3 s^{-1})
3.3	6	300	81.10	0.5	6.80	23	36	7	0	2	5	1.60	0.60	34	6	7	0.07	0.31	6.43E-06
4.2	8	300	85.50	0.4	9.20	24	25	10	1	3	3	1.20	0.60	28	3	8	0.04	0.33	3.29E-06
4.1	8	300	84.00	0.4	13.90	17	124	12	1	3	4	0.80	0.70	33	4	8	0.03	0.50	2.19E-06
4.8	8	300	144.50	0.4	9.10	41	45	10	2	4	3	0.50	1.10	35	6	9	0.04	0.80	1.37E-06
4.1	8	300	177.00	0.5	8.10	17	117	11	3	4	2	1.50	0.70	12	2	9	0.06	0.33	8.02E-06
4.5	8	300	111.50	0.6	8.50	10	50	8	1	4	5	0.70	1.10	26	4	8	0.07	0.86	6.47E-06
5.5	10	300	143.30	0.5	7.80	34	36	13	1	2	3	1.50	0.60	25	10	6	0.06	0.33	1.00E-05
5.8	10	300	153.90	0.5	9.20	25	43	13	0	2	1	1.00	0.60	27	6	9	0.05	0.50	6.67E-06
5.1	10	300	82.60	0.6	7.60	7	66	9	2	3	3	0.70	0.50	26	6	7	0.08	0.86	8.07E-06
5.3	10	300	189.10	0.7	6.10	55	45	7	3	2	4	0.50	1.20	29	7	4	0.11	1.40	9.15E-06
6.7	12	300	167.60	0.5	10.90	15	22	13	0	4	4	1.20	0.60	22	7	7	0.05	0.42	9.59E-06
6.9	12	300	200.00	0.5	4.60	44	12	9	1	2	1	1.20	0.40	12	7	5	0.11	0.42	9.59E-06

Table B.0.2 – Results of the volume variation suite of the analogue modelling experiments.

Exp. No.	Angle of Slope	Volume (cm^3)	Length (cm)	Height (cm)	Field Width Max (cm)	Field Width Min (cm)	Time to First Breakout (sec)	Time to Flow Max Length (s)	No of Flows	No of Tubes	No of Leveed Flows	No of Lobes	Max Flow Width (cm)	Min Flow Width (cm)	Angle of Breaches to Original Flow	No of Breaches	No of Over Flows	Flow Field Aspect Ratio (cm)	Flow Aspect Ratio (cm)	E_r (m^3 s^{-1})
1	2	200	95.00	0.5	8.20	0.40	n/a	n/a	6	2	1	4	7.90	2.20	25	n/a	n/a	0.06	0.06	1.06E-05
3	4	200	42.00	0.4	8.70	1.00	n/a	n/a	6	0	1	2	8.00	5.00	0	n/a	n/a	0.05	0.05	1.10E-05
4	4	200	93.00	0.2	8.50	0.30	n/a	n/a	2	0	0	2	6.00	2.00	27	n/a	n/a	0.02	0.03	1.03E-06
9	6	200	95.00	0.6	10.20	0.80	n/a	n/a	7	0	4	2	8.00	3.00	43	n/a	n/a	0.06	0.08	5.55E-05
10	6	200	95.00	0.6	5.90	0.40	n/a	n/a	4	1	3	1	4.40	2.80	15	n/a	n/a	0.10	0.14	3.05E-05
14	8	200	95.00	0.7	6.20	0.35	n/a	n/a	8	1	4	2	5.20	2.10	30	n/a	n/a	0.11	0.13	7.63E-05
13	8	200	95.00	0.6	8.10	0.60	n/a	n/a	6	0	1	6	5.40	2.60	13	n/a	n/a	0.07	0.11	4.99E-05
17	10	200	86.00	0.6	6.10	0.10	n/a	n/a	7	0	3	6	6.40	1.50	20	n/a	n/a	0.10	0.09	7.38E-05
18	10	200	50.50	0.4	4.80	0.10	n/a	n/a	4	0	0	0	6.20	2.40	0	n/a	n/a	0.08	0.06	2.12E-05
20	12	200	95.00	0.3	2.80	0.10	n/a	n/a	4	0	3	3	5.90	1.80	0	n/a	n/a	0.11	0.05	1.02E-05
19	12	200	95.00	0.3	1.60	0.30	n/a	n/a	6	1	3	2	4.50	1.50	0	n/a	n/a	0.19	0.07	7.76E-06
2	2	300	95.00	0.6	8.40	0.60	n/a	n/a	5	0	5	3	9.70	2.80	33	n/a	n/a	0.07	0.06	2.25E-05
6	4	300	95.00	0.4	9.80	0.60	n/a	n/a	9	2	6	1	7.00	4.50	0	n/a	n/a	0.04	0.06	9.61E-06
5	4	300	95.00	0.4	3.80	0.20	n/a	n/a	6	0	1	1	3.80	1.00	0	n/a	n/a	0.11	0.11	5.21E-06
7	6	300	95.00	1.0	10.00	0.60	n/a	n/a	3	0	2	0	6.20	2.10	15	n/a	n/a	0.10	0.16	1.99E-04
8	6	300	95.00	0.4	8.80	0.60	n/a	n/a	11	2	4	6	5.80	2.30	29	n/a	n/a	0.05	0.07	1.19E-05
12	8	300	78.30	0.4	6.00	0.70	n/a	n/a	6	0	3	5	7.80	5.20	22	n/a	n/a	0.07	0.05	2.14E-05
11	8	300	95.00	0.5	3.80	0.20	n/a	n/a	9	1	3	8	3.10	0.70	20	n/a	n/a	0.13	0.16	1.66E-05
15	10	300	95.00	0.3	9.50	0.40	n/a	n/a	11	2	6	6	5.10	1.90	29	n/a	n/a	0.03	0.06	7.35E-06
16	10	300	95.00	0.3	5.40	0.10	n/a	n/a	14	0	2	9	4.60	1.50	33	n/a	n/a	0.06	0.07	6.63E-06
21	12	300	95.00	0.5	9.90	0.80	n/a	n/a	10	1	1	0	6.60	2.30	44	n/a	n/a	0.05	0.08	5.27E-05
22	12	300	95.00	0.4	7.80	0.70	n/a	n/a	9	0	3	3	5.40	1.40	25	n/a	n/a	0.05	0.07	2.21E-05

Table B.0.3 – Results of the effusion rate variation suite of the analogue modelling experiments.

Exp. No.	Angle of Slope	Length (cm)	Height (cm)	Field Width Max (cm)	Time to First Break Out (sec)	Time to Flow Max Length (s)	No of Flows	No of Tubes	No of Leveed Flows	No of Lobes	Max Flow Width (cm)	Min Flow Width (cm)	Angle of Break Out to Original Channel	No of Breaches	No of Over flows	Flow Field Aspect ratio (cm)	Flow Aspect Ratio (cm)	E_r (m^3 s^{-1})	Effusion Rate Group
1.6	2	82.60	0.7	9.30	23	94	6	1	2	5	1.00	0.80	40	6	5	0.08	0.70	3.68E-06	ErL
1.1	2	157.50	0.6	12.90	24	84	10	0	2	6	1.50	0.90	28	6	2	0.05	0.40	3.48E-06	ErL
1.1	2	112.60	0.8	14.10	41	98	22	2	1	4	1.10	0.90	30	10	10	0.06	0.73	6.04E-06	ErM
1.9	2	83.30	0.8	10.70	15	79	6	2	0	4	0.95	0.80	35	3	4	0.07	0.84	5.22E-06	ErM
2.4	4	47.60	0.7	8.90	9	20	6	2	2	5	1.90	0.60	30	4	5	0.08	0.37	1.40E-05	ErH
2.3	4	48.30	0.8	13.30	25	26	8	3	1	5	1.10	0.60	35	3	7	0.06	0.73	1.21E-05	ErH
2.8	4	147.80	0.3	10.80	48	37	11	2	5	2	1.60	0.50	35	7	4	0.03	0.19	9.26E-07	ErL
2.1	4	149.20	0.4	7.60	42	47	8	0	4	2	1.40	0.60	30	4	4	0.05	0.29	1.92E-06	ErL
2.5	4	69.40	0.6	10.50	17	57	8	3	1	4	1.80	0.80	26	3	7	0.06	0.33	8.34E-06	ErM
3.2	6	103.70	0.6	12.00	28	28	12	1	5	4	1.40	0.90	33	6	6	0.05	0.43	9.72E-06	ErH
3.8	6	116.20	0.4	12.10	28	122	13	2	1	5	1.60	0.80	29	5	8	0.03	0.25	3.29E-06	ErL
3.6	6	103.90	0.4	6.40	35	168	10	0	2	3	1.30	0.60	31	5	5	0.06	0.31	2.67E-06	ErL
3.1	6	127.40	0.4	7.30	21	25	13	2	2	2	1.10	1.00	20	11	2	0.05	0.36	2.26E-06	ErL
3.4	6	79.10	0.5	10.10	28	79	7	0	2	3	1.60	0.50	32	4	6	0.05	0.31	6.43E-06	ErM
4.4	8	100.80	0.8	7.10	9	80	8	1	2	3	1.60	0.70	28	3	8	0.11	0.50	3.50E-05	ErH
4.3	8	63.60	0.4	6.20	5	32	6	1	1	3	1.40	1.10	35	3	6	0.06	0.29	3.83E-06	ErL
4.6	8	100.10	0.5	9.20	23	43	12	3	3	5	0.70	0.60	17	9	11	0.05	0.71	3.74E-06	ErL
4.9	8	108.10	0.5	9.10	24	33	7	3	4	1	1.20	0.60	12	9	7	0.05	0.42	6.42E-06	ErM
4.7	8	111.20	0.5	6.40	21	21	10	3	2	2	1.00	0.40	10	13	5	0.08	0.50	5.35E-06	ErM

Table B.0.3 (cont.)

Exp. No.	Angle of Slope	Length (cm)	Height (cm)	Field Width Max (cm)	Time to First Break Out (sec)	Time to Flow Max Length (s)	No of Flows	No of Tubes	No of Leveed Flows	No of Lobes	Max Flow Width (cm)	Min Flow Width (cm)	Angle of Break Out to Original Channel	No of Breaches	No of Over flows	Flow Field Aspect ratio (cm)	Flow Aspect Ratio (cm)	E_r (m^3 s^{-1})	Effusion Rate Group
5.9	10	184.50	0.7	4.40	18	42	7	0	2	1	1.90	0.70	22	7	4	0.16	0.37	3.48E-05	ErH
5.6	10	141.10	0.7	12.10	23	104	15	1	4	3	1.80	0.70	36	9	10	0.06	0.39	3.30E-05	ErH
5.1	10	196.10	0.5	8.20	17	117	9	2	2	3	1.90	0.70	25	18	9	0.06	0.26	1.27E-05	ErH
5.4	10	199.90	0.5	7.80	18	36	14	1	2	3	1.60	0.60	27	8	8	0.06	0.83	4.00E-06	ErL
5.2	10	180.10	0.5	10.10	10	104	11	2	5	5	1.20	0.70	32	10	4	0.05	0.42	8.01E-06	ErM
5.7	10	147.30	0.5	4.80	10	46	11	1	3	3	1.20	0.30	9	3	8	0.10	0.42	8.01E-06	ErM
6.4	12	156.90	0.7	9.60	9	68	12	2	6	3	1.30	0.40	12	4	9	0.07	0.54	2.85E-05	ErH
6.2	12	166.00	0.7	5.60	16	21	7	1	3	2	1.20	0.40	10	7	5	0.13	0.58	2.63E-05	ErH
6.6	12	200.00	0.7	6.10	23	32	10	1	3	4	1.20	0.60	25	4	9	0.11	0.58	2.63E-05	ErH
6.1	12	200.00	0.6	8.80	31	15	10	1	2	3	1.80	0.60	15	6	4	0.07	0.33	2.48E-05	ErH
6.8	12	200.00	0.6	5.60	60	20	8	1	2	3	1.80	0.60	15	6	3	0.11	0.33	2.48E-05	ErH
6.5	12	200.00	0.5	5.60	59	20	7	0	4	2	1.90	0.60	15	6	2	0.09	0.26	1.52E-05	ErH
6.1	12	200.00	0.5	6.40	26	55	8	1	3	2	1.20	0.40	10	2	13	0.08	0.42	9.59E-06	ErM
6.3	12	200.00	0.5	6.20	27	28	9	0	6	2	1.20	0.60	12	7	5	0.08	0.42	9.59E-06	ErM

Appendix C

Table C.0.1 - The table below lists the results of all uniaxial compression tests.

Sample No.	Field Site	Max Axial Strain x 10^{-3}	Max Compressive Stress MPa	Young's Modulus GPa	Ratio	Clean Break / Compressed
B.1 D O	Sicily	14.99	28.35	2.06	1.99	Yes
B.1 A V	Sicily	22.77	50.12	2.36	2.02	Yes
B.1 B V	Sicily	13.00	22.50	1.39	1.99	No
B.1 C V	Sicily	22.94	51.14	2.41	2.00	Yes
B1.2 C O	Sicily	12.96	7.97	1.35	2.01	Yes
B1.2 D O	Sicily	13.92	19.50	1.87	2.00	No
B1.2 A V	Sicily	19.86	44.26	2.45	2.01	Yes
B1.2 B V	Sicily	18.00	7.97	0.69	2.00	Yes
B1.3 D O	Sicily	45.53	48.62	1.08	2.01	Yes
B1.3 E O	Sicily	24.97	44.72	2.29	2.01	No
B1.3 F O	Sicily	15.98	26.11	1.87	1.99	No
B1.3 A V	Sicily	9.68	15.08	1.55	2.06	Yes
B1.3 B V	Sicily	21.82	44.29	2.37	2.01	Yes
B1.3 C V	Sicily	26.69	65.39	2.65	2.01	Yes
B1.4 E O	Sicily	22.76	22.70	0.93	2.02	Yes
B1.4 E O 1	Sicily	19.79	44.02	2.40	2.02	Yes
B1.4 F O	Sicily	12.91	32.09	2.51	2.01	Yes
B1.4 F O 1	Sicily	15.90	26.74	1.83	2.00	Yes
B1.4 G O	Sicily	16.00	42.79	2.88	2.00	Yes
B1.4 A V	Sicily	22.00	54.38	2.68	2.00	Yes
B1.4 B V	Sicily	25.10	68.53	2.89	1.99	Yes
B1.4 C V	Sicily	11.97	26.32	2.32	2.05	Yes
B1.4 D V	Sicily	12.97	29.61	2.32	2.01	Yes
B Flow 2	Sicily	13.97	26.13	1.99	2.01	Yes
B Flow 3	Sicily	16.93	45.41	2.95	2.02	Yes
B Flow 1	Sicily	9.95	15.78	1.96	2.02	yes
2003 45 9	Sicily	21.83	52.74	2.62	2.03	Yes
2003 45 2	Sicily	21.87	53.67	2.74	2.02	Yes
2003 45 4	Sicily	18.83	46.31	2.53	2.03	Yes
2003 45 3	Sicily	20.71	44.16	2.63	2.04	Yes
2003 45 1	Sicily	16.88	37.83	2.52	2.02	Yes
2003 45 8	Sicily	16.95	42.54	2.67	2.02	Yes
2003 45 5	Sicily	19.62	56.80	3.01	2.05	Yes
2003 45 10	Sicily	11.95	29.70	2.79	2.02	Yes
2003 45 7	Sicily	11.94	26.53	2.88	2.02	Yes
2003 45 6	Sicily	16.86	40.99	2.58	2.03	Yes
2003 90 9	Sicily	20.68	49.00	2.49	2.04	Yes
2003 90 10	Sicily	20.52	53.99	2.63	2.06	Yes
2003 90 7	Sicily	21.75	20.22	1.73	2.03	No
2003 90 4	Sicily	16.91	42.64	2.77	2.02	Yes
2003 90 1	Sicily	15.66	36.41	2.71	2.05	Yes
2003 90 6	Sicily	17.83	52.22	3.18	2.03	Yes
2003 90 2	Sicily	16.72	32.77	2.03	2.04	Yes
2003 90 8	Sicily	18.84	52.75	2.99	2.03	Yes

Table C.0.1 (cont.)

Sample No.	Field Site	Max Axial Strain x 10^{-3}	Max Compressive Stress MPa	Young's Modulus GPa	Ratio	Clean Break / Compressed
2003 90 5	Sicily	17.82	42.28	2.51	2.03	Yes
2003 90 3	Sicily	17.85	44.03	2.56	2.02	Yes
2003 Flow 1	Sicily	22.75	60.67	2.74	2.03	Yes
2003 Flow 6	Sicily	22.89	35.51	1.63	2.02	Yes
2003 Flow 7	Sicily	22.90	30.52	2.27	2.02	Yes
2003 Flow 5	Sicily	22.63	65.05	2.94	2.04	Yes
2003 Flow 8	Sicily	17.63	44.55	2.73	2.05	Yes
2003 Flow 4	Sicily	14.88	31.90	2.25	2.02	Yes
2003 Flow 9	Sicily	19.74	37.75	2.41	2.03	Yes
2003 Flow 10	Sicily	25.13	34.96	1.72	2.00	Yes
2003 Flow 2	Sicily	14.80	32.82	2.39	2.04	Yes
2003 Flow 3	Sicily	15.83	35.95	2.37	2.03	Yes
B 45 1	Sicily	14.86	24.67	1.88	2.03	Yes
B 45 2	Sicily	17.80	39.03	2.38	2.03	Yes
B 90 2	Sicily	17.66	35.49	2.14	2.05	Yes
B 90 1	Sicily	12.73	29.62	2.47	2.05	Yes
B 90 4	Sicily	12.89	18.02	1.40	2.03	Yes
B 90 3	Sicily	6.92	11.27	1.76	2.04	Yes
Gate 4	Sicily	23.75	62.16	2.87	2.03	Yes
Gate 1	Sicily	23.78	49.54	2.34	2.03	Yes
Gate 2	Sicily	18.81	31.56	1.83	2.03	Yes
Gate 3	Sicily	16.90	18.04	1.41	2.02	Yes
Gate 90 1	Sicily	19.82	54.43	2.83	2.03	Yes
Gate 90 5	Sicily	19.90	59.98	3.02	2.02	Yes
Gate 90 7	Sicily	10.88	28.88	2.72	2.03	Yes
Gate 90 2	Sicily	19.69	57.09	2.99	2.04	Yes
Gate 90 4	Sicily	15.81	55.97	3.17	2.04	Yes
Gate 90 3	Sicily	15.86	41.53	2.73	2.03	Yes
Gate 90 6	Sicily	9.93	21.63	2.38	2.03	No
Gate B 1	Sicily	17.79	43.23	2.59	2.03	Yes
Gate B 4	Sicily	16.71	42.01	2.84	2.05	Yes
Gate B 7	Sicily	11.94	25.27	2.21	2.02	Yes
Gate B 5	Sicily	19.90	55.59	2.92	2.02	Yes
Gate B 2	Sicily	18.65	41.27	2.25	2.04	Yes
Gate B 3	Sicily	17.90	42.32	2.58	2.02	Yes
Gate B 6	Sicily	19.61	42.41	2.35	2.05	Yes
Gate Flow 2	Sicily	16.89	39.55	2.45	2.02	Yes
Gate Flow 3	Sicily	17.04	31.03	1.97	2.00	Yes
Gate Flow 1	Sicily	14.86	26.12	1.77	2.00	Yes
Gate Flow 2	Sicily	11.97	9.01	0.76	2.02	Yes
Lava 4	Sicily	26.14	79.70	3.01	2.08	Yes
Lava 6	Sicily	24.83	75.89	3.11	2.03	Yes
Lava 1	Sicily	24.75	65.87	2.80	2.03	Yes
Lava 3	Sicily	22.84	58.60	2.70	2.02	Yes
Lava 2	Sicily	18.91	49.25	2.77	2.02	Yes
Lava 5	Sicily	17.74	44.67	2.76	2.04	Yes
Lava 90 3	Sicily	24.97	72.05	2.99	2.01	Yes
Lava 90 1	Sicily	16.87	24.30	1.46	2.03	Yes
Lava 90 5	Sicily	22.81	64.96	3.01	2.03	Yes
Lava 90 4	Sicily	24.85	67.99	2.99	2.02	Yes
Lava 90 2	Sicily	24.82	55.07	2.50	2.03	Yes
Lava 90 6	Sicily	11.96	26.96	2.68	2.02	No
Lava 90 3	Sicily	29.55	74.85	2.66	2.04	Yes
Lava 90 4	Sicily	24.81	38.77	1.77	2.03	Yes
Lava 90 1	Sicily	27.64	62.72	2.72	2.04	Yes

Table C.0.1 (cont.)

Sample No.	Field Site	Max Axial Strain x 10^{-3}	Max Compressive Stress MPa	Young's Modulus GPa	Ratio	Clean Break / Compressed
Chin 45 4	Tenerife	30.59	107.01	3.68	2.03	Yes
Chin 45 1	Tenerife	21.63	46.49	2.25	2.04	No
Chin 45 5	Tenerife	22.93	55.21	2.60	2.00	Yes
Chin 45 6	Tenerife	24.70	66.17	2.92	2.03	Yes
Chin 45 3	Tenerife	21.94	22.74	1.44	2.01	No
Chin 45 2	Tenerife	24.97	43.47	2.30	2.02	Yes
Chin 90 7	Tenerife	15.98	46.67	3.24	2.00	Yes
Chin 90 6	Tenerife	30.83	78.15	2.99	2.01	Yes
Chin 90 4	Tenerife	18.04	54.02	3.42	2.00	Yes
Chin 90 1	Tenerife	30.01	83.84	2.98	2.00	Yes
Chin 90 3	Tenerife	29.85	53.06	2.81	2.01	No
Chin 90 2	Tenerife	33.00	74.50	2.40	2.00	Yes
Chin 90 5	Tenerife	22.08	58.90	3.16	1.99	Yes
Gar 1 90 3	Tenerife	23.72	82.86	3.78	2.03	Yes
Gar 1 90 1	Tenerife	20.00	24.59	1.45	2.00	No
Gar 1 90 9	Tenerife	16.96	40.96	2.63	2.03	Yes
Gar 1 90 8	Tenerife	19.71	42.08	2.31	2.03	Yes
Gar 1 90 2	Tenerife	11.87	20.60	1.89	2.03	No
Gar 1 90 10	Tenerife	18.92	45.38	2.59	2.02	Yes
Gar 1 90 4	Tenerife	27.64	68.56	2.75	2.03	Yes
Gar 1 90 7	Tenerife	22.92	39.95	1.88	2.01	Yes
Gar 1 90 5	Tenerife	17.93	36.43	2.44	2.02	Yes
Gar 1 90 6	Tenerife	17.86	36.13	2.15	2.02	Yes
Gar 1 Flow 5	Tenerife	29.92	93.53	3.47	2.00	Yes
Gar 1 Flow 2	Tenerife	35.71	59.41	1.53	2.02	Yes
Gar 1 Flow 9	Tenerife	28.53	139.40	5.16	2.04	Yes
Gar 1 Flow 8	Tenerife	32.88	66.52	2.13	2.01	Yes
Gar 1 Flow 3	Tenerife	19.55	28.95	1.58	2.05	No
Gar 1 Flow 1	Tenerife	18.80	44.32	2.61	2.03	Yes
Gar 1 Flow 4	Tenerife	19.74	50.92	2.80	2.03	Yes
Gar 1 Flow 10	Tenerife	21.70	48.65	2.47	2.03	Yes
Gar 1 Flow 7	Tenerife	16.89	30.33	1.84	2.01	Yes
Gar 1 Flow 6	Tenerife	17.04	42.13	2.91	2.00	Yes
Gar 2 45 2	Tenerife	22.71	69.65	3.21	2.03	Yes
Gar 2 45 9	Tenerife	23.69	71.86	3.16	2.03	Yes
Gar 2 45 5	Tenerife	17.86	50.02	2.95	2.02	Yes
Gar 2 45 6	Tenerife	13.93	37.96	2.88	2.01	Yes
Gar 2 45 1	Tenerife	17.81	60.40	3.41	2.02	Yes
Gar 2 45 10	Tenerife	21.38	33.49	1.66	2.06	Yes
Gar 2 45 8	Tenerife	22.72	67.45	3.23	2.03	Yes
Gar 2 45 4	Tenerife	20.72	65.27	3.32	2.03	Yes
Gar 2 45 3	Tenerife	21.79	66.95	3.19	2.02	Yes
Gar 2 45 7	Tenerife	21.83	58.21	2.87	2.02	Yes
Gar 2 90 10	Tenerife	15.07	33.53	2.60	1.99	No
Gar 2 90 6	Tenerife	26.98	51.47	2.07	2.01	Yes
Gar 2 90 9	Tenerife	18.85	38.58	2.04	2.02	Yes
Gar 2 90 5	Tenerife	17.73	49.66	2.88	2.03	Yes
Gar 2 90 8	Tenerife	19.06	60.27	3.33	2.00	Yes
Gar 2 90 3	Tenerife	16.00	48.60	2.98	2.00	Yes
Gar 2 90 1	Tenerife	25.74	83.84	3.41	2.02	Yes
Gar 2 90 2	Tenerife	17.88	40.14	2.16	2.01	Yes
Gar 2 90 4	Tenerife	29.89	35.67	1.39	2.01	Yes
Gar 2 90 7	Tenerife	25.03	40.19	1.78	2.00	Yes
Gar 2 Flow 1	Tenerife	26.69	88.77	3.35	2.02	Yes
Gar 2 Flow 10	Tenerife	30.02	104.47	3.54	2.00	Yes
Gar 2 Flow 3	Tenerife	33.84	130.15	4.11	2.01	Yes

Table C.0.1 (cont.)

Sample No.	Field Site	Max Axial Strain x 10^{-3}	Max Compressive Stress MPa	Young's Modulus GPa	Ratio	Clean Break / Compressed
Gar 2 Flow 6	Tenerife	19.84	65.09	3.51	2.02	Yes
Gar 2 Flow 5	Tenerife	22.90	37.55	1.45	2.01	Yes
Gar 2 Flow 4	Tenerife	22.94	59.97	3.19	2.01	Yes
Gar 2 Flow 9	Tenerife	18.00	64.13	3.56	2.00	Yes
Gar 2 Flow 7	Tenerife	21.98	73.47	3.46	2.00	Yes
Gar 2 Flow 8	Tenerife	28.74	100.71	3.67	2.02	Yes
Gar 2 Flow 2	Tenerife	18.00	44.57	2.56	2.00	Yes
Gar 3 90 5	Tenerife	33.61	128.95	4.02	2.02	Yes
Gar 3 90 9	Tenerife	28.80	86.91	3.25	2.02	Yes
Gar 3 90 8	Tenerife	38.73	113.01	3.54	2.02	Yes
Gar 3 90 4	Tenerife	34.77	123.48	3.77	2.02	Yes
Gar 3 90 10	Tenerife	20.90	50.37	2.48	2.01	Yes
Gar 3 90 2	Tenerife	26.89	81.18	3.23	2.02	Yes
Gar 3 90 1	Tenerife	22.93	61.59	2.87	2.01	Yes
Gar 3 90 3	Tenerife	16.93	41.28	2.78	2.00	Yes
Gar 3 90 7	Tenerife	18.95	59.95	3.19	2.01	Yes
Gar 3 90 6	Tenerife	18.98	41.49	2.31	2.00	Yes
Gar 3 A 6	Tenerife	23.70	71.60	3.12	2.03	Yes
Gar 3 A 5	Tenerife	30.42	25.01	0.75	2.06	Yes
Gar 3 A 8	Tenerife	22.98	68.31	3.02	2.02	Yes
Gar 3 A 2	Tenerife	23.75	70.39	3.04	2.03	Yes
Gar 3 A 4	Tenerife	15.79	42.21	2.75	2.03	Yes
Gar 3 A 1	Tenerife	14.91	37.52	2.50	2.01	No
Gar 3 A 3	Tenerife	18.94	37.80	2.51	2.03	Yes
Gar 3 A 10	Tenerife	17.80	52.78	2.99	2.03	Yes
Gar 3 A 7	Tenerife	14.88	26.43	1.87	2.04	Yes
Gar 3 A 9	Tenerife	19.89	44.10	2.40	2.01	Yes
4.1.2 90	Tenerife	17.79	72.10	3.97	2.01	Yes
4.1.3 90	Tenerife	12.94	55.26	4.22	1.99	Yes
4.1.4 90	Tenerife	24.88	77.63	3.28	1.99	Yes
4.1.1 90	Tenerife	15.96	50.49	3.35	1.99	Yes
4.6.1 90	Tenerife	27.62	29.93	1.66	2.01	Yes
4.6.2 90	Tenerife	15.77	33.31	2.22	2.01	Yes
4.6.4 90	Tenerife	26.60	34.45	2.39	2.02	Yes
4.6.6 Flow	Tenerife	32.77	34.99	1.69	2.00	Yes
4.6.3 Flow	Tenerife	18.58	38.21	2.22	2.03	No
4.6.7 Flow	Tenerife	10.85	18.10	2.27	2.02	No
4.6.5 Flow	Tenerife	19.80	11.01	0.24	2.01	No
5.2.2 45	Tenerife	16.59	13.69	1.23	2.04	Yes
5.2.1 90	Tenerife	16.94	16.74	0.88	1.99	No
5.3.A 45	Tenerife	10.88	29.45	2.72	2.01	Yes
5.3.B 45	Tenerife	14.88	44.22	3.07	2.01	Yes
5.6.2 45	Tenerife	33.81	133.68	4.20	2.00	Yes
5.6.1 90	Tenerife	26.71	99.23	3.97	2.01	Yes
6.2.A 45	Tenerife	32.26	91.01	4.13	2.04	Yes
6.2.B 45	Tenerife	38.47	100.36	3.55	2.02	Yes
6.3.1 90	Tenerife	12.82	18.93	1.52	2.02	Yes
6.3.2 90	Tenerife	14.64	24.86	1.78	2.04	Yes
6.3.3 90	Tenerife	13.78	21.51	1.73	2.02	Yes
6.6.2 45	Tenerife	22.63	23.81	0.82	2.02	Yes
6.6.3 45	Tenerife	17.81	36.01	3.06	2.01	Yes
6.6.1 90	Tenerife	66.67	39.31	0.62	2.00	No
7.2.C 45	Tenerife	23.67	73.67	3.37	2.02	Yes
7.2.B 45	Tenerife	21.82	73.98	3.68	2.01	Yes
7.2.A 45	Tenerife	30.76	69.20	3.67	2.01	Yes
7.2.2 90	Tenerife	16.75	40.67	2.77	2.02	Yes

Table C.0.2 – Table shows a full list of porosity and density test results carried out on samples from Etna and Tenerife

Sample No.	Field Site	Porosity (n)	Dry Density ρ_d (g/cm^3)
2003 45 1	Sicily	6.43	2.47
2003 45 10	Sicily	6.85	2.43
2003 45 2	Sicily	5.75	2.49
2003 45 3	Sicily	5.86	2.49
2003 45 4	Sicily	5.75	2.48
2003 45 5	Sicily	6.60	2.46
2003 45 6	Sicily	9.57	2.41
2003 45 7	Sicily	8.23	2.39
2003 45 8	Sicily	6.57	2.45
2003 45 9	Sicily	4.67	2.44
2003 90 1	Sicily	6.17	2.44
2003 90 10	Sicily	5.60	2.46
2003 90 2	Sicily	6.18	2.44
2003 90 3	Sicily	6.90	2.43
2003 90 4	Sicily	5.97	2.44
2003 90 5	Sicily	6.65	2.44
2003 90 6	Sicily	6.17	2.45
2003 90 7	Sicily	5.65	2.44
2003 90 8	Sicily	6.59	2.44
2003 90 9	Sicily	5.03	2.45
2003 Flow 1	Sicily	5.33	2.47
2003 Flow 10	Sicily	6.56	2.40
2003 Flow 2	Sicily	7.07	2.39
2003 Flow 3	Sicily	7.29	2.38
2003 Flow 4	Sicily	6.29	2.44
2003 Flow 5	Sicily	5.66	2.46
2003 Flow 6	Sicily	5.36	2.46
2003 Flow 7	Sicily	5.52	2.46
2003 Flow 8	Sicily	5.97	2.46
2003 Flow 9	Sicily	6.38	2.45
B 45 1	Sicily	5.57	2.36
B 45 2	Sicily	10.15	2.13
B 90 1	Sicily	7.41	2.34
B 90 2	Sicily	6.98	2.22
B 90 3	Sicily	51.26	1.91
B 90 4	Sicily	11.12	1.90
B Flow 1	Sicily	11.38	1.99
B Flow 2	Sicily	6.83	2.32
B Flow 3	Sicily	8.07	2.36
B.1 A V	Sicily	12.69	2.38
B1.2 A V	Sicily	8.67	2.49

Table C.0.2 (Cont.)

Sample No.	Field Site	Porosity (n)	Dry Density ρ_d (g/cm^3)
B1.3 A V	Sicily	8.80	2.46
B1.4 A V	Sicily	7.97	2.50
Gate 1	Sicily	5.52	2.55
Gate 2	Sicily	7.68	2.45
Gate 3	Sicily	8.42	2.43
Gate 4	Sicily	5.35	2.55
Gate 90 1	Sicily	5.26	2.50
Gate 90 2	Sicily	6.16	2.47
Gate 90 3	Sicily	7.17	2.43
Gate 90 4	Sicily	6.25	2.48
Gate 90 5	Sicily	5.47	2.50
Gate 90 6	Sicily	8.64	2.40
Gate 90 7	Sicily	5.68	2.45
Gate B 1	Sicily	5.99	2.59
Gate B 2	Sicily	7.70	2.54
Gate B 3	Sicily	9.80	2.49
Gate B 4	Sicily	6.71	2.58
Gate B 5	Sicily	6.96	2.56
Gate B 6	Sicily	10.45	2.40
Gate B 7	Sicily	6.91	2.56
Gate Flow 1	Sicily	10.17	2.37
Gate Flow 2	Sicily	12.63	2.27
Gate Flow 2	Sicily	8.47	2.39
Gate Flow 3	Sicily	9.37	2.38
Lava 1	Sicily	4.13	2.68
Lava 2	Sicily	5.39	2.61
Lava 3	Sicily	5.04	2.65
Lava 4	Sicily	3.55	2.66
Lava 5	Sicily	7.13	2.46
Lava 6	Sicily	3.70	2.66
Lava 90 1	Sicily	2.29	2.68
Lava 90 1	Sicily	32.51	2.72
Lava 90 2	Sicily	5.05	2.65
Lava 90 3	Sicily	0.41	2.71
Lava 90 3	Sicily	3.66	2.71
Lava 90 4	Sicily	4.55	2.70
Lava 90 4	Sicily	5.41	2.65
Lava 90 5	Sicily	4.55	2.67
Lava 90 6	Sicily	6.44	2.59
4.1.1 90	Tenerife	2.12	2.73
4.1.2 90	Tenerife	1.27	2.86
4.1.3 90	Tenerife	1.52	2.77
4.1.4 90	Tenerife	2.00	2.80
4.6.1 90	Tenerife	0.60	2.47
4.6.2 90	Tenerife	11.55	2.46

Table C.0.2 (Cont.)

Sample No.	Field Site	Porosity (n)	Dry Density ρ_d (g/cm^3)
4.6.3 Flow	Tenerife	12.07	2.45
4.6.4 90	Tenerife	12.47	2.43
4.6.5 Flow	Tenerife	17.32	2.21
4.6.6 Flow	Tenerife	11.89	2.47
4.6.7 Flow	Tenerife	14.43	2.38
5.2.1 90	Tenerife	13.18	2.29
5.2.2 45	Tenerife	9.67	2.17
5.3.A 45	Tenerife	6.09	2.29
5.3.B 45	Tenerife	6.71	2.36
5.6.1 90	Tenerife	1.04	2.92
5.6.2 45	Tenerife	0.64	2.96
6.2.A 45	Tenerife	4.41	2.65
6.2.B 45	Tenerife	4.53	2.63
6.3.1 90	Tenerife	4.22	2.25
6.3.2 90	Tenerife	4.44	2.28
6.3.3 90	Tenerife	4.83	2.25
6.6.1 90	Tenerife	4.72	2.19
6.6.2 45	Tenerife	5.68	2.20
6.6.3 45	Tenerife	7.60	2.01
7.2.2 90	Tenerife	4.15	2.60
7.2.A 45	Tenerife	3.59	2.63
7.2.B 45	Tenerife	3.50	2.63
7.2.C 45	Tenerife	0.04	2.02
Chin 45 1	Tenerife	6.64	2.55
Chin 45 2	Tenerife	8.78	2.58
Chin 45 3	Tenerife	7.58	2.46
Chin 45 4	Tenerife	5.28	2.48
Chin 45 5	Tenerife	6.83	2.50
Chin 45 6	Tenerife	7.45	2.54
Chin 90 1	Tenerife	7.07	2.43
Chin 90 2	Tenerife	8.41	2.44
Chin 90 3	Tenerife	8.12	2.37
Chin 90 4	Tenerife	4.55	2.47
Chin 90 5	Tenerife	8.69	2.42
Chin 90 6	Tenerife	3.17	2.63
Chin 90 7	Tenerife	1.87	2.35
Gar 1 90 1	Tenerife	8.64	2.07
Gar 1 90 10	Tenerife	11.64	2.12
Gar 1 90 2	Tenerife	11.40	2.06
Gar 1 90 3	Tenerife	5.43	2.36
Gar 1 90 4	Tenerife	12.88	2.20
Gar 1 90 5	Tenerife	14.12	2.12
Gar 1 90 6	Tenerife	14.26	2.06
Gar 1 90 7	Tenerife	13.88	2.10
Gar 1 90 8	Tenerife	10.87	2.05

Table C.0.2 (Cont.)

Sample No.	Field Site	Porosity (n)	Dry Density ρ_d (g/cm^3)
Gar 1 90 9	Tenerife	10.06	2.20
Gar 1 Flow 1	Tenerife	10.38	2.11
Gar 1 Flow 10	Tenerife	11.73	2.06
Gar 1 Flow 2	Tenerife	6.41	2.37
Gar 1 Flow 3	Tenerife	9.93	2.10
Gar 1 Flow 4	Tenerife	11.71	2.08
Gar 1 Flow 5	Tenerife	5.69	2.35
Gar 1 Flow 6	Tenerife	12.75	2.13
Gar 1 Flow 7	Tenerife	12.21	2.12
Gar 1 Flow 8	Tenerife	7.98	2.25
Gar 1 Flow 9	Tenerife	6.92	2.38
Gar 2 45 1	Tenerife	9.73	2.27
Gar 2 45 10	Tenerife	10.06	2.26
Gar 2 45 2	Tenerife	5.37	2.48
Gar 2 45 3	Tenerife	10.69	2.37
Gar 2 45 4	Tenerife	10.66	2.31
Gar 2 45 5	Tenerife	8.81	2.24
Gar 2 45 6	Tenerife	8.99	2.33
Gar 2 45 7	Tenerife	12.08	2.28
Gar 2 45 8	Tenerife	10.54	2.25
Gar 2 45 9	Tenerife	6.21	2.46
Gar 2 90 1	Tenerife	9.14	2.45
Gar 2 90 10	Tenerife	7.69	2.24
Gar 2 90 2	Tenerife	10.06	2.40
Gar 2 90 3	Tenerife	9.11	2.37
Gar 2 90 4	Tenerife	10.37	2.05
Gar 2 90 5	Tenerife	8.71	2.16
Gar 2 90 6	Tenerife	8.07	2.40
Gar 2 90 7	Tenerife	11.51	2.42
Gar 2 90 8	Tenerife	8.77	2.40
Gar 2 90 9	Tenerife	8.60	2.36
Gar 2 Flow 1	Tenerife	4.85	2.39
Gar 2 Flow 10	Tenerife	5.48	2.43
Gar 2 Flow 2	Tenerife	11.71	2.33
Gar 2 Flow 3	Tenerife	6.38	2.49
Gar 2 Flow 4	Tenerife	7.72	2.40
Gar 2 Flow 5	Tenerife	7.54	2.43
Gar 2 Flow 6	Tenerife	7.41	2.45
Gar 2 Flow 7	Tenerife	8.63	2.49
Gar 2 Flow 8	Tenerife	9.75	2.44
Gar 2 Flow 9	Tenerife	8.36	2.36
Gar 3 90 1	Tenerife	8.88	2.40
Gar 3 90 10	Tenerife	8.16	2.39
Gar 3 90 2	Tenerife	8.27	2.55
Gar 3 90 3	Tenerife	9.83	2.50

Table C.0.2 (Cont.)

Sample No.	Field Site	Porosity (n)	Dry Density ρ_d (g/cm^3)
Gar 3 90 4	Tenerife	6.97	2.57
Gar 3 90 5	Tenerife	5.39	2.61
Gar 3 90 6	Tenerife	11.30	2.23
Gar 3 90 7	Tenerife	10.01	2.37
Gar 3 90 8	Tenerife	6.78	2.58
Gar 3 90 9	Tenerife	6.72	2.56
Gar 3 A 1	Tenerife	9.47	2.23
Gar 3 A 10	Tenerife	10.81	2.13
Gar 3 A 2	Tenerife	9.10	2.31
Gar 3 A 3	Tenerife	10.56	2.30
Gar 3 A 4	Tenerife	9.29	2.25
Gar 3 A 5	Tenerife	8.54	2.26
Gar 3 A 6	Tenerife	8.22	2.31
Gar 3 A 7	Tenerife	10.84	2.29
Gar 3 A 8	Tenerife	9.04	2.33
Gar 3 A 9	Tenerife	12.21	2.21